Functional diversity of sharks through time: past, present and future

Jack A. Cooper

College of Science

Swansea University

Swansea University
Prifysgol Abertawe

Submitted to Swansea University in fulfilment of the requirements for the degree of

Doctor of Philosophy

2024

Summary

Modern sharks have played multiple roles in marine ecosystems for over 250 million years. Yet, today, overfishing is driving over one-third of shark species towards extinction. Traditionally, scientists assess extinctions by evaluating changes in species diversity. However, the ecology of species depends on their functional traits, the diversity of which (functional diversity) dictates how species contribute to ecosystem structure and stability. Thus, to understand the ecological consequences of extinctions, it is imperative to record changes in functional diversity. Determining how shark functional diversity has changed through time through their rich, continuous dental fossil record could draw an unprecedented parallel on how extinctions have shaped past, present and future marine communities.

First, I assessed the extent to which dental characters can serve as proxies for functional traits in living sharks using a literature review and two validation analyses (chapter 2). This identified seven dental character proxies for body size, prey preference and feeding mechanism, providing a framework to infer these traits from fossil teeth. Second, I investigated changes in functional diversity over the last 66 million years using teeth (chapter 3). This found that shark functional diversity was relatively high for over 50 million years, before declining to its lowest level today over the last 10 million years due to the extinctions of functionally unique and specialised species that inordinately influence ecosystem functioning. Finally, I simulated future shark extinctions and quantified resulting changes in functional diversity (chapter 4). The results projected further declines, and poleward shifting of functional diversity by 2100 and near-worldwide increases in functional uniqueness, rendering virtually all marine habitats functionally susceptible to further extinctions, with the most functionally unique and specialised sharks at greatest risk.

Overall, this thesis highlights the importance of prioritising protections for sharks disproportionately contributing to functional diversity to conserve the health of our oceans.

Declaration and Statements

I, **Jack Cooper**, certify that this work has not previously been accepted in substance for any degree and is not being concurrently submitted in candidature for any degree.

Signed: ████████████ (candidate)

Date: 29/07/2024

STATEMENT 1

This thesis is the result of my own investigations, except where otherwise stated. Where correction services have been used, the extent and nature of the correction is clearly marked in a footnote(s).

Other sources are acknowledged by footnotes giving explicit references. A bibliography is appended.
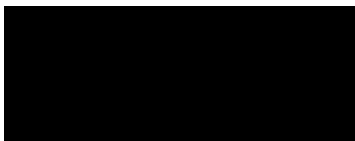
Signed: ████████████ (candidate)

Date: 29/07/2024

STATEMENT 2

I hereby give consent for my thesis, if accepted, to be available for electronic sharing.

Signed: ████████████ (candidate)

Date: 29/07/2024

STATEMENT 3

The University's ethical procedures have been followed and, where appropriate, that ethical approval has been granted.

Signed: (candidate)

Date: 29/07/2024

Authorship Declaration

The following people and institutions contributed to the preparation and publication of work undertaken as part of this thesis:

	Name	Institution	Contribution chapter
Candidate	Jack A. Cooper	Swansea University	Chapter 2, 3
Author 1	Prof Catalina Pimiento	University of Zurich Swansea University	Chapter 2, 3
Author 2	Dr John N. Griffin	Swansea University	Chapter 2
Author 3	René Kindlimann	Haimuseum und Sammlung R. Kindlimann	Chapter 2

Author details and their roles:

Paper 1, *Are shark teeth proxies for functional traits? A framework to infer ecology from the fossil record*, included as Chapter 2 of this thesis.

Candidate contributed to the research design, collected all data, performed all analyses, and wrote the manuscript. **Author 1** conceived the initial idea, contributed to the research design, aided with analysis, and wrote and contributed critically to the drafts and final version of the manuscript. **Author 2** contributed to the research design, aided with analysis, and wrote and contributed critically to the drafts and final version of the manuscript. **Author 3** provided data and corresponding inventory numbers from his collection and contributed critically to the final version of the manuscript.
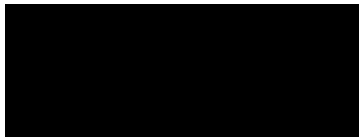
Paper 2, *The rise and fall of shark functional diversity over the last 66 million years*, included as Chapter 3 of this thesis.
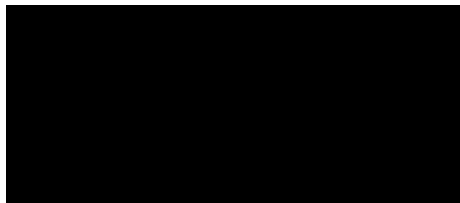
Candidate contributed to the research design, collected and curated all data, performed all analyses and wrote the manuscript. **Author 1** conceived the initial idea, contributed to the research design, and contributed critically to the drafts and final version of the manuscript.

We the undersigned agree with the above stated proportion of work undertaken for each of the above submitted peer-reviewed papers contributing to this thesis:
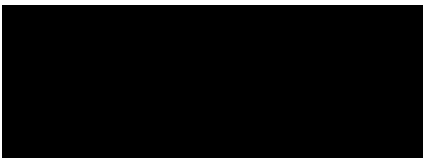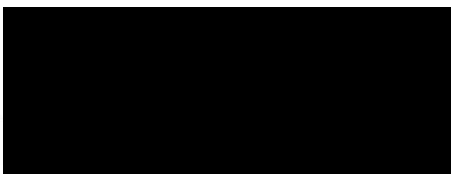
Candidate: Jack A. Cooper

Author 1: Prof Catalina Pimiento

Author 2: Dr John N. Griffin

Author 3: René Kindlimann

Contents

Acknowledgements

I've been lucky to have a very privileged PhD project. I've been able to do research I love; I've been part of an amazing team that has only grown through the years and will continue to produce cutting-edge science; I've been well supported by a generous scholarship; I've had numerous opportunities in collaborations and public engagement; and I've been able to travel the world – most notably to repeatedly visit the beautiful mountains of Switzerland for some truly wonderful group retreats. So naturally, after 4 years, I have a lot of people to thank.

First of all, my family: mum, dad, my brother Calum and my very old cat Cody, who all remained supportive even while not always fully understanding the scientific jargon.

This project would not have been possible without the funding from the Fisheries Society of the British Isles (FSBI). Thank you for supporting my work all these years and for your constant enthusiasm for my progress at your annual symposiums.

I am grateful to the curators and staff of all the museums I travelled to for my key data collection. In particular, I want to thank the following: René Kindlimann who let me use a whole heap of his critically important collection for two of my chapters and co-authored one of them; Emma Bernard who took me through the collection of London's natural history museum – a dream come true for any budding palaeontologist in the UK – and for her great chats about our shared love of Scotland, Bristol, sharks, and bad shark movies; Stephen Godfrey for his incredibly generous hospitality during my visit to the Calvert Marine Museum in Maryland; Gordon Hubbell for allowing me to visit his world-famous collection, a career peak for a young lad who spent far too much time watching fossil shark documentaries as a kid; and my "academic grandad" Bruce MacFadden for his support and hospitality during two weeks in Gainesville, Florida. I also want to thank the Royal Belgian Institute of Natural Sciences, who hosted me no fewer than three times over the years after I quickly became obsessed with their exceptional megalodon spinal column.

I am deeply thankful for the Pimiento Research Group. I have had endless amounts of fascinating conversations, good laughs, and insightful scientific discussions with all of you. There is no better team I could've worked with, and I know you will all go on to do remarkable things! I thank the current members Gregor Mathes, Kristína Kocáková and Lewis Williams; as well as past members Jaime Villafaña, Arianna Chiti, Amanda Gardiner, Dominik Spitznagel and Clement Prieul, for their support, collaboration, and friendship.

and I deeply thank Sophie Boitsios for including me. I've been creatively involved in two fantastic animations on research I've been a part of and thank Ian Cooke-Tapia at Cooked Illustrations and the staff at Ted-Ed for their wonderful work. Lastly, I want to shout out Sarah Buddery and MJ Smith at Let's Jaws for a Minute for being the best podcasting duo I've been able to chat to, and for referring to me as their podcast's "local shark boy".

Finally, and most importantly, I want to thank my supervisors: John Griffin for his words of wisdom in ecological analyses, looking after plants, and academic "taxes"; and *especially* my primary supervisor Catalina Pimiento, who has truly gone above and beyond in her guidance, advice, patience, and support of me and my research not just in these last 4 years, but extending back to my masters too. She has redirected me when I've been lost (many times); celebrated the big and small victories with me; supported and encouraged me in my past and future outreach endeavours; comforted me when I've faced adversity; helped me see things from different perspectives I perhaps would not have otherwise seen or appreciated without her friendship and insight; and all in all taught me how to be a better scientist and independent thinker. She took a chance on me to be her first PhD student and help launch her research group, and I owe my success and ability to study the animals I've loved since childhood to her. I am, and will forever be, grateful to her and will always remain a cheerleader of all the amazing future work that will come out of her lab group. Thank you, Catalina and John, for everything, and for allowing me to bond with your lovely cats, Mona and Frida.

<p style="text-align:center">***</p>

I dedicate this thesis to my late grandparents Peter and Eileen Hinde, who always championed education, and were always at home during my childhood encouraging my increasingly niche interests.

List of Tables

List of Figures

List of Abbreviations

Abbreviation	Definition
Chapter 1: Introduction	
Ecto	Ectothermy
FE	Functional entity
FM	Feeding mechanism
Hab	Habitat
Inverts	Invertebrates
m	Metres
Ma	Million years ago
Meso	Mesothermy
PCoA	Principal coordinate analysis
Terrest	Terrestriality
Thermo	Thermoregulation
TL	Total length
VP	Vertical position
Chapter 2: Are shark teeth proxies for functional traits? A framework to infer ecology from the fossil record	
AS	Acrocone serrations
CART	Classification and regression tree
CE	Cutting edge
CH	Crown height
CH_cat	Categorical crown height
CH_num	Numerical crown height
CNR	Cusp number ratio
Cur	Curvature
CS	Character state
CW	Crown width
CW_cat	Categorical crown width
CW_num	Numerical crown width
DC	Dental character
df	Degrees of freedom
Gi	Giant
High vert	High vertebrates
Inverts	Invertebrates
Lar	Large
LC	Lateral cusplets
LO	Longitudinal outline
m	Metres
Med	Medium
Mya	Million years ago
NoC	Number of cusps
PC	Principal component
PCA	Principal component analysis

Plank	Plankton
RL	Root lobes
SC	Serrational cusplets
Sm	Small
sp.	Species
ST	Serration type
T	Trait
TM	Trait modality
TTH	Total tooth height
Vest	Vestigial
XO	Cross-section outline

Chapter 3: The rise and fall of shark functional diversity over the last 66 million years

df	Degrees of freedom
FE	Functional entity
FOred	Functional over-redundancy
FOri	Functional originality
FRed	Functional redundancy
FRic	Functional richness
FSpe	Functional specialisation
IUCN	International union for the conservation of nature
K/Pg	Cretaceous-Paleogene
m	Metres
Ma	Million years ago
Myr	Million years
PBDB	Palaeobiology database
PCoA	Principal coordinate analysis
SD	Standard deviation
sp.	Species

Chapter 4: Poleward shift and functional decline of sharks and rays under future extinctions

AEP	Average extinction probaility
Avg Ext Prob	Average extinction probaility
CMIP6	Coupled model intercomparison project (6th phase)
CO_2	Carbon dioxide
CR	Critically endangered
DD	Data deficient
EN	Endangered
EX	Extinct
GE	Global endangerment
GLM	Generalised linear model
GLMM	Generalised linear mixed model
FRic	Functional richness
FSp	Functional specialisation
FUn	Functional uniqueness
FUS	Functionally unique and specialised
FUSE	Functionally unique, specialised and endangered
IPCC	Intergovernmental panel on climate change
IUCN	International union for the conservation of nature
LC	Least concern
m	Metres

MCMC	Markov Chain Monte Carlo
MPA	Marine protected area
NT	Near threatened
O_2	Oxygen
PCoA	Principal coordinate analysis
RCP	Regional concentration pathway
VU	Vulnerable

Chapter 5: General discussion

CART	Classification and regression tree
FOri	Functional originality
FRic	Functional richness
FSp	Functional specialisation
FUn	Functional uniqueness
FUS	Functionally unique and specialised
FUSE	Functionally unique, specialised and endangered
ISRA	Important shark and ray area
IUCN	International union for the conservation of nature
m	Metres
Ma	Million years ago
MPA	Marine protected area
PC	Principal component
PCA	Principal component analysis

List of Institutions

Abbreviation	Institute (city; state; country)	Relevant chapter(s)
CMM	Calvert Marine Museum; Solomons; Maryland; United States of America	Chapter 2, 3
GHC	Gordon Hubbell Collection (Jaws International); Gainesville; Florida; United States of America	Chapter 2, 3
NHM	Natural History Museum; London; United Kingdom	Chapter 2, 3
NHMW	Natural History Museum Wien; Vienna; Austria	Chapter 3
MUSM	Museo de Historia Natural, Universidad Nacional Mayor de San Marcos; Lima; Peru	Chapter 3
PIMUZ	Paleontological Institute and Museum, University of Zurich; Zurich; Switzerland	Chapter 2, 3
RBINS	Royal Belgian Institute of Natural Sciences; Brussels; Belgium	Chapter 2, 3
RKC	René Kindlimann Collection; Aathal-Seegräben; Switzerland	Chapter 2, 3
UF	University of Florida, Florida Museum of Natural History; Gainesville; Florida; United States of America	Chapter 3
USNM	Smithsonian Institution National Museum of Natural History; Washington DC; United States of America	Chapter 3

Chapter 1 | Introduction

This PhD thesis consists of three main chapters investigating the functional diversity of sharks in the past, present and future. Sharks are one of the oldest and most threatened groups of marine vertebrates on Earth. Their changes in species richness in the geological past and ongoing abundance declines are well documented in the scientific literature. Despite this, little is understood about the potential ecological consequences of these changes, both past and future. Ecological changes due to shark extinctions in the geological past could provide insights into future extinction effects. However, the shark fossil record consists primarily of isolated teeth and thus these teeth are often the only available tools for inferring functional traits that dictate the range of shark ecological functions (i.e., functional diversity). Chapter 2, therefore, assesses the extent to which measurements in shark teeth can be used as proxies for functional traits. Building from this chapter's findings, chapter 3 uses teeth to investigate how shark functional diversity changed over the last 66 million years. Lastly, chapter 4 simulates future shark extinctions and assesses the temporal and spatial effects on functional diversity by the year 2100. The overall aim of this thesis is to assess how shark functional diversity has changed across millions of years from the distant past to the present day, and how it might change in the future given the current extinction crisis, ultimately showcasing how shark extinctions affect their contributions to marine ecosystem functioning in their past and future evolutionary history.

1.1   Sharks are ecological linchpins

Modern sharks (Elasmobranchii; Selachii) are among the oldest and most evolutionarily distinct marine vertebrates in today's oceans (Stein et al. 2018). Their evolutionary history dates to at least 250 million years ago (Ma; Cappetta 2012), with shark-like elasmobranchs (Chondrichthyes; Elasmobranchii) extending even further back to at least 400 Ma (Maisey 2012). Throughout this long existence, sharks have experienced and survived many biotic and environmental changes. Notably, this includes the last two of the "big five" mass extinction events in geological history (i.e., the Triassic-Jurassic and Cretaceous-Paleogene events; Kriwet and Benton 2004, Guinot et al. 2012, Guinot and Condamine 2023), and multiple other extinction events (e.g., Pimiento et al. 2017, Sibert and Rubin 2021a). As such, sharks can be considered among nature's great survivors, having continuously played important, competitive roles in marine ecosystems for millions of years even amongst world-changing environmental

shifts and the rise and fall of various other marine vertebrate groups (Compagno 1990, Ciampaglio et al. 2005).

As well as their long history, living sharks are known for their high taxonomic and ecological diversity (Compagno 1990). Today's sharks are over 500 species strong and are distributed across nearly every marine habitat (Weigmann 2016, Ebert et al. 2021), and even some freshwater and estuarine systems (Martin 2005, Lucifora et al. 2015). Across these habitats, sharks play a variety of key ecological roles that aid in stabilising marine ecosystems (Dedman et al. 2024). A particularly well-known role is that of an apex predator, typically played by large macropredatory species such as the tiger shark (*Galeocerdo cuvier*), which regulate prey populations (Hammerschlag et al. 2019). Another is that of mesopredators such as reef sharks (e.g., *Carcharhinus amblyrhynchos*), which concurrently serve as both consumers and prey, and can additionally partake in local nutrient cycling (Heupel et al. 2014, Roff et al. 2016, Navia et al. 2017). Finally, a more recently studied ecological role of today's sharks is that of nutrient transporters, which connect long distance habitats and populations through annual, seasonal or transoceanic migrations; documented in both mesopredators (e.g., *C. amblyrhynchos*; Williams et al. 2018) and large apex predators like the great white shark (*Carcharodon carcharias*; Bonfil et al. 2005). Between these different ecological roles, many sharks evidently have large effects on marine ecosystems, and can be considered keystone species (Heupel et al. 2014, Hammerschlag et al. 2019, Dedman et al. 2024).

Despite their ecological importance, sharks and their elasmobranch relatives (i.e., rays and skates) are among the most threatened groups of marine vertebrates on Earth (Dulvy et al. 2014). Over one-third of today's shark and ray species are currently threatened with extinction (Dulvy et al. 2021), with large-bodied, tropical and coastal species being particularly at risk (Ferretti et al. 2010, Dulvy et al. 2021). While habitat destruction, climate change and pollution are all threats facing sharks today, overfishing is the overwhelming leading cause of this extinction risk, being the sole threat for more than two-thirds of threatened shark and ray species (Dulvy et al. 2021). Indeed, it is commonly reported that as many as 100 million sharks a year are killed as fishing catch (Ferretti et al. 2010, Worm et al. 2013). Furthermore, an 18-fold increase in relative fishing pressure over the last ~50 years alone has led to the abundance of oceanic sharks and rays declining by at least 71% (Pacoureau et al. 2021). Protections have been introduced over the last decade such as limiting the fishing trade of threatened species and the elimination of some shark finning trades, where sharks have fins removed before being

tossed back into the sea (Ferretti et al. 2020); however, global fishing mortality of sharks has worryingly continued to increase despite these efforts (Worm et al. 2024).

Declines and subsequent extinctions of sharks can compromise the functional balance of marine ecosystems. The most well-studied effect is that which occurs with the loss of apex predatory sharks. Since apex predators regulate the populations of lower trophic levels of the food web, their loss has been suggested to cause top-down cascading effects (Baum and Worm 2009, Estes et al. 2011). In the case of sharks, a classic case study concluded that the fishing-induced declines of 11 large apex predatory shark species on the east coast of the United States caused explosions of populations of mesopredatory prey such as crowned rays, so much so that populations of the ray's own prey – bay scallops – were decimated, reducing ecosystem stability and productivity and even causing the closure of local scallop fisheries (Myers et al. 2007). However, this is a nearly 20-year-old study, and the proposed cascading theory has since come under scrutiny. A more recent study has argued that there was little correlation between the loss of the sharks and the recorded increase in crowned ray abundance and decline of bay scallops, due to the slow-growing rays also being affected by fishing pressure and a lack of consideration for other bay scallop predators (Grubbs et al. 2016). Furthermore, empirical studies focusing on coral reef habitats have since found that fishing pressure resulted in simultaneous declines across all shark trophic levels: in other words, both apex predators and mesopredators (i.e., sharks across multiple ecological roles) were lost (Roff et al. 2016, Desbiens et al. 2021). Even some studies that have found evidence for mesopredator population increases following the decline of apex predatory sharks have stopped short of definitively calling this a trophic cascade (e.g., Ferretti et al. 2010). Ultimately, this debate indicates that the ecological effects of ongoing shark declines, both at individual and collective ecological roles, are still not fully understood. Since overfishing appears to affect sharks across their wide range of habitats and ecological roles (Desbiens et al. 2021), global declines of sharks as a collective could potentially disrupt worldwide marine ecosystem functioning across multiple different levels.

Notably, trophic effects of the loss of apex predatory sharks have also been inferred from the fossil record. Undoubtedly the most famous extinct shark is the "Megalodon" (*Otodus megalodon*). Reaching a maximum body length of 20 m (Perez et al. 2021), and weighing over 60 tonnes (Cooper et al. 2022), *O. megalodon* was the largest macropredatory shark that ever existed (Gottfried et al. 1996, Pimiento and Balk 2015); and one of the largest extinct marine megafauna the oceans have ever seen (Pimiento et al. 2024). Stable isotopes extracted from

fossilised teeth signify that its trophic level was likely comparable to or even higher than that of the apex predatory *C. carcharias* (Martin et al. 2015, Kast et al. 2022, McCormack et al. 2022). This trophic level reflects feeding on large organisms, with bite marks left behind on cetacean fossils suggesting that they were part of *O. megalodon*'s diet (Collareta et al. 2017). Significantly, several such fossil bites show signs of healing, indicating survival from the bite, while others have been found with *O. megalodon* teeth stuck inside the bitten fossil; both lines of evidence point to *O. megalodon* being an active predator (Godfrey and Altman 2005, Aguilera et al. 2008, Kallal et al. 2010, Godfrey and Beatty 2022). However, following the extinction of *O. megalodon* in the Pliocene epoch (5.3-2.6 Ma; Pimiento and Clements 2014, Pimiento et al. 2016, Boessenecker et al. 2019), fossils indicate that cetaceans reached larger body sizes than their ancestors, having been released from the strong predation pressure of *O. megalodon* (Pyenson and Sponberg 2011, Pimiento and Clements 2014, Cooper et al. 2022). In addition, *O. megalodon* has been proposed to have been an important nutrient transporter undertaking transoceanic migrations (Cooper et al. 2022; see Pollerspöck et al. (2023) for recent fossil evidence supporting this hypothesis), implying that nutrient transfer between distant habitats was disrupted following its extinction. Given that *O. megalodon* also had a cosmopolitan distribution (Pimiento et al. 2016, Pollerspöck et al. 2023), this in turn signals that such disruptions potentially occurred on a global scale (Cooper et al. 2022). As such, the case study of *O. megalodon*, although representing just one charismatic species, broadly indicates that previous shark extinctions have had large ecological effects on marine communities in the distant past.

Ultimately, losses of sharks have been documented as adversely affecting marine ecosystems both in the past (e.g., Cooper et al. 2022) and the present (e.g., Myers et al. 2007). This therefore indicates that the ongoing declines and extinction risk facing sharks today (e.g., Dulvy et al. 2021, Pacoureau et al. 2021) could have dire consequences for marine ecosystem functioning in the future. Nonetheless, as overfishing – the biggest threat to today's sharks (Dulvy et al. 2017, Dulvy et al. 2021) and something that sharks of the geological past would never have faced – causes ongoing shark declines across multiple trophic levels and ecological roles (Roff et al. 2016, Desbiens et al. 2021), the wider ecological effects of such collective declines lack a comprehensive understanding.

1.2 Past and present extinctions

Although sharks represent one of the most threatened groups of marine vertebrates (Dulvy et al. 2014), they are not alone in facing worldwide species decline. In fact, it is widely accepted by the scientific community that we are now on the road to a "sixth mass extinction", as current global species losses are already at a rate comparable to, and possibly even exceeding, the previous "big five" mass extinctions that have shaped worldwide biodiversity (Barnosky et al. 2011, Marshall 2023). Understanding the ecological effects of extinctions in general therefore remains a pressing issue.

While assessing effects of ongoing and future extinctions is a daunting task, the fossil record could provide a starting point of comparison. This is because the fossil record, although inherently incomplete (Foote and Sepkoski 1999, Benton et al. 2011), has recorded several past extinction events. The most notable of the "big five" mass extinction events (Raup and Sepkoski 1982) include the Permian-Triassic mass extinction event 252 Ma that eliminated around 81% of marine species (Benton and Twitchett 2003, Stanley 2016), and the Cretaceous-Paleogene mass extinction event 66 Ma where a bolide impact rendered between 55 and 76% of species extinct, most famously including all non-avian dinosaurs (Alvarez et al. 1980, Stanley 2016). Shark extinctions in the fossil record have been singled out by a few studies, including in the Cretaceous-Paleogene event, where ~60% of shark species were lost on a global scale (Kriwet and Benton 2004, Guinot and Condamine 2023). Other purported extinction events have also been investigated, with one study recently proposing a rapid extinction of unknown causes that was selective to pelagic sharks in the early Miocene epoch ~19 Ma based on a 90% abundance decline of fossilised shark dermal denticles from open ocean sentiments (Sibert and Rubin 2021a; but see also Feichtinger et al. 2021, Naylor et al. 2021, Sibert and Rubin 2021b, c). What the above fossil studies have in common is that they focus primarily on declines in taxonomic occurrence (i.e., species richness) as a metric of extinction, in a broadly similar vein to recent work assessing ongoing shark abundance declines (Pacoureau et al. 2021).

Studying taxonomic loss is a traditional approach for assessing both past and present extinctions (Raup 1994, Jablonski 2004, Barnosky et al. 2011). This effectively quantifies the intensity and rate of extinctions. However, it does not consider the ecological roles that may or may not be lost alongside species. For example, lost species may play the same ecological roles as surviving species, resulting in little to no change in efficient functioning of the wider ecosystem (e.g., Pimiento et al. 2020a). On the other hand, lost species may play a wide range

of different ecological roles of varying importance to the wider community. Indeed, some distinct ecological roles such as that of a large apex predator may be played by a single species in some ecosystems, which means that the loss of that species would cause a disproportionate change in ecosystem functioning (Mouillot et al. 2013a, Mouillot et al. 2014, Enquist et al. 2020, Griffin et al. 2020). Ecological roles may be quantified by traits like body size or diet (Mouillot et al. 2013b, Mouillot et al. 2014); and previous research has found that trait-based studies have been better at detecting the effects of extinctions on ecosystem functioning compared to the use of a traditional taxonomic approach (McGill et al. 2006, Mokany et al. 2008, Villéger et al. 2010, Gagic et al. 2015). Of relevance to shark extinctions, taxonomic changes of sharks and their relatives have been recorded from the fossil record over the last 300 million years (Guinot et al. 2012), but the ecological consequences of those changes have never been assessed, which could provide insights into how future marine ecosystem functioning may be disrupted by the collective loss of sharks. In sum, to gauge the implications of past and present extinctions on ecosystem functioning, it is imperative that the recorded taxonomic losses are linked with ecological roles (e.g., Pimiento et al. 2017).

1.3   Functional diversity

Functional diversity is the diversity of species' functional traits (**Table 1.1**). These are measurable characteristics that mediate how species perform within and interact with their ecosystem (McGill et al. 2006, Violle et al. 2007, Mouillot et al. 2013b). Functional traits can be morphological, behavioural, physiological or biochemical (Nock et al. 2016). Key examples of functional traits in sharks include: (1) body size, which reflects travelling capabilities and thus ability to transport nutrients (Doughty et al. 2016), as well as prey size and trophic level (Lucifora et al. 2009); (2) diet, which reflects how species partake in resource partitioning and distribution via direct (i.e., consumption) and indirect effects (i.e., altered behaviour) on prey (Burkholder et al. 2013); and (3) feeding mechanism, which reflects how species specialise in prey consumption, and thus how they can alter ecosystem structure and prey distribution via intraspecific competition (Munroe et al. 2013). Ultimately, traits like these collectively dictate how species stabilise ecosystems and fill diverse niches. In other words, functional traits are linked to a species' ecological role. As such, the loss of certain combinations of traits, whether it belongs to a single species or a larger collective, results in the loss of an ecological role, which in turn can reflect the relative impact of extinctions (Mouillot et al. 2013b).

Table 1.1. A glossary of terms and metrics associated with functional diversity calculations.

Term	Definition
Functional trait	Measurable intrinsic characters, measured at species or individual level, that influence species performance in ecosystems
Functional space	A multidimensional space defined by functional traits
Functional entities	Unique trait combinations broadly representing ecological functions/roles
Functional redundancy	Number of species filling functional entities
Functional over-redundancy	% of functional entities above the mean level of redundancy
Functional vulnerability	% of functional entities filled by a single species
Functional richness	Volume of occupied functional space
Functional originality	Distance of species to their closest single neighbour
Functional uniqueness	Distance of species to their closest five neighbours
Functional specialisation	Distance of species to the centroid of the functional space

Several approaches can be used to assess functional diversity. One significant approach is to quantify the number of functions (i.e., ecological roles) in a community. This is done using unique combinations of functional traits, referred to as functional entities (FEs; **Table 1.1, 1.2**). By assessing the number of species that occupy individual FEs, one can calculate up to three

additional functional diversity metrics: (1) functional redundancy, the number of species per FE; (2) functional over-redundancy, the % of species filling FEs above the mean level of redundancy; and (3) functional vulnerability, the % of FEs filled by just a single species (**Table 1.1**; Mouillot et al. 2014). In a biological sense, these three metrics respectively reflect the resilience, over-representation, and susceptibility of ecological roles in a community.

Table 1.2. A conceptual species-trait matrix documenting functional traits recorded in five example shark species: four extant species from the present day and one extinct species from the geological past. Each species' combination of traits represents a functional entity, and the diversity of these entities can be used at face value, or in a multidimensional space defined by the traits themselves, to quantify functional diversity. All traits, and values from extant sharks, are extracted from Pimiento et al. (2023), with the exception of basking shark (*Cetorhinus maximus*) thermoregulation, recently found to be mesothermic (Dolton et al. 2023a). For trait values of the extinct *Otodus megalodon*, references are provided in-table. Abbreviations are as follows: Hab = habitat; VP = vertical position; Terrest = terrestriality; Thermo = thermoregulation; FM = feeding mechanism; TL = total length (i.e., maximum body size in metres; m).

Species	Hab	VP	Terrest	Thermo	FM	Diet	TL (m)
Stegostoma fasciatum	Coastal	Benthic	Brackish	Ectotherm	Macropredator	Inverts/ Fish/ High verts	2
Cetorhinus maximus	Coastal/ Oceanic	Pelagic	Marine	Mesotherm	Filter feeder	Plankton	11
Pliotrema warreni	Coastal	Benthic	Marine	Ectotherm	Macropredator	Inverts/ Fish	1.36
Sphyrna lewini	Coastal/ Oceanic	Pelagic	Brackish	Ectotherm	Macropredator	Inverts/ Fish	4.3
Otodus megalodon	Coastal	Pelagic	Marine	Mesotherm	Macropredator	High verts	20
	(Pimiento et al. 2016)	(Pimiento et al. 2017)	(Pimiento et al. 2016)	(Ferrón 2017, Griffiths et al. 2023)	(Godfrey and Altman 2005, Godfrey and Beatty 2022)	(Collareta et al. 2017, Godfrey et al. 2021)	(Perez et al. 2021)

Another well-utilised approach for evaluating functional diversity is the use of a functional space, which visualises the range and diversity of functions. This approach quantifies the distribution of species in a multidimensional space defined by functional traits (Villéger et al. 2008, Mouillot et al. 2013b). From within this space, one can quantify functional richness (**Table 1.1**) – the % volume of space occupied by species within a community, which reflects the range of ecological roles and can change over time as ecological roles originate or disappear alongside species (Mouillot et al. 2013b). The species distribution within the functional space

further reveals which species may possess traits highly dissimilar to other species, or traits with extreme values. The former may be measured using the distance of species to their closest neighbours in space, defined as functional originality or functional uniqueness based on the number of neighbours used as measurement (**Table 1.1**; Mouillot et al. 2013b, Pimiento et al. 2020b). The latter is measured based on species distance from the centroid of space and is called functional specialisation (**Table 1.1**; Mouillot et al. 2013b). All functional diversity metrics calculated from a functional space should be done so diligently, as the quality of the space (Maire et al. 2015) and the number and weighting of traits (Lefcheck et al. 2015, Zhu et al. 2017, Legras et al. 2019) can influence the results and thus must be carefully considered. Other functional diversity-based approaches include measuring shifts in trait values (e.g., Henderson et al. 2024) or measuring functional richness based on kernel density estimation (i.e., incorporating the density of observations of species sharing the same trait values), sometimes called functional volume (Hedberg et al. 2021).

Trait-based studies assessing functional diversity in ecology have appeared exponentially in the literature over the last 20 years (Mammola et al. 2021, Palacio et al. 2022). These typically only require a species-trait matrix (e.g., **Table 1.2**) and species-assemblage matrix (i.e., a matrix of species occurrences in different habitats or designated time periods) as necessary inputs, making such studies highly reproducible under a simple, easy-to-replicate protocol (Palacio et al. 2022). Indeed, an abundance of software packages such as in R (R Core Team 2017) have begun to emerge in the last 15 years specialising in functional diversity analyses (e.g., Casanoves et al. 2010, Laliberté and Legendre 2010, Cardoso et al. 2014, Grenié et al. 2017, Magneville et al. 2022, Grenié and Gruson 2023, Carmona et al. 2024). This further highlights the usefulness and reproducibility of increasingly common trait-based work in ecology. In particular, the functional space approach has become a staple in ecological trait studies (**Figure 1.1**; Villéger et al. 2008, Laliberté and Legendre 2010, Mouillot et al. 2013b).

Functional diversity of sharks through time: past, present and future
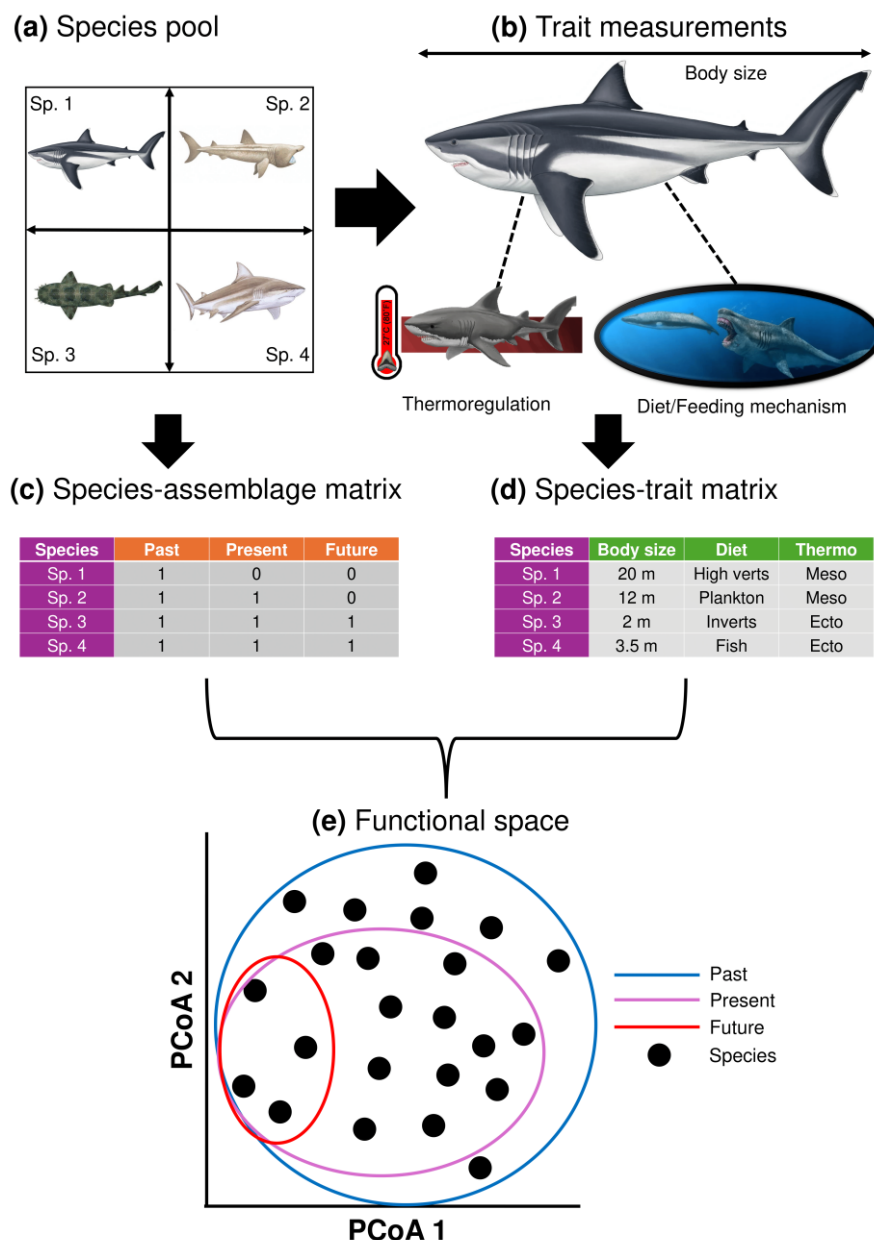
Figure 1.1. Schematic framework for the aim of this thesis to analyse functional diversity through time using the functional space approach. (a) A pool of species is collected, illustrated here with four examples. Sp. 1 = the extinct megalodon shark (*Otodus megalodon*); Sp. 2 = the basking shark (*Cetorhinus maximus*); Sp. 3 = the ornate wobbegong (*Orectolobus ornatus*); Sp. 4 = the bull shark (*Carcharhinus leucas*). The *O. megalodon* illustration is credited to Oliver E. Demuth, produced for Cooper et al. (2020). All other illustrations are credited to Marc Dando. (b) A set of traits are measured from the species. The palaeo-art representing megalodon thermoregulation is credited to Christina Spence Morgan, while the palaeo-art representing megalodon feeding is credited to Juan Jose Giraldo. (c) A species-assemblage matrix is produced, where the presence or absence of species in time periods is marked by 1 and 0 respectively, conceptually represented here by the past, present and future. (d) A species-trait matrix is produced from the trait measurements. Abbreviations include: thermo = thermoregulation; inverts = invertebrates; meso = mesothermy; ecto = ectothermy. (e) Both are used to create a multidimensional functional space based on trait values, the occupied volume of which (functional richness) declines through time as more species are lost from the past to the future (i.e., species in the future are also present in the present and past). PCoA refers to the axes of a principal coordinate analysis. This conceptual figure is inspired by and adapted from Figure 1 of Mouillot et al. (2013b).

In functional spaces, functionally unique and specialised species respectively occupy isolated and outlying portions of space (Mouillot et al. 2013b, Griffin et al. 2020). Biological examples of such species, distinguished from others due to their dissimilar or extreme trait values, may include large-bodied apex predators that are typically uncommon in ecological communities due to low population abundance and energy efficiency (e.g., Garcia et al. 2008, Ordiz et al. 2013, Estes et al. 2016). Indeed, these types of species are considered highly important for biosphere functioning (Estes et al. 2016, Enquist et al. 2020, Carmona et al. 2021). The loss (i.e., extinction) of functionally unique and specialised species from a community respectively leaves large portions of functional space unoccupied or reduces the range of occupied space (Pimiento et al. 2020b, Toussaint et al. 2021). As such, functionally unique and specialised species disproportionately contribute to maintaining functional diversity and, therefore, ecosystem functioning (Mouillot et al. 2013b, Griffin et al. 2020).

Recent work has come forward to propose conservation priorities for threatened species that are also important contributors to functional diversity, such as the novel prioritization index, FUSE (Griffin et al. 2020, Pimiento et al. 2020b). This index combines species' functional uniqueness and specialisation with their extinction risk, revealing which species extinctions are likely to have large impacts on ecosystem functioning. Quantifying functional diversity, and identifying the species most critical for maintaining it (i.e., with the highest functional uniqueness and/or specialisation), over time could serve as a powerful proxy for ecological changes through time, particularly those caused by extinctions.

A handful of studies have previously assessed changes in functional diversity following extinction events recorded in the marine fossil record. Most of these studies have focused on the extinctions of benthic marine communities, finding negligible impacts on functional diversity due to ecological roles persisting through surviving taxa (Dineen et al. 2014, Foster and Twitchett 2014, Aberhan and Kiessling 2015). Others have focused on large vertebrates, namely megafaunal taxa (i.e., species >45 kg in mass in the case of extant species (Estes et al. 2016) or >1 m in body length in the case of extinct species; Pimiento et al. 2024). One keynote study identified a Pliocene extinction event of marine megafauna and found that these extinctions resulted in larger-than-expected losses of functional diversity (Pimiento et al. 2017). Similar results have since been found in terrestrial mammalian megafauna, where continuous extinctions over the last 21,000 years caused a greater-than-expected loss of functional diversity considering the number of species lost (Hedberg et al. 2021). Collectively,

these previous studies indicate that distinct taxa in communities such as large vertebrates are crucial for maintaining functional diversity, including in the geological past.

Changes in functional diversity are far less studied over longer timescales, such as across more than one geological boundary. This is not particularly surprising as the fossil record is inherently incomplete, and most fossil species are known from only fragmented remains (Foote and Sepkoski 1999, Benton et al. 2011), making measuring functional traits directly difficult. Moreover, dating fossils comes with a high degree of uncertainty due to geological layers representing large time spans, so changes in functional diversity through geological time generally cannot be recorded on a fine-scale resolution (Bush et al. 2007, Novack-Gottshall 2007). Indeed, only a few studies so far have assessed functional diversity over long geological timescales (e.g., Villéger et al. 2011, Foster and Twitchett 2014, Dunhill et al. 2018, Pimiento et al. 2020a, Shupinski et al. 2024). Two such studies concentrated on benthic marine biota (Villéger et al. 2011, Pimiento et al. 2020a). The first of these studies focused on seafloor invertebrates, revealing that their functional diversity has increased from 500 Ma to the present (Villéger et al. 2011). The second examined functional diversity of Caribbean molluscs over the last 23 million years, which revealed that despite high extinction rates 3 Ma, these molluscs primarily lost functionally redundant species (i.e., species sharing the same trait combinations/functional entities), allowing their ecological roles to persist and thus buffering their functional diversity, which consistently grew over time (Pimiento et al. 2020a). Crucially, neither of these two studies investigated functional diversity changes for a group of large vertebrates, which have been established as having larger-than-expected contributions to functional diversity by fossil studies investigating individual or continuous extinction events occurring even at a single geological boundary (i.e., Pliocene-Pleistocene boundary) or across a single geological epoch (Pimiento et al. 2017, Hedberg et al. 2021). As such, assessing changes in functional diversity over a longer range of time could provide valuable information about the ecological consequences of past extinctions.

1.4   Applying functional diversity to the shark fossil record

Given their long evolutionary history (i.e., over 250 million years; Cappetta 2012), and their wide range of habitats and ecological roles (Compagno 1990, Dedman et al. 2024), sharks represent an ideal model for studying changes in functional diversity through time. Furthermore, understanding ecological effects of their past extinctions could be key to predicting the effects of their ongoing declines (Dulvy et al. 2021, Pacoureau et al. 2021). However, a key limitation to studying functional diversity across geological timescales is the inherent incompleteness of the fossil record, which hinders the ability to directly measure functional traits such as body size and diet that are needed to quantify functional diversity (Ciampaglio et al. 2001).

At first glance, sharks appear to have a highly limited fossil record because their soft cartilaginous skeletons do not typically fossilise (Maisey 2012). However, their teeth are much harder and thus easily preserve in the fossil record (Kent 1994, Cappetta 2012). Moreover, sharks constantly shed teeth throughout their lives, with a single individual losing as many as 30,000 teeth during its lifespan (Whitenack et al. 2011). This combination of high preservation potential and high rate of replacement has led to shark teeth being among the most abundant vertebrate fossils in the marine fossil record (Hubbell 1996, Cappetta 2012).

While teeth may not be direct measures of functional traits in sharks, they may have the potential to serve as proxies. Previous work has found quantitative support that tooth measurements such as size and shape (herein, dental characters) can be used to distinguish taxonomy to the species level in both extinct and extant sharks (Nyberg et al. 2006, Whitenack and Gottfried 2010, Marrama and Kriwet 2017). Indeed, there have since been calls for tooth morphology to be included in detail when describing new living shark species as well as fossils (Guinot et al. 2018). The next logical step is, therefore, to determine the extent to which dental characters may infer ecology in the form of functional traits. A few prior studies attempting to do so have so far produced mixed results. For example, tooth size (i.e., crown height or width) has been used as a linear predictor for body size in living shark species (e.g., *Carcharodon carcharias*; Shimada 2003, Perez et al. 2021) and subsequently extrapolated to extinct species (e.g., *Otodus megalodon*; Pimiento and Balk 2015, Shimada 2019, Perez et al. 2021). However, biomechanical studies have found little functional difference between different shark tooth morphologies, implying a murky relationship between tooth morphology and functional traits like diet and feeding mechanism (Whitenack and Motta 2010, Whitenack et al. 2011, Corn et al. 2016, Ballell and Ferrón 2021). Moreover, links between certain aspects of tooth

morphology like cutting edge and functional traits such as feeding mechanism have generally been assigned qualitatively (Frazzetta 1988) rather than quantitatively tested or validated. As such, the extent to which dental characters from shark teeth may relate to functional traits is currently unclear given the, at best, cloudy evidence of direct relationships. This is therefore a knowledge gap that must be filled before one can even attempt to assess shark functional diversity in the geological past.

In summary, the abundant dental fossil record of sharks, a record that is continuous through time from the past to the present (Cappetta 2012), may be our best available tool for inferring functional traits in extinct shark species (**Figure 1.2**). If verifiable relationships between dental characters and functional traits can be found, this would provide an opportunity to assess shark functional diversity over long geological timescales. Such an assessment would ultimately be key to evaluating their ecological responses to past extinctions, which in turn may well serve as a window into their possible ecological future under current threats.
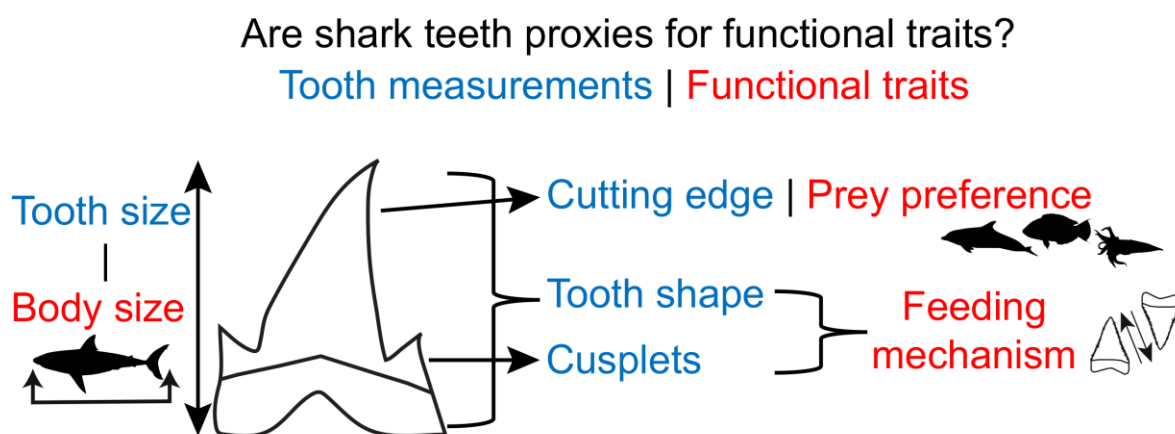
Figure 1.2. Schematic illustration of how different shark tooth measurements have been used as proxies for functional traits in previous works on extant sharks, which this thesis aims to explore as one of its research questions; and subsequently apply to the fossil record. Tooth illustrations were custom made while animal silhouettes were downloaded from Phylopic (www.phylopic.org) and are all in the public domain.

Overall, there are three research questions to address in this thesis:

1. Can shark tooth measurements serve as proxies for functional traits?
2. How has shark functional diversity changed over geological time up to the present?
3. Given their ongoing declines, how might future extinctions of sharks affect their functional diversity?

1.5   Aims and Objectives

This thesis aims to investigate how the functional diversity of sharks has changed from the past to the present, and how it may be expected to change from the present to the future. The following objectives were addressed in three data chapters:

- Chapter 2 investigates the extent to which dental characters from isolated shark teeth can serve as proxies for functional traits. To do so, I reviewed the scientific literature on extant species to evaluate how dental characters have been used as ecological proxies and then conducted two separate validation analyses. This chapter was published in the *Journal of Fish Biology* in January 2023 (Cooper et al. 2023).

- Chapter 3 explores how shark functional diversity changed over the last 66 million years using the dental characters identified as suitable trait proxies in chapter 2. I then subsequently identified which taxa were the most important contributors to functional diversity through time. This chapter was published in *Global Ecology and Biogeography* in June 2024 (Cooper and Pimiento 2024).

- Chapter 4 assesses the future functional diversity of sharks and rays. Using the year 2100 as a baseline extinction scenario, I first simulated future extinctions and quantified resulting functional diversity over the next 500 years. From there, I identified the species whose extinctions would have the largest ecological impacts by 2100; and examined global spatial shifts in functional diversity by 2100 under climate change and future extinctions. This chapter is in preparation for publication.

Citations for published chapters (candidate highlighted in bold):

- **Cooper JA**, Griffin JN, Kindlimann R & Pimiento C, (2023). Are shark teeth proxies for functional traits? A framework to infer ecology from the fossil record. *Journal of Fish Biology*, **103**, 798-814.

- **Cooper JA** & Pimiento C, (2024). The rise and fall of shark functional diversity over the last 66 million years. *Global Ecology and Biogeography*, **33**, e13881.

Additionally, I co-authored and published two further papers during my PhD which are not included as chapters in this thesis.

The first paper, published in *Science Advances* in August 2022, focuses on the extinct giant shark *Otodus megalodon*, in which I recreated the first 3D model of this charismatic species

based on an exceptional vertebral column specimen and inferred its movement and feeding ecology, allowing me to also discuss the ecological effects of its extinction (Cooper et al. 2022). This paper was a side project that was designed and developed by the corresponding authors (C. Pimiento and J. R. Hutchinson) several years before my involvement, with the majority of 3D scan material already collected by the time I joined the project. My involvement began in 2019, a year before I started my PhD, continuing from my MSc project in which I had calculated 2D body dimensions of *O. megalodon* based on five ecological analogues (Cooper et al. 2020). My contributions to the final paper were as follows: (1) measuring fossil vertebrae material; (2) establishing collaboration with the Kwa-Zulu Natal Sharks Board in South Africa for relevant great white shark data; (3) constructing the final 3D model; (4) performing several of the analyses, including collecting swimming speed data of living sharks from literature; and (5) co-writing the final manuscript with the senior author; all performed with input from the corresponding authors.

The second paper, published in *Cambridge Prisms: Extinction* in May 2024, provides a definition for, and subsequently identifies, extinct marine megafauna in the fossil record over the last 550 million years (Pimiento et al. 2024). This project was part of a course at the University of Zurich, for which I have served as a guest speaker. Furthermore, it was conducted alongside a large ensemble of collaborators, including two sets of students, a wide-ranging group of experts on different megafaunal clades, and most of the other members of the Pimiento Research Group. My specific role in the project was that of a "clade expert", focusing on the data collected for fossil sharks. My contributions to the final paper were as follows: (1) collecting an initial set of fossil shark data from literature; (2) collating ecological data for our taxa alongside the other members of the Pimiento Research Group; (3) checking additional data collected by the students and correcting errors where necessary; and (4) providing feedback on the first version of the final manuscript.

These papers, and the supplementary material of the first paper, can be found within Appendices 4-6.

Citations for additional published papers (candidate highlighted in bold):

> **Cooper JA**, Hutchinson JR, Bernvi DC, Cliff G, Wilson RP, Dicken ML, Menzel J, Wroe S, Pirlo J & Pimiento C, (2022). The extinct shark *Otodus megalodon* was a transoceanic superpredator: Inferences from 3D modeling. *Science Advances*, **8**, eabm9424.

Pimiento C, Kocáková K, Mathes GH, Argyriou T, Cadena EA, **Cooper JA**, Cortés D, Field DJ, Klug C, Scheyer TM, Valenzuela-Toro AM, Buess T, Günter M, Gardiner AM, Hatt P, Holdener G, Jacober G, Kobelt S, Masseraz S, Mehli I, Reiff S, Rigendinger E, Ruckstuhl M, Schneider S, Seige C, Senn N, Staccoli V, Baumann J, Flüeler L, Guevara LJ, Ickin E, Kissling KC, Rogenmoser J, Spitznagel D, Villafaña JA & Zanatta C, (2024). The extinct marine megafauna of the Phanerozoic. *Cambridge Prisms: Extinction*, **2**, e7, 1-17.

Chapter 2 | Are shark teeth proxies for functional traits? A framework to infer ecology from the fossil record

This work is published in the *Journal of Fish Biology* as:

2.1 Abstract

Modern sharks have an evolutionary history of at least 250 million years and are known to play key roles in marine systems, from controlling prey populations, to connecting habitats across oceans. These ecological roles can be quantified based on their functional traits, which are typically morphological (e.g., body size) or behavioural (e.g., feeding and diet). However, our understanding of such roles of extinct sharks is limited by the inherent incompleteness of their fossil record, which consists mainly of isolated teeth. As such, establishing links between tooth morphology and ecological traits in living sharks could provide a useful framework to infer sharks' ecology from the fossil record. Here, based on extant sharks from which morphological and behavioural characteristics are known, I assess the extent to which isolated teeth can serve as proxies for functional traits. To do so, I first review the scientific literature on extant species to evaluate the use of shark dental characters as proxies for ecology to then perform validation analyses based on an independent dataset collected from museum collections. My results reveal that 12 dental characters have been used in the shark literature as proxies for three functional traits: body size, prey preference and feeding mechanism. From all dental characters identified, tooth size and cutting edge are the most widely used. Validation analyses suggest that seven dental characters – crown height, crown width, cutting edge, lateral cusplets, curvature, longitudinal outline and cross-section outline – are the best proxies for the three functional traits. Specifically, tooth size (crown height and width) was found to be a reliable proxy of all three traits; the presence of serrations on the cutting edge was one of the best proxies for prey preference; and tooth shape (longitudinal outline) and the presence of lateral cusplets were among the best indicators of feeding mechanism. Taken together, my results suggest that in the absence of directly measurable traits in the fossil record, these seven dental characters (and different combinations of them) can be used to quantify the ecological roles of extinct sharks. This information has the potential of providing key insights into how shark functional diversity has changed through time, including their ecological responses to extinction events.

2.2 Introduction

With over 500 extant species living in almost all marine habitats (Weigmann, 2016), sharks (Elasmobranchii, Selachii) play key ecological roles in today's oceans. Some well-studied roles include: (1) apex predators (e.g., the tiger shark, *Galeocerdo cuvier*), consuming large quantities of biomass and regulating the populations of their prey (Myers et al. 2007, Ferretti et al. 2010, Hammerschlag et al. 2019); (2) mesopredators (e.g., the grey reef shark, *Carcharhinus amblyrhynchos*), a dual role as consumers of smaller organisms and as potential prey for larger carnivores (Heupel et al. 2014, Frisch et al. 2016, Roff et al. 2016, Barley et al. 2019); and (3) highly mobile animals (e.g., the great white shark, *Carcharodon carcharias*), connecting habitats and populations and potentially transferring nutrients across sites (Bonfil et al. 2005, Weng et al. 2007, Williams et al. 2018). Several sharks are therefore considered keystone species given the large effects they can have in ecosystems (Heupel et al. 2014, Hammerschlag et al. 2019; but see Roff et al. 2016).

Species' ecologies can be quantified based on their functional traits – measurable intrinsic characteristics that broadly reflect how resources are obtained, used and transported, which ultimately impact biodiversity and how the ecosystem operates (Petchey and Gaston 2006, Mouillot et al. 2013b). A key functional trait in sharks is body size, which is fundamental to inform on the size of the prey they consume (Lucifora et al. 2009, Heupel et al. 2014) and the distance they can travel, and thus their ability to connect habitats and transport nutrients (Doughty et al. 2016, Estupiñán-Montaño et al. 2021). Another essential trait in shark ecology is diet (i.e., the prey items they consume) which is inherently linked to trophic level, and therefore the ability of some sharks to alter ecosystem structure, resource distribution and partitioning via top-down control both directly through prey consumption and indirectly by altering of prey behaviour and distribution (Cortés 1999, Papastamatiou et al. 2006, Burkholder et al. 2013). Finally, feeding mechanism is an important functional trait in sharks, as it determines dietary specialisation (Ciampaglio et al. 2005), which can affect ecosystem structure by mitigating interspecific competition and influencing prey abundance and diversity (Munroe et al. 2013). Together, these functional traits can provide fundamental information on ecological roles shark species play in marine systems.

The fossil record of modern sharks has evidenced their long evolutionary history, which dates back to at least 250 mya (Cappetta 2012). Sharks are represented in the fossil record primarily by their isolated teeth, which they shed constantly throughout their lives and, unlike their cartilaginous skeletons, have a hard composition, resulting in high preservation potential (Kent

1994, Cappetta 2012). Shark teeth are therefore abundant in the marine fossil record (Hubbell 1996, Cappetta 2012) and are often the only information available for understanding the ecological roles sharks played in the past. Importantly, many fossil sharks have living representatives (Paillard et al. 2020, Pimiento and Benton 2020), allowing scientists to infer aspects of their natural history not preserved in the geological record.

Multiple studies have proposed that some shark functional traits are correlated to tooth morphology (e.g., Frazzetta 1988, Ciampaglio et al. 2005). As such, tooth measurements (herein, dental characters) have been used to infer the ecology of fossil taxa. For instance, tooth height has been widely used as an indicator of body size (e.g., Condamine et al. 2019, Shimada et al. 2020), while the presence of serrations on the cutting edge has been used to infer diet (i.e., prey preference) and feeding mechanism (e.g., Kent 1994, Ciampaglio et al. 2005). However, other studies have suggested that links between shark tooth morphology and ecology are uncertain at best. For example, biomechanical analyses indicate that different shark tooth morphologies lack functional differences, providing little support for their use as proxies for feeding mechanisms (Whitenack and Motta 2010, Whitenack et al. 2011). Hence, it remains unclear the extent to which measurable characteristics of shark dentition can be used to infer functional traits. A deeper understanding of the relationships between dental characters and functional traits could allow a wider use of shark teeth as ecological proxies. This would be particularly useful in palaeontology, as the fossil record of sharks is mostly limited to isolated teeth. Connecting shark teeth with ecological traits can therefore provide insight into the roles that sharks played in ancient ecosystems and how they responded to past environmental changes.

Here, I evaluate the use of shark dental characters as proxies for functional traits (**Figure 2.1**). I ask two questions: (Q1) which dental characters have been used as proxies for functional traits? and (Q2) which of these dental characters are the best proxies for functional traits? To answer these questions, I: (1) review the literature (**Figure 2.1a-c**) focusing on extant sharks because their ecology is well documented (Weigmann 2016, Ebert et al. 2021); and (2) use two validation analyses on an independent jaw dataset of extant species (**Figure 2.1e-g**). My results provide a framework to infer shark functional traits based on their teeth, which can potentially be applied to the fossil record.
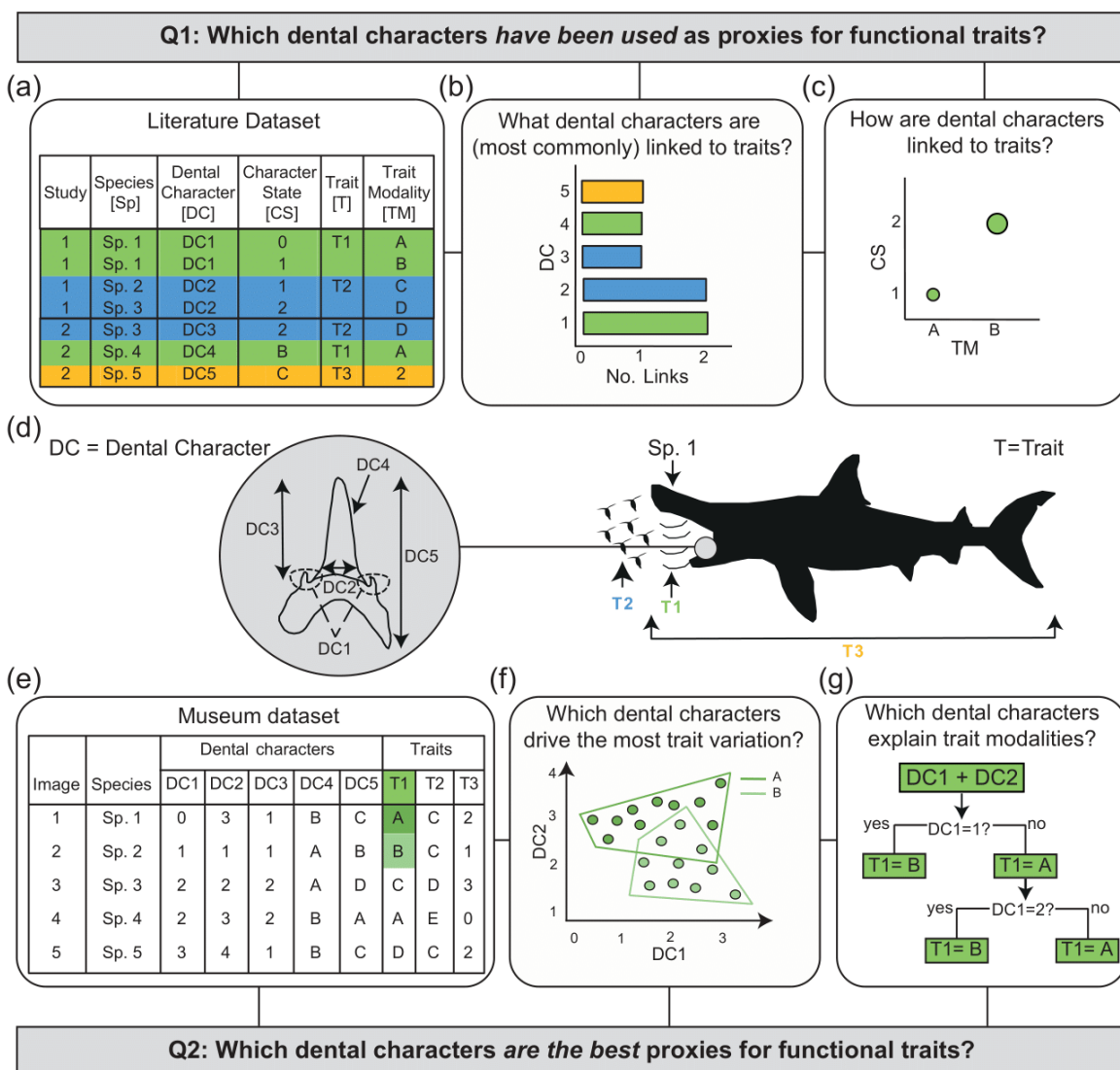
Figure 2.1. Conceptual approach. Q1 is answered using the following steps: (a) taxonomic, dental character (DC) and corresponding functional trait (T) data are extracted from the literature; (b) the dental characters most commonly and broadly used as proxies for individual traits are identified; and (c) individual links between dental character states (CS) and trait modalities (TM) are quantified. A graphical example of dental characters and their use as proxies for functional traits is shown in (d). Q2 is answered using the following steps: (e) dental characters and trait values are recorded from jaw specimens from museum collections; and validation analyses performed on this data, specifically (f) principal component analysis to identify which dental characters drive trait variation; and (g) classification tree analysis to find which dental characters best explain trait values.

2.3   Materials and Methods

Q1: Which shark dental characters have been used as proxies for functional traits?

Data: I conducted a survey of the literature to identify published studies that measure or record dental characters from extant shark teeth and link them to functional traits. The survey was performed in the academic search engines Google Scholar, Scopus and Web of Science, using the following terms: (1) Shark + tooth OR teeth + morphology; (2) Shark + tooth OR teeth + trait; (3) Shark + tooth OR teeth + ecology; and (4) Shark + tooth OR teeth + morphology + function. Once traits studied in literature were identified, I repeated these searches using those traits as additional terms; for example: (5) Shark + tooth OR teeth + body size.

From each study returned, I extracted the following information from the main text, tables, figures, and supplementary material: taxonomy (i.e., order, family, genus and species), tooth position if reported (i.e., upper or lower), dental character recorded (e.g., lateral cusplets; **Figure 2.2**) and its character state (e.g., present or absent; **Table 2.1**), the functional trait linked to the dental character (e.g., prey preference), and trait values (e.g., plankton, invertebrates, fishes, high vertebrates; **Figure 2.1a**; Supporting Information Data S1; see **Appendix 1**). Additionally, I recorded whether or not each taxon was represented in the fossil record by checking against Paillard et al. (2020) and the Paleobiology Database (http://paleobiodb.org/; last accessed August 2022).
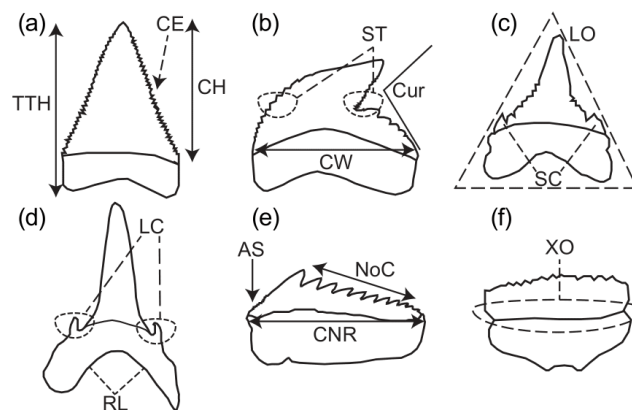
Figure 2.2. Schematic illustrations of all dental characters identified as proxies for functional trait in the literature review. Abbreviations are as follows: (a) CH = crown height; CE = cutting edge; TTH = total tooth height; (b) CW = crown width; Cur = curvature; ST = serration type; (c) LO = longitudinal outline; SC = serrational cusplets; (d) LC = lateral cusplets; RL = root lobes; (e) AS = acrocone serrations; NoC = number of cusps; CNR = cusp number ratio; (f) XO = cross-section outline. Descriptions for each dental character can be found in **Table 2.1**. Teeth used to illustrate these characters are from the following species: (a) *Carcharodon carcharias*; (b) *Galeocerdo cuvier*; (c) a juvenile *C. carcharias*; (d) *Carcharias taurus*; (e) *Hexanchus griseus*; and (f) *Mustelus canis*.

Table 2.1. Summary of 14 dental characters identified by the literature review as proxies for each recorded functional trait, including two that were linked only to life stage. States for crown height, crown width and total tooth height states are based on tooth size distributions (see **Appendix Figure S1.1**). States for curvature, longitudinal outline and cross-section outline are based on Ciampaglio et al. (2005). Number of cusps is recorded as count data (i.e. 1 = 1 cusp, 2 = 2 cusps, 3 = 3 cusps, etc). Illustrations for each dental character can be found in **Figure 2.2**.

Character [Abbreviation]	Description	States	Functional traits
Acrocone serrations [AS]	Serrations present on the main cusp of lower Hexanchiformes teeth (Adnet 2006)	0 – Absent; 1 – Present	Life stage
Cross-section outline [XO]	The shape profile of the tooth in a cross section (Ciampaglio et al. 2005)	1 – Round; 2 – Oval; 3 – Triangular; 4 – Lens; 5 – Rectangular; 6 – Polygonal; 7 – Multi indented lens	Feeding mechanism
Crown height [CH]	Maximum vertical enamel height	1 – Small (<5 mm) 2 – Medium (5-20 mm) 3 – Large (20-50 mm) 4 – Huge (>50 mm)	Body size, prey preference, feeding mechanism
Crown width [CW]	Width of the tooth crown	1 – Slender (<10 mm) 2 – Wide (10-35 mm) 3 – Vast (>35 mm)	Body size, prey preference, feeding mechanism
Curvature [Cur]	Angle of the main cusp	0 – None; 1 – Slight; 2 – Present	Prey preference, feeding mechanism
Cusp number ratio [CNR]	Number of cusps/crown width in Hexanchiformes (Adnet 2006)	Number of cusps/crown width	Body size
Cutting edge [CE]	The mesial and distal edge of the main cusp, which can be smooth or serrated	0 – None; 1 – Smooth; 2 – Serrated	Prey preference, feeding mechanism
Lateral cusplets [LC]	Small secondary cusps found on either side of the tooth's main cusp	0 – Absent; 1 – Present	Prey preference, feeding mechanism
Longitudinal outline [LO]	The shape profile of the whole tooth (Ciampaglio et al. 2005)	1 – Triangular; 2 – Semi-circular; 3 – Piercing; 4 – Rectangular; 5 – Polygonal	Prey preference, feeding mechanism
Number of cusps [NoC]	The total number of cusps on a single tooth, including lateral cusplets	Count data	Body size, feeding mechanism
Root lobes [RL]	Edges of the root at the mesial or distal created by the nutrient groove	0 – None; 1 – Short; 2 – Moderate; 3 – Elongated	Feeding mechanism
Serrational cusplets [SC]	Cusplets developing as serrations on the main cusp (Bemis et al. 2015)	0 – Absent; 1 – Present	Life stage
Serration type [ST]	Large primary serrations, or small secondary "serrations within serrations" (Moyer and Bemis 2017)	1 – Primary; 2 – Secondary	Prey preference
Total tooth height [TTH]	Maximum height of the tooth from tip to root edge	1 – Small (<5 mm) 2 – Medium (5-20 mm) 3 – Large (20-50 mm) 4 – Huge (>50 mm)	Body size

The functional trait data were tabulated as follows: (1) Body size was recorded as total length (distance from the snout to the tip of the caudal fin) in cm. We further assigned this data to four size classes to facilitate analyses (**Table 2.2**). (2) Prey preference was defined as the most common prey item consumed as adults and was assigned using four broad categorisations (**Table 2.2**) following previous work (Pimiento et al. 2020b). It should be noted that many shark species are opportunistic generalists feeding on a variety of food (Wetherbee and Cortés 2004), with the prey preference of some species varying seasonally (MacNeil et al. 2005, Baremore et al. 2010, Dicken et al. 2017). Previous works attempting to standardise sharks' diet composition have outlined up to 11 prey categories (Cortés 1999). However, even this fine categorisation scheme fails to fully capture the complex dietary spectrum of sharks. For example, the bonnethead shark (*Sphyrna tiburo*) primarily feeds on crustaceans (Mara et al. 2010), but also consumes seagrass (Leigh et al. 2018). Similarly, the whale shark (*Rhincodon typus*) mostly filter-feeds on plankton, but it has also been reported to feed on macroalgae (Meekan et al. 2022). Although our broad prey preference categorisation scheme does not account for the full range of prey sharks can have during their lifetime, it allows to capture the most common diet of shark species, facilitating extrapolation to the fossil record. (3) Feeding mechanism was defined in terms of dentition types, which describe how sharks capture and process prey (Kent 1994, Motta 2004, Ciampaglio et al. 2005, Cappetta 2012). We identified four different schemes defining such dentition types from the literature (**Appendix Table S1.1**) and selected Kent (1994) to record feeding mechanism hereafter as it was the only one that considered filter feeding as a separate mechanism ('Vestigial'). Finally, although life stage is another trait associated with sharks' ecological roles (Tavares et al. 2019) and has been suggested to be linked to crown width changes in *C. carcharias*, particularly in males (French et al. 2017), I did not consider it here as its relations with tooth morphology have not been widely studied across shark species (Cappetta 2012).

I defined links between dental characters and functional traits as any occurrence in literature in which a dental character is considered explanatory of a functional trait (**Figure 2.1d**). I assigned each link to two categories based on whether it was made quantitatively (i.e., established using an analytical approach such as a linear regression) or qualitatively (i.e., assigned based on observations or assumptions). Finally, I evaluated whether the collected data were independent (i.e., if the link was made using the study's own data and not based on previous studies; Supporting Information Data S2; see **Appendix 1**) in order to remove possible influence of prior assumptions.

Table 2.2. Summary of the functional traits in sharks linked to dental character proxies in the literature review. Categorisations of body size are based on classes from Shimada et al. (2020); broad categorisations of prey preference are based on Pimiento et al. (2020b) and feeding mechanism categorisations are based on homodont dentition types from Kent (1994). Ecosystem functions and services are also recorded following Tavares et al. (2019). Example studies returned by the literature review that linked dental characters to each functional trait are included.

Functional trait	Description	Functions	Services	Example study
Body size	Total length in cm; and categorised in the following classes: 1 – Small (1-200 cm); 2 – Medium (201-400 cm); 3 – Large (401-600 cm); 4 – Giant (>600 cm)	Nutrient storage and transport	Nutrient cycling, food provision and promotion of biodiversity	Shimada (2003)
Prey preference	Categories: 1 – Plankton; 2 – Invertebrates; 3 – Fishes; 4 – High vertebrates	Nutrient storage and trophic-dynamic regulations of populations	Nutrient cycling, biological control and maintenance of trophic interactions and ecosystem stability	Moyer and Bemis (2017)
Feeding mechanism	Categories: 1 – Crushing; 2 – Clutching; 3 – Grasping; 4 – Cutting; 5 - Vestigial	Nutrient storage and trophic-dynamic regulations of populations	Nutrient cycling, biological control and maintenance of trophic interactions and ecosystem stability	Frazzetta (1988)

Analyses: All analyses were made using the data from the literature deemed to be independent. I first quantified the motivation for each study. Then, I assessed the number of extant orders, families, genera and species represented in the data following the nomenclature by Weigmann (2016). I additionally examined the distribution of crown heights and crown widths to assign size-based categorisations to these dental characters (**Figure 2.2a-b**; **Table 2.1; Appendix Figure S1.1**). Finally, I assessed the frequency in which dental characters are used as a proxy to each functional trait (**Figure 2.1b**), determined the dental characters most broadly used across the shark phylogeny and quantified the times each character state was linked to specific trait values (**Figure 2.1c**). Although all tooth positions were considered in the analyses, for body size I ran an additional analysis using only anterior teeth as they have been proposed to be more directly associated to sharks' total length than other positions (Condamine et al. 2019, Shimada et al. 2020).

Q2: Which shark dental characters are the best proxies for functional traits?

Data: I collected an independent tooth dataset from all species identified in the literature review (**Figure 2.1e**) based on images of authentic jaw specimens (Supporting Information Data S3; see **Appendix 1**). Specimens were housed at the following museum collections: the British Natural History Museum (NHM); the Paleontological Institute and Museum, University of Zurich (PIMUZ); the collection of Haimuseum und Sammlung R. Kindlimann (RKC; a private collection with public access); the Royal Belgian Institute of Natural Sciences (RBINS); the Calvert Marine Museum (CMM); and the Gordon Hubbell Collection (GHC; Jaws International, Gainesville, FL), where each specimen was photographed.

To take specimen images, jaws were positioned on a flat surface and photographed from above (i.e., at a 90° angle) at the maximum open gape angle to mitigate potential parallax error. Seven specimens were displayed on vertical walls, in which case they were photographed at 0°. One exception to this protocol was a *Megachasma pelagios* specimen (GHC-9; Supporting Information Data S3), where each jaw was photographed individually due to being separated during its curation. Whenever a taxon was identified to the genus-level in the literature review, a jaw of a species of such a genus was selected in its place based on availability.

From each jaw, I selected the following upper and lower teeth to measure: (1) first anterior, (2) third lateral, and (3) final posterior tooth on the left side of the jaw, from the first functional row. The first anterior is the first tooth adjacent to the symphysis, and the final posterior is the last tooth along the mesio-distal axis of the jaw ramus. The third lateral is defined here as the sixth tooth adjacent to the symphysis, following an assumption of three anterior teeth in each jaw, a pattern typically seen in all macrophagous Lamniformes and some Carcharhiniformes (Shimada 2002, Cullen and Marshall 2019). These tooth positions were selected to account for monognathic (i.e., differences in tooth morphology across individual jaws, which is gradual in most species but particularly strong in Lamniformes and Heterodontiformes; Shimada 2002, Cappetta 2012) and dignathic heterodonty (i.e., differences between the upper and lower jaws, which is widespread in many species) as this can result in different relationships between dental characters and functional traits. Although the number of tooth files varies significantly between species, the chosen positions account for morphological differences between anterior and posterior teeth (Cappetta 2012) while also including more distinct lateral teeth of sharks like Lamniformes.

For each tooth selected, I measured crown height and crown width in millimetres (mm) using ImageJ (Abràmoff et al. 2004) and a scale bar present in all photographs. Furthermore, I

recorded the states of all other dental characters identified as a trait-proxy in literature (**Table 2.1**), including tooth size categories as described above (**Table 2.1; Appendix Figure S1.1**). Total tooth height was not measured from the jaws due to its categorisations being identical to crown height (**Table 2.1**). Finally, to each species, I assigned functional trait values (**Table 2.2**; **Figure 2.1e**) based on Weigmann (2016) and Ebert et al. (2021).

Some limitations to the dataset should be acknowledged. First, given the reduced availability of jaw specimens, I was able to only photograph a single specimen per taxon. Second, only 12 specimens (20.7%) had sex data and 21 (36.2%) had body size or life stage data available. As such, neither gynandric nor ontogenetic heterodonty (i.e., differences in tooth morphology between sexes and life stages, respectively) could be accounted for in these analyses. However, while monognathic and dignathic heterodonty are known in many shark species, gynandric and ontogenetic heterodonty are more poorly studied in sharks and better studied in rays (Cappetta, 2012). Of the studies that have been conducted, gynandric and ontogenetic heterodonty have been described in only a few species (e.g., *C. carcharias*, *Carcharhinus leucas*, *Scyliorhinus stellaris*, *Etmopterus spinax* and *G. cuvier*; French et al. 2017, Cullen and Marshall 2019, Berio et al. 2020, Straube and Pollerspöck 2020, Turtscher et al. 2022). Nonetheless, because the aim of this research is to apply resulting dental character-functional trait relationships to isolated fossil teeth (from which life stage and sex is often unknown), I contend that the absence of gynandric and ontogenetic heterodonty from the analyses should not distort the interpretation and application of the resulting framework to fossils.

Analyses: With the museum dataset, I performed two separate sets of analyses in the R environment (R Core Team 2017). Firstly, I used Principal Component Analysis (PCA) to illustrate variation in tooth morphology (i.e., morphospace) and associated trait values. Recorded dental characters were used as the variables for these analyses. I used crown height and crown width both as numerical (i.e., measured in mm) and categorical (i.e., size classes) variables to assess the different contributions to morphological variation. Functional trait values (**Table 2.2**) were used to define convex hulls along the morphospace, allowing me to identify morphological clusters. Overall, my analyses allowed me to identify which dental characters were the most important drivers of variation along the tooth morphospace (**Figure 2.1f**). Although exploratory, PCA has been previously used to link shark ecology to both tooth (Ciampaglio et al. 2005) and dermal denticle morphology (Dillon et al. 2017).

Secondly, a Classification and Regression Tree (CART) analysis was used to assess which dental characters best explain functional trait values (**Figure 2.1g**). This approach uses decision tree modelling to explain each response variable by splitting the explanatory data into mostly homogenous groups with the *rpart* R package (De'ath and Fabricius 2000, Therneau et al. 2015). I used classification rather than regression trees to perform the analyses, whereby functional traits were the response variables and dental characters the explanatory variables, because most of the data collected were categorical. As such, crown height and crown width categorisations were considered in these analyses (**Table 2.1**; **Appendix Figure S1.1**). Tooth position was also included as an explanatory variable to account for monognathic and dignathic heterodonty, which can, for example, lead to different feeding mechanisms across or between jaws (Kent 1994, Cappetta 2012, Cullen and Marshall 2019). Including tooth position further allowed me to determine if it was a more important predictor of functional trait values than the dental characters. To assess reliability of the trees, I used cross-validation in which I partitioned the data into two sets: (1) the train set, comprising of 2/3 of the data, used to fit the tree; and (2) the test set, composing the last 1/3 of the data and run against the tree to evaluate its accuracy (De'ath and Fabricius 2000). My two sets of analyses were performed considering all tooth positions, and then repeated considering only anterior teeth given their supposed more direct correlation with traits such as body size (Condamine et al. 2019, Shimada et al. 2020).

2.4   *Results and Discussion*

Q1: Which dental characters have been used as proxies for functional traits in sharks?

My review returned 56 studies published between 1959 and 2020. I obtained data from 5,056 teeth (Supporting Information Data S1) across 63 extant shark species belonging to 39 genera, 25 families and 7 orders (**Appendix Table S1.2**). Five taxa were identified only to genus-level, resulting in a total of 68 taxa in the whole dataset. From teeth data collected, 68% belonged to modern taxa and the remaining to fossil specimens of extant taxa, with the majority (90%) of modern taxa having a fossil record (Paillard et al. 2020). All extant orders except Echinorhiniformes and Pristiophoriformes were represented in the dataset (**Appendix Figure S1.2a**). This was unsurprising as both orders are relatively poorly studied (Ebert et al. 2021). Data were notably skewed towards two orders: Lamniformes (64.5%) and Carcharhiniformes (32.1%; Supporting Information Data S1; **Appendix Figure S1.2a**); suggesting that these are the most well-studied shark orders in the literature on tooth morphology. Carcharhiniformes is by far the most species-rich order today (~290 species; Ebert et al. 2021) whereas Lamniformes, with just 15 living species, displays high ecological and dental disparity (Ebert et al. 2021). Moreover, several species in these orders have relatively large tooth sizes (Cappetta 2012), likely explaining this bias.

The subset of data deemed to be independent included 40 studies (71% of the full dataset). These studies investigated the relationship between tooth morphology and functional traits to: (1) apply it to specimens (both fossil and extant) with unknown trait data (e.g., unknown body size; 19 studies; 47.5%); (2) assess it through tooth replacement and/or ontogeny (6 studies; 15%); (3) verify trait values (7 studies; 17.5%); (4) study tooth performance in cutting prey (7 studies; 17.5%); and (5) perform evolutionary analyses (1 study; 2.5%). From these studies, I extracted 4,605 teeth data (91% of the total data collected; **Appendix Table S1.2**) comprising all 68 taxa. Of these data, 72% belong to modern specimens and the remaining to fossil specimens of extant taxa. I initially identified 14 dental characters (**Figure 2.2**) used as proxies for three functional traits in sharks (body size, prey preference and feeding mechanism; see Materials and Methods and **Table 2.1**). Two of these dental characters (i.e., acrocone serrations and serrational cusplets) were linked to life stage (**Table 2.1**). However, life stage and associated dental characters were discarded from the analyses because they were not found broadly across shark phylogeny. Specifically, acrocone serrations were unique to Hexanchiformes (Adnet 2006) and serrational cusplets were only described in juvenile *C.*

carcharias teeth (Bemis et al. 2015). As such, my analyses considered the remaining 12 dental characters. A total of 400 links (i.e., where a dental character was considered explanatory of trait values) were identified from the literature (Supporting Information Data S2) – 150 (37.5%) attributed to body size, 71 (17.8%) to prey preference and 173 (43.3%) to feeding mechanism. All three identified traits are among the most relevant for studying ecological function in marine megafauna (Tavares et al. 2019).

Body size: The literature review found five dental characters used as proxies for body size: crown height, crown width, total tooth height, cusp number ratio and number of cusps (**Table 2.1**; **Figure 2.3a**). These characters were identified from 24 studies, recorded numerically (i.e., measured in mm) and used across 52 shark taxa belonging to four orders: Hexanchiformes, Squaliformes, Lamniformes, and Carcharhiniformes (**Appendix Table S1.2**; **Appendix Figure S1.2b**). Crown height was by far the most common proxy for body size (112 links; 74.7%), followed by crown width (20 links; 13.3%; **Figure 2.3a**). Despite its commonness, crown height was linked to body size in just two orders, Carcharhiniformes and Lamniformes, while crown width was the only proxy used across all four orders (**Appendix Table S1.2**; **Appendix Figure S1.3a**). Cusp number ratio and number of cusps were proxies limited only to Hexanchiformes (Adnet 2006, Adnet and Martin 2007), whereas total tooth height was a proxy used in Squaliformes, Lamniformes and Carcharhiniformes (**Appendix Table S1.2**; **Appendix Figure S1.3a**). Total tooth height had only four recorded links to body size while cusp number ratio and number of cusps each had two (**Figure 2.3a**). Consistent results were found when only anterior teeth were considered, where crown height and crown width were the most commonly used dental characters (**Appendix Figure S1.4a**). Overall, my literature review reveals that the most common and most broadly used proxies for body size are crown height and crown width respectively.
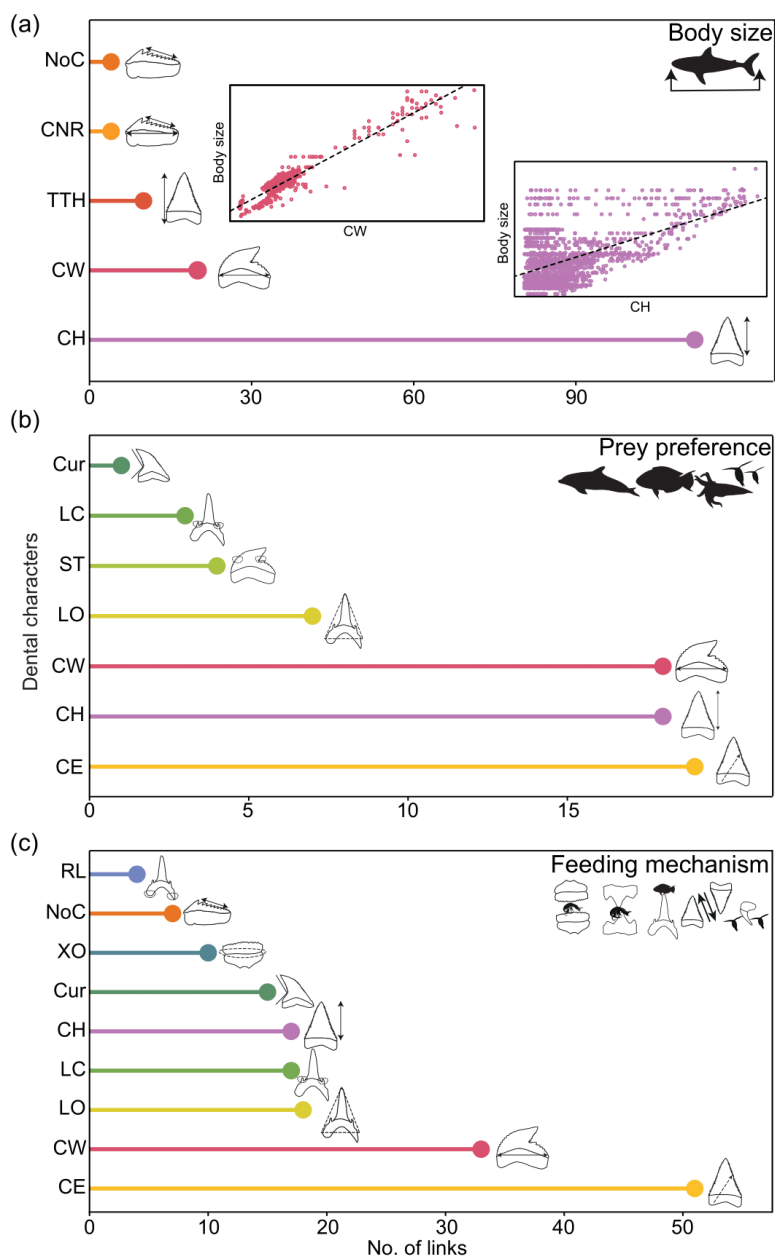
Figure 2.3. Dental characters used in literature as proxies for (a) body size; (b) prey preference and (c) feeding mechanism. Dental character abbreviations are as follows: NoC = number of cusps; CNR = cusp number ratio; TTH = total tooth height; CW = crown width; CH = crown height; Cur = curvature; LC = lateral cusplets; ST = serration type; LO = longitudinal outline; CE = cutting edge; RL = root lobes; and XO = cross-section outline. Scatter plots in (a) show linear regressions between crown height (purple plot) and crown width (pink plot) versus body size considering all tooth positions (see text and **Appendix Figure S1.5** for details).

With regard to this finding, I performed linear regressions considering body size versus crown height and crown width from the literature. I found that both dental characters were positively correlated with body size even when examining all taxonomic orders together (**Figure 2.3a**; **Appendix Figure S1.5**). The correlation between crown height and body size was weaker when all tooth positions were considered ($R^2 = 0.32$, $P < 0.001$; **Figure 2.3a**; **Appendix Figure**

S1.5a) and stronger when only anterior teeth were used ($R^2 = 0.71$, $P < 0.001$; **Appendix Figure S1.5c**). This is most likely due to shark teeth progressively decreasing in crown height antero-posteriorly along the jaw (e.g., Pimiento et al. 2010). As such, large sharks can have tall anterior teeth, as well as short lateral and posterior teeth. Conversely, crown width was found to be highly correlated with body size when considering both all tooth positions ($R^2 = 0.90$, $P < 0.001$; **Figure 2.3a**; **Appendix Figure S1.5b**) and only anterior teeth ($R^2 = 0.89$, $P < 0.001$; **Appendix Figure S1.5d**). A positive linear relationship between tooth size and body size was also observed when using categorised size classes where larger body size classes are linked with larger tooth sizes (**Figure 2.4a, b**; crown height Kruskal-Wallis test: $X^2 = 431.08$, df = 3, $P < 0.001$; crown width Kruskal-Wallis test: $X^2 = 250.24$, df = 2, $P < 0.001$). This was also found when only using anterior teeth (**Appendix Figure S1.4b-c**; crown height Kruskal-Wallis: $X^2 = 206.5$, df = 3, $P < 0.001$; crown width Kruskal-Wallis: $X^2 = 202.5$, df = 2, $P < 0.001$). My results are in-line with current knowledge of the relationship between shark tooth size and total length (e.g., Strasburg 1963, Litvinov et al. 1983, Shimada 2003, Chavez et al. 2012). In fact, these relationships in individual species are often extrapolated to extinct sharks to predict body size. For example, the relationship between tooth size and total length in *C. carcharias* is commonly used to predict the size of the extinct *Otodus megalodon* (Pimiento et al. 2010, Pimiento and Balk 2015, Shimada 2019). In this species, crown width has recently been shown to be a more robust proxy than crown height across different tooth positions (Perez et al. 2021), mirroring my regression results (**Figure 2.3a**; **Appendix Figure S1.5**). It should be noted; however, that non-macrophagous sharks (*M. pelagios*; *Cetorhinus maximus* and *R. typus*) represent exceptions to these findings given their small teeth (i.e., <5 mm in crown height; **Table 2.1**) relative to their large body sizes (5-18 m; **Table 2.2**; Ebert et al. 2021). As such, there were no studies in the literature linking body size and tooth size in these species. Taken together, my linear regression analyses indicate that from the two most common proxies for body size, crown width displays a stronger linear correlation across tooth positions than crown height (crown width vs. body size $R^2 > 0.85$; crown height vs. body size $R^2 > 0.32 < 0.71$; **Figure 2.3a**; **Appendix Figure S1.5**).
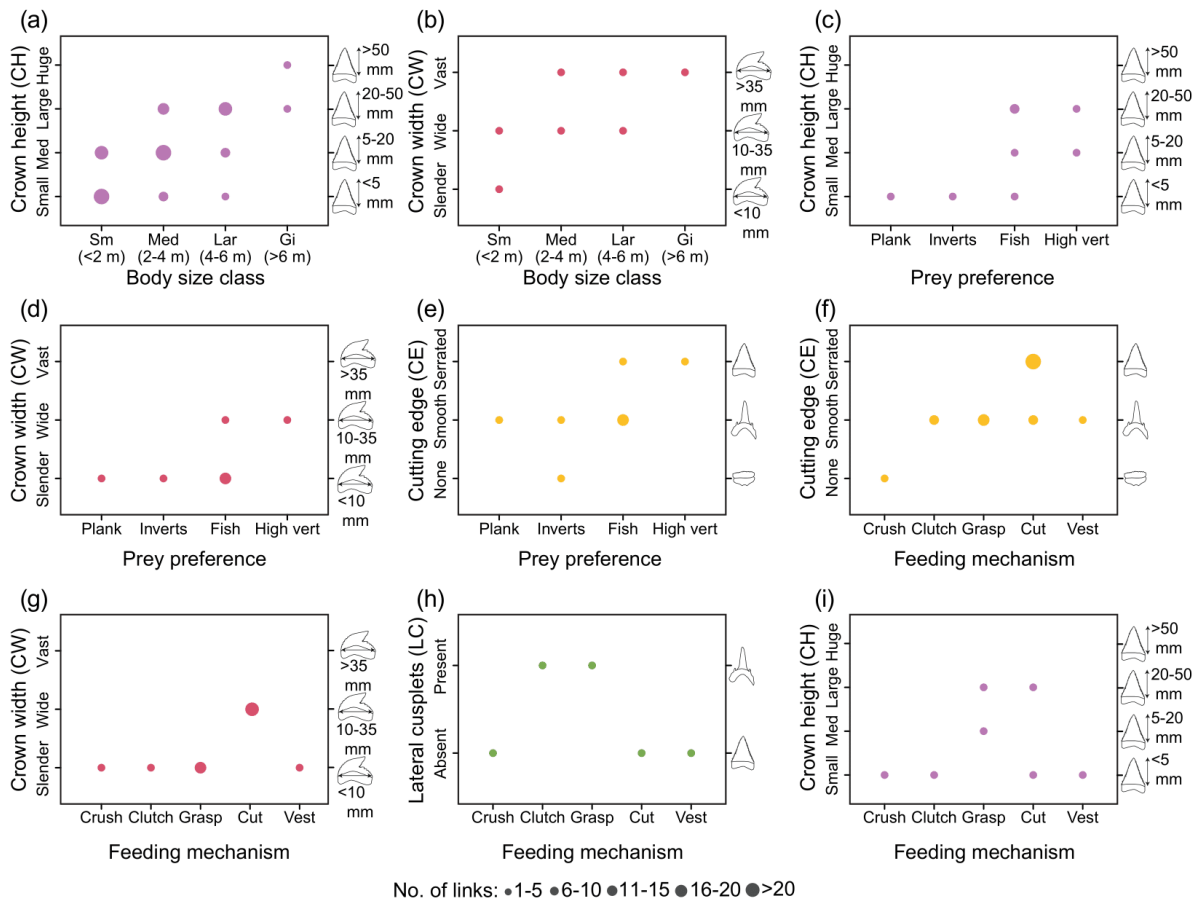
Figure 2.4. Links between dental character states and functional trait values recorded from literature. (a-b) Links to body size classes from (a) crown height; and (b) crown width. (c-e) Links to prey preference from (c) crown height; (d) crown width; and (e) cutting edge. (f-i) Links to feeding mechanism from (f) cutting edge; (g) crown width; (h) lateral cusplets; and (i) crown height. Note that crown height and crown width and body size were recorded numerically via measurement data, but here are converted to categorical values (**Tables 2.1-2**). Abbreviations are as follows: Sm = small; Med = medium; Lar = large; Gi = giant; Plank = plankton; Inverts = invertebrates; Fish = fishes; High vert = high vertebrates; Crush = crushing; Clutch = clutching; Grasp = grasping; Cut = cutting; Vest = vestigial.

Prey preference: I identified seven dental characters used as proxies for prey preference in the literature review: cutting edge, crown height, crown width, longitudinal outline, serration type, lateral cusplets and curvature (**Table 2.1**; **Figure 2.3b**). These were recorded categorically (e.g., cutting edge: smooth, serrated or absent; **Table 2.1**) in nine studies across five orders (Squantiniformes, Heterodontiformes, Orectolobiformes, Lamniformes and Carcharhiniformes) and 25 taxa (**Appendix Table S1.2**; **Appendix Figure S1.2c**). A robust correlation between tooth morphology and prey preference is expected given that the primary function of teeth is to capture and process prey (Cappetta 2012). Of the seven identified dental characters, all except curvature were used as proxies across multiple orders (**Appendix Table S1.2**; **Appendix Figure S1.3b**), with crown height being studied in all five above orders,

cutting edge being studied in all except Heterodontiformes, and crown width and lateral cusplets being studied in three orders (Orectolobiformes, Lamniformes and Carcharhiniformes; **Appendix Table S1.2**; **Appendix Figure S1.3b**). Cutting edge, crown height and crown width were by far the most common proxies for prey preference (20, 18 and 18 links respectively; **Figure 2.3b**), making up 78.9% of all documented links. As such, they were selected for further analysis.

Quantifying links between dental character states and functional trait values revealed that small and slender crowns and smooth cutting edges were associated with smaller prey (i.e., plankton and invertebrates), whereas large and wide crowns and serrated cutting edges were associated with larger prey items (i.e., fishes and high vertebrates; **Figure 2.4c-e**). Prey preferences of plankton and invertebrates were exclusively linked to small crown heights (<5 mm) and widths (<10 mm), and smooth cutting edges. Moreover, the absence of cutting edges was linked only to invertebrate preferences; representing plate-like teeth used in the consumption of typically armoured prey (Kent 1994, Cappetta 2012, Cullen and Marshall 2019). A dietary preference for fishes occurred across multiple states for the most common dental characters (i.e., cutting edge, crown height and crown width), likely reflecting the fact that fishes are widely consumed across shark species (Wetherbee and Cortés 2004, Ebert et al. 2021). Moreover, fishes display a wide diversity of body forms, with shark tooth morphologies varying accordingly. Prey preferences for high vertebrates, on the other hand, were associated only with larger tooth sizes (i.e., medium-large crown heights, wide crown widths) and serrated cutting edges, likely reflecting the need of slicing chunks of flesh in order to consume large prey with thick skin such as marine mammals (Frazzetta 1988, Cortés 1999, Ciampaglio et al. 2005, Lucifora et al. 2009). My results therefore suggest that the combination of crown size and cutting edge are the most common proxies for prey preference in sharks.

Feeding mechanism: I found nine dental characters used as proxies for shark feeding mechanism in literature: cutting edge, crown width, longitudinal outline, lateral cusplets, crown height, curvature, cross-section outline, number of cusps and root lobes (**Table 2.1**; **Figure 2.3c**). All were measured categorically (e.g., lateral cusplets: absent or present; **Table 2.1**) in relation to this functional trait, with the exception of number of cusps which was recorded based on countable elements (i.e., discrete numerical data; Supporting Information Data S1). Both qualitative (without analysis) and quantitative links (with analysis) – 86 (49.7%) and 87 (50.3%) respectively – were returned within the literature review across 11 studies and 37 taxa from six orders: Hexanchiformes, Squaliformes, Heterodontiformes, Orectolobiformes,

Lamniformes and Carcharhiniformes (**Appendix Table S1.2**; **Appendix Figure S1.2d**). Of the nine identified dental characters, cutting edge, cross-section outline and longitudinal outline were proxies used in all six orders above. The presence of lateral cusplets was used as a proxy for feeding mechanism within five orders, while crown height, crown width and number of cusps were used in four orders. Finally, curvature and root lobes were proxies used in three and two orders respectively (**Appendix Table S1.2**; **Appendix Figure S1.3c**). Root lobes was the least common (5 links) and least broadly used proxy, so was discarded from subsequent analyses. Number of cusps was also not investigated further due to redundancy as this character includes all lateral cusplets (Ciampaglio et al. 2005). As such, the seven most commonly used dental characters (**Figure 2.3c**) were selected for further analyses.

Of the seven dental characters investigated further, three – curvature, longitudinal outline and cross-section outline – did not have clear relationships with feeding mechanism that could be detected from literature (**Appendix Figure S1.6**). For instance, although curvature was found to be present in teeth with grasping and vestigial feeding mechanisms, and absent in cutting feeding, no data was found for clutching or crushing feeding (**Appendix Figure S1.6a**). Not all character states of longitudinal outline and cross-section outline were accounted for in the data either. Notably, some states of both characters were linked to multiple feeding mechanisms and vice versa (**Appendix Figure S1.6b-c**). For example, a "lens" cross-section outline was found in clutching, grasping and cutting feeding (**Appendix Figure S1.6c**). As both longitudinal outline and cross-section outline are shape-based metrics (Ciampaglio et al. 2005), the lack of a clear relationship between these dental characters and feeding mechanism in the literature may support suggestions that although overall tooth morphology appears to correspond to dietary preference (Frazzetta 1988, Cappetta 2012, Bazzi et al. 2021), its relationship with feeding function may be more cloudy (Whitenack and Motta 2010, Whitenack et al. 2011).

The remaining four dental characters (i.e., cutting edge, crown width, lateral cusplets and crown height) had clearer associations with feeding mechanisms (**Figure 2.4f-i**). For instance, serrated cutting edges and wide crowns were exclusively linked to cutting feeding (**Figure 2.4f-g**); the absence of a cutting edge was only linked to crushing feeding (**Figure 2.4f**); and the presence of lateral cusplets was linked only to clutching and grasping feeding (**Figure 2.4h**). The links between other dental character states and feeding mechanisms were less clear, with single character states being linked to multiple feeding mechanisms (**Figure 2.4f-i**). Notably, while large crown heights were only linked to both grasping and cutting feeding

mechanisms, small crowns were also linked to cutting, and medium crowns also to grasping (**Figure 2.4i**). The literature review therefore indicates that cutting edge, crown width and lateral cusplets are the most widely used proxies for feeding mechanisms, with crown height also being largely used, but showing less clear associations.

Q2: Which dental characters are the best proxies for functional traits in sharks?

My museum dataset included 63 of the 68 taxa initially collated in the literature review – 58 identified to species level and five to genus level; for which proxy species were used based on collection availability (Supporting Information Data S3). Missing species included: *Carcharhinus sealei*, *C. maximus*, *Rhizoprionodon longurio*, *Scoliodon laticaudus* and *Scyliorhinus retifer*. From the 12 dental characters identified in the literature review as proxies for functional traits (**Table 2.1**), cusp number ratio and serration type (**Figure 2.2**) were excluded due to limited representation across shark phylogeny. Specifically, cusp number ratio only occurs in Hexanchiformes (Adnet 2006, Adnet and Martin 2007) while serration type only occurs in serrated teeth. Indeed, secondary serrations (**Table 2.1**) have only been reported in *G. cuvier* teeth (Moyer and Bemis 2017). I also excluded total tooth height because crown height was found to be much more widely used in literature (**Figure 2.3**). As a result, nine dental characters were included in the analyses.

The PCA showcased which of the nine remaining dental characters contributed most to variation across tooth morphology and associated trait values (**Figure 2.5**; **Appendix Figure S1.7**). PC1 explained 34% of shark tooth morphology variation whereas PC2 explained 18% when considering all teeth and anteriors only (**Table 2.3**; **Appendix Table S1.3**). Morphological variation in PC1 was mostly related to crown height and crown width, and to a lesser extent to cutting edge (**Figure 2.2**; **Table 2.3**; **Appendix Table S1.3**). This is the case when considering all teeth and anteriors only (**Appendix Figure S1.7**). As such, positive PC1 values were occupied primarily by large crowns and serrated cutting edges and negative values were occupied by smaller crowns and smooth or absent cutting edges. Numerical and categorical crown height and crown width were found to make very similar contributions to morphospace variation (**Table 2.3**; **Appendix Figure S1.3**), suggesting that the nature of these variables has negligible effect on interpretation. The contributions of dental characters to PC2 differed when considering all teeth vs. anteriors only. When all teeth were included, PC2 was mostly related to the presence of lateral cusplets and number of cusps (**Figure 2.2**; **Table 2.3**), with positive values occupied by teeth with multiple cusps, including lateral cusplets, and

negative values occupied by single-cusp teeth with no lateral cusplets (**Table 2.3**). However, when only anterior teeth were considered, PC2 was mostly related to longitudinal outline (**Figure 2.2c**; **Appendix Table S1.3**). As such, positive PC2 values were occupied by triangular longitudinal outlines whereas negative PC2 values were occupied by teeth with a "piercing" longitudinal outline (**Table 2.1**). Taken together, the PCA results indicate that tooth size (crown height and crown width), cutting edge and lateral cusplets are drivers of variation in shark tooth morphology, with longitudinal outline also driving variation in anterior teeth.

Table 2.3. Contribution of shark dental characters to morphospace variation in the first two axes of the PCA based on the museum dataset and all tooth positions being considered. All results are accurate to three decimal places. Bold values denote highest contributions.

Character	Abbreviation	PC1 contribution	PC2 contribution
Crown height (numerical)	CH_num	**0.401**	-0.092
Crown height (categorical)	CH_cat	**0.379**	-0.061
Crown width (numerical)	CW_num	**0.475**	-0.117
Crown width (categorical)	CW_cat	**0.422**	-0.086
Cutting edge	CE	**0.362**	-0.091
Lateral cusplets	LC	-0.041	**0.534**
Curvature	Cur	-0.054	-0.291
Cross-section outline	XO	0.289	0.314
Longitudinal outline	LO	-0.140	0.289
Root lobes	RL	0.123	0.319
Number of cusps	NoC	0.184	**0.552**

Body size: The PCA revealed great overlap between body size classes across tooth morphologies both when considering all teeth (**Figure 2.5a**) and only anterior teeth (**Appendix Figure S1.7a**). This likely reflects how similar-sized sharks can have different ecologies. For example, the dental morphospace of giant sharks (>6 m; **Table 2.2**; darkest blue polygon in **Figure 2.5a**) included both large and serrated teeth (e.g., *C. carcharias*; maximum body size = 7 m) as well as minute and smooth teeth (e.g., *R. typus*; maximum body size = 18 m; McClain et al. 2015). Nevertheless, unlike the morphospace of mid-body sizes, the smallest and largest morphospaces (i.e., small and giant body size classes; **Table 2.2**) showed clear peaks in PC values. For instance, the small body size morphospace (light green curve in **Figure 2.5a**) showed a distinct single peak between -2 and -1 along PC1, suggesting small tooth sizes. This morphospace also diverged from the main cluster that encompasses all other body sizes along the most negative PC1 values (**Figure 2.5a**). This was the case both when considering all teeth and anteriors only (light green polygon diverging between -4 to -2 along PC1; **Figure 2.5a**; **Appendix Figure S1.7a**). These divergent, extreme morphologies include the smallest tooth sizes (i.e., crown height < 5 mm; crown width <10 mm) and the absence of a cutting edge

(**Table 2.1**), suggesting that plate-like teeth (i.e., flat crowns) are associated with some of the smallest body sizes. Also notably, the giant morphospace was mostly restricted to positive PC1 values when considering all teeth and anteriors only (darkest blue polygon in **Figure 2.5a**; **Appendix S1.7a**), suggesting a general association between giant sharks and large tooth sizes. Along PC2, the giant morphospace was associated with a single cusp morphology with no lateral cusplets. This is evidenced by the concentration of negative values along PC2 (darkest blue curve peaks around -2 in **Figure 2.5a**) when all teeth are considered, and of positive PC2 values (darkest blue curve peaks around 2 in **Appendix Figure S1.7a**) when only anterior teeth are considered. Together, these results suggest that even though there is great overlap between body size classes across tooth morphologies, the morphospace of small body sizes is generally associated with small crowns and smooth cutting edges (PC1), and the giant morphospace is associated with large, single cusp teeth (PC2).
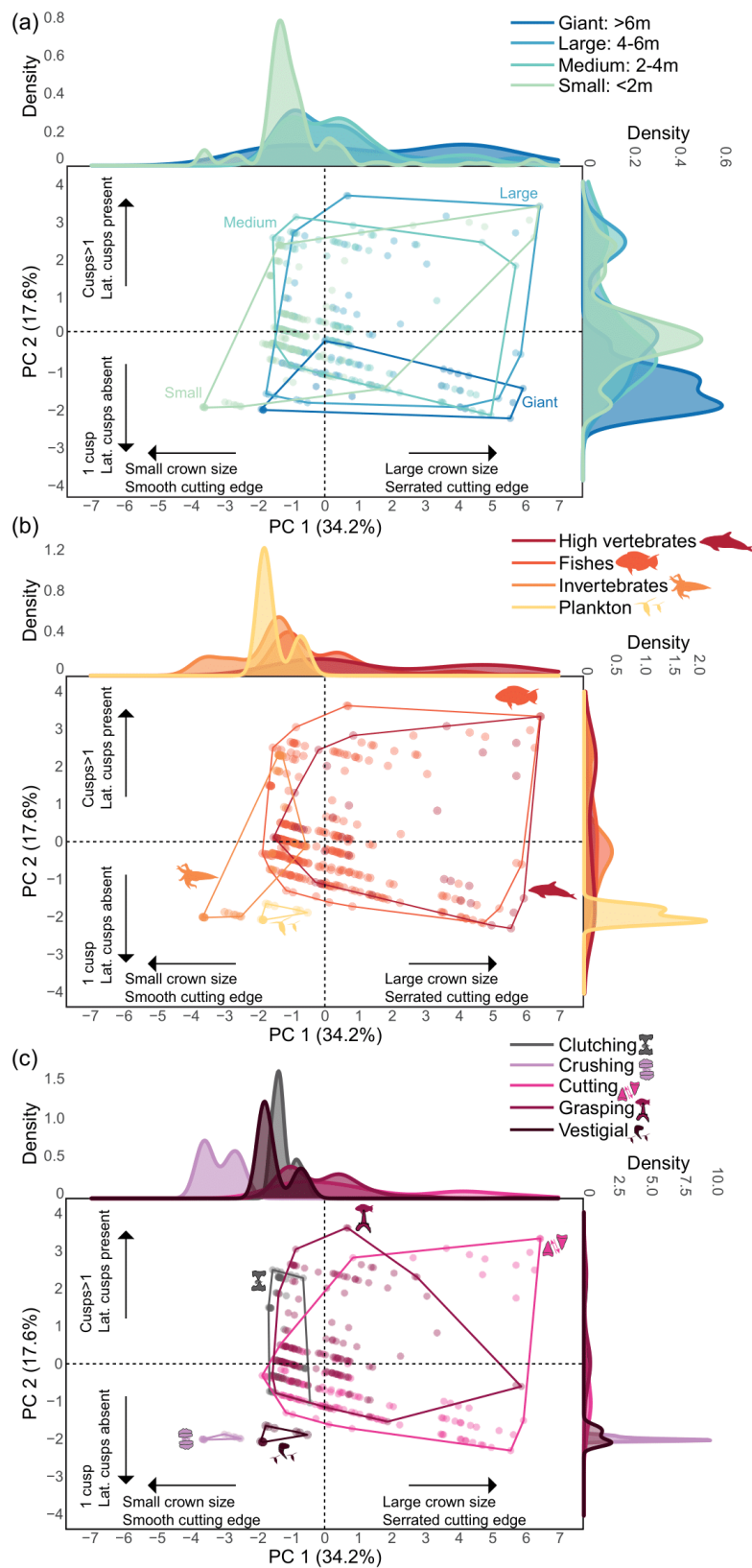
Figure 2.5. PCA of dental characters across functional traits based on the museum dataset. Each set of analysis is linked to a single functional trait as follows: (a) body size; (b) prey preference; and (c) feeding mechanism, with values for each trait defining convex hulls following **Table 2.2**. Arrows summarise how dental characters are correlated to each axis, based on their contributions recorded in **Table 2.3**. Density plots show the distribution of trait values along each axis.

The body size classification tree indicated that crown height was the main predictor of body size (**Figure 2.6a**; **Appendix Table S1.4**). Cross-validation analyses aimed to assess tree reliability produced an accuracy of 53.1% on the test set. Repeating the analysis on only anterior teeth produced a near-identical tree (**Appendix Figure S1.8a**), but with a test set accuracy of 68.2%. The difference in accuracy is likely due to the purported more direct association between crown height and body size in anterior teeth (Condamine et al. 2019, Shimada et al. 2020). Nevertheless, this accuracy difference is only modest (i.e., 15.1%) given that tooth position was not returned as an important predictor of body size (**Figure 2.6a**; **Appendix Figure S1.8**). These findings differ from those obtained from the linear regressions based on data from the literature review, in which crown width was found to be more strongly correlated to body size than crown height across tooth positions (**Figure 2.3a**; **Appendix Figure S1.5**). This difference could be explained by the broader categorical nature of the classification tree's variables (De'ath and Fabricius 2000) compared to the numerical nature of the linear regressions. Nevertheless, the classification tree (**Figure 2.6a**) supports my general findings that large crown sizes are associated with large bodies in sharks (**Figure 2.3a**, **2.4a**, **b**, **2.5a**; **Appendix Figure S1.4-5**). Taken together, my analyses suggest that crown height and crown width are the most common and best proxies for body size in sharks.
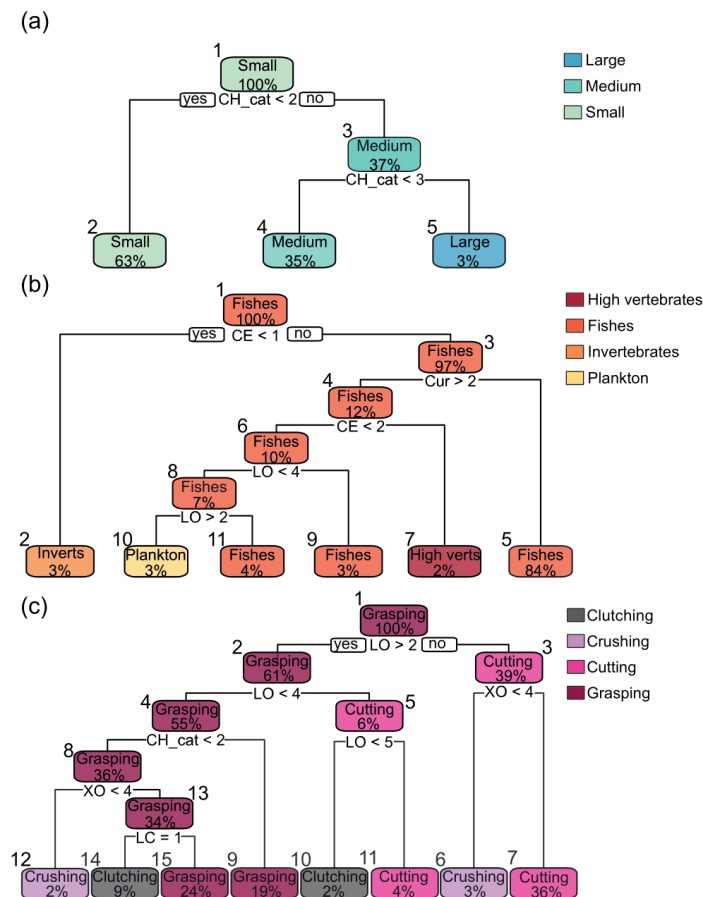
Figure 2.6. Classification tree analyses on dental characters recorded from the museum dataset. Each tree is related to a single functional trait as follows: (a) body size; (b) prey preference; and (c) feeding mechanism. Nodes are produced by splitting the data based on the presence of the dental character states recorded as predictors. The proportional node contributions to the entire dataset are included alongside the most common trait value making up each node (**Appendix Table S1.4-S6**). Abbreviations are as follows: CH_cat = categorical crown height; CE = cutting edge; Cur = curvature; LO = longitudinal outline; XO = cross-section outline; and LC = lateral cusplets (**Table 2.1**).

Prey preference: The PCA showed some overlap in prey preference across tooth morphologies (**Figure 2.5b**; **Appendix Figure S1.7b**), likely representing the generalist diets of most shark species (Wetherbee and Cortés 2004). A fish prey preference occupied the largest extent of the dental morphospace both when considering all teeth and only anterior teeth (orange polygon in **Figure 2.5b**; **Appendix Figure S1.7b**), reflecting diversity of shark tooth morphologies linked to piscivory. In both sets of analyses, the morphospace for high vertebrates (red polygon in **Figure 2.5b**; **Appendix Figure S1.7b**) was contained inside the fish morphospace, likely due to the fact that (1) sharks that prey upon large organisms such as high vertebrates tend to feed on a wide range of prey (Lucifora et al. 2009); and (2) sharks such as *C. carcharias* that consume high vertebrates as adults specialise in fishes as juveniles (Estrada et al. 2006), this dietary shift likely reflected in ontogenetic heterodonty where crowns get wider as the shark

grows (French et al. 2017). My analyses further showed that the high vertebrates and the fishes morphospaces mostly extended along positive PC values, indicating an association with large crown sizes, serrated cutting edges and the presence of cusplets. However, unlike the high vertebrate morphospace, which largely extended along most PC1 values (red curve in **Figure 2.5b**), the fish morphospace concentrated at mid PC1 values (orange curve peaks mostly at -1, and to a lesser degree at 1; **Figure 2.5b**), reflecting mid tooth sizes (i.e., 5-20 mm crown height) and both smooth and serrated cutting edges. Furthermore, the fishes morphospace of anterior teeth extended into the most negative PC2 values, reflecting piercing longitudinal outlines and lateral cusplets, while the high vertebrates morphospace is restricted to more positive values representing triangular longitudinal outlines lacking lateral cusplets (**Appendix Figure S1.7b**).

The invertebrates morphospace overlapped with the fishes morphospace on negative PC1 values, with a main peak around -1.5 (light orange polygon and curve in **Figure 2.5b**) reflecting small crowns and smooth cutting edges associated with both prey preferences. However, the invertebrates morphospace diverged further into the most negative PC1 and PC2 values (extending across values of -3 to -4 in PC1 and around -2 in PC2), reflecting even smaller crowns, no cutting edge, and no cusp (i.e., the unique plate-like morphology, especially useful to consume invertebrates). This was also the case when only anterior teeth are analysed (**Appendix Figure S1.7b**). However, in anterior teeth, the diverging invertebrates morphospace occupied a PC2 value of around 0, reflecting the semi-circular longitudinal outlines of these teeth. The plankton morphospace completely diverged from all others, exclusively occupying negative values along PC1 and PC2, with a peak around -2 in both PCs (yellow polygon and curves in **Figure 2.5b**). This area of the morphospace was associated with small (<5 mm crown height; <10 mm crown width) single-cusped teeth with smooth cutting edges. A similarly distinct divergence was seen in anterior teeth (**Appendix Figure S1.7b**). As such, this divergence likely indicates a dietary specialisation. Taken together, the results suggest that: (1) the dietary preferences for high vertebrates and fishes are associated with large to mid-sized crowns, and serrated cutting edges, though may be distinguished by lateral cusplets and longitudinal outline; (2) the dietary preferences for invertebrates and plankton are associated with small crown sizes, a lack of lateral cusplets and smooth or absent cutting edges; and (3) crown size and cutting edge are the dental characters that drive most of the observed variation in prey preference.

The classification tree analysis revealed cutting edge to be the main predictor of prey preference at the root node (**Figure 2.6b**), in line with our findings from the literature where the lack of a

cutting edge was linked to invertebrate specialisation, smooth cutting edges were associated with multiple prey preferences, and serrated cutting edges were linked to preferences for high vertebrates (**Figure 2.4c-e**). Curvature and longitudinal outline were also predictors at subsequent decision nodes, indicating their use to distinguish teeth associated with planktivory (**Figure 2.6b**; **Appendix Table S1.5**). Cross-validation analyses indicated an accuracy of 83.9% on the test set, suggesting that the dental characters used in the tree are strong predictors of prey preference. When only anterior teeth were analysed, cross-section outline was the main predictor at the root node, albeit primarily to distinguish teeth linked to planktivory from the rest of the subset (**Appendix Figure S1.8b**). Of the remaining sample, the tree indicated crown width, lateral cusplets and crown height could be used to distinguish prey preferences of fishes from invertebrates. Specifically, larger crown sizes were associated with piscivory and smaller crown sizes were associated with a dietary preference for invertebrates (**Appendix Figure S1.8b; Appendix Table S1.5**). The resulting tree's test set had an accuracy of 78.8%. Tooth position was not returned as a predictor of prey preference by either tree, suggesting lesser importance compared to the returned dental characters (**Figure 2.6b**; **Appendix Figure S1.8b**). The classification trees therefore indicate that cutting edge is the most important predictor of prey preference, but that crown size and shape (i.e., longitudinal and cross-section outline), as well as curvature and lateral cusplets, can be subsequently used in combination to distinguish specific prey preferences. Overall, my results collectively suggest that cutting edge and crown size are the most common and best dental character proxies for prey preference.

Feeding mechanism: The PCA showed morphospace overlap between clutching, cutting, and grasping feeding both when considering all teeth and anterior teeth only (**Figure 2.5c**; **Appendix Figure S1.7c**). This could be reflective of a lack of functional difference between these mechanisms previously suggested by biomechanical studies (Whitenack and Motta 2010, Whitenack et al. 2011). However, some variation between the tooth morphologies of these feeding mechanisms was detected. The clutching morphospace concentrated at negative PC1 values both when considering all teeth and anteriors only, peaking at around -1.5 (grey polygon and curve in **Figure 2.5c**; **Appendix Figure S1.7c**) and reflecting small crowns and smooth cutting edges. Some of this morphospace overlapped with the grasping morphospace, suggesting some similar tooth morphology, a result also obtained from the literature review (**Figure 2.4f-i**). For example, both morphospaces occupied both positive and negative PC2 values due to variation in number of cusps or the presence of lateral cusplets (**Figure 2.5c**). However, the grasping morphospace extended along mid to positive PC1 values (purple

polygon in **Figure 2.5c**), suggesting that this mechanism is also associated with larger tooth sizes (i.e., medium crown heights of 5-20 mm). The cutting morphospace extended across even more positive PC1 values (pink polygon in **Figure 2.5c**). This suggests that cutting feeding is primarily associated with large crowns and serrated cutting edges. Across PC2 when considering all teeth, the cutting morphospace mostly occupied negative values, reflecting single-cusped and no lateral cusplets morphologies. However, some divergence into positive PC2 values represented the unique lower tooth morphologies of Hexanchiformes, known for having multiple cusps (i.e., >5; **Figure 2.5c**; Adnet 2006). In anterior teeth, the cutting and grasping morphospaces diverged into positive and negative PC2 values respectively. This suggests that cutting feeding is linked to teeth with triangular longitudinal outlines and no lateral cusplets, while grasping mechanism teeth are associated with piercing longitudinal outlines and the presence of lateral cusplets.

The PCA further revealed that crushing and vestigial feeding mechanisms were associated with unique tooth morphologies, as both morphospaces diverged from the main cluster when considering all teeth and anteriors only (light pink and darkest purple polygons respectively in **Figure 2.5c**; **Appendix Figure S1.7c**). Crushing feeding was linked to small crowns with no cutting edge (e.g., plate-like teeth typically seen in *Mustelus canis*, *Heterodontus francisci* and *S. tiburo*; Kent 1994, Cappetta 2012). Meanwhile, vestigial feeding was linked to the small non-functional teeth of planktivorous sharks (e.g., *M. pelagios*, *C. maximus* and *R. typus*; Kent 1994). Indeed, the vestigial morphospace mirrored the morphospace for plankton prey preference (**Figure 2.5b**; **Appendix Figure S1.7b**), suggesting a one-to-one correspondence in tooth morphology between these two trait values. When considering all teeth, the crushing and vestigial morphospaces both concentrated at the most negative PC1 and PC2 values, overlapping in density along PC2 (curves peaking around -2) due to the absence of lateral cusplets. The crushing morphospace peaked at more negative PC1 values (between -4 and -3) than vestigial morphospace (peaking at -2). This reflects that, despite both morphologies including the smallest teeth (i.e., <5 mm crown height; **Figure 2.5c**), the (plate-like) crushing morphology lacks a cutting edge, whereas the vestigial morphology displays a smooth cutting edge. When analysing anterior teeth, crushing feeding was represented by just two teeth from a single species (*M. canis*; Supporting Information Data S3), thus constituting outliers that caused large density peaks along both PC1 and PC2 (**Appendix Figure S1.7c**). Despite this, the crushing morphospace occupied PC2 values of around 0 due to a semi-circular longitudinal outline and the absence of lateral cusplets. The vestigial morphospace displayed more positive

PC2 values (1 to 2; darkest purple polygon in **Appendix Figure S1.7c**), associated with more triangular outlines than crushing morphologies in anterior teeth.

Taken together, the PCAs on feeding mechanism suggest that: (1) despite overlap between the clutching, grasping and cutting morphospaces, these dentitions can be distinguished by crown size (small, medium and large crown heights respectively), cutting edge (serrated in cutting feeding and smooth in clutching and grasping feeding) and lateral cusplets (absent in cutting feeding and present in clutching and grasping feeding); (2) there are unique tooth morphologies associated to specific mechanisms (i.e., absent cutting edge (= plate-like) and semi-circular longitudinal outline represent the crushing mechanism and the smallest crowns and triangular longitudinal outlines represent the vestigial mechanism); and (3) crown size, cutting edge, lateral cusplets and longitudinal outline are the dental characters that drive the most observed variation in feeding mechanisms.

The classification tree analysis found longitudinal outline to be the main predictor of feeding mechanism, both in the root node and in subsequent decision nodes (**Figure 2.6c**). Cross-section outline, crown height and lateral cusplets were also predictors at subsequent decision nodes, used to predict specific feeding mechanisms from smaller subsamples (**Figure 2.6c**; **Appendix Table S1.6**). Tree accuracy was found to be 74.4% for the test set during cross-validation analyses. Longitudinal outline was also the main predictor at the root node when the classification tree used only anterior teeth, with crown height and curvature being predictors of subsequent decision nodes (**Appendix Figure S1.8c**), producing a test set of 74.4% accuracy. Tooth position was not returned as a predictor of feeding mechanism by either tree (**Figure 2.6c**; **Appendix Figure S1.8c**). The trees thus suggest that longitudinal outline is an important predictor of feeding mechanism in sharks. For example, the cutting morphology typically includes a triangular longitudinal outline whereas the grasping morphology typically has a piercing longitudinal outline (**Figure 2.6c**; Ciampaglio et al. 2005), something also supported by the PCA on anterior teeth (**Appendix Figure S1.7c**). Moreover, crushing morphology was associated with unique plate-like tooth morphologies (i.e., no cutting edge; **Figure 2.6c**; Kent 1994, Cappetta 2012). Overall, my analyses collectively suggest that tooth size (crown height and width), cutting edge and lateral cusplets are the most commonly used and among the best proxies for feeding mechanism, with tooth shape (longitudinal outline) being less widely used in the literature, but also showing strong associations with feeding mechanisms.

2.5   Conclusions

Based on a literature review of 56 studies, I identified 12 dental characters from extant shark teeth that have been used as proxies for three functional traits: body size, prey preference and feeding mechanism (**Table 2.1**). Following two separate sets of analyses on an independent dataset of jaw specimens from museum collections, I determined that tooth size (crown height and crown width) and cutting edge contributed the most to the variation we observed in tooth morphology (**Table 2.3**; **Figure 2.5**; **Appendix Figure S1.7**). I further found that seven dental characters – crown height, crown width, cutting edge, lateral cusplets, curvature, cross-section outline and longitudinal outline – were suggested to be predictors of functional trait values by the classification trees (**Figure 2.6**; **Appendix Figure S1.8**). Importantly, I found that tooth position was not a predictor of any functional trait, suggesting that heterodonty, while important to acknowledge, has little influence on the relationship between functional traits and dental characters in isolated teeth. Overall, the results suggest that tooth size is a key and commonly used proxy for body size; tooth size and cutting edge are the dental characters most used and best suited to predict prey preference; and that tooth size, cutting edge, lateral cusplets and overall shape (i.e., longitudinal outline), are the most common and useful proxies for feeding mechanism (**Figures 2.3-2.6**). The key implication of these findings is that the proposed dental character proxies can be applied to extinct sharks whose fossil records are primarily composed of isolated teeth. This would thus provide insights into the ecological roles sharks played in marine systems millions of years ago and their ecological responses to environmental changes.

Chapter 3 | The rise and fall of shark functional diversity over the last 66 million years

This work is published in *Global Ecology and Biogeography* as:

Cooper JA & Pimiento C, (2024). The rise and fall of shark functional diversity over the last 66 million years. *Global Ecology and Biogeography*, **33**, e13881.

3.1   Abstract

Aim: Modern sharks are a diverse and highly threatened group playing important roles in ecosystems. They have an abundant fossil record spanning at least 250 million years (Myr), consisting primarily of isolated teeth. Throughout their evolutionary history, sharks have faced multiple environmental changes and extinction events. Here, I aim to use dental characters to quantify how shark functional diversity has changed during the last 66 Myr.

Location: Global.

Time period: Cenozoic era (66-0 million years ago; Ma).

Major taxa studied: Sharks (Selachii).

Methods: I complied a dataset of over 9,000 shark teeth belonging to 537 taxa from museum collections and scientific literature, and measured six dental characters strongly linked with functional traits. I then quantified different functional diversity metrics across Cenozoic time bins, compared them against null expectations, and identified the most important taxa contributing to maintaining functional diversity.

Results: Sharks displayed relatively high functional diversity during the Cenozoic, with 66-87% of the functional space being occupied for ~60 Myr (Paleocene to Miocene). High levels of functional redundancy during this time resulted in larger-than-expected functional richness; but a large decline (-45%) in redundancy in the Oligocene (~30 Ma) left shark functional diversity highly vulnerable to further loss. Shark functional diversity declined from the late Miocene (~10 Ma) onwards, losing 44% of functional richness by the Recent. Extinct sharks disproportionally contributed to the Cenozoic functional diversity and spanned a wider range of functional space than extant sharks, with the loss of mid-sized suction feeders and large-bodied predators driving functional declines.

Main conclusions: After maintaining high levels of functional diversity for most of the Cenozoic, sharks lost nearly half of their functional diversity in the last ~10 Myr. Current anthropogenic pressures are therefore likely eroding an already diminished shark functional diversity, leaving future communities ecologically deprived compared with their thriving geological past.

3.2   Introduction

Sharks (Elasmobranchii, Selachii) are a diverse and ecologically disparate group of marine vertebrates (Compagno 1990). With over 500 living species across nearly all marine habitats (Weigmann 2016), they play a range of critical functions in marine systems such as apex predators controlling prey populations (Myers et al. 2007), mesopredators acting as food sources for larger predators (Navia et al. 2017), and nutrient transporters connecting distant populations and habitats (Williams et al. 2018). Notably, modern sharks are evolutionary distinct compared to other marine vertebrates (Stein et al. 2018) and have a 250-million-year-old fossil record consisting mostly of well-preserved teeth, which are highly abundant in marine sediments worldwide (Kent 1994, Cappetta 2012).

Throughout their long evolutionary history, sharks have experienced numerous environmental changes and survived several extinction events (Kriwet and Benton 2004, Guinot et al. 2012, Belben et al. 2017, Sibert and Rubin 2021a, Guinot and Condamine 2023). While previous studies have examined shark morphological disparity through time (Belben et al. 2017, Bazzi et al. 2021), how their functional diversity has changed remains largely unexplored. Exploring this question is possible by examining fossil shark teeth, which have been demonstrated to be good proxies of traits such as body size, prey preference and feeding mechanism (Cooper et al. 2023). Because these traits can reflect how sharks obtain and move resources across systems, they can be used as a basis to quantify the diversity of their ecological functions (herein, functional diversity; Mouillot et al. 2013b).

Functional diversity can be assessed using different approaches. One approach involves quantifying the ecological functions in a community (i.e., number of unique trait combinations, or functional entities; herein, FEs) and the number of species filling them. This approach allows assessing the level of functional resilience in a community by measuring functional redundancy (i.e., number of species per entity; herein, FRed) and over-redundancy (i.e. % of species filling entities above mean level of redundancy, which measures the over-representation of some functions; herein, FOred; Mouillot et al. 2013b, Mouillot et al. 2014). Furthermore, functional diversity can be quantified based on the distribution of species in a multidimensional space defined by their traits (Villéger et al. 2008, Mouillot et al. 2013b). Such an approach allows to quantify the range of ecological functions based on the volume of trait space occupied by a community (i.e., functional richness; herein, FRic; Mouillot et al. 2013b). Similarly, the distribution of species in trait space allows identifying species possessing dissimilar or extreme traits. In this context, "functional originality" is measured as the distance of species to their

closest neighbour (herein, FOri) and "functional specialisation" is measured based on the distance of species to the centroid of the space (herein, FSpe; Mouillot et al. 2013b), which in turn enables identifying species whose loss would result in disproportional declines of functional diversity (e.g., Pimiento et al. 2020b). By assessing functional diversity using these different approaches, it is possible to quantify changes over time, identify the species contributing the most to maintaining ecological functions and quantify the potential ecological consequences of extinctions (Villéger et al. 2011, Pimiento et al. 2017, Pimiento et al. 2020b, Pimiento et al. 2023).

Here, I use shark teeth to evaluate how shark functional diversity has changed throughout the Cenozoic, from 66 million years ago (Ma) to the present. I focus on this era as many shark taxa in the Cenozoic fossil record have living representatives (Paillard et al. 2020, Pimiento and Benton 2020) and therefore, the tooth-trait links in extant sharks can be applied (Cooper et al. 2023). I first compiled a global image dataset of over 9,000 shark teeth belonging to 537 taxa from which I took measurements of dental characters known to be proxies to ecological traits. I then characterised the structure of the shark functional space and calculated several functional diversity metrics across different time bins (i.e., geological epochs and stages) across the Cenozoic. I included a time-bin representing the present-day (i.e., Recent), for which I only used extant species with a fossil record [i.e., 21.3% of extant species (Ebert et al. 2021); see below] to allow a suitable comparison with the inherently incomplete fossil record. Finally, I quantified individual contributions to functional diversity to identify the taxa whose extinctions had the largest impacts, and to determine whether extinct or extant taxa had larger contributions. My results provide insights into the range of shark ecological functions through a significant portion of their long evolutionary history and provide a deep-time perspective to their present-day functional diversity.

3.3 Materials and Methods

Data

Specimen collection

I searched for shark tooth specimens spanning the Cenozoic era (66-0 Ma; Gradstein et al. 2012) and the present-time (i.e., the Recent). I did this from: (1) nine museum collections in which all specimens found were photographed with a scale bar to allow subsequent measurements; (2) images in online museum repositories; and (3) tooth images from the literature (see supplementary methods; **Appendix 2**). Literature was searched using Shark-References (https://shark-references.com; last accessed May 2023; Pollerspöck and Straube 2014), from which I could extract images from 208 scientific publications (Data S1; see **Appendix 2**). All images used in this data collection can be found in the Zenodo Repository (https://doi.org/10.5281/zenodo.10076354).

From each tooth, I recorded: (1) taxonomic information from museum labels or the scientific publications, which was corrected when necessary based on the taxonomy from Shark-References (Pollerspöck and Straube 2014); (2) tooth position to account for heterodonty using museum labels or the publications where the specimen came from, and comparisons to associated dentitions from the literature; and (3) geological information (i.e., longitude, latitude, formation, locality, and age) from museum labels, the literature, and the Palaeobiology Database (PBDB; https://paleobiodb.org/; last accessed May 2023). Age (epoch and stage) was assigned following Gradstein et al. (2012). Finally, I assessed whether a taxon was extinct or extant based on Shark-References (Pollerspöck and Straube 2014) and the PBDB.

In total, I gathered images of 8,595 Cenozoic fossil shark teeth belonging to 537 taxa, 454 identified to the species-level (75.6% of all Cenozoic fossil species; Pollerspöck and Straube 2014) and 83 to the genus-level. I additionally collected images of 965 teeth of living sharks (i.e., from the Recent), 115 identified to species (21.5% of all known extant species; Ebert et al. 2021), and one to genus (Data S1). I then degraded the Recent sample to ensure it was comparable to the fossil record (see below). My data covered all continents; however, data distribution had a notable bias towards Europe and North America (**Appendix Figure S2.1**) given that eight of the nine museums visited were located in these continents; and the sampling of the fossil record is known to be highly skewed towards wealthy regions (Raja et al. 2022).

Dental measurements

I examined the following six dental characters from each specimen collected: crown height, crown width, cutting edge, lateral cusplets, cross-section outline and longitudinal outline (**Appendix Table S2.1**). I chose these six characters as they were previously found to be proxies for three main ecological traits in extant sharks: body size, prey preference and feeding mechanism (Cooper et al. 2023). Specifically, tooth size (i.e., crown height and crown width) is a strong proxy for body size; tooth size and cutting edge are strong proxies for prey preference; and all of these characters in addition to lateral cusplets and tooth shape (i.e., longitudinal outline and cross-section outline) are strong proxies for feeding mechanism (**Appendix Table S2.2**; Cooper et al. 2023). Crown height and crown width were measured directly from the specimens examined in museum collections using digital callipers (in mm), and from the images (which had a scale bar) using ImageJ (Abràmoff et al. 2004) for specimens collected from online museum repositories and the literature. The rest of the characters were categorical and assigned to each specimen based on a visual inspection. Dental characters were treated as either ordinal or nominal variables in our analyses (see supplementary methods).

Time-binning

Based on the geological information collected from each specimen, I assigned each taxon a Cenozoic epoch (Paleocene, 66-56 Ma; Eocene, 56-33.9 Ma; Oligocene, 33.9-23.03 Ma; Miocene, 23.03-5.333 Ma; Pliocene, 5.333-2.58 Ma; and Pleistocene, 2.58-0.01 Ma; Gradstein et al. 2012). I excluded the Holocene (0.01-0 Ma) from the analyses because I only collected two fossil specimens from this epoch (a *Carcharodon carcharias* and an *Isurus* sp.). All present-day specimens were assigned to the Recent (0 Ma). To ensure that this sample was comparable with the rest of the Cenozoic, I followed Villéger et al. (2011) and only included extant taxa with a fossil record. I assessed whether an extant taxon had a fossil record based on Pimiento and Benton (2020) and Paillard et al. (2020), which resulted in the exclusion of 53 species.

I used a range-through approach to fill the gaps in non-consecutive epochs from each taxon's age range (e.g., if a taxon was recorded in the Oligocene and Pliocene, I assumed it was also present in the Miocene). Following this data treatment of the fossil record, I extended the range of all extant taxa to the Recent, even if they were not recorded from the present-day sample, except for genus-level taxa for which all their species were already present in the Recent, which were recorded as extinct. This resulted in the addition of 51 taxa to the Recent, 16 species and 35 genera, for a total of 114 taxa in the degraded Recent sample.

I additionally assigned each taxon to a Cenozoic stage and repeated the steps described above. This additional binning was done to: (1) assess whether the uneven duration of geological epochs affected the results; and (2) capture more detailed changes in functional diversity over time. However, my main analyses were done to the epoch level to facilitate interpretability due to the high number of geological stages (i.e., 22; Gradstein et al. 2012).

Final dataset

The degradation of the Recent (i.e., including only extant taxa with a fossil record) resulted in a final dataset of 9,178 shark teeth. The total number of taxa remained the same: 454 identified to the species-level and 83 to the genus-level. My dataset included 100% of the Cenozoic orders and families, 92% of the genera and 75.6% of the fossil species deemed to be valid by Shark-References (Pollerspöck and Straube 2014). My degraded Recent sample included 85% of extant taxa known to have a fossil record (Paillard et al. 2020) and 21.3% of all living shark species (Weigmann 2016, Ebert et al. 2021). I consider this acceptable for my comparison with the fossil record as we cannot assume that the Cenozoic sample represents the true shark diversity of the geological past due to the inherently incomplete fossil record (Foote and Sepkoski 1999, Benton et al. 2011, Marshall 2019). Nevertheless, given the relatively low representation of current diversity in the Recent sample, I performed additional analyses to assess how the inclusion of additional living taxa affects the results (see below).

Analyses

Trait analyses

All analyses were conducted in the R environment (R Core Team 2017). Association between tooth position and each dental character was tested to assess the influence of monognathic (within jaws) and dignathic (between jaws) heterodonty. To do so, I used polychoric correlations (**Appendix Table S2.3**) in the *DescTools* package (Signorell et al. 2019). All dental characters (**Appendix Table S2.1**) were found to have weak associations with tooth position (rho < 0.35; **Appendix Table S2.3**), suggesting that heterodonty does not influence our results.

Iterative Functional Taxonomic Units

Shark tooth morphology can display intraspecific variation due to differences in life stage, sex, and jaw position (Kent 1994, Cappetta 2012, Cullen and Marshall 2019). To account for

intraspecific variation in tooth morphology, and hence in functional traits (Cianciaruso et al. 2009, de Bello et al. 2011, Albert et al. 2012), I quantified all different dental character combinations per taxon. I refer to these as Functional Taxonomic Units (FTUs; Pimiento et al. 2017). A total of 1,442 FTUs were computed across 537 taxa. However, in order to retain the taxonomic identity of each FTU, I performed the functional diversity analyses described below using one randomly selected FTU per taxon and repeating this process across 1,000 iterations.

Functional diversity analyses

I used two approaches to quantify functional diversity, one based on unique trait combinations, or functional entities (FEs; Mouillot et al. 2013b, Mouillot et al. 2014) and one based on the distribution of taxa in a multidimensional trait space (Villéger et al. 2008, Mouillot et al. 2013b). All functional diversity metrics under both approaches were computed using the *mFD* package (Magneville et al. 2022) and were computed per time bin and across each FTU iteration (see above).

For the first approach, I first quantified the number of functional entities (i.e., FE richness) per time bin using the "sp.to.fe" function. I identified a total of 122 FEs, corresponding to 5.65% of a possible 2,160 FEs. Then, based on the number of FEs per iteration (see above), I used the "alpha.fd.fe" function to calculate functional redundancy (i.e., FRed; the average number of taxa per entity) and over-redundancy (i.e., FOred; % of taxa that fill FEs above the mean level of redundancy) per time bin.

For the second approach, I created a multidimensional functional space based on the dental characters assigned to each taxon (Mouillot et al. 2013b). To do so, I first computed a trait distance matrix using the "funct.dist" function, which is based on Gower's distance (Gower 1971) and adapted from the "gawdis" function (de Bello et al. 2020). This allows for the treatment of multiple variable types (e.g., ordinal and nominal; **Appendix Table S2.1**; supplementary methods), to give different weights to each dental character (see below), and to retrieve the axes of a Principal Coordinate Analysis (herein, PCoA; Magneville et al. 2022). Given that the associations between dental characters and functional traits are not always one-to-one, I assigned weights to some dental characters to avoid the overrepresentation of some aspects of tooth morphology and therefore, functional traits (Pavoine et al. 2009, de Bello et al. 2020). Accordingly, I assigned a weight of 0.5 to crown height and to crown width, as both are tooth-size characters and proxies for body size (**Appendix Table S2.2**; Cooper et al. 2023 and references therein). I further weighted cross-section outline and longitudinal outline at 0.33

and 0.67 respectively, as both are tooth-shape-related characters and proxies for feeding mechanism, with longitudinal outline being a more important proxy (**Appendix Table S2.2**; Cooper et al. 2023). The remaining dental characters (i.e., cutting edge and lateral cusplets) were assigned weights of one each, as they are independently associated to prey preference and feeding mechanism respectively (Cooper et al. 2023).

Using the "quality.fspaces" function, I determined that my data were best represented in four dimensions (**Appendix Figure S2.2**; Maire et al. 2015). However, I built the space using three dimensions because: (1) the difference in mean absolute deviation values between a three- and four-dimensional space was negligible (<0.0001; **Appendix Figure S2.2**); and (2) 78.4% of the total inertia was represented within the first three axes. Based on the functional space built using all taxa, I assessed the relationship between axes and dental characters (**Appendix Table S2.4; Appendix Figure S2.3**) using the "traits.faxes.cor" function. To test the effect of my dental character weightings on these relationships, I repeated the above steps without weighting dental characters (**Appendix Table S2.4**). I used the "alpha.fd.multidim" function to calculate functional richness (FRic; % volume of the functional space occupied), mean originality (FOri; the distance of each taxa to its closest neighbour) and mean specialisation (FSpe; the distance of each taxa to the functional space centroid) per time bin. I also calculated the FRic and mean FOri and FSpe of extinct and extant taxa and the mean FOri and FSpe across shark orders. Finally, I used the "fuse" function to compute species' individual FOri and FSpe (Griffin et al. 2020, Pimiento et al. 2020b) and ranked taxa according to their scores to identify the top 5% contributors.

For all metrics described above, I reported the median and standard deviation (SD) per time bin, as the data across FTU iterations were not normally distributed (Shapiro-wilk; $P < 0.05$). Based on median values, I plotted the functional space of the entire Cenozoic assemblage and identified its vertices using the functions "background.plot" and "vertices", respectively. I also built the functional spaces of each time bin and of extinct and extant taxa using the "alpha.multidim.plot" function. I additionally used Mann-Whitney U-tests to assess whether the differences across epochs (i.e., assessed in pairwise time bins) were statistically significant. Furthermore, I performed a Welch two sample t-test to assess whether mean FOri and FSpe values of extinct and extant taxa were statistically different, and two-sided 90th quantile permutation tests (n=5000; Cooke et al. 2022) to assess if outliers in FSpe or FOri distributions of the extinct or extant samples deviated due to random chance.

Assessment of sampling biases

First, I assessed how sampling biases might affect the number of taxa recorded in each time bin (i.e., empirical taxonomic richness), and consequently the functional diversity metrics. To do so, I randomly resampled each time bin based on the lowest sample size in the dataset (Pleistocene = 309 teeth) using the "sample" R function and re-calculated the number of taxa as well as all functional diversity metrics per time bin 1,000 times without replacement. I also assessed whether changes in the empirical number of taxa through time were statistically different from those seen when taxonomic richness was resampled. I did this by (1) calculating the net-changes of taxonomic richness between successive time bins in both the empirical and resampled data; (2) subtracting the empirical net-changes from their resampled counterparts to find the difference in net-changes between the two samples, done for all 1,000 resampled iterations (see above); (3) bootstrapping the resampled net-changes to obtain a median of differences per net-change and assessing the central tendency and uncertainty with confidence interval tests; and (4) performing a one-tailed bootstrap hypothesis test per net-change to determine if the returned differences were statistically significant.

I also assessed how the degradation of the Recent sample (i.e., including only extant taxa with a fossil record) affected the results. To do so, I re-calculated FRic (i.e., % volume of the functional space occupied) for (1) all taxa from the present-day (i.e., herein "Recent-plus", which includes taxa without a fossil record; n = 162); and (2) a random subsample of the "Recent-plus" based on the number of taxa with a fossil record (i.e., herein "Resampled Recent-plus"; n = 114) 1,000 times without replacement. I compared these values against those from the degraded Recent sample.

Finally, I performed a complementary analysis (see supplementary methods) to assess (1) how much of a functional space comprising the total diversity of living sharks is represented by the degraded Recent sample; and (2) whether the degraded Recent sample is missing the most extreme trait values from today's diversity. To do this, I collected trait data of all living species based on the literature (Data S2; see **Appendix 2**). Specifically, I collected data on the traits that the dental characters serve as proxies of (i.e., body size, prey preference and feeding mechanism; Cooper et al. 2023). Body size and prey preference were obtained from Pimiento et al. (2023), whereas feeding mechanism was obtained from Kent (1994, 2018) and Cappetta (2012).

Null model

I compared all functional diversity metrics per time bin against a null model to examine whether my results differ from random expectations based on empirical taxonomic richness. Accordingly, for each time bin, I randomised taxonomic identity while maintaining the empirical number of taxa and re-calculated all functional diversity metrics 1,000 times. To compare the median values from this null model against those obtained empirically I used *Z*-scores (i.e., [empirical median – null model median]/null model SD). *Z*-scores with an absolute value of >|1.96| were considered statistically significant and indicative of empirical results falling beyond 95% of the null distribution (Hedberg et al. 2021).

Sensitivity analyses

To assess the sensitivity of my functional diversity analyses to individual traits (Lefcheck et al. 2015), I computed all functional diversity metrics described above, but removing one dental character at a time.

Random simulations of species loss

I examined how changes in FRic over time differ from expectations based on a random simulation of taxonomic loss. Accordingly, I computed FRic in randomised subsamples sequentially going from 10 to the total number of taxa (537), 100 times without replacement (Pimiento et al. 2020b). This procedure allowed me to establish the expected relationship between FRic and taxonomic richness and assess deviations from expectations.

3.4 Results and Discussion

Structure of Cenozoic shark functional space

The Principal Coordinate Analysis (PCoA) based on dental measurements (trait-proxies) revealed that the Cenozoic shark assemblage can be represented within a reduced three-dimensional trait space (representing 78.4% of the total inertia; **Figure 3.1a**, **Appendix Figure S2.2**). The first axis (50.5% inertia) was most correlated to lateral cusplets and longitudinal outline (**Appendix Table S2.4**), which, based on Cooper et al. (2023), are associated with feeding mechanism (**Appendix Table S2.2**). Although these dental characters were weighted at one and 0.67 respectively (see Methods), they were also found to be the most correlated to PCoA1 when unweighted (**Appendix Table S2.4**). An extinct megamouth shark, †*Megachasma alisonae,* scored the lowest value along this axis (**Figure 3.1a**), with teeth displaying the presence of lateral cusplets and piercing longitudinal outlines, representing clutching and vestigial feeding mechanisms (Cooper et al. 2023). Such inferences broadly agree with literature, where †*M. alisonae* has been interpreted as a filter feeder (Shimada and Ward 2016). The highest value along this axis was scored by the extinct "megalodon" †*Otodus megalodon* (**Figure 3.1a**), whose teeth lack lateral cusplets and had triangular longitudinal outlines, representing a cutting feeding mechanism (Cooper et al. 2023). Indeed, †*O. megalodon* likely fed by slicing large prey (Kent 1994, Cappetta 2012).

The second axis (19.5% inertia) was most correlated with cutting edge and crown height (**Appendix Table S2.4**), which collectively relate mainly to prey preference (**Appendix Table S2.2**; Cooper et al. 2023). The lowest scoring species was an extinct nurse shark †*Ginglymostoma maroccanum* (**Figure 3.1a**), with teeth displaying smooth cutting edges and small crown heights, broadly indicating a preference for invertebrates, in line with the ecology of its extant relatives (Ebert et al. 2021, Cooper et al. 2023). The highest scoring species was †*Otodus nodai* (**Figure 3.1a**), an extinct megatoothed shark possessing teeth with serrated cutting edges and large crown heights, suggesting a prey preference for high vertebrates (e.g., seabirds and marine mammals; Cortés 1999, Cooper et al. 2023). Interestingly, the highest values along PCoA2 were largely unoccupied (**Figure 3.1a**), suggesting that some possible forms of shark tooth morphology were not realised. Indeed, only 5.65% of all possible dental character combinations were filled (see Methods). The highest scoring values along this axis represent the tooth morphology of top predators (i.e., the largest teeth with serrated edges; Cooper et al. 2023). The empty space along PCoA2 could be due to the fact that top predatory traits are rare in ecosystems because large body sizes and specialised diets result in low energy

efficiency and population abundance (Garcia et al. 2008, Munroe et al. 2013). Therefore, large top predators are functionally distinct compared to smaller, more generalist sharks, which is reflected in their extreme and/or solitary positions in trait space.

The third axis (8.4% inertia) of the functional space was most correlated with crown height (**Appendix Table S2.4**), which is strongly related to body size and prey preference (**Appendix Table S2.2**; Cooper et al. 2023). The lowest scoring species was an extinct whale shark †*Palaeorhincodon dartevellei,* which is inferred to have been planktivorous based on its small teeth (Kent 1994). An extinct mako shark, †*Isurus retroflexus,* scored the highest value (**Figure 3.1a**), which is inferred to have fed on large fishes based on its large teeth and extant counterparts (Ebert et al. 2021, Cooper et al. 2023). Interestingly, the species scoring the highest and lowest values along PCoA3 do not display contrasting body sizes. Indeed, planktivorous species can reach large sizes despite their small teeth, with the extant whale shark *Rhincodon typus*, reaching up to 21 m in total length (Ebert et al. 2021). Therefore, PCoA3 appears to largely display variation in prey size, rather than body size.

Overall, examining the Cenozoic shark functional space (**Figure 3.1**, **Appendix Figure S2.4**) revealed that low values of the trait-space were occupied by teeth broadly associated with benthic feeding ecology (i.e., small, smooth, and piercing or semi-circular teeth indicating sharks feeding on small prey such as invertebrates via clutching and vestigial mechanisms), whereas high values were occupied by teeth associated with high-level macropredators (i.e., large, serrated, and triangular teeth reflecting cutting mechanisms and a prey preference for large prey such as high vertebrates).
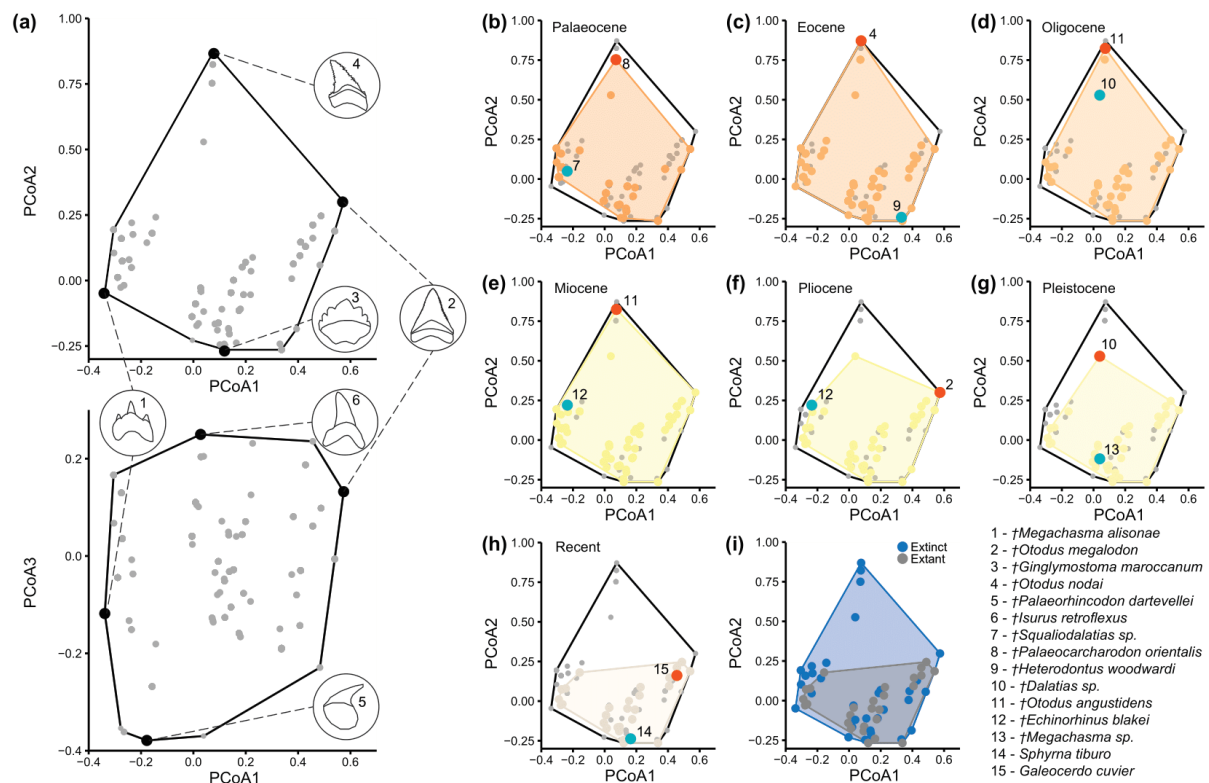
Figure 3.1. Functional space of Cenozoic sharks. (a) Structure of the three-dimensional functional space for all sharks. Black dots represent the highest and lowest scoring taxon per axis, with their corresponding teeth illustrated and numbered following an accompanying legend. Grey dots mark all other taxa. (b-h) Shark functional spaces over time (only two dimensions shown here; see **Appendix Figure S2.4**), with space occupied in each time bin depicted by coloured convex hulls. Note that the Holocene was excluded from our analyses (see text). Coloured dots denote taxa present in each assemblage, while grey dots represent absent taxa. Turquoise and orange dots denote taxa with the highest FOri and FSpe scores respectively, which are detailed in the legend. (i) Convex hulls of extinct (blue) and extant (grey) sharks.

How has functional diversity of sharks changed through time?

The number of collected taxa (i.e., empirical sample) was lowest in the Paleocene, at the beginning of the Cenozoic (**Appendix Figure S2.5a**). This number more than doubled in the Eocene, where maximum richness was reached, marking the largest increase in taxonomic diversity in the Cenozoic based on my sample. Sampled taxa subsequently dropped by 55% in the Oligocene, which represents the largest taxonomic decline observed, followed by a 93% increase in the Miocene. Thereafter, the number of collected taxa decreased in the Pliocene, Pleistocene and Recent, by 37%, 9%, and 15% respectively (**Appendix Figure S2.5a**). When accounting for uneven sampling based on my resampling procedure (see Methods), I found the same general pattern (**Appendix Figure S2.5**). However, I also found small differences, including an almost negligible (3%) increase from the Pliocene to the Pleistocene (as opposed

61

to a 9% decrease), and that the Recent (and not the Paleocene) was the time bin with the lowest taxonomic richness (empirical Paleocene = 105, Recent = 114; resampled Paleocene = 87, Recent = 83; **Appendix Figure S2.5**). Nevertheless, the results found using the empirical data provide a useful representation of the changes in taxonomic richness throughout the last ~66 million years (Myr) given that: (1) the differences in the general pattern of taxonomic richness over time were small; and (2) the difference in net-change between empirical and resampled data displayed small uncertainty (i.e., a range within ±1 of the central tendency for all net-changes) and were not statistically significant (P > 0.05; **Appendix Table S2.5**).

Paleocene

The FE approach showed that the Paleocene epoch (66-56 Ma) had the lowest FE richness and FRed of the Cenozoic (**Table 3.1**; **Figure 3.2a**, **b**), specifically during the early and middle Paleocene respectively (i.e., Danian-Selandian, 66-59.2 Ma; **Appendix Figure S2.6a**, **b**). The functional space approach further revealed that Paleocene sharks spanned over half of the functional space (FRic = 66%; **Table 3.1**; **Figure 3.1b**, **3.2d**). Relatively high FOri and FSpe values compared to the rest of the Cenozoic were established in the Paleocene; however, these values only marginally changed thereafter at the epoch level (**Table 3.1**; **Figure 3.2e**, **f**). At the stage level, FOri displayed the highest values in the middle Paleocene (Selandian, ~60 Ma; **Table 3.1**; **Appendix Figure S2.6e**). Of all the functional diversity metrics considered, FOred and FRic significantly differed from the null model (i.e., where we randomised species identities while maintaining the empirical taxonomic richness; see violin plots in **Figure 3.2**), with values respectively 6% and 23% higher than expected in the Paleocene (**Table 3.2**, **Appendix Table S2.6**), and 6% and 19% higher than expected in the Danian and Selandian, respectively (~63.5 Ma and ~60 Ma; **Appendix Table S2.7-S2.9**). These results suggest that although the Paleocene was poor in terms of number of ecological functions and redundancy, it displayed a considerably wide range of different functions, more so than expected. Indeed, examining FRic changes in response to taxonomic richness showed that FRic approaches 50% on average with as few as 70 taxa (**Appendix Figure S2.7**), suggesting that even species-poor shark assemblages can have a broad range of functions in the Cenozoic.

Table 3.1. Diversity metrics per time bin ("Epoch"). Functional diversity metric values are medians calculated from 1,000 iterations of empirical analyses, accurate to three decimal places for FOri and FSpe, and up to two for all other metrics. Proportional changes from one epoch to the other are in parentheses, calculated based on values within the table. Abbreviations are as follows: Ma = million years ago; FEs = number of functional entities; FRed = functional redundancy (average number of species per FE); FOred = functional over-redundancy (% of species filling entities above mean level FRed); FRic = functional richness (% of space volume occupied); FOri = functional originality (mean distance of taxa to their closest neighbour); FSpe = functional specialisation (mean distance of species to the centroid of the space). Bold denotes largest proportional changes (black = increases; grey = decreases; asterisk = overall highest values).

Epoch	Time (Ma)	FEs	FRed	FOred (%)	FRic (%)	FOri	FSpe
Paleocene	66-56	32	3.25	48	66	0.022	0.308
Eocene	56-33.9	55	4.82*	50*	86	0.016	0.304
		(+72%)	**(+48%)**	(+2%)	**(+20%)**	(-27%)	(-1%)
Oligocene	33.9-23.03	43	2.67	40	78	0.021	0.300
		(-22%)	(-45%)	(-10%)	(-8%)	**(+31%)**	(-1%)
Miocene	23.03-5.33	56*	4.18	46	87*	0.020	0.302
		(+30%)	**(+56%)**	(+6%)	(+9%)	(-5%)	(+1%)
Pliocene	5.33-2.58	49	2.92	41	69	0.024*	0.309*
		(-12%)	(-30%)	(-5%)	(-18%)	(+20%)	**(+2%)**
Pleistocene	2.58-0.01	44	3.02	42	60	0.020	0.302
		(-10%)	(+4%)	(+1%)	(-6%)	(-17%)	(-2%)
Recent	0	36	3.17	43	43	0.012	0.293
		(-18%)	(+5%)	(+1%)	(-17%)	**(-40%)**	(-3%)

The Paleocene represents the aftermath of the Cretaceous-Paleogene (K/Pg) mass extinction, in which elasmobranchs lost at least 60% of their diversity, with durophagous sharks (those eating shelled invertebrates) being the most affected (Kriwet and Benton 2004, Guinot and Condamine 2023). This depletion of species diversity likely explains the low FE richness of this epoch. Moreover, the K/Pg extinction particularly diminished large-bodied teleosts (Friedman and Sallan 2012), suggesting that shark prey may have been somewhat limited, potentially resulting in functional redundancy being packed into few FEs (i.e., higher than expected FOred). However, during this time, ocean temperature and eustatic sea level increased (Zachos et al. 2001, Miller et al. 2005), and ray-finned fishes diversified and became highly abundant, taking advantage of the vacant niches left after the K/Pg (Sibert and Norris 2015, Alfaro et al. 2018). As such, the higher-than-expected range of ecological functions (i.e., FRic) of the Paleocene could be linked to the highly productive and extensive coastal habitats of the time (e.g., Pimiento et al. 2017), and to the availability of prey for piscivore diets.
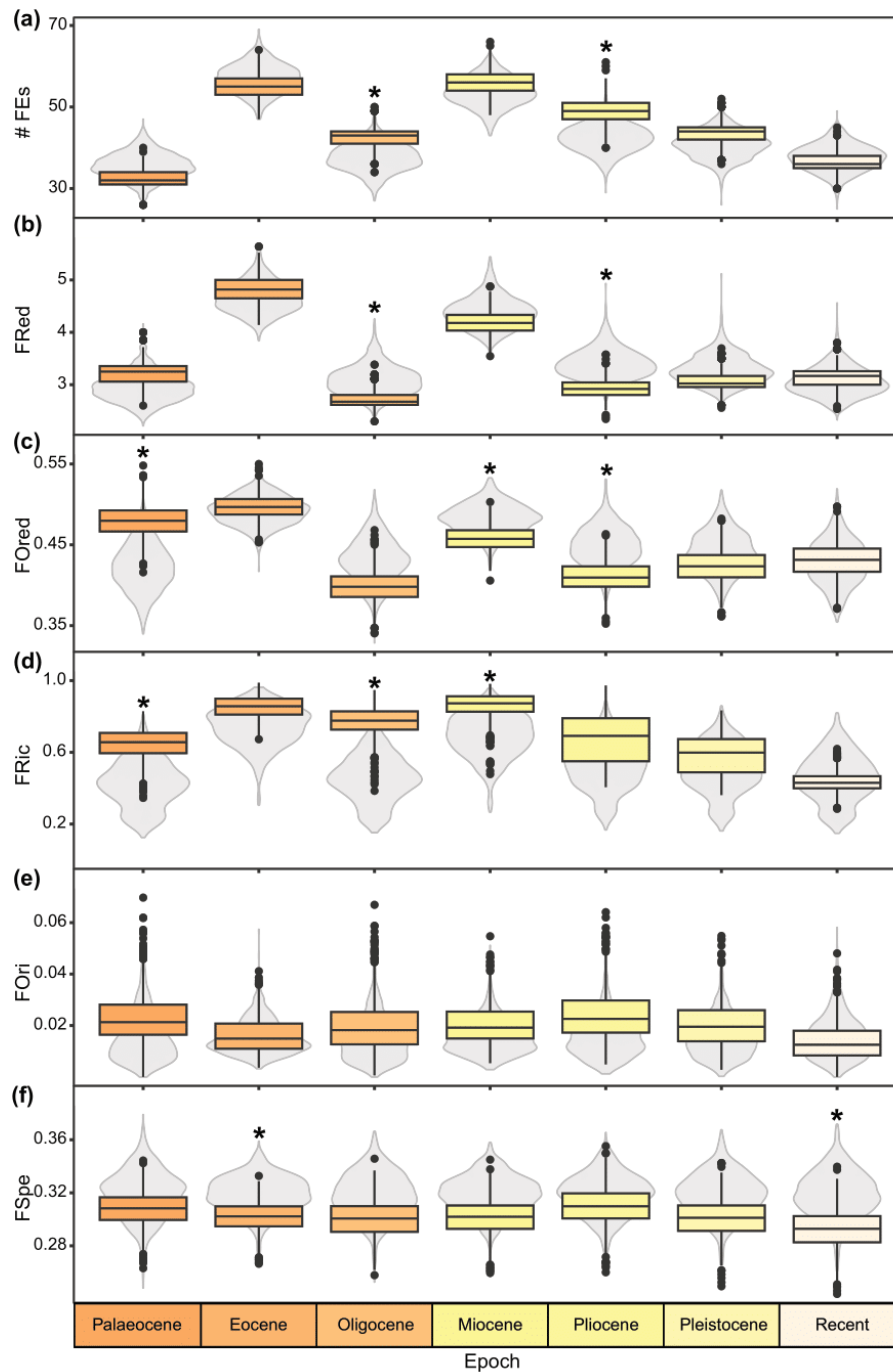
Figure 3.2. Changes in shark functional diversity through time. (a) number of functional entities (# FEs); (b) functional redundancy (FRed); (c) functional over-redundancy (FOred); (d) functional richness (FRic); (e) functional originality (FOri); and (f) functional specialisation (FSpe). Boxplots showcase values across 1,000 iterations in which random dental character combinations (i.e., FTUs; see Methods) were selected per taxon to account for intraspecific variation. Grey violin plots display the range of values from the null model across 1,000 iterations. See **Table 3.1** for all values per time bin. Asterisks denote significant deviations from null expectations.

Eocene

The Eocene (56-33.9 Ma) showcased a marked increase in FE richness and FRed, the latter reaching its highest Cenozoic value during this time (**Table 3.1**; **Figure 3.2**), specifically

during the middle Eocene (Lutetian; ~45 Ma; **Appendix Figure S2.6b**; **Appendix Table S2.7**). FRic also expanded, reaching near-maximum levels (**Table 3.1**; **Figure 3.1c**, **3.2d**), specifically in the late Eocene (Priabonian; ~35 Ma; **Appendix Figure S2.6d**; **Appendix Table S2.7**). FE richness, FRed and FSpe slightly deviated from null expectations, with FSpe being 5% lower than expected for the Eocene (**Table 3.2**, **Appendix Table S2.6**) and FE richness and FRed being 12% higher and 11% lower, respectively, than null expectations for the Priabonian (**Appendix Figure S2.6**; **Appendix Table S2.8**, **S2.9**). Together, these results indicate a significant rise in shark functional diversity during the Eocene, as indicated by the increase of FEs and FRic. Taxa were also slightly less specialised than expected which, together with the high levels of functional redundancy (maximum FRed), likely conferred the Eocene assemblage some level of ecological insurance.

The Eocene marked the warmest epoch in the Cenozoic (Zachos et al. 2001), which has been linked to increased productivity (Rabosky and Sorhannus 2009) and the emergence of marine mammals (Uhen 2007). These environmental and biotic changes likely enhanced habitat complexity and expanded prey availability for sharks (Ciampaglio et al. 2005), which may have, in turn, enabled the emergence of new ecological functions and facilitated functional space expansion (i.e., increasing FEs and FRic; **Table 3.1**). Indeed, it is during the Eocene that sharks feeding on high vertebrates start occupying the highest scores along PCoA2 (**Figure 3.1c**). Moreover, invertebrates and fishes – prey already available to sharks prior to this epoch – continued to diversify during the Eocene (Alroy et al. 2008, Guinot and Cavin 2016), potentially allowing functional redundancy to consolidate (i.e., peak FRed; decreasing FOri and FSpe; **Table 3.1**).

Table 3.2. *Z*-scores for all functional diversity metrics calculated, indicating how the empirical result of each metric differs from random chance expectations based on the number of taxa. All values are accurate to two decimal places. *Z*-scores marked in bold are considered statistically significant ($Z > |1.96|$), marking a value that falls outside of 95% of the null distribution. Abbreviations are as follows: FE = functional entities; FRed = functional redundancy; FOred = functional over-redundancy; FRic = functional richness; FOri = functional originality; FSpe = functional specialisation.

Epoch	FE	FRed	FOred	FRic	FOri	FSpe
Paleocene	-1.81	1.89	**3.33**	**2.91**	1.14	-1.06
Eocene	-0.91	0.88	0.36	1.60	0.16	**-1.98**
Oligocene	**2.59**	**-2.41**	-1.87	**4.12**	0.67	-1.67
Miocene	1.10	-0.95	**-2.25**	**2.38**	1.00	-1.77
Pliocene	**3.28**	**-2.98**	**-2.46**	1.66	1.37	-0.89
Pleistocene	1.43	-1.30	-1.07	0.99	0.82	-1.62
Recent	-0.74	0.75	0.18	-0.30	-0.34	**-2.24**

Oligocene

The Oligocene (33.9-23.03 Ma) experienced the largest declines of FE richness, FRed and FOred, the latter two hitting their lowest values of the Cenozoic at the epoch level (**Table 3.1**; **Figure 3.2a-c**). Despite these changes, FRic declined only by 8% (**Table 3.1**; **Figure 3.1d, 3.2d**), largely retaining the Eocene functional space, even at stage level (**Appendix Figure S2.6d**; **Appendix Table S2.7**). Meanwhile, FOri underwent its largest increase, signifying increased taxon isolation in trait space (**Table 3.1**; **Figure 3.2e**). Of all metrics, FE richness, FRed, FRic and FOred significantly deviated from null expectations (**Table 3.2**; **Appendix Table S2.9**). Specifically, FE richness and FRic were respectively 16% and 32% higher than expected, while FRed was 14% lower than expected (**Table 3.2**, **Appendix Table S2.6**). Similar deviations were also found in both Oligocene stages, though the FRic deviation was restricted to the early Oligocene (Rupelian; ~30 Ma), and FOred was 5% lower than expected only at the stage level (**Appendix Figure S2.6a-d**; **Appendix Table S2.8**). These results indicate that although the Oligocene shark assemblage experienced important redundancy losses (**Table 3.1**; **Figure 3.2**), there was not a significant reduction of ecological functions, as indicated by the FE and FRic values, which were higher than expected. Indeed, the relationship between FRic and taxonomic richness becomes more asymptotic as FRic approaches 80% (**Appendix Figure S2.7**). Interestingly, these changes in functional diversity did not result in the overrepresentation of some FEs, as indicated by the low FOred values (**Figure 3.2**, **Appendix S2.6c**), which were significantly lower than expected at stage level (**Appendix Table S2.8**, **S2.9**). The relative resilience of functional diversity during the Oligocene was likely the result of the ecological insurance reached during the Eocene. Nevertheless, functional redundancy was largely depleted during the Oligocene, as evidenced by the increase in FOri and decrease in FRed, the latter being lower than expected based on taxon numbers (**Figure 3.2**; **Table 3.2**). Overall, the results collectively suggest that the Oligocene shark functional diversity was somewhat buffered by the ecological redundancy reached in the Eocene, but the loss of this redundancy in the Oligocene (**Appendix Figure S2.6**), likely left the assemblage highly vulnerable.

During most of the Oligocene, the oceans were cooler than in the Eocene (Zachos et al. 2001), likely resulting in a decline in eustatic sea level (Miller et al. 2005, De Boer et al. 2010). These changes may have led to a reduction in the extent of coastal habitats for sharks and their prey (e.g., Pimiento et al. 2017) which could be linked to the declines in functional diversity (i.e., 22% decline in FE richness and 45% decline in FRed). However, the continued diversification

of fishes and marine mammals during this time (Uhen 2007, Guinot and Cavin 2016) may have ensured access to diverse prey, as evidenced by the lower-than-expected functional losses and the maintenance of most of the extent of functional space.

Miocene

In the Miocene (23.03-5.33 Ma), shark functional diversity displayed marked recoveries from the Oligocene: FE richness and FRic reached the maximum values of the Cenozoic (**Table 3.1**; **Figure 3.1e**, **3.2a-d**), with FRic being 17% higher than expected (**Table 3.2**, **Appendix Table S2.6**). These peaks in functional diversity were specifically observed in the early and middle Miocene (FEs peak in the Aquitanian-Burdigalian, 23.03-15.97 Ma; FRic peaks in the Aquitanian-Serravallian, 23.03-11.63 Ma; **Appendix Figure S2.6**, **Appendix Table S2.7**). In the late Miocene (Tortonian and Messinian; 11.63-5.333 Ma), however, shark functional diversity declined, as evidenced by a decrease in FEs and FRic (**Appendix Figure S2.6**; **Appendix Table S2.7**). Miocene functional redundancy metrics did not experience the same level of recovery as other functional diversity metrics. Although FRed increased from the Oligocene to the Miocene, values were lower than expected throughout most Miocene stages (**Appendix Figure S2.6**; **Appendix Table S2.8**, **S2.9**). Similarly, FOred increased in the Miocene, despite being lower than expected (**Figure 3.2**, **Appendix Figure S2.6**; **Table 3.2**, **Appendix Table S2.9**). When taken together, the results suggest that although shark assemblages exploited the maximum range of ecological functions in the early and middle Miocene, they did not necessarily increase their ecological resilience due to their lower-than expected functional redundancy and high over-redundancy (**Appendix Figure S2.6**; **Appendix Table S2.7-S2.9**).

The Miocene epoch was a time of large environmental and biological changes. Temperatures were relatively high throughout the early and middle Miocene (Zachos et al. 2001), resulting in increased eustatic sea level (De Boer et al. 2010) and ocean productivity (Marx and Uhen 2010). Consequently, cetaceans diversified, reaching their highest diversity in the Tortonian (lower late Miocene; ~10 Ma; Marx and Uhen 2010). Although these conditions became volatile from the late Miocene onwards, overall, the first half of the Miocene provided sharks warm temperatures and, importantly, diverse, large prey. These favourable conditions likely enabled the larger-than-expected expansion of the functional space, with the Miocene being the epoch with the largest space occupation of the entire Cenozoic, (i.e., FRic = 87%; **Table 3.1**). Some of this expansion was driven by the appearance of new, highly specialised species,

specifically, the largest macropredatory shark that has ever lived, †*O. megalodon*, which likely preyed upon marine mammals (e.g., Collareta et al. 2017, Godfrey et al. 2021, Godfrey and Beatty 2022) and sits at the extreme of PCoA1 (**Figure 3.1a**, **e**).

Pliocene

Pliocene (5.33-2.58 Ma) sharks experienced dwindling FE richness, FRed, FOred, and FRic relative to the Miocene (**Table 3.1**, **Appendix Table S2.7**; **Figure 3.1f**, **3.2a-d**, **Appendix Figure S2.6**). Notably, Pliocene sharks experienced the highest loss of functional space of the entire Cenozoic (i.e., 18% loss; **Table 3.1**). Moreover, taxa became more isolated in and occupied extreme positions of the trait space, as denoted by rising FOri and FSpe, which reached their maximum Cenozoic values (**Table 3.1**, **Appendix Figure S2.7**; **Figure 3.2**, **Appendix Figure S2.6**). From these metrics, FE richness, FRed and FOred exceeded null expectations (**Table 3.2**). FE richness was 17% higher than expected, while FRed and FOred were respectively 14% and 4% lower than expected (**Table 3.2**, **Appendix Table S2.6-S2.9**; **Appendix Figure S2.6a-c**). Together, these results suggest that the number of shark ecological functions (FEs) and functional redundancy (FRed) diminished in the Pliocene, with taxa becoming more functionally specialised than in any other time bin (**Table 3.1**; **Figure 3.2f**). Despite these changes being less dramatic than expected, the Pliocene assemblage was likely highly vulnerable to further losses.

From the late Miocene and throughout the Pliocene, ocean temperature, productivity, eustatic sea levels and the extent of coastal habitats underwent significant fluctuations, with an overall trend of decline (Zachos et al. 2001, Miller et al. 2005, De Boer et al. 2010, Marx and Uhen 2010, Pimiento et al. 2017). Cetacean diversity largely mirrored this trend, with an initial increase in the early Pliocene (Zanclean; ~4.5 Ma) and a dramatic decrease towards the late Pliocene (Piacenzian; ~3 Ma; Marx and Uhen 2010, Pimiento et al. 2017). These changing conditions likely resulted in limited prey availability for sharks, potentially explaining the loss of functional diversity observed in the Pliocene, specifically the contraction of trait space along PCoA2 (**Figure 3.1f**), which is mostly related with a prey preference for high vertebrates (**Appendix Table S2.2**).

Pleistocene

In the Pleistocene (2.58-0.01 Ma), FE richness and FRic continued to decline from the Pliocene, while FRed and FOred maintained Pliocene levels (**Table 3.1**; **Figure 3.1g**, **3.2**). All

functional diversity metrics maintained similar values throughout all stages of the Pleistocene (**Appendix Figure S2.6**; **Appendix Table S2.7**). Moreover, no metric deviated from null expectations at either epoch or stage level (**Table 3.2**, **Appendix Table S2.9**). Overall, these results suggest that the Pleistocene shark functional diversity represents a continuation from the Pliocene assemblage, with functional diversity remaining as expected given the losses from the previous epoch.

The Pleistocene oceans experienced violent temperature and sea level oscillations (Zachos et al. 2001, Miller et al. 2005, De Boer et al. 2010), which resulted in ample fluctuations of neritic area available, and ultimately, a significant decrease of the extent of productive coastal habitats (Pimiento et al. 2017). It has been proposed that these area changes were key drivers in the extinction of one third of the marine megafauna in the Plio-Pleistocene transition, which mostly affected homeothermic animals, including mesothermic sharks (Pimiento et al. 2017). Indeed, the giant macropredator †*O. megalodon* became extinct during this event, specifically in the late Pliocene (Pimiento and Clements 2014, Boessenecker et al. 2019). Although most of the functional space had already been lost by the Pliocene, the extinction of †*O. megalodon* resulted in further loss of trait space, particularly along PCoA1 and PCoA2, which, combined, represent the ecological role of a super predator (Cooper et al. 2022, Kast et al. 2022).

Recent

In the Recent sample, FE richness continued to decrease, while FRed and FOred largely retained Pleistocene values (**Table 3.1**; **Figure 3.2a-c**). Meanwhile, FRic, FOri and FSpe reached their lowest Cenozoic values (**Table 3.1**; **Figure 3.1h**, **3.2e-f**, **Appendix Figure S2.6d**; **Appendix Table S2.7**). FSpe and FRic were the only metrics significantly deviating from null expectations, FSpe at the epoch level (**Table 3.2**, **Appendix Table S2.6**) and FRic at the stage level (**Appendix Figure S2.6**; **Appendix Table S2.9**). My sampling bias assessments revealed that the FRic decline in the Recent is not likely to be a sampling artefact. Specifically, when assessing whether my findings are the result of the degradation of the Recent (see Methods), I found that the inclusion of present-day species without a fossil record (i.e., the "Recent-plus" sample) does not extend the space occupied in this time bin (**Appendix Figure S2.8**), nor does it when resampling the "Recent-plus" based on the degraded Recent sample size ("resampled Recent-plus"; **Appendix Figure S2.8**). Indeed, the "Recent-plus" FRic was significantly lower than expected ($Z = -4.56$; **Appendix Figure S2.8**). As such, the FRic found based on empirical data is a conservative estimate. Furthermore, when assessing the space occupied by the

degraded Recent sample in a functional space built using the total extant diversity (see Methods), I found that the degraded Recent sample occupies 98% of the modern functional space and includes the most functionally specialised living species (**Appendix Figure S2.9**). This indicates that my Recent sample largely captures the extent of ecological functions of modern sharks. Finally, the decline in FRic in the Recent was significantly different than expected based on random taxonomic loss (**Appendix Figure S2.7**). Indeed, the loss of taxa from the Pleistocene to the Recent was expected to approach Paleocene values based on simulations of randomised taxonomic loss (FRic = ~60%; **Appendix Figure S2.7**), instead of the values found empirically (FRic = 43%; **Figure 3.2**, **Appendix Figure S2.6**).

Taken together, my results suggest that although shark taxa are less isolated in trait space in the Recent than in the Pleistocene (i.e., decreased FOri and FSpe), the Recent sample occupied less than half of the Cenozoic functional space (FRic = 43%), a level of FRic not even seen in the Paleocene after the K/Pg extinction (**Figure 3.1**; **Table 3.1**), which is a conservative estimate based on tests (see above). As such, shark functional diversity is potentially depleted today compared with the last ~66 Myr. Considering the losses of shark functional diversity since the late Miocene, this level of ecological loss appears to be the continuation of a long-term decline (**Figure 3.1f-h**, **3.2**). Nevertheless, the extent of functional space of the Recent is markedly diminished compared with the Pleistocene, especially along PCoA2. This erosion of functional space resulted from the loss of †*Dalatias sp.* an extinct form of kitefin shark, which represents the ecological role of deep-water species potentially specialised in preying upon large fish (Navarro et al. 2014). Although the functional space of the Recent sample provides a useful comparison with the geological past and with modern assemblages (see Methods and above), it is still a subsample of the current shark functional diversity. Nevertheless, when examining vertices of the Recent functional space, we can identify the species holding the extremes of the functional volume still preserved from the geological past. These include the bluntnose sixgill shark (*Hexanchus griseus*; IUCN Red List status = Near Threatened) and the Iceland catshark (*Apristurus laurussonii*; IUCN = Least Concern)*,* which preserve the remains of the highest and lowest values along the Cenozoic PCoA1. Similarly, the horn shark (*Heterodontus francisci*; IUCN = Data Deficient) and the great white shark (*Carcharodon carcharias*; IUCN = Vulnerable) preserve the lowest and highest ends along the Cenozoic PCoA2. Finally, the tiger shark (*Galeocerdo cuvier*; IUCN = Near Threatened) and the short-tail nurse shark (*Pseudoginglymostoma brevicaudatum*: IUCN = Critically Endangered; IUCN 2023) preserve the extreme portions of the Cenozoic functional space along PCoA3 (**Appendix**

Figure S2.10). The protection of these species could potentially complement current recommendations for the conservation shark functional diversity (Pimiento et al. 2023).

The rise and fall

Collectively, my tooth-based analyses revealed that shark functional diversity was generally high in the Cenozoic past (i.e., FRic = 60-87%) compared with the Recent (i.e. FRic =43%). This diversity experienced fluctuations through time, with peaks in the Eocene and Miocene (**Table 3.1**; **Figure 3.1**, **3.2**), and a steady decline from the late Miocene onwards. All functional diversity changes over time were significantly different across consecutive time bins, as evidenced by pairwise statistical comparisons (Mann-Whitney U-tests; $P \leq 0.01$; **Appendix Table S2.10**). My results are robust in the face of sampling artefacts, different trait treatments, and uneven time bin durations. Specifically, my functional diversity estimates do not appear to be affected by uneven sampling (**Appendix Figure S2.5**), or by the removal of individual traits (**Appendix Figure S2.11**), and were upheld when analysed at the stage level (**Appendix Figure S2.6**). Lastly, my estimates of Recent FRic appear to be largely conservative and to capture the extent of functions of the modern assemblage (**Appendix Figure S2.8**, **S2.9**).

This study does not allow me to establish the causal mechanisms behind the observed changes in functional diversity. However, fluctuations in global temperature, productivity, sea level, and prey availability largely coincide with the rise and fall of shark functional diversity. Despite the environmental fluctuations of the Cenozoic era, the overall trend of the last ~66 Myr has been of cooling (Zachos et al. 2001, Burke et al. 2018). Today, however, modern shark communities are encountering markedly different conditions, with ocean temperatures rapidly increasing due to human-produced greenhouse gas emissions (Smith et al. 2015). Future projections suggest that under unmitigated scenarios, temperatures by the year 2150 could resemble those of the Eocene epoch, potentially reversing a 50-million-year cooling trend in less than 200 years (Burke et al. 2018). Although I found that functional diversity peaks coincided with global warming events in the geological past, studies indicate that modern sharks are being adversely affected by anthropogenic global warming and ocean acidification (Rummer et al. 2022). Specifically, critical habitats for shark survival, such as coral reefs and nursery areas are diminishing, and shark native ranges are becoming less suitable (Dulvy et al. 2021, Coulon et al. 2024). Nevertheless, these oceanographic changes are not the primary threat to sharks today; instead, overfishing is directly driving around 40% of living shark species

towards extinction (Dulvy et al. 2021, Pimiento et al. 2023). Understanding the mechanisms shaping shark functional diversity across evolutionary timescales requires careful consideration of multiple confounding factors and their interactions, presenting a promising avenue for future research.

Which species had the largest contributions to functional diversity?

Extinct vs. extant

I found no clear difference between mean functional originality (FOri) and specialisation (FSpe) of extinct vs. extant sharks (Welch two sample t-test; FOri: t = 0.046, df = 208.01, p = 0.96; FSpe: t = -0.9, df = 212.81, p = 0.37; **Figure 3.3a**, **c**). However, there were several high-scoring outliers in the FSpe distribution, almost all of which are extinct (**Figure 3.3c**). Moreover, these outliers were not found to deviate from the FSpe distribution by chance (Two-sided 90th quantile permutation tests; P = 0.016, see Methods). As such, extinct sharks spanned a considerably wider range of the functional space (FRic = 98.7%) than extant sharks (FRic = 43%; **Figure 3.1i**, **Appendix Figure S2.4a**). Indeed, the highest and lowest scoring species of all three functional axes were extinct (**Figure 3.1a**).

Ranking the top 5% FOri and FSpe taxa further revealed that most of these taxa were extinct (**Figure 3.3b**, **d**). This included the top six FOri and the top 20 FSpe taxa. Interestingly, seven of the top ten FSpe taxa (**Figure 3.3d**) belonged to a single genus: †*Otodus* (i.e., the "megatoothed" sharks), a clade well known for their gigantic body sizes (8-20 m long) and high trophic levels (Cooper et al. 2022, Kast et al. 2022). It can thus be inferred that the †*Otodus* clade performed a specialised ecological function during the Cenozoic; a function that would have been lost in the Pliocene following the extinction of its last surviving species, †*O. megalodon* (Pimiento and Clements 2014, Pimiento et al. 2016, Boessenecker et al. 2019, Kast et al. 2022). Together, these results indicate that extinct species disproportionally contributed to Cenozoic shark functional diversity, more so than their extant counterparts (**Figure 3.1i**, **3.3**), largely explaining the diminishing of functional diversity in the Recent when compared to the past (**Figure 3.2**, **Appendix Figure S2.6**).
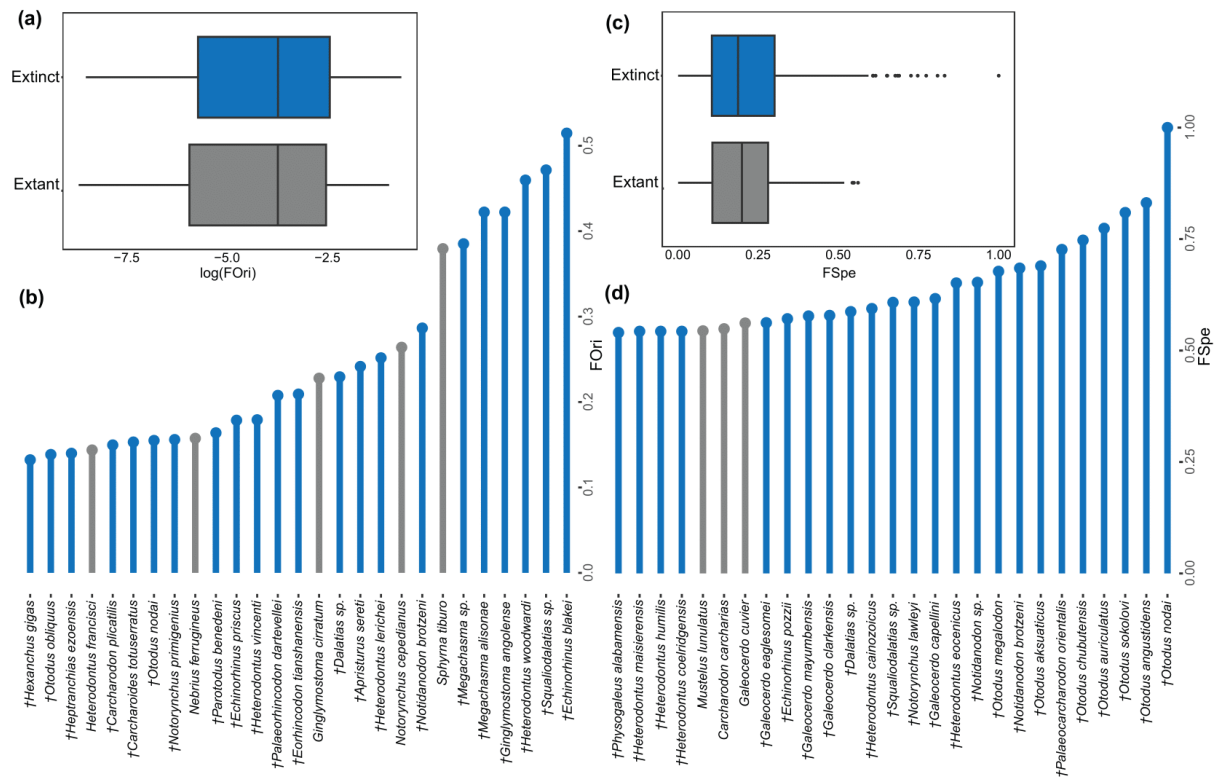
Figure 3.3. Functional originality (FOri) and specialisation (FSpe) of extinct and extant Cenozoic sharks. (a) mean FOri, log transformed for visualisation; (b) top 5% FOri taxa; (c) mean FSpe; (d) top 5% FSpe taxa. Taxa are coloured based on their status as extinct (blue) or extant (grey).

Functionally original taxa

In the Paleocene, the highest scoring FOri taxon was an extinct kitefin shark †*Squaliodatalias* sp., which occupied the lower end of PCoA1 and PCoA2 (**Figure 3.1b**), denoting small, smooth, and piercing teeth with lateral cusplets. Based on Cooper et al. (2023), this indicates a prey preference for invertebrates and a clutching feeding mechanism. The Eocene's highest scoring FOri species was an extinct bullhead shark †*Heterodontus woodwardi*, which occupied intermediate trait values along PCoA1, and the lowest values along PCoA2 (**Figure 3.1c**). This represents small, semi-circular teeth with no lateral cusplets or cutting edge, typical of a crushing feeding mechanism and a hard-shelled invertebrate prey preference seen also in its living representatives (Hovestadt 2018, Cooper et al. 2023). The extinctions of †*Squaliodalatias* sp. and †*H. woodwardi* did not result in gaps in the functional space as close neighbours playing similar ecological roles survived (**Figure 3.1b-d**). The most functionally original taxon of the Oligocene was †*Dalatias* sp., a kitefin shark which occupied intermediate trait values along PCoA2 (**Figure 3.1e**), marking medium-sized teeth with serrated cutting edges and thus suggesting a medium body size and prey preference for fishes (Cooper et al. 2023). Today, there is a single extant species of this genus, *Dalatias licha*, which occupies a

high trophic level due to being able to occasionally take bites out of prey larger than itself (Navarro et al. 2014). Although *D. licha* has a fossil record dating as far back as the Eocene (Paillard et al. 2020), †*Dalatias* sp. differed in space by occupying higher trait values along PCoA2, implying larger, more heavily serrated teeth (Cooper et al. 2023). I therefore consider this taxon extinct and separately from its living counterpart. This taxon persisted into the Pleistocene, but its absence from the Recent sample left a significant gap in the functional space (Figure 1g, h), indicating the loss of a distinct ecological role played by mid-sized deep-sea predators.

The highest scoring FOri species in the Miocene and Pliocene was an extinct bramble shark †*Echinorhinus blakei*, which was also the most functionally original of the whole Cenozoic (**Figure 3.3b**). This species occupied low trait values along PCoA1 (**Figure 3.1e**, **f**), denoting piercing longitudinal outlines and lateral cusplets, and indicating a clutching and grasping feeding mechanism (Cooper et al. 2023). However, this species also occupied intermediate values along PCoA2, marking smooth cutting edges and medium crown heights, implying a medium body size and a prey preference of fishes (Cooper et al. 2023). Indeed, Echinorhiniformes was the order with the highest mean FOri (**Appendix Figure S2.12a**). Both extinct and extant echinorhiniforms are poorly studied (Bogan and Agnolín 2022), but the order is known for medium to large body sizes (reaching 4-4.5 m long) and suction feeding (Ebert et al. 2021). Notably, the extinction of †*E. blakei* between the Pliocene and Pleistocene left a gap in the shark functional space (**Figure 3.1g**, **h**), indicating the loss of an ecological role played by medium-sized suction feeders. A megamouth shark, †*Megachasma* sp., was the most functionally original taxon of the Pleistocene, and occupied low PCoA1 values (**Figure 3.1g**), denoting teeth with lateral cusplets and piercing longitudinal outlines and thus a clutching or vestigial morphology, typical of a filter feeding mechanism (Cooper et al. 2023). The space left by †*Megachasma* sp. was retained in the Recent by close neighbours with similar ecological roles. The highest scoring FOri species of the Recent sample was the bonnethead shark *Sphyrna tiburo*. This species occupied intermediate trait values along PCoA1 and the lowest values along PCoA2 (**Figure 3.1h**), indicating small, semi-circular teeth with no cutting edge or lateral cusplets, and thus suggesting crushing feeding and prey preferences of invertebrates (Cooper et al. 2023), in line with the species' known ecology (Mara et al. 2010, Leigh et al. 2018).

Overall, these results suggest that mid-sized sharks feeding on invertebrates and fishes displayed high FOri values, and thus were highly isolated in trait space through time. The

Pliocene extinction of †*E. blakei*, a presumed mid-sized suction feeder, and the Pleistocene extinction of †*Dalatias* sp., a presumed mid-sized piscivore, left the largest gaps in the trait space.

Functionally specialised taxa

The highest scoring FSpe taxa of the Paleocene and Eocene epochs were †*Palaeocarcharodon orientalis* and †*Otodus nodai,* respectively, with †*O. nodai* also being the most functionally specialised species of the Cenozoic (**Figure 3.1b**, **c**, **3.3d**). These species sat in the upper end of PCoA2 (**Figure 3.1c**, **d**), denoting a prey preference for high vertebrates based on their large and serrated teeth (Cooper et al. 2023). The extinction of these species did not result in the loss of functional space, as other taxa playing similar macropredatory ecological roles occupied neighbouring sections of the space (**Figure 3.1b-d**). The highest scoring FSpe species of the Oligocene and Miocene was †*O. angustidens*, which was a close neighbour of †*O. nodai* from the Eocene (**Figure 3.1d**, **e**) and had an inferred prey preference of high vertebrates (Cooper et al. 2023). The extinction of this species in the Miocene resulted in the loss of the highest trait values along PCoA2 (**Figure 3.1e**, **f**). †*O. megalodon* was the highest FSpe species of the Pliocene, occupying the highest end of PCoA1 (**Figure 3.1f**). This marks triangular teeth with no lateral cusplets and thus a cutting feeding mechanism (Cooper et al. 2023). †*O. megalodon*'s extinction in the Pliocene left a notable gap in the Pleistocene trait space (**Figure 3.1f**, **g**). Overall, the extinctions of the different †*Otodus* species in the Miocene and Pliocene resulted in the loss of ecological roles played by giant apex predators. The highest FSpe taxon of the Pleistocene was †*Dalatias* sp. (**Figure 3.1g**), which occupied the highest remaining values along PCoA2. The absence of this taxon in the Recent suggests a further loss of predatory ecological roles (**Figure 3.1g**, **h**). This left the tiger shark *Galeocerdo cuvier* as the most functionally specialised species of the Recent, which occupied high values along PCoA1 (**Figure 3.1h**), marking teeth with polygonal longitudinal outlines and no lateral cusplets; and a cutting feeding mechanism (Cooper et al. 2023).

The most functionally specialised taxa of the Cenozoic belong to the orders Squaliformes (†*Dalatias* sp.), Carcharhiniformes (*G. cuvier*), and Lamniformes (†*P. orientalis* and †*Otodus* spp.). While none of these orders had the highest mean FSpe scores, all had high-ranking outliers represented by the above-mentioned taxa and others, particularly Lamniformes (**Appendix Figure S2.12b**). These results collectively indicate that the Miocene-Pliocene extinctions of †*Otodus* species, followed by the Pleistocene extinction of †*Dalatias* sp. (i.e.,

the reduction of the *Dalatias* genus to a single living species; *D. licha*), were probable drivers of functional diversity losses between the Miocene and the Recent.

Overall, when examining the contributions of individual taxa to the Cenozoic functional diversity, my results revealed that (1) extinct sharks spanned a larger extent of the functional space and were generally more functionally distinct than extant sharks (**Figure 3.1i**, **3.3**); and (2) specialised suction feeders, mid-sized deep-sea predators and gigantic apex predators were important contributors to functional diversity, with their Miocene-Pleistocene extinctions resulting in losses inside the functional space, likely explaining the overall decline of functional diversity from the late Miocene onwards (**Figure 3.1f-h**, **3.2**, **Appendix Figure S2.6**).

3.5   Conclusions

My tooth-based analyses revealed that shark functional diversity was generally high throughout most of the Cenozoic (e.g., FRic > 60%; **Table 3.1**), peaking at 86-87% FRic in the Eocene and Miocene (56-33.9 and 23.03-5.333 Ma; **Figure 3.1c**, **e**, **3.2d**, **Appendix Figure S2.6**). Despite the loss of species in the K/Pg (Kriwet and Benton 2004, Guinot and Condamine 2023), shark functional diversity was higher than expected between the Paleocene and Miocene epochs (FRic Z > 1.96 in the Paleocene, Oligocene, and Miocene; **Table 3.2**). However, I found that shark functional diversity has steadily declined since its Miocene peak, with 44% of FRic being lost between then and the present (**Table 3.1**, **Appendix Table S2.7**; **Figure 3.1e-h**, **3.2d**, **Appendix Figure S2.6d**). Consequently, shark functional diversity today is likely diminished compared with the Cenozoic past. Indeed, I found that extinct sharks inordinately contributed to functional diversity compared with extant sharks (**Figure 3.1i**, **3.3**). The functional diversity decline from the late Miocene onwards was likely driven by the loss of giant apex predators (i.e., †*Otodus* spp. in the Miocene and Pliocene), suction feeders (e.g., †*Echinorhinus blakei* in the Pliocene) and deep-sea sharks at high trophic levels (i.e., the extinction of †*Dalatias* sp. in the Pleistocene). Today, sharks rank among the most imperilled marine vertebrates on Earth, with overfishing emerging as the primary driver of extinction (Dulvy et al. 2014, Stein et al. 2018, Dulvy et al. 2021). My findings forewarn that ongoing anthropogenic-driven shark declines might be eroding an already diminished functional diversity. Current recommendations to safeguard elasmobranch functional diversity include the identification of functionally unique, specialised, and endangered species, as well as the areas harbouring hotspots of functional diversity (Pimiento et al. 2023). This study further highlights the modern shark species holding some of the Cenozoic functional space, potentially complementing our knowledge on the current priorities for the preservation of shark functional diversity in the changing world.

Chapter 4 | Poleward shift and functional decline of sharks and rays under future extinctions

This work is in preparation for publication.

4.1   Abstract

Elasmobranchs (sharks, rays and skates) are among the most imperilled marine vertebrates on Earth, with over one-third of their species at risk of extinction, primarily due to overfishing. Simultaneously, elasmobranch populations are widely predicted to shift their spatial ranges poleward by 2100 due to human-induced climate change. Despite these threats, their future impacts on global elasmobranch functional diversity are yet to be investigated. Here, based on extinction simulations, I quantify future changes in elasmobranch functional diversity, identify the projected extinctions by 2100 that will have the biggest ecological impacts, and assess global spatial shifts in functional diversity by 2100 under extinctions and climate change. Simulated extinction scenarios projected marked declines in functional diversity over the next 500 years. Alarmingly, the most functionally unique and specialised (FUS) species of utmost importance for maintaining functional diversity were found to have the greatest extinction risk by 2100, with the extinctions of two iconic and distinct shark species – the whale shark and the Greenland shark – predicted to have the largest ecological impacts. On top of this, more than half of the ten highest-scoring FUS species were forecast to become extinct within the next 200 years. Finally, my spatial analyses indicated depletions of functional diversity across coastal and tropical habitats, at greatest risk from overfishing and climate change, by 2100. High latitudes were projected to gain functional diversity, signifying a poleward shift of ecological functions as well as species. However, a near-worldwide increase in functional uniqueness was detected, suggesting reductions of elasmobranchs sharing ecological functions in virtually every marine habitat and thus rendering global elasmobranch functional diversity highly susceptible to further extinctions beyond 2100. Swift action to curb overfishing and climate change is urgently needed to prevent the potential collapse of elasmobranch functional diversity and thus the ecological compromising of oceans worldwide.

4.2 Introduction

Sharks, rays and skates (elasmobranchs) are a highly diverse and evolutionarily distinct group of marine vertebrates, with over 1,000 living species distributed across nearly all marine habitats (Weigmann 2016, Stein et al. 2018). Importantly, elasmobranchs also contribute a wide range of critical ecological functions (Dedman et al. 2024). For example, elasmobranchs can affect marine ecosystem functioning by: (1) consuming large quantities of biomass and thus potentially restructuring trophic communities via direct or indirect top-down predation effects (Myers et al. 2007, Hammerschlag et al. 2019; but see Desbiens et al. 2021); (2) simultaneously serving as both a consumer of lower trophic level organisms and prey to higher level predators (Roff et al. 2016, Navia et al. 2017); or (3) transporting nutrients within individual habitats or between long-distance habitats via migration (Doughty et al. 2016, Roff et al. 2016, Williams et al. 2018). However, despite this widespread ecological importance, over a third of today's elasmobranch species are at risk of extinction, with overfishing being the overwhelmingly primary cause of this risk (Dulvy et al. 2021). Indeed, recent research has suggested that increased fishing pressure has led to a ~71% abundance decline of oceanic elasmobranchs since ~1970 (Pacoureau et al. 2021). Worryingly, the global overfishing mortality of elasmobranchs has continued to increase over the last decade despite protective regulations being introduced (Worm et al. 2024). Given their range of ecological roles, this widespread loss of elasmobranchs is likely to disrupt marine ecological processes on a near-worldwide scale.

While overfishing is the main direct threat to elasmobranchs, their populations are also expected to be globally redistributed in the near-future due to anthropogenically induced climate change (Dulvy et al. 2021). Human-produced greenhouse gas emissions have led to rapid increases in ocean temperature (Smith et al. 2015). This has made native ranges of elasmobranchs, including critical areas like nurseries, less habitable, particularly in coral reefs and the tropics (Dulvy et al. 2021, Rummer et al. 2022, Coulon et al. 2024). Several studies have attempted to predict future distribution of individual elasmobranch species under climate change (i.e., generally in the years 2050-2100) using environmental climate modelling and have universally found that their spatial ranges are likely to shift polewards (e.g., Sequeira et al. 2014, Birkmanis et al. 2020, Diaz-Carballido et al. 2022). In fact, some of these range shifts are already being documented today. For example, large elasmobranchs such as the great white (*Carcharodon carcharias*) and tiger sharks (*Galeocerdo cuvier*) have been found to have expanded their spatial ranges poleward due to ocean warming in the last decade (Tanaka et al.

2021, Hammerschlag et al. 2022). More recently still, three smalltooth sandtiger sharks (*Odontaspis ferox*) were recorded in UK and Irish waters in 2023 despite no prior records, a northerly shift of three degrees of latitude suspected to be climate-induced (Curnick et al. 2023). An understanding of how the collective shifts of elasmobranchs could affect global marine ecosystem functioning in the future is currently lacking, particularly in combination with projected extinctions due to factors like overfishing that are considered much graver threats to elasmobranchs than climate change (Dulvy et al. 2021, Jorgensen et al. 2022).

Although ongoing taxonomic declines and range shifts of elasmobranchs are well documented (e.g., Ferretti et al. 2010, Roff et al. 2018, Pacoureau et al. 2021, Hammerschlag et al. 2022), their ecological functions, and thus how they contribute to marine ecosystems, are dictated by functional traits (Mouillot et al. 2013b, Gagic et al. 2015). These traits, including body size, diet and habitat among others, broadly reflect how species acquire and transport resources across systems (Mouillot et al. 2013b). The diversity of these traits, functional diversity, is therefore a fundamental dimension of biodiversity. This can be quantified based on how species are distributed in a multidimensional functional space defined by traits (Villéger et al. 2008, Mouillot et al. 2013b). Such an approach allows the calculation of three important facets of functional diversity: (1) the variety of ecological functions based on the occupied volume of functional space (i.e., functional richness); (2) the distance of species from their nearest neighbours in space, which identifies which species are most dissimilar to others (i.e., functional uniqueness); and (3) the distance of species from the centroid of the space, which reveals which species have the most extreme trait values on the edge of space (i.e., functional specialisation; Mouillot et al. 2013b). Identification of the most functionally unique and specialised elasmobranchs critically reveals which species contribute the most to ecosystem functioning (Griffin et al. 2020, Pimiento et al. 2020b, Pimiento et al. 2023), yet the relative impact of their purported extinctions is yet to be evaluated.

Previous works exploring the functional diversity of elasmobranchs have shown that they are expected to suffer the largest losses among the marine megafauna (>45 kg) if current trajectories assessed by the IUCN Red List (IUCN 2023) are maintained (Pimiento et al. 2020b). However, overfishing can simultaneously cause declines of elasmobranchs across multiple trophic levels and ecological roles rather than only the largest species, as recorded in habitats such as coral reefs (Roff et al. 2016, Desbiens et al. 2021), forewarning widespread ecological consequences. The spatial range of present-day elasmobranch functional diversity has also been investigated, both in specific regions (Siders et al. 2022) and across the entire

world (Pimiento et al. 2023). The global study found that today's elasmobranch functional diversity is not only acutely vulnerable due to threatened species occupying a greater extent of functional richness than non-threatened species; but also inadequately protected from overfishing by the global network of marine protected areas (MPAs; Pimiento et al. 2023). Moreover, analysis of the shark fossil record indicates that today's elasmobranchs already have a diminished functional diversity compared to their geological past (Cooper and Pimiento 2024). Together, these past works suggest grave peril for elasmobranch functional diversity. Given this, it is imperative to understand how future elasmobranch extinctions, and climate-induced redistribution, could influence their remaining functional diversity, and thus their ability to retain global ecological functioning.

Here, I simulate future elasmobranch extinctions and combine this with functional traits from earlier work (Pimiento et al. 2023) to predict future temporal and spatial effects on functional diversity. I use the year 2100 as a baseline extinction scenario due to its common use in climate modelling (e.g., Gissi et al. 2023, Hodapp et al. 2023). First, I simulate future extinction scenarios, quantify resulting changes in functional diversity, and compare them against null expectations. I then identify species whose extinctions by 2100 would have the largest ecological effects based on their combined functional uniqueness and specialisation. Finally, I assess global spatial shifts in elasmobranch distribution by 2100 under climate change and simulated extinctions and the resulting effects on functional diversity. My results reveal the potential ecological consequences of future elasmobranch extinctions, and climate-induced range shifts, on a global scale.

4.3   Materials and Methods

All analyses were conducted in the R environment version 4.2.2 (R Core Team 2017). IUCN simulations and functional diversity analyses were done via the Supercomputing Wales Project (https://www.supercomputing.wales/; Redfern 2013).

Future extinction scenarios

In order to simulate future extinction scenarios, I first downloaded a list of Chondrichthyes species (i.e., cartilaginous fishes) and their threat statuses (i.e., Data Deficient, DD; Least Concern, LC; Near Threatened, NT; Vulnerable, VU; Endangered, EN; Critically Endangered, CR) from the IUCN Red List of Threatened Species (www.iucnredlist.org/; last accessed November 2023). I then checked all species names and contrasted them against the taxonomic nomenclature of Weigmann (2016), allowing me to merge or eliminate synonyms. This was done using the *rredlist* version 0.7.2 (Gearty et al. 2022) and *janitor* version 2.2 packages (Firke et al. 2023). I removed all chimeras from the data, producing an initial dataset of 1,181 species.

I simulated yearly future extinctions for all elasmobranch species in my dataset over the next 500 years using the *iucnsim* package (version 0.0.0.9000; Andermann et al. 2021). To perform this, I first downloaded the "Chondrichthyes" reference list directly from the package, as well as the corresponding Red List history, that is, historic status changes per species between 1990 and 2019. I then updated the Red List history file by inserting present-day (i.e., 2023) status. Based on these inputs, the *iucnsim* program can predict future status in two models: (1) based on extinction probabilities assigned to all species sharing an IUCN status (sensu Mooers et al. 2008); or (2) based on empirical status transitions within the Red List history file per species (sensu Monroe et al. 2019), which characterises potential future transitions away from current threat status (i.e., from VU to EN or vice versa) with a Markov-Chain Monte Carlo (MCMC) algorithm (Andermann et al. 2021). Both models come with their own assumptions that need to be considered. The first assumes the same chance of extinction for all species with the same IUCN status in a given future, which does not necessarily consider external factors affecting species with different ecologies and life-histories that may influence extinction probability (Andermann et al. 2021, Pavoine and Ricotta 2023). *Iucnsim* accounts for this by tailoring generation length, but such data are not readily available for elasmobranchs (Mull et al. 2022). The second model, meanwhile, allows for unique, species-specific, extinction probabilities due to relying on past IUCN status changes, but does not yet discriminate between status changes due to taxonomic changes, improved knowledge of a given species, or actual changes to its

populations (Andermann et al. 2021, Ali et al. 2022, Pavoine and Ricotta 2023). Moreover, due to an inherent time lag between a species extinction and the registration of this by the IUCN, it is likely that extinction probabilities may be underestimated (Andermann et al. 2021). As such, both models have notable limitations that I acknowledge here. Due to status transitions being (1) more readily available than generation length data; and (2) providing species-specific extinction probabilities; I selected the second model for the simulation analyses.

I estimated status transition rate and simulated future status, performing these simulations 10,000 times to increase accuracy of extinction times (i.e., how many years it takes for IUCN status to transition to EX; extinct) for species with low extinction probabilities, as recommended by the *iucnsim* package (Andermann et al. 2021). For data deficient species, *iucnsim* samples 100 transition rates for all transition types to draw a probable threat status (Andermann et al. 2021). Correcting for data deficiency is important for simulating extinctions as it has been suggested that many data deficient elasmobranch species likely have a high probability of extinction risk (Walls and Dulvy 2020). Although the study period spanned 500 years into the future, the simulations were performed up to 1,000 years into the future to establish a comprehensive distribution of extinction times and minimise the risk of any influence of potential artefacts like edge effects (e.g., Willmer et al. 2022).

From the simulated future in IUCN status changes, I extracted the estimated times of extinction per species per simulation to form six extinction scenarios. The first was based on simulated extinctions by the year 2100, simulated as 77 years in the future from 2023. This specific scenario was selected as the baseline future scenario to complement my climate modelling analysis that is based on environmental changes by the year 2100 (see below). Additionally, to investigate potential long-term changes in elasmobranch functional diversity under simulated extinctions, I set five additional extinction scenarios at 100, 200, 300, 400 and 500 years in the future. To nullify any influence of outlying extinction times among the simulations, I extracted the modal value of extinction times per species across all 10,000 simulations, which due to commonness was treated as the projected future extinctions in all subsequent analyses. Species extinctions in each scenario were simulated by removing species from the pool with modal extinction times of ≤ 77, 100, 200, 300, 400 and 500 years. However, relying solely on modal extinction times would overlook the inherent variability in predicting future extinction events. It is essential to account for this variability, as no single prediction can be deemed the definitive future. Moreover, the modal extinction times cannot and should not be considered completely accurate due to: (1) unpredictable, external anthropogenic factors that can affect species

indiscriminately regardless of traits or IUCN status (Purvis et al. 2000); or (2) inherent discrepancies between actual extinction times and the recording of that extinction by the IUCN (Andermann et al. 2021). As such, to account for inherent variation in extinction predictions, I added a "buffer" sequentially adding and subtracting one to 25 years to the predicted extinction times in each scenario prior to functional diversity calculations.

Functional diversity analyses

Trait data

A dataset of 1,100 elasmobranch species, already corrected for synonyms, and accompanying trait data was extracted from Pimiento et al. (2023). This dataset assigned seven functional traits to each species: habitat (coastal, oceanic, or both); vertical position (benthic, pelagic or benthopelagic); terrestriality (marine, brackish, or freshwater); thermoregulation (ectothermic or mesothermic); feeding mechanism (filter feeder or macropredator); diet (plankton, invertebrates, fish, high vertebrates, or different combinations of these); and maximum body size (total length or disk width), assigned mainly from primary literature (see supplementary material of Pimiento et al. 2023). However, I made one minor adjustment to the downloaded dataset. Specifically, I reassigned the thermoregulation of two species – the basking shark, *Cetorhinus maximus*, and the smalltooth sand tiger shark, *Odontaspis ferox* – from ectothermic to mesothermic based on recent work that has found anatomical evidence of mesothermy in both species (Dolton et al. 2023a, Dolton et al. 2023b).

All subsequent analyses described below were performed based on this dataset of 1,100 species as all were present within the reference list from *iucnsim* and had been corrected for synonyms. For missing trait data, I used the modal value of multiple imputations based on Pimiento et al. (2023).

Functional diversity metrics

Based on extinction forecasts (see above), I quantified the future functional diversity of elasmobranchs in the year 2100 (i.e., 77 years in the future) and in 100, 200, 300, 400 and 500 years (herein, "scenarios"). To create a multidimensional functional space based on trait values, I followed Cooper and Pimiento (2024), whereby I used the *mFD* package (version 1.0.6; Magneville et al. 2022) to compute a trait dissimilarity matrix based on Gower's distance, that incorporates multiple trait types (i.e., nominal, ordinal and quantitative). All traits were weighted equally, as I did not have *a priori* expectations regarding the relative importance of

traits. I subsequently performed a principal coordinate analysis (PCoA) where my data were best represented by four dimensions, accounting for 75.54% of the total inertia (**Appendix Table S3.1**, **S3.2**; **Appendix Figure S3.1**, **S3.2**). This showcased both a low number of axes and the least distortion of the original trait dissimilarity matrix, as indicated by having the lowest mean absolute deviation value (**Appendix Table S3.1**; **Appendix Figure S3.1**; Maire et al. 2015). Based on the produced functional space, I then calculated functional diversity metrics using the methods of Pimiento et al. (2020b). Specifically, I calculated species richness, as well as functional richness (FRic; the % volume of occupied functional space), mean functional uniqueness (FUn; the distance of each species from their five nearest neighbours), and mean functional specialisation (FSp; the distance of each species to the functional space centroid) for each future scenario.

I assessed individual species' contributions to functional diversity by using the "fuse" function in *mFD* (Magneville et al. 2022) to calculate per-species FUn and FSp. To capture extinction risk by 2100 in my "fuse" calculations, the GE (i.e., global endangerment metric) was assigned as the probability of extinction in 77 years based on IUCN status (Mooers et al. 2008, Davis et al. 2018). Specifically, I followed Davis et al. (2018), who converted IUCN status into extinction probabilities given 100 years of status quo conservation, assuming for simplicity that species populations followed exponential decay. To identify which species were the most important for maintaining functional diversity, I calculated species-specific FUS scores (functionally unique and specialised; (FUn + FSp)/2; Griffin et al. 2020) and ranked species scores accordingly.

To determine if high-ranking FUS species were at greater risk of extinction than low-ranking species in each future scenario (i.e., 2100 and 100, 200, 300, 400 and 500 years in the future), I marked species presence (i.e., survival) and absence (i.e., extinction) per scenario based on modal extinction times and ran generalised linear mixed effect models (GLMMs) implemented in the *lme4* package (version 1.1-35.1; Bates et al. 2014), using partial pooling within taxonomic orders to account for random trends (Harrison et al. 2018). I additionally calculated the predicted average extinction probability across individual taxonomic orders from GLMMs to uncover which were at the greatest extinction risk by 2100. Finally, I ranked the top ten FUS species and marked their simulated extinction times to identify the extinctions that will have the largest ecological effects by 2100.

Based on per-scenario FRic and per-species FUn and FSp calculations, I additionally used the "alpha.multidim.plot" function of *mFD* to visualise functional space occupation of all future scenarios (FRic) and the FUn and FSp scores of all species within each space and thus compliment the above analyses. In all future spaces, species simulated as extinct were removed to visualise changes in FRic and species-specific FUn and FSp (**Appendix Figure S3.3**, **S3.4**).

Null model

I compared my functional diversity metrics per scenario to a null model to assess if the projected shifts were more extreme than expected by chance based on species richness. This model was created by randomising the species present in each extinction scenario with the "sample_n" R function and subsequently re-calculating all functional diversity metrics as above 1,000 times. For each scenario, I compared the randomised null results against the "buffered" results obtained empirically (see above) using Wilcoxon signed-rank tests because the data were not normally distributed (Shapiro-Wilk normality test; $P < 0.05$).

Spatial analyses

To assess global distribution of elasmobranch species and functional diversity by 2100 under climate change, I used a species distribution model based on AquaMaps (v.10/2019; www.aquamaps.org; Kaschner et al. 2019). This model combines global occurrence data with ecological information to infer habitat suitability through preferred environmental parameters (e.g., Hodapp et al. 2023). The eleven parameters used are: (1) mean, (2) minimum, and (3) maximum depth, (4) mean sea surface and (5) bottom surface temperature, (6) mean surface and (7) bottom salinity, (8) mean primary productivity, (9) mean sea ice concentration, (10) mean dissolved oxygen concentration and (11) mean dissolved bottom oxygen concentration. Specifically, AquaMaps computes habitat suitability from annual averages of species occurrences and temporal mean values of all environmental parameters from 2000 to 2014 (Gissi et al. 2023, Hodapp et al. 2023). Its algorithm records probabilities of occurrence data and the eleven environmental parameters mentioned above at 0.5º x 0.5º grid cells, allowing visualisation using global maps. This information is compiled based on occurrence and environmental data collected from global open-access biodiversity databases, namely GBIF (Global Biodiversity Information Facility; https://www.gbif.org/), OBIS (Ocean Biodiversity Information system; https://obis.org/), FishBase (www.fishbase.org/; Froese and Pauly 2017) and SeaLifeBase (https://www.sealifebase.ca/).

Data

Although the trait dataset comprises 1,100 species, AquaMaps only has available occurrence data for 862 elasmobranch species (78.4% of species). This can be attributed to several sampling-based reasons: specifically, a lack of distribution data availability for some species, and geographic sampling gaps. For example, distribution data for several shark species are uncertain due to being identified from only 1-3 individual specimens, resulting in a lack of occurrence data recorded in global databases (Ebert et al. 2021); and in some cases, due to being known only from historical records and not being sighted for several decades (e.g., the "lost shark" *Carcharhinus obsoletus*; White et al. 2019). In terms of geographic sampling, such data are inherently unevenly sampled. For example, coastal waters of the northern hemisphere are very well sampled while polar and remote oceanic waters tend to be under-sampled (Hughes et al. 2021, Hodapp et al. 2023). Deep seas, a known habitat of several shark species (e.g., Simpfendorfer and Kyne 2009), are also particularly poorly sampled in global occurrence databases (Hughes et al. 2021). As such, it is essential to determine if this limited species sample can adequately capture elasmobranch functional diversity before assessing its changes in 2100 due to climate change and extinctions.

I performed complementary analyses to assess (1) how much of the present-day elasmobranch functional space is represented by the species recorded in AquaMaps; and (2) whether the AquaMaps data included the most functionally unique, specialised and endangered (FUSE) species (i.e., threatened species of particular importance for maintaining functional diversity; Griffin et al. 2020, Pimiento et al. 2020b). These analyses were performed using the *mFD* package's "fric.plot" and "fuse" functions respectively (Magneville et al. 2022). To capture extinction risk based on present-day IUCN status, the GE metric was set in the "fuse" calculation to a numerical vector based on IUCN status (i.e., 0 = LC; 1 = NT; 2 = VU; 3 = EN; 4 = CR). My analyses found that: (1) the AquaMaps sample occupied 97.3% of elasmobranch functional space (i.e., FRic); and (2) 90%, 84%, 82% and 72% of the top 20, 25, 50 and 100 FUSE species respectively were present in AquaMaps (**Appendix Table S3.3**; **Appendix Figure S3.5**). As such, I contend that the AquaMaps sample largely captures the extent of elasmobranch functional diversity and thus can be used to assess its global distribution in 2100.

I extracted probabilities of occurrence data for all 862 elasmobranch species from AquaMaps for the present day and for the year 2100 under three different representative concentration pathways (herein, RCP): RCP 2.6, 4.5, and 8.5. These three pathways relate to different

scenarios regarding the mitigation of carbon dioxide (CO_2) emissions. RCP 2.6 is a pathway in which strong mitigation is taken and all net-zero targets by 2050 are assumed to have been met; RCP 4.5 is a pathway where only moderate mitigation is taken, and is considered the most probable future of the three pathways due to the exhaustible nature of non-renewable fossil fuels; and RCP 8.5 is a "worst-case" pathway involving no mitigation, and thus increased CO_2 emissions (Moss et al. 2010).

Grid-based functional diversity

To conduct distribution analyses based on AquaMaps data, I filtered occurrence probability to a cut-off of ≥ 0.3 to minimise grid cells with no data while also broadly reflecting habitat suitability. Based on this cut-off, I converted occurrence data to presence/absence data per grid cell for functional diversity analyses. I first quantified species richness in all grid cells following Pimiento et al. (2023). I then also computed FRic and FSp using the *mFD* package's "alpha.fd.multidim" function (Magneville et al. 2022) in grid cells with five or more species since four functional space axes were found to be most optimal for the analyses (**Appendix Table S3.1**; Maire et al. 2015). In these same grid cells, I additionally calculated FUn using the "uniqueness" function of the *funrar* package (version 1.5.0; Grenié et al. 2017). These packages were used for the spatial analyses, with hundreds of thousands of grid-cell based assemblages, due to their quick and memory-efficient computations in the supercomputer (Grenié et al. 2017, Magneville et al. 2022). These analyses were conducted using (1) present-day AquaMaps data; and (2) AquaMaps data from 2100 under each RCP to evaluate future functional diversity distribution under each climate change pathway.

I then assessed functional diversity distribution in 2100 under both climate change and simulated extinctions to evaluate how a combination of extinctions and climate-induced range shifts affect global marine ecosystem functioning. To incorporate extinctions, I repeated the above analyses, but removing species with a modal extinction time of ≤ 77 (i.e., 77 years) from the AquaMaps data as per my 2100-based extinction scenario (see above). This was repeated under each RCP to examine the effect of worsening climate change on functional diversity distribution. Finally, to investigate if any environmental parameters in AquaMaps were strong predictors of future functional diversity following climate change and extinctions, I ran binomial generalised linear models (GLMs) of each parameter against the calculated functional diversity metrics per RCP.

Turnover calculations and mapping

To evaluate shifts in functional diversity by 2100 under climate change and extinctions, I evaluated turnovers in species richness and all three functional diversity metrics by 2100 per grid cell following previous work (Gissi et al. 2023). This was done by subtracting present-day values from those calculated in 2100 for each RCP, both with and without simulated extinctions being applied. Following these calculations, I then visualised the resulting shifts in global maps using the *ggplot2* package (version 3.4.4; Wickham 2016) of the *tidyverse* collection (version 2.0.0; Wickham et al. 2019).

4.4   Results and Discussion

Forecasted changes in functional diversity following simulated extinctions

How will future extinctions affect functional diversity?

In the baseline future extinction scenario, the year 2100 (i.e., 77 years in the future), 74 species (~6.7%; **Figure 4.1a**) were simulated as extinct based on the modal extinction time extracted from my *iucnsim* analyses (Andermann et al. 2021). This, in turn, was predicted to reduce functional richness (FRic) by 2.5% (**Table 4.1**; **Figure 4.1b**), a result not found to be significantly different from chance expectations (Wilcoxon signed-rank test; P = 0.17; **Appendix Table S3.4**). FRic only slightly declined (i.e., by <1%) between 2100 and 100 years into the future, but over the following 100 years, another 13.2% of FRic was lost. The next 200 years saw FRic decline by 23.4% and 28.8% compared to the present by 300 and 400 years in the future respectively. By 500 years in the future, 32% of species and 41% of FRic were projected to be lost based on the modal extinction times (**Table 4.1**; **Figure 4.1a**, **b**). Notably, from 100 years in the future onwards, the empirical FRic was significantly lower than expected by chance (P < 0.05; **Appendix Table S3.4**). Functional uniqueness (FUn) was projected to increase through time in the aftermath of simulated extinctions, increasing by 5% by 2100, and by 7% and 10% compared to the present by 100 and 200 years in the future. Subsequently, FUn was then projected to drastically increase over the next 300 years, rising by 37%, 68% and 90% compared to the present by 300, 400 and 500 years in the future (**Table 4.1**; **Figure 4.1c**). These changes did not deviate from chance expectations except in the 200-year and 300-year extinction scenarios, where FUn was found to be significantly lower than null expectations (P < 0.05; **Appendix Table S3.4**). Finally, functional specialisation (FSp) only had marginal declines in the future extinction scenarios compared to the present (i.e., by < 4%; **Table 4.1**; **Figure 4.1d**) but was consistently found to be significantly lower than null expectations (P < 0.05; **Appendix Table S3.4**).

Table 4.1. Future elasmobranch functional diversity. Metric values per scenario are based on the modal extinction time per species from our *iucn_sim* simulations, accurate to one decimal place for FRic; and four for FUn and FSp results for precise representation of changes. Proportional changes from the present-day value (i.e., 1,100 species; 100% FRic) are included in parentheses, accurate to one decimal place. Abbreviations are as follows: FRic = functional richness (% of functional space volume occupied); FUn = functional uniqueness (mean distance of species to their closest five neighbours in space); FSp = functional specialisation (mean distance of species to the centroid of the space).

Future scenario	FRic (%)	FUn	FSp
2100 (i.e., 77 years)	97.5	0.0075	0.1978
	(-2.5%)	(+5.4%)	(-1.1%)
100 years	96.8	0.0077	0.1967
	(-3.2%)	(+7.4%)	(-1.7%)
200 years	83.6	0.0079	0.1924
	(-16.4%)	(+10.8%)	(-3.9%)
300 years	77.6	0.0098	0.1936
	(-23.4%)	(+36.7%)	(-3.2%)
400 years	71.2	0.0112	0.1929
	(-28.8%)	(+67.5%)	(-3.6%)
500 years	59.0	0.0136	0.1947
	(-41%)	(+90.1%)	(-2.7%)

Functional diversity of sharks through time: past, present and future

Figure 4.1. Future proportional changes in species and functional diversity in the extinction scenarios. Changes are recorded in: (a) species richness; (b) functional richness (FRic); (c) functional uniqueness (FUn); and (d) functional specialisation (FSp). Boxplots represent the range of values from 10,000 *iucnsim* simulations in (a) and across the +/- 25-year buffer (see Methods) in (b-d). Red dots mark the modal value from simulations in all plots. Grey violin plots in (b-d) denote distribution from the null model across 1,000 iterations.

These results signal that the projected extinctions will lead to reductions of functional space occupation (i.e., FRic) over the next 500 years alongside lower-than-expected FSp (**Figure 4.1b**, **d**), demonstrating the sensitivity of functional diversity to species loss and particularly the loss of those with extreme trait values contributing distinct functions. Indeed, visualising the functional space of each extinction scenario revealed that space occupation shrank through time due to the loss of high-scoring FSp species with the most extreme trait values at the edge

of space (**Appendix Figure S3.3**, **S3.4**). These findings indicate declines in the range of ecological functions played by elasmobranchs. Furthermore, as species are lost in the near- and far-future, FUn was projected to increase. This denotes a loss of functional redundancy (i.e., the number of species playing similar ecological roles; Mouillot et al. 2014) as surviving species become more isolated in trait space (Mouillot et al. 2013b). Although FRic did not exceed null expectations based on extinctions by 2100 (**Figure 4.1b**; **Appendix Table S3.4**), an increase of FUn can leave communities more susceptible to further species losses and thus destabilise ecosystems (Micheli and Halpern 2005, Biggs et al. 2020). Indeed, this may be reflected in proportional increases of FUn exponentially growing to as high as 90% in subsequent extinction scenarios (**Figure 4.1c**). Strikingly, the >40% loss of FRic over the next 500 years continues and broadly replicates a trend of functional diversity decline recorded over the last 10 million years in the shark fossil record (Cooper and Pimiento 2024), but at a much more accelerated rate (i.e., in 0.005% of the time), implying greater severity of anthropogenic extinction risk to elasmobranchs today compared to threats they faced in the geological past.

Are the most functionally unique and specialised species at greatest extinction risk?

As the most functionally unique and specialised elasmobranch species disproportionately maintain functional diversity (Griffin et al. 2020, Pimiento et al. 2020b), their losses are expected to have the largest ecological impacts in the future. Indeed, the >40% shark functional diversity loss over the last 10 million years was likely due to the extinction of highly functionally unique and specialised species such as the extinct "megalodon" (*Otodus megalodon*), supporting this assertion (Cooper and Pimiento 2024). This necessitated quantifying and ranking species-specific FUS to evaluate its relationship with extinction risk in the future extinction scenarios.

Our GLMM revealed a clear and statistically significant negative relationship between extinction probability and FUS ranking in 2100 ($P = 0.035$; **Figure 4.2a**; **Appendix Table S3.5**). Moreover, half of the 12 taxonomic orders showed the same general trend (**Appendix Figure S3.6**). This was maintained under partial pooling of the orders (**Figure 4.2b**), as well as in future scenarios of 100 and 200 years in the future (**Appendix Figure S3.7**), though statistical significance was lost in these extinction scenarios ($P > 0.05$; **Appendix Table S3.5**). This trend reversed 300 years in the future, reappeared 400 years in the future, and then reversed again by 500 years in the future (**Appendix Figure S3.7**), with no statistical significance in any of these extinction scenarios (**Appendix Table S3.5**).
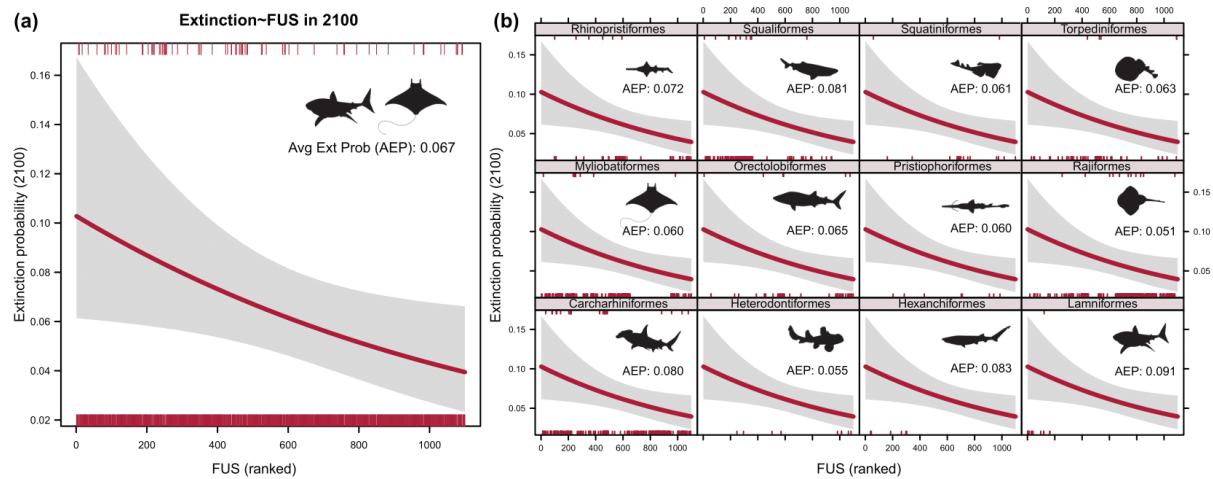
Figure 4.2. Generalised linear mixed effect model using ranked FUS scores of elasmobranchs to predict extinction probability by 2100. (a) the overall trend across all species; (b) trends across individual taxonomic orders, treated as a random effect in the random trend model and utilising partial pooling. Avg Ext Prob = average extinction probability. Silhouettes were downloaded from Phylopic (https://www.phylopic.org/). All are in the public domain, except for the Hexanchiformes silhouette, which is credited to Ignacio Contreras with an Attribution 3.0 Unported licence (https://creativecommons.org/licenses/by/3.0/).

Of the taxonomic orders, the mackerel sharks (Order Lamniformes) were found to have the highest average extinction probability by 2100 at 0.091, followed by the cow sharks (Order Hexanchiformes) and the dogfish sharks (Order Squaliformes) at 0.083 and 0.081 respectively (**Figure 4.2b**). Notably, Order Lamniformes has been found to be the taxonomic order with the highest mean FUn, FSp and FUSE scores by previous work (Pimiento et al. 2023). By stark contrast, the low-FUSE scoring sawsharks (Order Pristiophoriformes), bullhead sharks (Order Heterodontiformes) and skates (Order Rajiformes; Pimiento et al. 2023) had the lowest average extinction probabilities (0.06, 0.055 and 0.051 respectively; Figure 2b). As such, the taxonomic orders with the highest average contributions to functional diversity appear to be most at risk of extinction by 2100.

Overall, these results indicate that species with high FUS scores are at greater risk of extinction over the next 200 years compared to low-scoring species; a trend maintained even at the much higher taxonomic order level (**Figure 4.2**, **Appendix Figure S3.7**). Worryingly, two of the top ten FUS species were projected as becoming extinct by as soon as 2100. The first of these was the whale shark (*Rhincodon typus*), ranked 7th (**Appendix Table S3.6**) and distinguished in terms of its traits by being the largest living elasmobranch (~21 m; Ebert et al. 2021), and being a filter feeder that also consumes fish (Pimiento et al. 2023, Whitehead and Gayford 2023). The second was the Greenland shark (*Sominosus microcephalus*), ranked 9th (**Appendix Table S3.6**) and a benthopelagic shark which also reaches very large body sizes (> 7 m), occupies a

high trophic level due to being able to feed on high vertebrates, and can live in brackish waters (Ebert et al. 2021). Outside of the traits studied here, this species is also distinguished from other elasmobranchs for living in Arctic waters and being the longest-lived vertebrate on Earth, with lifespans estimated between 200 and 500 years (Nielson et al. 2016). By 200 years in the future, where the highest-ranked FUS species still have higher extinction probabilities than lower-ranked counterparts (**Appendix Figure S3.7**), and notably right before FUn starts to exponentially increase (**Figure 4.1c**), four more of the top 10 FUS species are projected to be lost, all from the Order Lamniformes (**Appendix Table S3.6**). This included the highest-ranked species, the basking shark (*Cetorhinus maximus*; **Appendix Table S3.6**), distinct for being the second-largest living elasmobranch (~11 m; Ebert et al. 2021), and a mesothermic filter feeder, a characteristic unique to this species (Dolton et al. 2023a). The other three were: (1) the great white shark (*Carcharodon carcharias*), ranked 2nd; (2) the longfin mako (*Isurus paucus*), ranked 8th; and (3) the shortfin mako (*Isurus oxyrinchus*), ranked 10th (**Appendix Table S3.6**). All are large-bodied (4-6 m long) and mesothermic macropredators able to feed on large prey (Ebert et al. 2021). All six species detailed above are threatened according to the IUCN (*C. carcharias* and *S. microcephalus* = VU; all other species = EN; IUCN 2023). Moreover, all have large body sizes (>4 m) and can live in coastal waters (Ebert et al. 2021), in line with current knowledge that over 75% of threatened elasmobranch species are coastal (Dulvy et al. 2021), and that large body size is generally associated with extinction risk in marine vertebrates (Harnik et al. 2012, Payne et al. 2016). The large body sizes represent extreme trait values (i.e., high FSp) while filter feeding and mesothermy represent trait values dissimilar to other species (i.e., high FUn); thus, their loss will inordinately reduce functional diversity. Taken together, my findings suggest that over half of the most functionally unique and specialised species could be lost within the next 200 years (**Appendix Table S3.6**), including at least two by the baseline extinction scenario of 2100, which reiterates the peril facing elasmobranch functional diversity and the vitality of conservation actions focusing on FUSE (functionally unique, specialised and endangered; Griffin et al. 2020, Pimiento et al. 2020b) species for protecting it.

Future global elasmobranch distribution

How will species redistribute in 2100 under climate change and extinctions?

I assessed collective and spatial redistribution of elasmobranch species in the baseline extinction scenario of 2100 using AquaMaps (Kaschner et al. 2019) to evaluate global ecological consequences of extinctions in combination with climate change. While climate

change indirectly causes species to shift their distributional ranges as a result of ocean warming degrading their native habitats (e.g., Sequeira et al. 2014, Hammerschlag et al. 2022, Rummer et al. 2022), it is not considered the main threat against elasmobranchs; with overfishing being a much more direct cause of decline, and the sole threat against two-thirds of all threatened elasmobranch species (Dulvy et al. 2021). Together, these two threats paint a more complete picture of the spatial future of elasmobranch biodiversity.

Under climate change and extinctions, I found that tropical and coastal regions will suffer the greatest elasmobranch losses by 2100 (**Figure 4.3**). My analysis of present-day elasmobranch distribution using AquaMaps found that species richness is most concentrated across coastlines of the Americas, northeast and southern Africa, India, and the Indo-Pacific across southern Japan, eastern China, Indonesia and northern Australia (**Appendix Figure S3.8a**), a result that was comparable to previous assessments (Lucifora et al. 2011, Derrick et al. 2020). However, under RCP 2.6 alone, considered a "best-case scenario" for near-future climate change (Moss et al. 2010), species were projected to widely decline across grid patches along tropical latitudes covering most of the above habitats (**Figure 4.3a**, **b**). When extinctions were also incorporated, the spatial range of losses dramatically expanded to higher latitudes (i.e., up to absolute latitudes of 50°), for example as far north as the UK, and steep species declines (i.e., >25 species lost) were projected in all hotspots noted above (**Figure 4.3b**). Under RCP 4.5, the most probable future under climate change (Moss et al. 2010), tropical losses intensified, losing more species across a wider range than RCP 2.6 (**Figure 4.3c**). When extinctions were also considered, the range of species losses again expanded into higher latitudes, and further intensified, particularly in the Indo-Pacific where between 34 and 70 species were lost across grid cells (**Figure 4.3d**). Under RCP 8.5, a pathway where CO_2 emissions are not mitigated (Moss et al. 2010), these same and exacerbated trends were detected – species loss across tropical and coastal habitats under climate change (**Figure 4.3e**), and a greater range and intensity of species losses when extinctions were incorporated, with the largest losses occurring around the Indonesia islands, where as many as 132 species were lost in some grids (**Figure 4.3f**). By comparison, the highest latitudes in poleward directions (i.e., $\geq 50°$ absolute latitude) were consistently projected to gain species across all climate change pathways, though the intensity of species gains in these regions was considerably lower when extinctions were incorporated into the analyses (**Figure 4.3**).
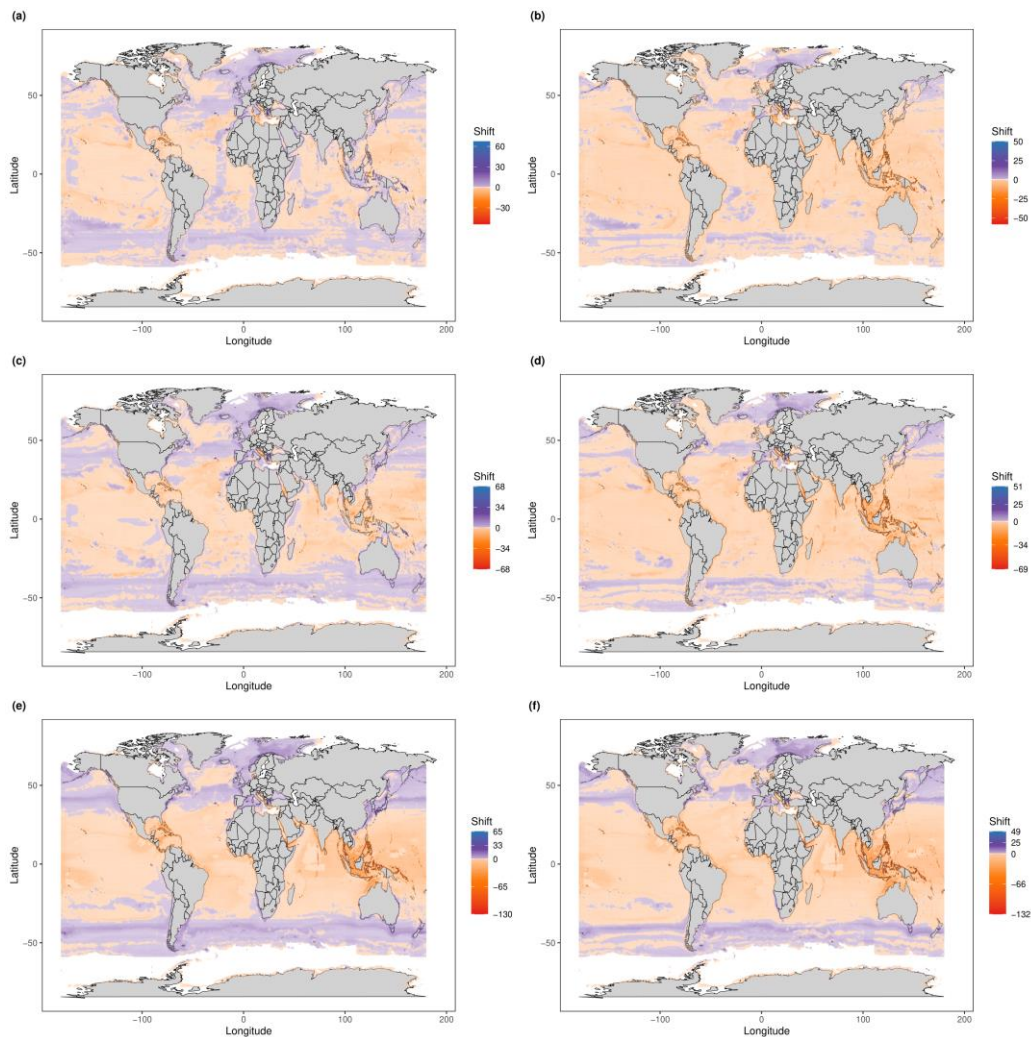
Figure 4.3. Biogeographic shifts of elasmobranch species richness by 2100. Values showcase changes in species richness between the present day and 2100 under (a, b) RCP 2.6; (c, d) RCP 4.5; and (e, f) RCP 8.5. The left column (a, c, e) represents calculated shifts when considering climate change only; while the right column denotes calculated shifts following both climate change and the exclusion of species simulated as extinct by 2100. In all plots, blue and purple represent grid cells gaining species while orange and red mark grid cells losing species, with blue and red denoting the largest gains and losses respectively.

These findings broadly parallel previous works that have suggested that (1) elasmobranch ranges are likely to shift polewards under climate change (Sequeira et al. 2014, Birkmanis et al. 2020, Diaz-Carballido et al. 2022); and (2) coastal and tropical habitats are at particular risk of species decline (Dulvy et al. 2021). Indeed, sea temperature and mean and minimum depth broadly indicating coastal habitats were found by my GLMs to be the best environmental predictors of future species richness under climate change and extinctions (**Appendix Table S3.7**). However, my results also imply that extinctions will greatly exacerbate the observed trends. Across all climate pathways, extinctions worsened species losses in the tropics, and reduced species gains in poleward latitudes (**Figure 4.3b**, **d**, **f**). Most strikingly, extinctions extended the spatial range of species losses under RCP 2.6 beyond that of even RCP 8.5 when

only climate change was considered (**Figure 4.3b**, **e**). My results therefore suggest that previous works predicting climate-induced distributions are underestimating tropical species decline by not accounting for more direct threats such as overfishing, which is the biggest driver of extinction risk in elasmobranchs (Dulvy et al. 2021). This highlights that predicting future elasmobranch distribution requires careful consideration of multiple confounding variables, namely direct anthropogenic threats on top of occurrence and environmental data.

How will functional diversity redistribute in 2100 under climate change and extinctions?

Given the sensitivity of functional diversity to species loss (**Figure 4.1**), and current knowledge that invasions into new habitats due to climate change can affect regional functional diversity (Toussaint et al. 2018, Renault et al. 2022), my assessment of spatial functional diversity in 2100 considered both climate change and simulated extinctions (**Figure 4.4**, **Appendix Figure S4.9**). My analysis of present-day FRic distribution using AquaMaps showed that FRic was concentrated within continental shelves and oceanic islands in the tropics, particularly in northern Australia and the Indo-Pacific (**Appendix Figure S3.8b**), a comparable finding to earlier work (Pimiento et al. 2023). Under extinctions, and the most probable climate future RCP 4.5 (Moss et al. 2010), however, FRic was projected to widely decline in continental shelves, particularly at tropical latitudes such as losses of 25-45% around the Indonesian islands and the Red Sea (**Figure 4.4a**). By contrast, gains in FRic were projected at high latitudes, the largest of which were found at absolute latitudes of $\geq 50^\circ$ in northern Europe and southmost Chile and Argentina. However, FRic gains were less than 15% on average, with a highest gain of 31%, potentially indicating that FRic was on the whole being lost as well as redistributed (**Figure 4.4a**). Most strikingly, virtually every spatial FRic hotspot identified by previous work (Pimiento et al. 2023), a range of coastal habitats including around oceanic islands, was predicted to undergo declines in FRic (**Figure 4.4a**). My FRic results suggest that the functional range of elasmobranchs in coastal and tropical areas will contract by 2100 as species abandon these regions due to ocean warming (e.g., Hammerschlag et al. 2022), or become extinct as fishing pressures threatening these species mount (Dulvy et al. 2021). Indeed, these trends of FRic decline intensified under worsening climate change (**Appendix Figure S3.9a**, **b**), and my GLMs found that temperature and depth were the key environmental predictors of FRic in 2100 under climate change and extinctions (**Appendix Table S3.8**). Such constrictions of functional space at these regional levels indicate that coastal and tropical waters, including identified FRic hotspots (Pimiento et al. 2023), will lose their variety of ecological functions, compromising the functioning of these ecosystems.

Functional diversity of sharks through time: past, present and future
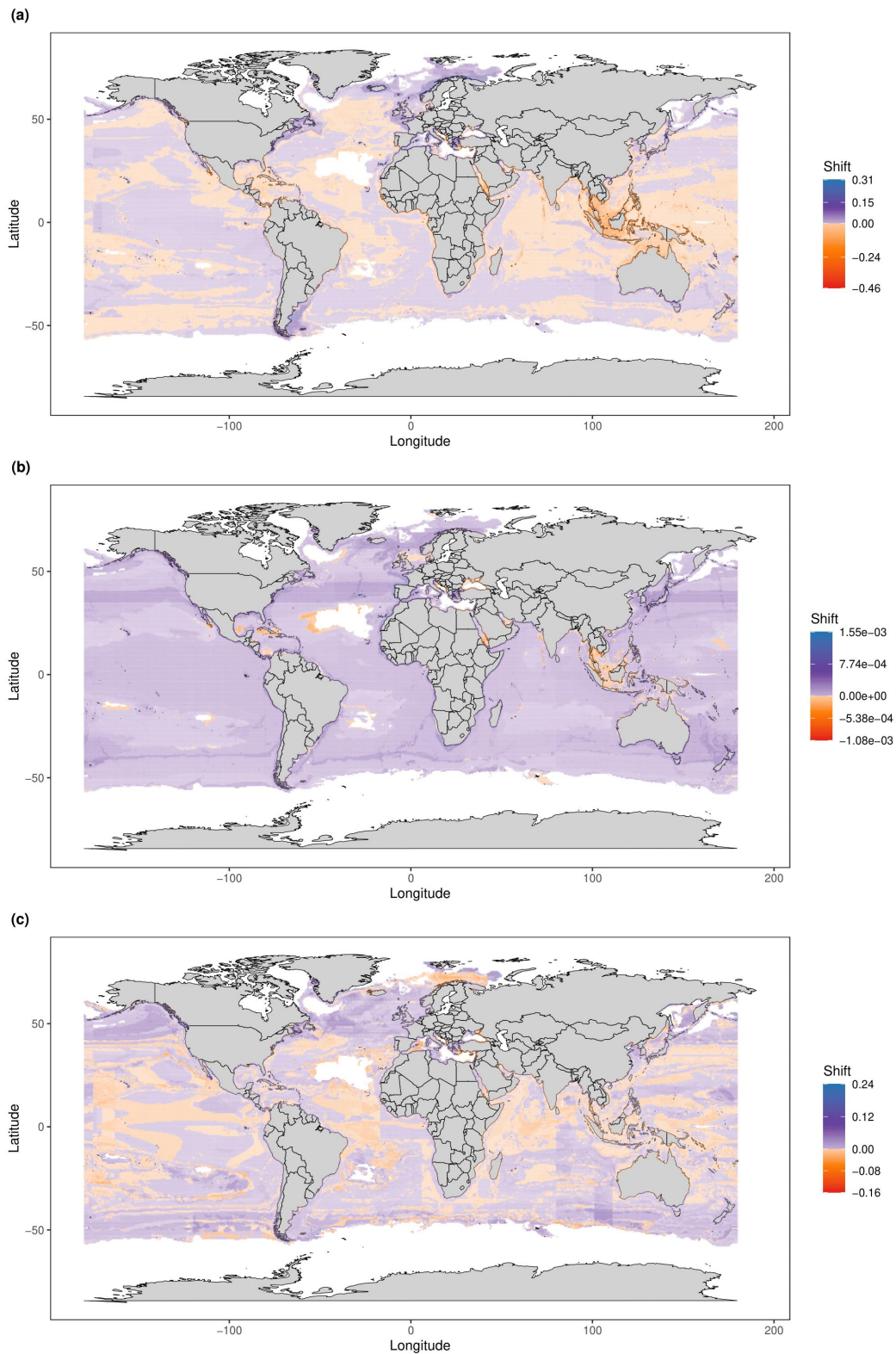
Figure 4.4. Biogeographic shifts in elasmobranch functional diversity by 2100 under RCP 4.5, the most probable future of the three analysed climate change pathways (Moss et al. 2010). Shifts are visualised for (a) functional richness; (b) functional uniqueness; and (c) functional specialisation. Shift values are based on calculations from the present day to 2100 following species extinctions. See **Appendix Figure S3.9** for shifts under RCP 2.6 and 8.5. In all plots, blue and purple represent grid cells with increased functional diversity metrics while orange and red mark grid cells with decreased functional diversity metrics, with blue and red denoting the largest gains and losses respectively.

Evaluating spatial shifts in FUn and FSp by 2100 provides insights into which regions could be most vulnerable to species loss and may aid in directing spatial conservation efforts towards protecting important ecological functions as well as species (Pimiento et al. 2023). My analysis of present-day elasmobranch FUn and FSp using AquaMaps found that FUn was highest around the Indonesian islands, and relatively high at high latitudes (**Appendix Figure S3.8c**), while FSp was relatively homogeneous in distribution and highest in open ocean (**Appendix Figure S3.8d**); broadly similar to previous evaluations (Pimiento et al. 2023). Alarmingly, I uncovered that by 2100, FUn was projected to predominantly increase on an almost complete global scale (**Figure 4.4b**, **Appendix Figure S9c**, **d**). Even high latitudes with high present-day FUn (Pimiento et al. 2023) were projected to experience gains (**Figure 4.4b**). In light of species and FRic tropical losses and poleward gains (**Figure 4.3**, **4.4a**), this finding indicates that elasmobranchs in co-existing habitats will be further apart in trait space compared to the present, a sign of reduced functional redundancy (i.e., fewer co-existing species will be playing the same ecological function). My GLMs suggested that sea temperature and mean dissolved oxygen concentration were the best predictors of spatial FUn in 2100 (**Appendix Table S3.9**). Ocean warming and acidification (i.e., depletion of O_2 as CO_2 is increasingly absorbed; Gobler and Baumann 2016) adversely affect elasmobranch habitat, behaviour and physiology (Rosa et al. 2017, Hammerschlag et al. 2022); implying widespread effects across species, likely including those sharing the same common trait values such as coastal habitats, macropredation and ectothermy (i.e., functionally redundant species). However, it should be noted that the effects of ocean acidification on species with unique trait values such as filter feeding, mesothermy, or capability of entering freshwater or estuaries have not yet been thoroughly investigated (Rosa et al. 2017). The low functional redundancy that comes with global FUn increases, as species sharing trait values migrate or become extinct, ensures that global elasmobranch habitats will become highly susceptible to future species loss, weakening the stability of worldwide marine ecosystems (Micheli and Halpern 2005).

Meanwhile, FSp was projected to broadly decline in tropical open oceans and increase at high poleward latitudes by 2100 under climate change and extinctions (**Figure 4.4c**). These trends exacerbated under unmitigated climate change (**Appendix Figure S3.9e**, **f**). Supporting oceanic declines were my GLMs suggesting that depth was the best predictor of FSp under extinctions and climate change (**Appendix Table S3.10**). These declines indicate constriction of regional functional space in tropical and remote waters (i.e., loss of FRic due to the loss of high-scoring FSp species with extreme trait values at the edge of space; Mouillot et al. 2013b,

Pimiento et al. 2020b), which could destabilise the ecological processes in these regions. Notably, only 5% of FSp hotspots, typically out in open ocean, are covered by the global network of MPAs (Pimiento et al. 2023), and thus the detected declines in these unprotected areas emphasise the need to expand protections to these distant but functionally important regions. The FSp gains at high latitudes, where FUn is already high and projected to further increase by 2100 (**Figure 4.4b**; Pimiento et al. 2023) indicates that while these areas are likely to gain a wider breadth and specialisation of ecological functions, those same functions will be highly vulnerable to species loss due to a lack of redundancy, further jeopardising ecological processes in these regions in the event of future species loss.

Taken together, the spatial distributions in 2100 indicate that, under the combined factors of projected extinctions and climate change, global elasmobranch functional diversity will decline, particularly within tropical and coastal areas, and will become more susceptible to further species loss on a near-worldwide scale (**Figure 4.4**). Declines are likely to be driven by the decimation of coastal tropical habitats, which are at the highest risk from overfishing and are most adversely affected by ocean warming brought about by climate change (Dulvy et al. 2021, Rummer et al. 2022). Poleward waters will gain elasmobranch functional diversity as well as species (**Figure 4.3**, **4.4**), as indicated by increases in FRic and FSp, but a global reduction in functional redundancy (i.e., increasing FUn) will render both native and newly arriving ecological functions highly vulnerable to further species losses detected beyond 2100 (**Figure 4.1**, **4.4b**). Ultimately, these results forewarn that the global balance of marine ecosystem functioning provided by elasmobranchs is under significant and near-immediate threat under current extinction trajectories.

Limitations

Given the inherent uncertainty of predicting future extinctions (Purvis et al. 2000), there are naturally limitations to my approaches that are worth noting. Namely, my model choice from the *iucnsim* program is based on historical IUCN status transitions across a ~30-year period being extrapolated to much more distant futures (Andermann et al. 2021). The recorded changes by the IUCN inherently lag behind precise population changes, and indeed this model is not yet able to distinguish if recorded transitions are definitively due to population changes rather than external factors such as taxonomic naming updates (Andermann et al. 2021, Ali et al. 2022, Pavoine and Ricotta 2023). Nevertheless, my chosen model is a more cautious and species-specific approach compared to assuming the same extinction probabilities for all

species based on IUCN status, regardless of differing population trends, ecology or life-history (sensu Mooers et al. 2008). As such, using the alternative model would almost certainly project even greater losses of functional diversity if applied to my analyses (Andermann et al. 2021). My projected results are therefore likely to be, at worst, conservative predictions.

Furthermore, although my spatial results offer global projections of future elasmobranch functional diversity under climate change and simulated extinctions (**Figure 4.3**, **4.4**), some limitations inherent to environmental and ecological niche modelling should be acknowledged (Araújo et al. 2019). These come in the form of model assumptions surrounding occurrence and environmental data. Firstly, given that global biodiversity is unevenly sampled (Hughes et al. 2021, Hodapp et al. 2023), the occurrence data are also inherently unevenly sampled. Indeed, my maps clearly showed patches of grid cells where no functional diversity results could be extracted due to under-sampled species (i.e., grids with <5 species; see Methods) and environmental data (**Figure 4.4**). Such areas include polar regions and remote ocean where elasmobranch species richness is low and/or poorly sampled (Lucifora et al. 2011, Derrick et al. 2020). Another limitation is the equilibrium assumption, which presumes that species are always present in all grid cells considered suitable (i.e., occurrence probabilities ≥ 0.3 in my case) with regards to environmental and climate data, and absent from unsuitable habitats; an assumption that naturally is not always met in biological reality (Araújo and Pearson 2005). For example, some elasmobranch species such as the great white shark (*Carcharodon carcharias*) and basking shark (*Cetorhinus maximus*) can travel the length of entire ocean basins during migration (Bonfil et al. 2005, Gore et al. 2008), and thus may well travel through under-sampled or presumably unsuitable areas where they have not been previously recorded. As such, it should be emphasised that the AquaMaps model assigns probabilities of occurrence per species per grid based on local environmental conditions. Despite these limitations, my results can be considered conservative as the environmental data are based on annual means (see Methods) rather than a range of environmental variability, including extremities which can influence species distribution and even risk extinctions (e.g., Cheung and Frolicher 2020).

A further limitation is that projected environmental parameters also rely on assumptions, driving uncertainty. AquaMaps specifically relies on single model estimates for its parameters rather than multi-model averages which are more common for climate change projections (Hodapp et al. 2023). Despite this, most projection models have large uncertainty, as well as bias and assumptions, and so an average of multiple models would not necessarily provide a more robust projection of future climate change (Power et al. 2021). Indeed, it has been

suggested that multi-model average approaches such as the intergovernmental panel on climate change's (IPCC) sixth phase of the coupled model intercomparison project (i.e., IPCC CMIP6) are highly sensitive to variability (Zelinka et al. 2020). Lastly, AquaMaps uses finer grid cell resolution than other models that do incorporate multi-model averages such as the IPCC CMIP6-based approach (i.e., 0.5° rather than 1°) and thus potentially provides a more complete picture of global climate change (Hodapp et al. 2023).

4.5   *Conclusions*

My scenario-based extinction simulations forecasted that elasmobranchs will undergo declines in functional diversity in every extinction scenario projected, from as soon as 2100 to as far as 500 years in the future (**Figure 4.1**; **Table 4.1**). These declines are likely to be driven by the loss of species with extreme trait values, as indicated by the greater-than-expected losses of FSp (**Figure 4.1d**), constricting the range of ecological functions (i.e., FRic; **Figure 4.1b**). Concurrently, these losses will lead to increases in FUn (i.e., reduced functional redundancy; **Figure 4.1c**), meaning that even the ecological functions persisting into the future will be less buffered against future extinctions (Mouillot et al. 2013b, Pimiento et al. 2020b). Furthermore, I found that the most functionally unique and specialised (i.e., FUS) species were at greatest risk of extinction by 2100 and up to 200 years in the future (**Figure 4.2**, **Appendix Figure S3.7**), the loss of which will cause the biggest erosions in functional diversity (Griffin et al. 2020, Pimiento et al. 2020b). More worryingly still, more than half of the top ten most functionally unique and specialised elasmobranchs were projected to become extinct within 200 years, with two of them – the whale shark (*Rhincodon typus*) and Greenland shark (*Somniosus microcephalus*) – projected as extinct by 2100 (**Appendix Table S3.6**). As such, the loss of these two iconic and distinct shark species will have the largest impacts on elasmobranch functional diversity by the end of this century. Lastly, evaluating spatial shifts in elasmobranch functional diversity by 2100 indicated global losses of ecological functions (i.e., reduced FRic) in coastal and tropical waters (**Figure 4.4a**), regions likely to be the most adversely affected by climate change and overfishing (Dulvy et al. 2021). High-latitude seas were projected to gain functional diversity, indicating a poleward shifting of ecological functions by 2100; however, my results projected near-worldwide gains in FUn (**Figure 4.4b**), signifying reduced functional redundancy due to surviving and redistributed ecological functions not sharing trait values. This ultimately forewarns vulnerability of elasmobranch functional diversity to further species losses in virtually every marine habitat across the world by the end of the century (Micheli and Halpern 2005, Pimiento et al. 2020b). Rapid efforts to curb climate change and overfishing (Dulvy et al. 2021), with spatial and taxonomic conservation priorities towards functionally unique, specialised and endangered (FUSE) species of key importance to ecosystem functioning (Griffin et al. 2020, Pimiento et al. 2023), are therefore urgently needed to prevent the potential collapse of elasmobranch functional diversity.

Chapter 5 | General discussion

In this thesis, I investigated how the functional diversity of sharks has changed over the last 66 million years to the present day, and how this may change in the future considering the current climate and extinction crises. Here, I synthesise and discuss the key results of each data chapter and explore future conservation managements that may help preserve shark functional diversity.

In chapter 2, because sharks in the fossil record are represented primarily by isolated teeth (Kent 1994, Cappetta 2012), I assessed the extent to which dental characters (i.e., tooth measurements) can serve as proxies for functional traits used to quantify functional diversity. Between a literature review and two subsequent validation analyses on extant sharks where trait values are already known, I identified seven dental characters that can be used as suitable proxies for three functional traits: body size, prey preference and feeding mechanism (Cooper et al. 2023). Across these traits, tooth size was found to be the best predictor of body size, tooth size and cutting edge were the best predictors of prey preference, and tooth shape and the presence or absence of lateral cusplets were the best predictors of feeding mechanism (**Table 5.1**).

Table 5.1. Summary of the relationships between dental characters and functional traits found in chapter 2. The top three predicting dental characters are ranked accordingly. Abbreviations are as follows: PCA = principal component analysis; CART = classification and regression tree.

Trait	Best predicting dental character (s)					
	Most common (# links; Figure 2.3)	Linear regression (Figure 2.3a)	Distinct links (Figure 2.4)	PCA (ranked by variation contribution; Figure 2.5)	CART (% accuracy; Figure 2.6)	Overall (ranked)
Body size	Crown height (112)	Crown width ($R^2 = 0.9$; $P < 0.001$)	Crown height, Crown width	Crown width, Crown height	Crown height (53.1%)	1. Crown width 2. Crown height
Prey preference	Cutting edge (20), Crown height (18), Crown width (18)	NA	Cutting edge	Crown width, Crown height, Cutting edge	Cutting edge (83.9%)	1. Cutting edge 2. Crown width 3. Crown height
Feeding mechanism	Cutting edge (51), Crown width (32)	NA	Lateral cusplets, Cutting edge	Crown width, Crown height, Cutting edge (all PC1), Lateral cusplets (PC2)	Longitudinal outline (74.4%)	1. Longitudinal outline 2. Lateral cusplets 3. Cutting edge

In chapter 3, using the dental characters identified as trait proxies in chapter 2, I assessed how the functional diversity of sharks changed from 66 million years ago (Ma) right up to the present day and identified the taxa whose extinctions had the largest effects on functional diversity through time. I found that shark functional diversity was relatively high for the first ~55 million years of the Cenozoic (Paleocene to middle Miocene epoch), peaking at 87% functional richness (FRic) in the early Miocene, approximately 20 Ma. However, I also detected a loss of 44% FRic over the last 10 million years (from the late Miocene to the Recent), leaving today's shark functional diversity lower than at any point in the last 66 million years (Cooper and Pimiento 2024). Most significantly, identifying the species with the highest functional originality (FOri) and specialisation (FSp) allowed me to determine which species extinctions through time were most responsible for the detected functional diversity loss. Specifically, the Pliocene loss of extinct bramble sharks (i.e., *Echinorhinus blakei*) led to the ecological role of suction feeder being mostly vacated in the Cenozoic shark functional space; indeed, today, there are just two species remaining that play this ecological role, both of which continue to be poorly studied in scientific literature (*E. brucus* and *E. cookei*; Ebert et al. 2021, Bogan and Agnolín 2022). Furthermore, the Pliocene extinction of the megalodon (*Otodus megalodon*), as well as that of its ancestors by the Miocene, rendered an entire trophic level unavailable to surviving sharks – specifically that of an apex superpredator (Cooper et al. 2022, Kast et al. 2022). The key implication from chapter 3 is that, as a result of these extinctions, shark functional diversity today is already diminished compared to at least the last 66 million years (Cooper and Pimiento 2024), meaning that their current extinction risks like anthropogenically-induced overfishing and climate change (Dulvy et al. 2021) threaten to further decimate their already dwindling contributions to marine ecosystem functioning, as subsequently explored in chapter 4.

In chapter 4, I projected future shifts in the functional diversity of elasmobranchs (sharks, rays and skates) by the year 2100 and over the next 500 years under simulated extinctions. Furthermore, I determined which extinctions by 2100 would have the largest ecological impacts and assessed spatial shifts in the global distribution of functional diversity in 2100 under both climate change and simulated extinctions. My results found that, under the simulated extinctions, elasmobranch functional richness (FRic) will decline through time, with greater-than-expected losses of FSp driving this decline and resulting in increased functional uniqueness (FUn), reducing resilience of the remaining ecological functions. Notably, almost half of FRic was projected to be lost over the next 500 years, replicating the trend recorded in

the last 10 million years by chapter 3 (Cooper and Pimiento 2024), but at a much more accelerated rate. Even more pressingly, I found that the highest-ranked FUS (functionally unique and specialised) species were at the highest risk of extinction by 2100, with two of the top ten FUS species – the iconic whale shark (*Rhincodon typus*) and Greenland shark (*Somniosus microcephalus*) – projected to become extinct by this time and thus having the biggest impacts on elasmobranch functional diversity. Most striking of all were my spatial analysis results. These found that functional diversity would be depleted in coastal and tropical areas, and that high latitudes would gain functional diversity, suggesting a poleward shift of elasmobranch ecological functions by 2100. However, a near-global increase in FUn was also detected, forewarning that the vast majority of marine habitats were losing functional redundancy and thus elasmobranch ecological functions will not only decline, but become more vulnerable to future species loss on a virtually worldwide scale. Collectively, these results tell of a worrying ecological future for sharks and their relatives, given that their functional diversity is already acutely vulnerable (Pimiento et al. 2023), and was found by chapter 3 to be already depleted compared to the geological past (Cooper and Pimiento 2024). They predict a future where sharks will continue to lose distinct ecological roles of great importance for maintaining marine ecosystem functioning, and where the remaining functions will only be at greater risk of extinction across the world, putting the health of every ocean in jeopardy.

Taken together, chapters 2 and 3 tested the hypothesis that isolated teeth in the shark fossil record could be used to detect ecological function and therefore ecological consequences of extinction in the geological past. Chapter 2's results provided a framework of how dental characters relate to functional traits (**Table 5.1**), partially resolving a series of mixed and mostly qualitative results in prior attempts to link tooth morphology to function (e.g., Randall 1973, Frazzetta 1988, Whitenack and Motta 2010). The application of this framework to the fossil record could, therefore, allow palaeontologists to detect shark ecology through time. Indeed, as well as the functional diversity analyses explored here, a potential future avenue of research for this framework could possibly be its use to infer traits for extinct species in phylogenetic analyses. Not only are phylogenetic analyses strengthened by the inclusion of fossil taxa (e.g., Albert et al. 2009, Pimiento et al. 2019), but this would potentially reveal patterns of adaptation or niche differentiation, providing insight into how both ecological and evolutionary processes have shaped shark biodiversity through deep time (e.g., Marion et al. 2024). Nevertheless, caveats to this framework include: (1) the detected dental character-trait relationships were not always one to one, particularly with tooth shape as the main predictor

of feeding mechanism (Cooper et al. 2023); and (2) its basis in extant species which cannot always be applied to extinct species older than the Cenozoic era studied in chapter 3. Indeed, some sharks from the Cretaceous period immediately preceding the Cenozoic are unlike any species living today, as revealed by exceptional body preservation fossils rather than deduced from teeth. For example, *Aquilolamna milarcae* was an unusually small (~1 m) filter feeder with wing-like pectoral fins, displaying a unique body plan (Vullo et al. 2021), and species of *Ptychodus* were 10 m long crushing feeders consuming large, shelled prey like turtles and ammonites (Vullo et al. 2024). Nevertheless, many extinct species from the Cenozoic have living representatives (Paillard et al. 2020, Pimiento and Benton 2020), allowing chapter 2's framework to be applied to fossils of this age. This approach, where the dental characters stood in as trait proxies, was shown to be effective in broadly reflecting the ecology of extinct species with living relatives or analogues (Cooper and Pimiento 2024), ultimately showcasing the usefulness of extant species as ecological analogues for extinct sharks.

With this capture of ecological function, the results of chapter 3 highlight the importance of functionally unique and specialised species in geological time. The disproportionate contributions of such species to functional diversity has led to calls for conservation priorities towards endangered species that are highly functionally unique and/or specialised in today's extinction crisis; most notably through the FUSE index (Griffin et al. 2020, Pimiento et al. 2020b). Indeed, recent work on crocodylians has already shown that conservation priorities towards endangered species with distinctly high ecological importance helps recover predicted losses of functional diversity (Griffith et al. 2022). As such, the results of chapter 3 give palaeontological credence to such conservation calls by highlighting how the extinctions of functionally unique and specialised species in the distant past have had the largest ecological effects on sharks through time.

Additionally, the combined results of chapters 3 and 4 offer a long-term perspective of ecological changes following collective shark extinctions in the geological past (chapter 3) that can be quantifiably compared to the ecological effects of human impacts on shark biodiversity (chapter 4). This highlights how palaeobiological research could be a fundamental aid to future conservation (Dietl et al. 2015, Dietl 2019, Kiessling et al. 2019, Dillon et al. 2022, Pimiento and Antonelli 2022, Dillon and Pimiento 2024). Over the last 20 years, a growing research community has come together to use geohistorical records that document long-term biodiversity changes to help in mitigating today's climate and extinction crises (Dillon et al. 2022). This emerging field, conservation palaeobiology, shows stirring potential for informing

shark conservation thanks to the development of rich and novel frameworks and datasets such as those produced in chapters 2 and 3, as well as recent advances in biomechanical reconstructions and fossil tooth geochemistry that further reflect ecological function (Dillon and Pimiento 2024). In this thesis specifically, chapter 2 highlights how the limited shark fossil record can be used to inform past ecological functions comparable to those of today's sharks, while chapter 3 openly shows how the loss of functionally unique and specialised species has historically reduced functional diversity in the distant past, a direct parallel to the projected losses of today's sharks in chapter 4. This further stresses the importance of considering functional diversity, such as via the FUSE index (Griffin et al. 2020, Pimiento et al. 2020b), in conservation practises for sharks and their relatives (Pimiento et al. 2023).

Ultimately, urgent conservation action will be needed to prevent the global collapse of shark functional diversity. Generally, conservation actions have focused on species that are the most endangered as deemed by the IUCN Red List (IUCN 2023), with at least 30-40% of ocean area requiring protections in order to conserve these species (Dulvy et al. 2017, Jefferson et al. 2021). Indeed, in terms of the threatened marine megafauna, sharks are expected to incur a disproportionate loss of FRic even under IUCN-based extinction probabilities (Pimiento et al. 2020b). Marine protected areas (MPAs) have been devised around the globe to protect threatened marine species from overexploitation (West et al. 2009, Takashina and Mougi 2014, Magris 2021); a crucial step for protecting shark species which are greatest risk from excessive fishing (Dulvy et al. 2017, Dulvy et al. 2021). However, the global MPA network currently only protects 26% of elasmobranch FRic and, alarmingly, just 10% and 5% of their FUn and FSp respectively (Pimiento et al. 2023). Given that the highest-ranking FUS species (i.e., species with the highest FUn and/or FSp) are at the highest risk of extinction by 2100, with more than half of the top ten FUS species projected to become extinct within 200 years (chapter 4), it is evident that MPAs need to be widely expanded worldwide to cover hotspots of FUn and FSp. These areas, comprised of mainly oceanic habitats, are not necessarily hotspots for fishing pressure but are nonetheless exposed to intense longline fishing (Kroodsma et al. 2018, Queiroz et al. 2019, Pimiento et al. 2023). One promising development in conserving shark biodiversity hotspots like these is the Important Shark and Ray Area (ISRA) proposal, which identifies discrete, three-dimensional areas of important habitat that can be manageably conserved (Hyde et al. 2022). Three-dimensional assessments of marine habitats for conservation needs are becoming increasingly important to achieve sustainability as the footprint of overfishing has been found across all depths (Jacquemont et al. 2024).

Furthermore, extinction risk and life-history are already considered when designating ISRAs, thus incorporating species-specific FUSE scores into the ISRA conservation proposal could be key to securing the global future of shark functional diversity.

In conclusion, this thesis has demonstrated that: (1) measurements from isolated shark teeth can be used as proxies for functional traits to inform deep time functional diversity analyses (chapter 2; Cooper et al. 2023); (2) present-day shark functional diversity is likely diminished compared to the last 66 million years following an ongoing decline that began ~10 Ma (chapter 3; Cooper and Pimiento 2024); and (3) shark functional diversity will continue to decline, unevenly redistribute, and become even more vulnerable to extinctions in the near-future without rapid conservation action prioritising the most functionally unique and specialised species (chapter 4).

References

Aberhan M & Kiessling W, (2015). Persistent ecological shifts in marine molluscan assemblages across the end-Cretaceous mass extinction. *Proceedings of the National Academy of Sciences* **112**, 7207-7212.

Abràmoff MD, Magalhães, PJ & Ram, SJ, (2004). Image processing with ImageJ. *Biophotonics international* **11**, 36-42.

Adnet S, (2006). Biometric analysis of the teeth of fossil and Recent hexanchid sharks and its taxonomic implications. *Acta Palaeontologica Polonica* **51**, 477-488.

Adnet S, & Martin, RA, (2007). Increase of body size in sixgill sharks with change in diet as a possible background of their evolution. *Historical Biology* **19**, 279-289.

Aguilera OA, García L & Cozzuol MA, (2008). Giant-toothed white sharks and cetacean trophic interaction from the Pliocene Caribbean Paraguaná Formation. *Paläontologische Zeitschrift* **82**, 204-208.

Albert CH, de Bello F, Boulangeat I, Pellet G, Lavorel S & Thuiller W, (2012). On the importance of intraspecific variability for the quantification of functional diversity. *Oikos* **121**, 116-126.

Albert JS, Johnson DM & Knouft JH, (2009). Fossils provide better estimates of ancestral body size than do extant taxa in fishes. *Acta Zoologica* **90**, 357-384.

Alfaro ME, Faircloth BC, Harrington RC, Sorenson L, Friedman M, Thacker CE, Oliveros CH, Cerny D & Near TJ, (2018). Explosive diversification of marine fishes at the Cretaceous-Paleogene boundary. *Nature Ecology and Evolution* **2**, 688-696.

Ali JR, Blonder BW, Pigot AL & Tobias JA, (2022). Bird extinctions threaten to cause disproportionate reductions of functional diversity and uniqueness. *Functional Ecology* **37**, 162-175.

Alroy J, Aberhan M, Bottjer DJ, Foote M, Fürsich FT, Harries PJ, Hendy AJ, Holland SM, Ivany LC, Kiessling W, Kosnik MA, Marshall CR, McGowan AJ, Miller AI, Olszewski TD, Patzkowsky ME, Peters SE, Villier L, Wagner PJ, Bonuso N, Borkow PS, Brenneis B, Clapham ME, Fall LM, Ferguson CA, Hanson VL, Krug AZ, Layou KM, Leckey EH, Nürnberg S, Powers CM, Sessa JA, Simpson C, Tomašových A & Visaggi CC, (2008). Phanerozoic trends in the global diversity of marine invertebrates. *Science* **321**, 97-100.

Alvarez LW, Alvarez W, Asaro F & Michel HV, (1980). Extraterrestrial cause for the Cretaceous-Tertiary extinction. *Science* **208**, 1095-1108.

Andermann T, Faurby S, Cooke R, Silvestro D & Antonelli A, (2021). iucn_sim: a new program to simulate future extinctions based on IUCN threat status. *Ecography* **44**, 162-176.

Araújo MB, Anderson RP, Márcia Barbosa A, Beale CM, Dormann CF, Early R, Garcia RA, Guisan A, Maiorano L, Naimi B, O'Hara RB, Zimmermann NE & Rahbek C, (2019). Standards for distribution models in biodiversity assessments. *Science Advances* **5**, eaat4858.

Araújo MB, & Pearson RG, (2005). Equilibrium of species' distributions with climate. *Ecography* **28**, 693-695.

Ballell A & Ferrón HG, (2021). Biomechanical insights into the dentition of megatooth sharks (Lamniformes: Otodontidae). *Scientific Reports* **11**, 1232.

Baremore IE, Murie DJ & Carlson JK, (2010). Seasonal and size-related differences in diet of the Atlantic angel shark Squatina dumeril in the northeastern Gulf of Mexico. *Aquatic Biology* **8**, 125-136.

Barley SC, Clark TD & Meeuwig JJ, (2019). Ecological redundancy between coral reef sharks and predatory teleosts. *Reviews in Fish Biology and Fisheries* **30**, 153-172.

Barnosky AD, Matzke N, Tomiya S, Wogan GO, Swartz B, Quental TB, Marshall C, McGuire JL, Lindsey EL, Maguire KC, Mersey B & Ferrer EA, (2011). Has the Earth's sixth mass extinction already arrived? *Nature* **471**, 51-57.

Bates D, Mächler M, Bolker B & Walker S, (2014). Fitting linear mixed-effects models using lme4. *Journal of Statistical Software* **67**, 1-48.

Baum JK, & Worm B, (2009). Cascading top-down effects of changing oceanic predator abundances. *Journal of Animal Ecology* **78**, 699-714.

Bazzi M, Campione NE, Kear BP, Pimiento C & Ahlberg PE, (2021). Feeding ecology has shaped the evolution of modern sharks. *Current Biology* **31**, 1-11.

Belben RA, Underwood CJ, Johanson Z & Twitchett RJ, (2017). Ecological impact of the end-Cretaceous extinction on lamniform sharks. *PLoS One* **12**, e0178294.

Bemis WE, Moyer JK & Riccio ML, (2015). Homology of lateral cusplets in the teeth of lamnid sharks (Lamniformes: Lamnidae). *Copeia* **103**, 961-972.

Benton MJ, Dunhill AM, Lloyd GT & Marx FG, (2011). Assessing the quality of the fossil record: insights from vertebrates. *Geological Society, London, Special Publications* **358**, 63-94.

Benton MJ & Twitchett RJ, (2003). How to kill (almost) all life: the end-Permian extinction event. *Trends in Ecology and Evolution* **18**, 358-365.

Berio F, Evin A, Goudemand N & Debiais-Thibaud M, (2020). The intraspecific diversity of tooth morphology in the large-spotted catshark *Scyliorhinus stellaris*: insights into the ontogenetic cues driving sexual dimorphism. *Journal of Anatomy* **237**, 960-978.

Biggs CR, Yeager LA, Bolser DG, Bonsell C, Dichiera AM, Hou Z, Keyser SR, Khursigara AJ, Lu K, Muth AF, Negrete B, & Erisman BE, (2020). Does functional redundancy affect ecological stability and resilience? A review and meta-analysis. *Ecosphere* **11**, e03184.

Birkmanis CA, Freer JJ, Simmons LW, Partridge JC & Sequeira AMM, (2020). Future distribution of suitable habitat for pelagic sharks in Australia under climate change models. *Frontiers in Marine Science* **7**, 570.

Boessenecker RW, Ehret DJ, Long DJ, Churchill M, Martin E & Boessenecker SJ, (2019). The Early Pliocene extinction of the mega-toothed shark *Otodus megalodon*: a view from the eastern North Pacific. *PeerJ* **7**, e6088.

Bogan S & Agnolín FL, (2022). The fossil record of the Bramble-shark *Echinorhinus* (Echinorhiniformes, Echinorhinidae) in South America. *Journal of South American Earth Sciences* **120**, 104083.

Bonfil R, Meÿer M, Scholl MC, Johnson R, O'Brien S, Oosthuizen H, Swanson S, Kotze D & Paterson M, (2005). Transoceanic migration, spatial dynamics, and population linkages of white sharks. *Science* **310**, 100-103.

Burke KD, Williams JW, Chandler MA, Haywood AM, Lunt DJ & Otto-Bliesner BL, (2018). Pliocene and Eocene provide best analogs for near-future climates. *Proceedings of the National Academy of Sciences* **115**, 13288-13293.

Burkholder DA, Heithaus MR, Fourqurean JW, Wirsing A & Dill LM, (2013). Patterns of top-down control in a seagrass ecosystem: could a roving apex predator induce a behaviour-mediated trophic cascade? *Journal of Animal Ecology* **82**, 1192-1202.

Bush AM, Bambach RK & Daley GM, (2007). Changes in theoretical ecospace utilization in marine fossil assemblages between the mid-Paleozoic and late Cenozoic. *Paleobiology* **33**, 76-97.

Cappetta H, (2012). Handbook of Paleoichthyology—Chondrichthyes—Mesozoic and Cenozoic Elasmobranchii: Teeth. In HP Schultze (Ed.), *Handbook of paleoichthyology*. Volume 3E (pp. 1-512). Munich: Verlag Dr. Friedrich Pfiel.

Cardoso P, Rigal F, Carvalho JC & Kembel S, (2014). BAT – Biodiversity Assessment Tools, an R package for the measurement and estimation of alpha and beta taxon, phylogenetic and functional diversity. *Methods in Ecology and Evolution* **6**, 232-236.

Carmona CP, Pavanetto N & Puglielli G, (2024). funspace: An R package to build, analyse and plot functional trait spaces. *Diversity and Distributions* **30**, e13820.

Carmona CP, Tamme R, Pärtel M, de Bello F, Brosse S, Capdevila P, González-M R, González-Suárez M, Salguero-Gómez R, Vásquez-Valderrama M & Toussaint A, (2021). Erosion of global functional diversity across the tree of life. *Science Advances* **7**, eabf2675.

Casanoves F, Pla L, Di Rienzo JA & Díaz S, (2010). FDiversity: a software package for the integrated analysis of functional diversity. *Methods in Ecology and Evolution* **2**, 233-237.

Chavez S, Zufan S, Kim SH & Shimada K, (2012). Tooth sizes as a proxy for estimating body lengths in the porbeagle shark, *Lamna nasus*. *Journal of Fossil Research* **45**, 1-5.

Cheung WWL, & Frolicher TL, (2020). Marine heatwaves exacerbate climate change impacts for fisheries in the northeast Pacific. *Scientific Reports* **10**, 6678.

Ciampaglio CN, Kemp M & McShea DW, (2001). Detecting changes in morphospace occupation patterns in the fossil record: characterization and analysis of measures of disparity. *Paleobiology* **27**, 695-715.

Ciampaglio CN, Wray GA, & Corliss BH, (2005). A toothy tale of evolution: convergence in tooth morphology among marine Mesozoic–Cenozoic sharks, reptiles, and mammals. *The Sedimentary Record* **3**, 4-8.

Cianciaruso MV, Batalha MA, Gaston KJ & Petchey OL, (2009). Including intraspecific variability in functional diversity. *Ecology* **90**, 81-89.

Collareta A, Lambert O, Landini W, Di Celma C, Malinverno E, Varas-Malca R, Urbina M & Bianucci G, (2017). Did the giant extinct shark *Carcharocles megalodon* target small prey? Bite marks on marine mammal remains from the late Miocene of Peru. *Palaeogeography, Palaeoclimatology, Palaeoecology* **469**, 84-91.

Compagno LJV, (1990). Alternative life-history styles of cartilaginous fishes in time and space. *Environmental Biology of Fishes* **28**, 33-75.

Condamine FL, Romieu J & Guinot G, (2019). Climate cooling and clade competition likely drove the decline of lamniform sharks. *Proceedings of the National Academy of Sciences* **116**, 20584-20590.

Cooke R, Gearty W, Chapman ASA, Dunic J, Edgar GJ, Lefcheck JS, Rilov G, McClain CR, Stuart-Smith RD, Lyons SK & Bates AE, (2022). Anthropogenic disruptions to longstanding patterns of trophic-size structure in vertebrates. *Nature Ecology and Evolution* **6**, 684-692.

Cooper JA, Griffin JN, Kindlimann R & Pimiento C, (2023). Are shark teeth proxies for functional traits? A framework to infer ecology from the fossil record. *Journal of Fish Biology* **103**, 798-814.

Cooper JA, Hutchinson JR, Bernvi DC, Cliff G, Wilson RP, Dicken ML, Menzel J, Wroe S, Pirlo J, & Pimiento C, (2022). The extinct shark *Otodus megalodon* was a transoceanic super-predator: inferences from 3D modeling. *Science Advances* **8**, eabm9424.

Cooper JA & Pimiento C, (2024). The rise and fall of shark functional diversity over the last 66 million years. *Global Ecology and Biogeography* **33**, e13881.

Cooper JA, Pimiento C, Ferrón HG & Benton MJ, (2020). Body dimensions of the extinct giant shark *Otodus megalodon*: a 2D reconstruction. *Scientific Reports* **10**, 14596.

Corn KA, Farina SC, Brash J & Summers AP, (2016). Modelling tooth-prey interactions in sharks: the importance of dynamic testing. *Royal Society Open Science* **3**, 160141.

Cortés E, (1999). Standardized diet compositions and trophic levels of sharks. *ICES Journal of Marine Science* **56**, 707-117.

Coulon N, Elliott S, Teichert N, Auber A, McLean M, Barreau T, Feunteun E & Carpentier A, (2024). Northeast Atlantic elasmobranch community on the move: Functional reorganization in response to climate change. *Global Change Biology* **30**, e17157.

Cullen JA, & Marshall CD, (2019). Do sharks exhibit heterodonty by tooth position and over ontogeny? A comparison using elliptic Fourier analysis. *Journal of Morphology* **280**, 687-700.

Curnick DJ, Deaville R, Bortoluzzi JR, Cameron L, Carlsson JEL, Carlsson J, Dolton HR, Gordon CA, Hosegood P, Nilsson A, Perkins MW, Purves KJ, Spiro S, Vecchiato M, Williams RS & Payne NL, (2023). Northerly range expansion and first confirmed records of the smalltooth sand tiger shark, *Odontaspis ferox*, in the United Kingdom and Ireland. *Journal of Fish Biology* **103**, 1549-1555.

Davis M, Faurby S & Svenning JC, (2018). Mammal diversity will take millions of years to recover from the current biodiversity crisis. *Proceedings of the National Academy of Sciences* **115**, 11262-11267.

De'ath G & Fabricius KE, (2000). Classification and regression trees: a powerful yet simple technique for ecological data analysis. *Ecology* **81**, 3178-3192.

de Bello F, Botta-Dukát Z, Lepš J, Fibich P & Goslee S, (2020). Towards a more balanced combination of multiple traits when computing functional differences between species. *Methods in Ecology and Evolution* **12**, 443-448.

de Bello F, Lavorel S, Albert CH, Thuiller W, Grigulis K, Dolezal J, Janeček Š & Lepš J, (2011). Quantifying the relevance of intraspecific trait variability for functional diversity. *Methods in Ecology and Evolution* **2**, 163-174.

De Boer B, Van de Wal R, Bintanja R, Lourens L & Tuenter E, (2010). Cenozoic global ice-volume and temperature simulations with 1-D ice-sheet models forced by benthic δ 18 O records. *Annals of Glaciology* **51**, 23-33.

Dedman S, Moxley JH, Papastamatiou YP, Braccini M, Caselle JE, Chapman DD, Cinner JE, Dillon EM, Dulvy NK, Dunn RE, Espinoza M, Harborne AR, Harvey ES, Heupel MR, Huveneers C, Graham NAJ, Ketchum JT, Klinard NV, Kock AA, Lowe CG, MacNeil MA, Madin EMP, McCauley DJ, Meekan MG, Meier AC, Simpfendorfer CA, Tinker MT, Winton M, Wirsing AJ & Heithaus MR, (2024). Ecological roles and importance of sharks in the Anthropocene Ocean. *Science* **385**, adl2362.

Derrick DH, Cheok J & Dulvy NK, (2020). Spatially congruent sites of importance for global shark and ray biodiversity. *PLoS One* **15**, e0235559.

Desbiens AA, Roff G, Robbins WD, Taylor BM, Castro-Sanguino C, Dempsey A & Mumby PJ, (2021). Revisiting the paradigm of shark-driven trophic cascades in coral reef ecosystems. *Ecology* **102**, e03303.

Diaz-Carballido PL, Mendoza-González G, Yañez-Arenas CA & Chiappa-Carrara X, (2022). Evaluation of shifts in the potential future distributions of carcharhinid sharks under different climate change scenarios. *Frontiers in Marine Science* **8**, 745501.

Dicken ML, Hussey NE, Christiansen HM, Smale MJ, Nkabi N, Cliff G & Wintner SP, (2017). Diet and trophic ecology of the tiger shark (*Galeocerdo cuvier*) from South African waters. *PLoS One* **12**, e0177897.

Dietl GP, (2019). Conservation palaeobiology and the shape of things to come. *Philosophical Transactions of the Royal Society B* **374**, 20190294.

Dietl GP, Kidwell SM, Brenner M, Burney DA, Flessa KW, Jackson ST & Koch PL, (2015). Conservation paleobiology: leveraging knowledge of the past to inform conservation and restoration. *Annual Review of Earth and Planetary Sciences* **43**, 79-103.

Dillon EM, Norris RD & O'Dea A, (2017). Dermal denticles as a tool to reconstruct shark communities. *Marine Ecology Progress Series* **566**, 117-134.

Dillon EM, Pier JQ, Smith JA, Raja NB, Dimitrijević D, Austin EL, Cybulski JD, De Entrambasaguas J, Durham SR, Grether CM, Haldar HS, Kocáková K, Lin CH, Mazzini I, Mychajliw AM, Ollendorf AL, Pimiento C, Regalado Fernández OR, Smith IE, & Dietl GP, (2022). What is conservation paleobiology? Tracking 20 years of research and development. *Frontiers in Ecology and Evolution* **10**, 1031483.

Dillon EM & Pimiento C, (2024). Aligning paleobiological research with conservation priorities using elasmobranchs as a model. *Paleobiology*, 1-20.

Dineen AA, Fraiser ML & Sheehan PM, (2014). Quantifying functional diversity in pre- and post-extinction paleocommunities: A test of ecological restructuring after the end-Permian mass extinction. *Earth-Science Reviews* **136**, 339-349.

Dolton HR, Jackson AL, Deaville R, Hall J, Hall G, McManus G, Perkins MW, Rolfe RA, Snelling EP, Houghton JDR, Sims DW, & Payne NL, (2023a). Regionally endothermic traits in planktivorous basking sharks *Cetorhinus maximus*. *Endangered Species Research* **51**, 227-232.

Dolton HR, Snelling EP, Deaville R, Jackson AL, Perkins MW, Bortoluzzi JR, Purves K, Curnick DJ, Pimiento C & Payne NL, (2023b). Centralized red muscle in *Odontaspis ferox* and the prevalence of regional endothermy in sharks. *Biology Letters* **19**, 20230331.

Doughty CE, Roman J, Faurby S, Wolf A, Haque A, Bakker ES, Malhi Y, Dunning, Jr JB & Svenning JC, (2016). Global nutrient transport in a world of giants. *Proceedings of the National Academy of Sciences* **113**, 868-873.

Dulvy NK, Fowler SL, Musick JA, Cavanagh RD, Kyne PM, Harrison LR, Carlson JK, Davidson LN, Fordham SV, Francis MP, Pollock CM, Simpfendorfer CA, Burgess GH, Carpenter KE, Compagno LJV, Ebert DA, Gibson C, Heupel MR, Livingstone SR, Sanciangco JC, Stevens JD, Valenti S, & White WT. (2014). Extinction risk and conservation of the world's sharks and rays. *Elife* **3**, e00590.

Dulvy NK, Pacoureau N, Rigby CL, Pollom RA, Jabado RW, Ebert DA, Finucci B, Pollock CM, Cheok J, Derrick DH, Herman KB, Sherman CS, VanderWright WJ, Lawson JM, Walls RHL, Carlson JK, Charvet P, Bineesh KK, Fernando D, Ralph GM, Matsushiba JH, Hilton-Taylor C, Fordham SV & Simpfendorfer CA, (2021). Overfishing drives over one-third of all sharks and rays toward a global extinction crisis. *Current Biology* **31**, 4773-4787.

Dulvy NK, Simpfendorfer CA, Davidson LNK, Fordham SV, Brautigam A, Sant G & Welch DJ, (2017). Challenges and priorities in shark and ray conservation. *Current Biology* **27**, R565-R572.

Dunhill AM, Foster WJ, Sciberras J & Twitchett RJ, (2018). Impact of the Late Triassic mass extinction on functional diversity and composition of marine ecosystems. *Palaeontology* **61**, 133-148.

Ebert DA, Dando M, & Fowler S, (2021). *Sharks of the world: a complete guide*. Princeton University Press, Plymouth.

Enquist BJ, Abraham AJ, Harfoot MBJ, Malhi Y & Doughty CE, (2020). The megabiota are disproportionately important for biosphere functioning. *Nature Communications* **11**, 699.

Estes JA, Heithaus M, McCauley DJ, Rasher DB & Worm B, (2016). Megafaunal impacts on structure and function of ocean ecosystems. *Annual Review of Environment and Resources* **41**, 83-116.

Estes JA, Terborgh J, Brashares JS, Power ME, Berger J, Bond WJ, Carpenter SR, Essington TE, Holt RD, Jackson JB, Marquis RJ, Oksanen L, Oksanen T, Paine RT, Pikitch EK, Ripple WJ, Sandin SA, Scheffer M, Schoener TW, Shurin JB, Sinclair AR, Soule ME, Virtanen R & Wardle DA, 2011. Trophic downgrading of planet Earth. *Science* **333**, 301-306.

Estrada JA, Rice AN, Natanson LJ & Skomal GB, (2006). Use of isotopic analysis of vertebrae in reconstructing ontogenetic feeding ecology in white sharks. *Ecology* **87**, 829-834.

Estupiñán-Montaño C, Tamburin E & Delgado-Huertas A, (2021). Stable isotope evidence for movements of hammerhead sharks *Sphyrna lewini*, connecting two natural protected areas in the Colombian Pacific. *Marine Biodiversity* **51**, 74.

Feichtinger I, Adnet S, Cuny G, Guinot G, Kriwet J, Neubauer TA, Pollerspöck J, Shimada K, Straube N, Underwood C & Vullo R, (2021). Comment on "An early Miocene extinction in pelagic sharks". *Science* **374**, eabk0632.

Ferretti F, Jacoby DMP, Pfleger MO, White TD, Dent F, Micheli F, Rosenberg AA, Crowder LB & Block BA, (2020). Shark fin trade bans and sustainable shark fisheries. *Conservation Letters* **13**, e12708.

Ferretti F, Worm B, Britten GL, Heithaus MR & Lotze HK, (2010). Patterns and ecosystem consequences of shark declines in the ocean. *Ecology Letters* **13**, 1055-1071.

Ferrón HG, (2017). Regional endothermy as a trigger for gigantism in some extinct macropredatory sharks. *PLoS One* **12**, e0185185.

Firke S, Denney B, Haid C, Knight R, Grosser M & Zadra J, (2023). janitor: simple tools for examining and cleaning dirty data. R package version 2.2.0: https://CRAN.R-project.org/package=janitor.

Foote M & Sepkoski JJ, (1999). Absolute measures of the completeness of the fossil record. *Nature* **398**, 415-417.

Foster WJ, & Twitchett RJ, (2014). Functional diversity of marine ecosystems after the Late Permian mass extinction event. *Nature Geoscience* **7**, 233-238.

Frazzetta TH (1988). The mechanics of cutting and the form of shark teeth. *Zoomorphology* **108**, 93-107.

French GCA, Sturup M, Rizzuto S, van Wyk JH, Edwards D, Dolan RW, Wintner SP, Towner AV & Hughes WOH, (2017). The tooth, the whole tooth and nothing but the tooth: tooth shape and ontogenetic shift dynamics in the white shark *Carcharodon carcharias*. *Journal of Fish Biology* **91**, 1032-1047.

Friedman M & Sallan LC, (2012). Five hundred million years of extinction and recovery: a phanerozoic survey of large-scale diversity patterns in fishes. *Palaeontology* **55**, 707-742.

Frisch AJ, Ireland M, Rizzari JR, Lönnstedt OM, Magnenat KA, Mirbach CE & Hobbs JPA, (2016). Reassessing the trophic role of reef sharks as apex predators on coral reefs. *Coral Reefs* **35**, 459-472.

Froese R, & Pauly D, (2017). FishBase World wide web electronic publication. www.fishbase.org.

Gagic V, Bartomeus I, Jonsson T, Taylor A, Winqvist C, Fischer C, Slade EM, Steffan-Dewenter I, Emmerson M, Potts SG, Tscharntke T, Weisser W & Bommarco R, (2015). Functional identity and diversity of animals predict ecosystem functioning better than species-based indices. *Proceedings of the Royal Society B* **282**, 20142620.

Garcia VB, Lucifora LO & Myers RA, (2008). The importance of habitat and life history to extinction risk in sharks, skates, rays and chimaeras. *Proceedings of the Royal Society B* **275**, 83-89.

Gearty W, Chamberlain S & Salmon M, (2022). rredlist: 'IUCN' Red List Client. R package version 0.7.1:https://CRAN.R-project.org/package=rredlist.

Gissi E, McDevitt-Irwin JM, Kaschner K, Kesner-Reyes K, Hazen E, Santoleri R & Micheli F, (2023). Identifying climate refugia through analysis of functional diversity. *Research Square*, 1-34.

Gobler CJ, & Baumann H, (2016). Hypoxia and acidification in ocean ecosystems: coupled dynamics and effects on marine life. *Biology Letters* **12**, 20150976.

Godfrey SJ & Altman J, (2005). A Miocene cetacean vertebra showing a partially healed compression fracture, the result of convulsions or failed predation by the Giant White Shark, *Carcharodon megalodon*. *Jeffersoniana* **16**, 1-12.

Godfrey SJ & Beatty BL, (2022). A Miocene cetacean vertebra showing a partially healed longitudinal shear-compression fracture, possibly the result of domoic acid toxicity or failed predation. *Palaeontologia Electronica* **25**, a28.

Godfrey SJ, Nance JR & Riker NL, (2021). *Otodus*-bitten sperm whale tooth from the Neogene of the Coastal Eastern United States. *Acta Palaeontologica Polonica* **66**, 599-603.

Gore MA, Rowat D, Hall J, Gell FR & Ormond RF, (2008). Transatlantic migration and deep mid-ocean diving by basking shark. *Biology Letters* **4**, 395-398.

Gottfried MD, Compagno LJV & Bowman SC, (1996). Size and skeletal anatomy of the giant "megatooth" shark *Carcharodon megalodon*. Pages 55-66 *in* AP Klimley & Ainley DG, (Ed.). *Great white sharks: the biology of Carcharodon carcharias*. Academic Press, San Diego.

Gower JC, (1971). A general coefficient of similarity and some of its properties. *Biometrics* **27**, 857.

Gradstein FM, Ogg JG, Schmitz MD & Ogg GM, (2012). *The geologic time scale 2012*. Elsevier.

Grenié M, Denelle P, Tucker CM, Munoz F & Violle C, (2017). funrar: An R package to characterize functional rarity. *Diversity and Distributions* **23**, 1365-1371.

Grenié M & Gruson H, (2023). fundiversity: a modular R package to compute functional diversity indices. *Ecography* **2023**, e06585.

Griffin JN, Leprieur F, Silvestro D, Lefcheck JS, Albouy C, Rasher DB, Davis M, Svenning JC & Pimiento C, (2020). Functionally unique, specialised, and endangered (FUSE) species: towards integrated metrics for the conservation prioritisation toolbox. *BioRxiv*, 2020.05.09.084871.

Griffith P, Lang JW, Turvey ST & Gumbs R, (2022). Using functional traits to identify conservation priorities for the world's crocodylians. *Functional Ecology* **37**, 112-124.

Griffiths ML, Eagle RA, Kim SL, Flores RJ, Becker MA, Maisch HM, Trayler RB, Chan RL, McCormack J, Akhtar AA, Tripati AK & Shimada K, (2023). Endothermic physiology of extinct megatooth sharks. *Proceedings of the National Academy of Sciences* **120**, e2218153120.

Grubbs RD, Carlson JK, Romine JG, Curtis TH, McElroy WD, McCandless CT, Cotton CF & Musick JA, (2016). Critical assessment and ramifications of a purported marine trophic cascade. *Scientific Reports* **6**, 20970.

Guinot G, Adnet S & Cappetta H, (2012). An analytical approach for estimating fossil record and diversification events in sharks, skates and rays. *PLoS One* **7**, e44632.

Guinot G, Adnet S, Shimada K, Underwood CJ, Siversson M, Ward DJ, Kriwet J & Cappetta H, (2018). On the need of providing tooth morphology in descriptions of extant elasmobranch species. *Zootaxa* **4461**, 118-126.

Guinot G & Cavin L, (2016). 'Fish' (Actinopterygii and Elasmobranchii) diversification patterns through deep time. *Biological Reviews* **91**, 950-981.

Guinot G & Condamine FL, (2023). Global impact and selectivity of the Cretaceous-Paleogene mass extinction among sharks, skates and rays. *Science* **379**, 802-806.

Hammerschlag N, McDonnell LH, Rider MJ, Street GM, Hazen EL, Natanson LJ, McCandless CT, Boudreau MR, Gallagher AJ, Pinsky ML & Kirtman B, (2022). Ocean warming alters the distributional range, migratory timing, and spatial protections of an apex predator, the tiger shark (*Galeocerdo cuvier*). *Global Change Biology* **28**, 1990-2005.

Hammerschlag N, Schmitz OJ, Flecker AS, Lafferty KD, Sih A, Atwood TB, Gallagher AJ, Irschick DJ, Skubel R & Cooke SJ, (2019). Ecosystem function and services of aquatic predators in the Anthropocene. *Trends in Ecology and Evolution* **34**, 369-383.

Harnik PG, Lotze HK, Anderson SC, Finkel ZV, Finnegan S, Lindberg DR, Liow LH, Lockwood R, McClain CR, McGuire JL, O'Dea A, Pandolfi JM, Simpson C & Tittensor DP, (2012). Extinctions in ancient and modern seas. *Trends in Ecology and Evolution* **27**, 608-617.

Harrison XA, Donaldson L, Correa-Cano ME, Evans J, Fisher DN, Goodwin CED, Robinson BS, Hodgson DJ & Inger R, (2018). A brief introduction to mixed effects modelling and multi-model inference in ecology. *PeerJ* **6**, e4794.

Hedberg CP, Lyons SK & Smith FA, (2021). The hidden legacy of megafaunal extinction: Loss of functional diversity and resilience over the Late Quaternary at Hall's Cave. *Global Ecology and Biogeography* **31**, 294-307.

Henderson CJ, Gilby BL, Turschwell MP, Goodridge Gaines LA, Mosman JD, Schlacher TA, Borland HP & Olds AD, (2024). Long term declines in the functional diversity of sharks in the coastal oceans of eastern Australia. *Communications Biology* **7**, 611.

Heupel MR, Knip DM, Simpfendorfer CA & Dulvy NK, (2014). Sizing up the ecological role of sharks as predators. *Marine Ecology Progress Series* **495**, 291-298.

Hodapp D, Roca IT, Fiorentino D, Garilao C, Kaschner K, Kesner-Reyes K, Schneider B, Segschneider J, Kocsis AT, Kiessling W, Brey T & Froese R, (2023). Climate change disrupts core habitats of marine species. *Global Change Biology* **29**, 3304-3317.

Hovestadt DC, (2018). Reassessment and revision of the fossil Heterodontidae (Chondrichthyes: Neoselachii) based on tooth morphology of extant taxa. *Palaeontos* **30**, 3-120.

Hubbell G, (1996). Using tooth structure to determine the evolutionary history of the white shark. Pages 9-18 *in* AP Klimley & Ainley DG (Ed.), *Great white sharks: the biology of Carcharodon carcharias.* Academic Press, San Diego.

Hughes AC, Orr MC, Ma K, Costello MJ, Waller J, Provoost P, Yang Q, Zhu C & Qiao H, (2021). Sampling biases shape our view of the natural world. *Ecography* **44**, 1259-1269.

Hyde CA, Notarbartolo di Sciara G, Sorrentino L, Boyd C, Finucci B, Fowler SL, Kyne PM, Leurs G, Simpfendorfer CA, Tetley MJ, Womersley F & Jabado RW, (2022). Putting sharks on the map: A global standard for improving shark area-based conservation. *Frontiers in Marine Science* **9**, 968853.

IUCN, (2023). The IUCN Red List of Threatened Species. Retrieved from www.iucnredlist.org.

Jablonski D, (2004). Extinction: past and present. *Nature* **427**, 589.

Jacquemont J, Loiseau C, Tornabene L & Claudet J, (2024). 3D ocean assessments reveal that fisheries reach deep but marine protection remains shallow. *Nature Communications* **15**, 4027.

Jefferson T, Costello MJ, Zhao Q & Lundquist CJ, (2021). Conserving threatened marine species and biodiversity requires 40% ocean protection. *Biological Conservation* **264**, 109368.

Jorgensen SJ, Micheli F, White TD, Van Houtan KS, Alfaro-Shigueto J, Andrzejaczek S, Arnoldi NS, Baum JK, Block B, Britten GL, Butner C, Caballero S, Cardeñosa D, Chapple TK, Clarke S, Cortés E, Dulvy NK, Fowler S, Gallagher AJ, Gilman E, Godley BJ, Graham RT, Hammerschlag N, Harry AV, Heithaus MR, Hutchinson M, Huveneers C, Lowe CG, Lucifora LO, MacKeracher T, Mangel JC, Barbosa Martins AP, McCauley DJ, McClenachan L, Mull C, Natanson LJ, Pauly D, Pazmiño DA, Pistevos JCA, Queiroz N, Roff G, Shea BD, Simpfendorfer CA, Sims DW, Ward-Paige C, Worm B & Ferretti F, (2022). Emergent research and priorities for shark and ray conservation. *Endangered Species Research* **47**, 171-203.

Kallal RJ, Godfrey SJ & Ortner DJ, (2010). Bone reactions on a pliocene cetacean rib indicate short-term survival of predation event. *International Journal of Osteoarchaeology* **22**, 253-260.

Kaschner K, Kesner-Reyes K, Garilao C, Segschneider J, Rius-Barile J, Rees T & Froese R, (2019). AquaMaps: Predicted range maps for aquatic species.

Kast ER, Griffiths ML, Kim SL, Rao ZC, Shimada K, Becker MA, Maisch HM, Eagle RA, Clarke CA, Neumann AN, Karnes ME, Lüdecke T, Leichliter JN, Martínez-García A, Akhtar AA, Wang XT, Haug GH & Sigman DM, (2022). Cenozoic megatooth sharks occupied extremely high trophic positions. *Science Advances* **8**, eabl6529.

Kent BW, (1994). *Fossil sharks of the Chesapeake Bay region*. Egan Rees & Boyer, Inc., Columbia, Maryland.

Kent BW, (2018). The cartilaginous fishes (chimaeras, sharks and rays) of Calvert Cliffs, Maryland, USA. Pages 45-157 *in* SJ Godfrey, (Ed.). The Geology and Vertebrate Paleontology of Calvert Cliffs, Maryland, USA. Smithsonian Institution Scholarly Press, Washington D.C.

Kiessling W, Raja NB, Roden VJ, Turvey ST & Saupe EE, (2019). Addressing priority questions of conservation science with palaeontological data. *Philosophical Transactions of the Royal Society B* **374**, 20190222.

Kriwet J & Benton MJ, (2004). Neoselachian (Chondrichthyes, Elasmobranchii) diversity across the Cretaceous–Tertiary boundary. *Palaeogeography, Palaeoclimatology, Palaeoecology* **214**, 181-194.

Kroodsma DA, Mayorga J, Hochberg T, Miller NA, Boerder K, Ferretti F, Wilson A, Bergman B, White TD, Block BA, Woods P, Sullivan B, Costello C & Worm B, (2018). Tracking the global footprint of fisheries. *Science* **359**, 904-908.

Laliberté E & Legendre P, (2010). A distance-based framework for measuring functional diversity from multiple traits. *Ecology* **91**, 299-305.

Lefcheck JS, Bastazini VAG & Griffin JN, (2015). Choosing and using multiple traits in functional diversity research. *Environmental Conservation* **42**, 104-107.

Legras G, Loiseau N, Gaertner JC, Poggiale JC & Gaertner-Mazouni N, (2019). Assessing functional diversity: the influence of the number of the functional traits. *Theoretical Ecology* **13**, 117-126.

Leigh SC, Papastamatiou YP & German DP, (2018). Seagrass digestion by a notorious 'carnivore'. *Proceedings of the Royal Society B* **285**, 20181583.

Litvinov F, Agapov S, Katalimov V, & Mironov S, (1983). Rate of tooth replacement in blue shark, *Prionace glauca* (Carcharhinidae), in relation to feeding. *Journal of Ichthyology* **23**, 143-145.

Lucifora LO, Carvalho MR, Kyne PM & White WT, (2015). Freshwater sharks and rays. *Current Biology* **25**, R971-973.

Lucifora LO, García VB, Menni RC, Escalante AH & Hozbor NM, (2009). Effects of body size, age and maturity stage on diet in a large shark: ecological and applied implications. *Ecological Research* **24**, 109-118.

Lucifora LO, Garcia VB & Worm B, (2011). Global diversity hotspots and conservation priorities for sharks. *PLoS One* **6**, e19356.

MacNeil MA, Skomal GB & Fisk AT, (2005). Stable isotopes from multiple tissues reveal diet switching in sharks. *Marine Ecology Progress Series* **302**, 199-206.

Magneville C, Loiseau N, Albouy C, Casajus N, Claverie T, Escalas A, Leprieur F, Maire E, Mouillot D & Villéger S, (2022). mFD: an R package to compute and illustrate the multiple facets of functional diversity. *Ecography* **2022**, e05904.

Magris RA, (2021). Effectiveness of large-scale marine protected areas in the Atlantic Ocean for reducing fishing activities. *Frontiers in Marine Science* **8**, 711011.

Maire E, Grenouillet G, Brosse S & Villéger S, (2015). How many dimensions are needed to accurately assess functional diversity? A pragmatic approach for assessing the quality of functional spaces. *Global Ecology and Biogeography* **24**, 728-740.

Maisey JG, (2012). What is an 'elasmobranch'? The impact of palaeontology in understanding elasmobranch phylogeny and evolution. *Journal of Fish Biology* **80**, 918-951.

Mammola S, Carmona CP, Guillerme T & Cardoso P, (2021). Concepts and applications in functional diversity. *Functional Ecology* **35**, 1869-1885.

Mara KR, Motta PJ & Huber DR, (2010). Bite force and performance in the durophagous bonnethead shark, *Sphyrna tiburo*. *Journal of Experimental Zoology Part A: Ecological Genetics and Physiology* **313**, 95-105.

Marion AFP, Condamine FL & Guinot G, (2024). Sequential trait evolution did not drive deep-time diversification in sharks. *Evolution* **78**, 1405-1425.

Marrama G & Kriwet J, (2017). Principal component and discriminant analyses as powerful tools to support taxonomic identification and their use for functional and phylogenetic signal detection of isolated fossil shark teeth. *PLoS One* **12**, e0188806.

Marshall CR, (2019). Using the fossil record to evaluate timetree timescales. *Frontiers in Genetics* **10**, 1049.

Marshall CR, (2023). Forty years later: The status of the "Big Five" mass extinctions. *Cambridge Prisms: Extinction* **1**, e5, 1-13.

Martin JE, Tacail T, Adnet S, Girard C & Balter V, (2015). Calcium isotopes reveal the trophic position of extant and fossil elasmobranchs. *Chemical Geology* **415**, 118-125.

Martin RA, (2005). Conservation of freshwater and euryhaline elasmobranchs: a review. *Journal of the Marine Biological Association of the United Kingdom* **85**, 1049-1073.

Marx FG & Uhen MD, (2010). Climate, critters, and cetaceans: Cenozoic drivers of the evolution of modern whales. *Science* **327**, 993-996.

McClain CR, Balk MA, Benfield MC, Branch TA, Chen C, Cosgrove J, Dove AD, Gaskins LC, Helm RR, Hochberg FG, Lee FB, Marshall A, McMurray SE, Schanche C, Stone SN & Thaler AD, (2015). Sizing ocean giants: patterns of intraspecific size variation in marine megafauna. *PeerJ* **3**, e715.

McCormack J, Griffiths ML, Kim SL, Shimada K, Karnes ME, Maisch HM, Pederzani S, Bourgon N, Jaouen K, Becker MA, Jöns N, Sisma-Ventura G, Straube N, Pollerspöck J, Hublin JJ, Eagle RA & Tütken T, (2022). Trophic position of *Otodus megalodon* and great white sharks through time revealed by zinc isotopes. *Nature Communications* **13**, 2980.

McGill BJ, Enquist BJ, Weiher E & Westoby M, (2006). Rebuilding community ecology from functional traits. *Trends in Ecology and Evolution* **21**, 178-185.

Meekan M, Virtue P, Marcus L, Clements K, Nichols P & Revill A, (2022). The world's largest omnivore is a fish. *Ecology* **103**, e3818.

Micheli F, & Halpern BS, (2005). Low functional redundancy in coastal marine assemblages. *Ecology Letters* **8**, 391-400.

Miller KG, Kominz MA, Browning JV, Wright JD, Mountain GS, Katz ME, Sugarman PJ, Cramer BS, Christie-Blick N & Pekar SF, (2005). The Phanerozoic record of global sea-level change. *Science* **310**, 1293-1298.

Mokany K, Ash J & Roxburgh S, (2008). Functional identity is more important than diversity in influencing ecosystem processes in a temperate native grassland. *Journal of Ecology* **96**, 884-893.

Monroe MJ, Butchart SHM, Mooers AØ & Bokma F, (2019). The dynamics underlying avian extinction trajectories forecast a wave of extinctions. *Biology Letters* **15**, 20190633.

Mooers AØ, Faith DP & Maddison WP, (2008). Converting endangered species categories to probabilities of extinction for phylogenetic conservation prioritization. *PLoS One* **3**, e3700.

Moss RH, Edmonds JA, Hibbard KA, Manning MR, Rose SK, van Vuuren DP, Carter TR, Emori S, Kainuma M, Kram T, Meehl GA, Mitchell JF, Nakicenovic N, Riahi K, Smith SJ, Stouffer RJ, Thomson AM, Weyant JP & Wilbanks TJ, (2010). The next generation of scenarios for climate change research and assessment. *Nature* **463**, 747-756.

Motta PJ, (2004). Prey capture behavior and feeding mechanics of elasmobranchs. Pages 165-202 *in* J. C. Carrier, J. A. Musick, and M. R. Heithaus, (Ed.). *Biology of sharks and their relatives*. CRC Press, New York.

Mouillot D, Bellwood DR, Baraloto C, Chave J, Galzin R, Harmelin-Vivien M, Kulbicki M, Lavergne S, Lavorel S, Mouquet N, Paine CE, Renaud J & Thuiller W, (2013a). Rare species support vulnerable functions in high-diversity ecosystems. *PLoS Biology* **11**, e1001569.

Mouillot D, Graham NA, Villéger S, Mason NW & Bellwood DR, (2013b). A functional approach reveals community responses to disturbances. *Trends in Ecology and Evolution* **28**, 167-177.

Mouillot D, Villéger S, Parravicini V, Kulbicki M, Arias-Gonzalez JE, Bender M, Chabanet P, Floeter SR, Friedlander A, Vigliola L & Bellwood DR, (2014). Functional over-redundancy and high functional vulnerability in global fish faunas on tropical reefs. *Proceedings of the National Academy of Sciences* **111**, 13757-13762.

Moyer JK & Bemis WE, (2017). Shark teeth as edged weapons: serrated teeth of three species of selachians. *Zoology* **120**, 101-109.

Mull CG, Pacoureau N, Pardo SA, Ruiz LS, Garcia-Rodriguez E, Finucci B, Haack M, Harry A, Judah AB, VanderWright W, Yin JS, Kindsvater HK & Dulvy NK, (2022). Sharkipedia: a curated open access database of shark and ray life history traits and abundance time-series. *Scientific Data* **9**, 559.

Munroe SEM, Simpfendorfer CA & Heupel MR, (2013). Defining shark ecological specialisation: concepts, context, and examples. *Reviews in Fish Biology and Fisheries* **24**, 317-331.

Myers RA, Baum JK, Shepherd TD, Powers SP & Peterson CH, (2007). Cascading effects of the loss of apex predatory sharks from a coastal ocean. *Science* **315**, 1846-1850.

Navarro J, López L, Coll M, Barría C & Sáez-Liante R, (2014). Short- and long-term importance of small sharks in the diet of the rare deep-sea shark *Dalatias licha*. *Marine Biology* **161**, 1697-1707.

Navia AF, Mejía-Falla PA, López-García J, Giraldo A, & Cruz-Escalona VH, (2017). How many trophic roles can elasmobranchs play in a marine tropical network? *Marine and Freshwater Research* **68**, 1342-1353.

Naylor GJ, de Lima A, Castro JI, Hubbell G & de Pinna MC, (2021). Comment on "An early Miocene extinction in pelagic sharks". *Science* **374**, eabj8723.

Nielson J, Hedeholm RB, Heinemeier J, Bushnell PG, Christiansen JS, Olsen J, Ramsey CB, Brill RW, Simon M, Steffensen KF & Steffensen JF, (2016). Eye lens radiocarbon reveals centuries of longevity in the Greenland shark (*Somniosus microcephalus*). *Science* **353**, 702-704.

Nock CA, Vogt RJ & Beisner BE, (2016). Functional Traits. *Encyclopedia of Life Sciences*, 1-8.

Novack-Gottshall PM, (2007). Using a theoretical ecospace to quantify the ecological diversity of Paleozoic and modern marine biotas. *Paleobiology* **33**, 273-294.

Nyberg KG, Ciampaglio CN & Wray GA, (2006). Tracing the ancestry of the great white shark, *Carcharodon carcharias*, using morphometric analyses of fossil teeth. *Journal of Vertebrate Paleontology* **26**, 806-814.

Ordiz A, Bischof R & Swenson JE, (2013). Saving large carnivores, but losing the apex predator? *Biological Conservation* **168**, 128-133.

Pacoureau N, Rigby CL, Kyne PM, Sherley RB, Winker H, Carlson JK, Fordham SV, Barreto R, Fernando D, Francis MP, Jabado RW, Herman KB, Liu KM, Marshall AD, Pollom RA, Romanov EV, Simpfendorfer CA, Yin JS, Kindsvater HK & Dulvy NK, (2021). Half a century of global decline in oceanic sharks and rays. *Nature* **589**, 567-571.

Paillard A, Shimada K & Pimiento C, (2020). The fossil record of extant elasmobranchs. *Journal of Fish Biology* **98**, 445-455.

Palacio FX, Callaghan CT, Cardoso P, Hudgins EJ, Jarzyna MA, Ottaviani G, Riva F, Graco-Roza C, Shirey V & Mammola S, (2022). A protocol for reproducible functional diversity analyses. *Ecography* **2022**, e06287.

Papastamatiou YP, Wetherbee BM, Lowe CG & Crow GL, (2006). Distribution and diet of four species of carcharhinid shark the the Hawaiian Islands: evidence for resource partitioning and competitive exclusion. *Marine Ecology Progress Series* **320**, 239-251.

Pavoine S & Ricotta C, (2023). Identifying functionally distinctive and threatened species. *Biological Conservation* **284**, 110170.

Pavoine S, Vallet J, Dufour AB, Gachet S & Daniel H, (2009). On the challenge of treating various types of variables: application for improving the measurement of functional diversity. *Oikos* **118**, 391-402.

Payne JL, Bush AM, Heim NA, Knope ML & McCauley DJ, (2016). Ecological selectivity of the emerging mass extinction in the oceans. *Science* **14**, aaf2416.

Perez VJ, Leder RM & Badaut T, (2021). Body length estimations of Neogene lamniform sharks (*Carcharodon* and *Otodus*) derived from associated dentitions. *Palaeontologia Electronica* **24**, a09.

Petchey OL & Gaston KJ, (2006). Functional diversity: back to basics and looking forward. *Ecology Letters* **9**, 741-758.

Pimiento C, Albouy C, Silvestro D, Mouton TL, Velez L, Mouillot D, Judah AB, Griffin JN, & Leprieur F, (2023). Functional diversity of sharks and rays is highly vulnerable and supported by unique species and locations worldwide. *Nature Communications* **14**, 7691.

Pimiento C & Antonelli A, (2022). Integrating deep-time palaeontology in conservation prioritisation. *Frontiers in Ecology and Evolution* **10**, 959364.

Pimiento C, Bacon CD, Silvestro D, Hendy A, Jaramillo C, Zizka A, Meyer X & Antonelli A, (2020a). Selective extinction against redundant species buffers functional diversity. *Proceedings of the Royal Society B* **287**, 20201162.

Pimiento C & Balk MA, (2015). Body-size trends of the extinct giant shark *Carcharocles megalodon*: a deep-time perspective on marine apex predators. *Paleobiology* **41**, 479-490.

Pimiento C & Benton MJ, (2020). The impact of the Pull of the Recent on extant elasmobranchs. *Palaeontology* **63**, 369-374.

Pimiento C, Cantalapiedra JL, Shimada K, Field DJ & Smaers JB, (2019). Evolutionary pathways toward gigantism in sharks and rays. *Evolution* **73**, 588-599.

Pimiento C & Clements CF, (2014). When did *Carcharocles megalodon* become extinct? A new analysis of the fossil record. *PLoS One* **9**, e111086.

Pimiento C, Ehret DJ, MacFadden BJ & Hubbell G, (2010). Ancient nursery area for the extinct giant shark megalodon from the Miocene of Panama. *PLoS One* **5**, e10552.

Pimiento C, Griffin JN, Clements CF, Silvestro D, Varela S, Uhen MD & Jaramillo C (2017). The Pliocene marine megafauna extinction and its impact on functional diversity. *Nature Ecology and Evolution* **1**, 1100-1106.

Pimiento C, Kocáková K, Mathes GH, Argyriou T, Cadena EA, Cooper JA, Cortés D, Field DJ, Klug C, Scheyer TM, Valenzuela-Toro AM, Buess T, Günter M, Gardiner AM, Hatt P, Holdener G, Jacober G, Kobelt S, Masseraz S, Mehli I, Reiff S, Rigendinger E, Ruckstuhl M, Schneider S, Seige C, Senn N, Staccoli V, Baumann J, Flüeler L, Guevara LJ, Ickin E, Kissling KC, Rogenmoser J, Spitznagel D, Villafaña JA & Zanatta C, (2024). The extinct marine megafauna of the Phanerozoic. *Cambridge Prisms: Extinction* **2**, 1-17.

Pimiento C, Leprieur F, Silvestro D, Lefcheck JS, Albouy C, Rasher DB, Davis M, Svenning JC & Griffin JN, (2020b). Functional diversity of marine megafauna in the Anthropocene. *Science Advances* **6**, eaay7650.

Pimiento C, MacFadden BJ, Clements CF, Varela S, Jaramillo C, Velez-Juarbe J & Silliman BR, (2016). Geographical distribution patterns of *Carcharocles megalodon* over time reveal clues about extinction mechanisms. *Journal of Biogeography* **43**, 1645-1655.

Pollerspöck J, Cares D, Ebert DA, Kelley KA, Pockalny R, Robinson RS, Wagner D & Straube N, (2023). First in situ documentation of a fossil tooth of the megatooth shark *Otodus* (*Megaselachus*) *megalodon* from the deep sea in the Pacific Ocean. *Historical Biology*, 1-6.

Pollerspöck J, & Straube N, (2014). Shark-references. Retrieved from www.shark-references.com.

Power S, Lengaigne M, Capotondi A, Khodri M, Vialard J, Jebri B, Guilyardi E, McGregor S, Kug JS, Newman M, McPhaden MJ, Meehl G, Smith D, Cole J, Emile-Geay J, Vimont D, Wittenberg AT, Collins M, Kim GI, Cai W, Okumura Y, Chung C, Cobb KM, Delage F, Planton YY, Levine A, Zhu F, Sprintall J, Di Lorenzo E, Zhang X, Luo JJ, Lin X, Balmaseda M, Wang G & Henley BJ, (2021). Decadal climate variability in the tropical Pacific: Characteristics, causes, predictability, and prospects. *Science* **374**, eaay9165.

Purvis A, Gittleman JL, Cowlishaw G & Mace GM, (2000). Predicting extinction risk in declining species. *Proceedings of the Royal Society B* **267**, 1947-1952.

Pyenson ND & Sponberg SN, (2011). Reconstructing body size in extinct crown Cetacea (Neoceti) using allometry, phylogenetic methods and tests from the fossil record. *Journal of Mammalian Evolution* **18**, 269-288.

Queiroz N, Humphries NE, Couto A, Vedor M, da Costa I, Sequeira AMM, Mucientes G, Santos AM, Abascal FJ, Abercrombie DL, Abrantes K, Acuna-Marrero D, Afonso AS, Afonso P, Anders D, Araujo G, Arauz R, Bach P, Barnett A, Bernal D, Berumen ML, Bessudo Lion S, Bezerra NPA, Blaison AV, Block BA, Bond ME, Bonfil R, Bradford RW, Braun CD, Brooks EJ, Brooks A, Brown J, Bruce BD, Byrne ME, Campana SE, Carlisle AB, Chapman DD, Chapple TK, Chisholm J, Clarke CR, Clua EG, Cochran JEM, Crochelet EC, Dagorn L, Daly R, Cortes DD, Doyle TK, Drew M, Duffy CAJ, Erikson T, Espinoza E, Ferreira LC, Ferretti F, Filmalter JD, Fischer GC, Fitzpatrick R, Fontes J, Forget F, Fowler M, Francis MP, Gallagher AJ, Gennari E, Goldsworthy SD, Gollock MJ, Green JR, Gustafson JA, Guttridge TL, Guzman HM, Hammerschlag N, Harman L, Hazin FHV, Heard M, Hearn AR, Holdsworth JC, Holmes BJ, Howey LA, Hoyos M, Hueter RE, Hussey NE, Huveneers C, Irion DT, Jacoby DMP, Jewell OJD, Johnson R, Jordan LKB, Jorgensen SJ, Joyce W, Keating Daly CA, Ketchum JT, Klimley AP, Kock AA, Koen P, Ladino F, Lana FO, Lea JSE, Llewellyn F, Lyon WS, MacDonnell A, Macena BCL, Marshall H, McAllister JD, McAuley R, Meyer MA, Morris JJ, Nelson ER, Papastamatiou YP, Patterson TA, Penaherrera-Palma C, Pepperell JG, Pierce SJ, Poisson F, Quintero LM, Richardson AJ, Rogers PJ, Rohner CA, Rowat DRL, Samoilys M, Semmens JM, Sheaves M, Shillinger G, Shivji M, Singh S, Skomal GB, Smale MJ, Snyders LB, Soler G, Soria M, Stehfest KM, Stevens JD, Thorrold SR, Tolotti MT, Towner AV, Travassos P, Tyminski JP, Vandeperre F, Vaudo JJ, Watanabe YY, Weber SB, Wetherbee BM, White TD, Williams S, Zarate PM, Harcourt R, Hays GC, Meekan MG, Thums M, Irigoien X, Eguiluz VM, Duarte CM, Sousa LL, Simpson SJ, Southall EJ & Sims DW, (2019). Global spatial risk assessment of sharks under the footprint of fisheries. *Nature* **572**, 461-466.

R Development Core Team (2017). *R: A Language and Environment for Statistical Computing*. R Foundation for Statistical Computing, Vienna, Austria.

Rabosky DL & Sorhannus U, (2009). Diversity dynamics of marine planktonic diatoms across the Cenozoic. *Nature* **457**, 183-186.

Raja NB, Dunne EM, Matiwane A, Khan TM, Natscher PS, Ghilardi AM & Chattopadhyay D, (2022). Colonial history and global economics distort our understanding of deep-time biodiversity. *Nature Ecology and Evolution* **6**, 145-154.

Randall JE, (1973). Size of the great white shark (*Carcharodon*). *Science* **181**, 169-170.

Raup DM, (1994). The role of extinctions in evolution. *Proceedings of the National Academy of Sciences* **91**, 6758-76763.

Raup DM & Sepkoski JJ, (1982). Mass extinctions in the marine fossil record. *Science* **215**, 1501-1503.

Redfern LM, (2013). High Performance Computing (HPC) Wales and the next generation workforce: Strategies to ensure propagation. *MRS Online Proceedings Library* **1583**, 307.

Renault D, Hess MCM, Braschi J, Cuthbert RN, Sperandii MG, Bazzichetto M, Chabrerie O, Thiebaut G, Buisson E, Grandjean F, Bittebiere AK, Mouchet M & Massol F, (2022). Advancing biological invasion hypothesis testing using functional diversity indices. *Science of the Total Environment* **834**, 155102.

Roff G, Brown CJ, Priest MA & Mumby PJ, (2018). Decline of coastal apex shark populations over the past half century. *Communications Biology* **1**, 1-11.

Roff, G, Doropoulos C, Rogers A, Bozec YM, Krueck NC, Aurellado E, Priest M, Birrell C & Mumby PJ, (2016). The ecological role of sharks on coral reefs. *Trends in Ecology and Evolution* **31**, 395-407.

Rosa R, Rummer JL & Munday PL (2017). Biological responses of sharks to ocean acidification. *Biology Letters* **13**, 20160796.

Rummer JL, Bouyoucos IA, Wheeler CR, Santos CP & Rosa R, (2022). Climate change and sharks. Page 840 *in* JC Carrier, CA Simpfendorfer, MR Heithaus & KE Yopak, (Ed.). *Biology of sharks and their relatives*. CRC Press, Boca Raton, FL.

Sequeira AM, Mellin C, Fordham DA, Meekan MG & Bradshaw CJ, (2014). Predicting current and future global distributions of whale sharks. *Global Change Biology* **20**, 778-789.

Shimada K, (2002). Dental homologies in lamniform sharks (Chondrichthyes: Elasmobranchii). *Journal of Morphology* **251**, 38-72.

Shimada K, (2003). The relationship between the tooth size and total body length in the white shark. *Journal of Fossil Research* **35**, 28-33.

Shimada K, (2019). The size of the megatooth shark, *Otodus megalodon* (Lamniformes: Otodontidae), revisited. *Historical Biology* **33**, 904-911.

Shimada K, Becker MA & Griffiths ML, (2020). Body, jaw, and dentition lengths of macrophagous lamniform sharks, and body size evolution in Lamniformes with special reference to 'off-the-scale' gigantism of the megatooth shark, *Otodus megalodon*. *Historical Biology* **33**, 2543-2559.

Shimada K, & Ward DJ, (2016). The oldest fossil record of the megamouth shark from the late Eocene of Denmark, and comments on the enigmatic megachasmid origin. *Acta Palaeontologica Polonica* **61**, 839-845.

Shupinski AB, Wagner PJ, Smith FA & Lyons SK, (2024). Unique functional diversity during early Cenozoic mammal radiation of North America. *Proceedings of the Royal Society B* **291**, 20240778.

Sibert EC & Norris RD, (2015). New age of fishes initiated by the Cretaceous-Paleogene mass extinction. *Proceedings of the National Academy of Sciences* **112**, 8537-8542.

Sibert EC & Rubin LD, (2021a). An early Miocene extinction in pelagic sharks. *Science* **372**, 1105-1107.

Sibert EC & Rubin LD, (2021b). Response to comment on "An early Miocene extinction of pelagic sharks". *Science* **374**, abk1733.

Sibert EC & Rubin LD (2021c). Response to comment on "An early Miocene extinction of pelagic sharks". *Science* **374**, eabj9522.

Siders ZA, Trotta LB, Caltabellotta FP, Loesser KB, Baiser B & Ahrens RNM, (2022). Functional and phylogenetic diversity of sharks in the Northeastern Pacific. *Journal of Biogeography* **49**, 1313-1326.

Signorell A, Aho K, Alfons A, Anderegg N, Aragon T, Arppe A, Baddeley A, Barton K, Bolker B & Borchers HW, (2019). DescTools: Tools for descriptive statistics. *R package version 0.99* **28**,17.

Simpfendorfer CA & Kyne PM, (2009). Limited potential to recover from overfishing raises concerns for deep-sea sharks, rays and chimaeras. *Environmental Conservation* **36**, 97-103.

Smith SJ, Edmonds J, Hartin CA, Mundra A & Calvin K, (2015). Near-term acceleration in the rate of temperature change. *Nature Climate Change* **5**, 333-336.

Stanley SM, (2016). Estimates of the magnitudes of major marine mass extinctions in earth history. *Proceedings of the National Academy of Sciences* **113**, E6325-E6334.

Stein RW, Mull CG, Kuhn TS, Aschliman NC, Davidson LNK, Joy JB, Smith GJ, Dulvy NK & Mooers AO, (2018). Global priorities for conserving the evolutionary history of sharks, rays and chimaeras. *Nature Ecology and Evolution* **2**, 288-298.

Strasburg DW, (1963). The diet and dentition of *Isistius brasiliensis*, with remarks on tooth replacement in other sharks. *Copeia*, 33-40.

Straube N & Pollerspöck J, (2020). Intraspecific dental variations in the deep-sea shark *Etmopterus spinax* and their significance in the fossil record. *Zoomorphology* **139**, 483-491.

Takashina N & Mougi A, (2014). Effects of marine protected areas on overfished fishing stocks with multiple stable states. *Journal of Theoretical Biology* **341**, 64-70.

Tanaka KR, Van Houtan KS, Mailander E, Dias BS, Galginaitis C, O'Sullivan J, Lowe CG & Jorgensen SJ, (2021). North Pacific warming shifts the juvenile range of a marine apex predator. *Scientific Reports* **11**, 3373.

Tavares DC, Moura JF, Acevedo-Trejos E & Merico A, (2019). Traits shared by marine megafauna and their relationships with ecosystem functions and services. *Frontiers in Marine Science* **6**, 262.

Therneau T, Atkinson B & Ripley MB, (2015). Package 'rpart'. *The Comprehensive R Archive Network*.

Toussaint A, Brosse S, Bueno CG, Partel M, Tamme R & Carmona CP, (2021). Extinction of threatened vertebrates will lead to idiosyncratic changes in functional diversity across the world. *Nature Communications* **12**, 5162.

Toussaint A, Charpin N, Beauchard O, Grenouillet G, Oberdorff T, Tedesco PA, Brosse S & Villéger S, (2018). Non-native species led to marked shifts in functional diversity of the world freshwater fish faunas. *Ecology Letters* **21**, 1649-1659.

Turtscher J, Jambura PL, Lopez-Romero FA, Kindlimann R, Sato K, Tomita T & Kriwet J, (2022). Heterodonty and ontogenetic shift dynamics in the dentition of the tiger shark *Galeocerdo cuvier* (Chondrichthyes, Galeocerdidae). *Journal of Anatomy* **241**, 372-392.

Uhen MD, (2007). Evolution of marine mammals: back to the sea after 300 million years. *The Anatomical Record* **290**, 514-522.

Villéger S, Mason NW & Mouillot D, (2008). New multidimensional functional diversity indices for a multifaceted framework in functional ecology. *Ecology* **89**, 2290-2301.

Villéger S, Novack-Gottshall PM & Mouillot D, (2011). The multidimensionality of the niche reveals functional diversity changes in benthic marine biotas across geological time. *Ecology Letters* **14**, 561-568.

Villéger S, Ramos Miranda J, Flores Hernandez D & Mouillot D, (2010). Contrasting changes in taxonomic vs. functional diversity of tropical fish communities after habitat degradation. *Ecological Applications* **20**, 1512-1522.

Violle C, Navas ML, Vile D, Kazakou E, Fortunel C, Hummel I & Garnier E, (2007). Let the concept of trait be functional! *Oikos* **116**, 882-892.

Vullo R, Frey E, Ifrim C, González González MA, Stinnesbeck ES & Stinnesbeck W, (2021). Manta-like planktivorous sharks in Late Cretaceous oceans. *Science* **371**, 1253-1256.

Vullo R, Villalobos-Segura E, Amadori M, Kriwet J, Frey E, Gonzalez Gonzalez MA, Padilla Gutierrez JM, Ifrim C, Stinnesbeck ES & Stinnesbeck W, (2024). Exceptionally preserved shark fossils from Mexico elucidate the long-standing enigma of the Cretaceous elasmobranch *Ptychodus*. *Proceedings of the Royal Society B* **291**, 20240262.

Walls RHL & Dulvy NK, (2020). Eliminating the dark matter of data deficiency by predicting the conservation status of Northeast Atlantic and Mediterranean Sea sharks and rays. *Biological Conservation* **246**, 108459.

Weigmann S, (2016). Annotated checklist of the living sharks, batoids and chimaeras (Chondrichthyes) of the world, with a focus on biogeographical diversity. *Journal of Fish Biology* **88**, 837-1037.

Weng KC, Boustany AM, Pyle P, Anderson SD, Brown A, & Block BA, (2007). Migration and habitat of white sharks (*Carcharodon carcharias*) in the eastern Pacific Ocean. *Marine Biology* **152**, 877-894.

West CD, Dytham C, Righton D & Pitchford JW, (2009). Preventing overexploitation of migratory fish stocks: the efficacy of marine protected areas in a stochastic environment. *ICES Journal of Marine Science* **66**, 1919-1930.

Wetherbee BM & Cortés E, (2004). Food consumption and feeding habits. CRC Press, Boca Raton.

White WT, Kyne PM & Harris M, (2019). Lost before found: A new species of whaler shark *Carcharhinus obsolerus* from the Western Central Pacific known only from historic records. *PLoS One* **14**, e0209387.

Whitehead DA & Gayford J, (2023). First record of bottom-feeding behaviour in the whale shark (*Rhincodon typus*). *Journal of Fish Biology* **103**, 448-452.

Whitenack LB & Gottfried MD, (2010). A morphometric approach for addressing tooth-based species delimitation in fossil mako sharks, *Isurus* (Elasmobranchii: Lamniformes). *Journal of Vertebrate Paleontology* **30**, 17-25.

Whitenack LB & Motta PJ, (2010). Performance of shark teeth during puncture and draw: implications for the mechanics of cutting. *Biological Journal of the Linnean Society* **100**, 271-286.

Whitenack LB, Simkins, Jr DC & Motta PJ, (2011). Biology meets engineering: the structural mechanics of fossil and extant shark teeth. *Journal of Morphology* **272**, 169-179.

Wickham H, (2016). Getting Started with ggplot2. *ggplot2: Elegant graphics for data analysis*, 11-31.

Wickham H, Averick M, Bryan J, Chang W, McGowan L, François R, Grolemund G, Hayes A, Henry L, Hester J, Kuhn M, Pedersen T, Miller E, Bache S, Müller K, Ooms J, Robinson D, Seidel D, Spinu V, Takahashi K, Vaughan D, Wilke C, Woo K, & Yutani H, (2019). Welcome to the Tidyverse. *Journal of Open Source Software* **4**, 1686.

Williams JJ, Papastamatiou YP, Caselle JE, Bradley D & Jacoby DMP, (2018). Mobile marine predators: an understudied source of nutrients to coral reefs in an unfished atoll. *Proceedings of the Royal Society B* **285**, 20172456.

Willmer JNG, Püttker T & Prevedello JA, (2022). Global impacts of edge effects on species richness. *Biological Conservation* **272**, 109654.

Worm B, Davis B, Kettemer L, Ward-Paige CA, Chapman D, Heithaus MR, Kessel ST & Gruber SH, (2013). Global catches, exploitation rates, and rebuilding options for sharks. *Marine Policy* **40**, 194-204.

Worm B, Orofino S, Burns ES, D'Costa NG, Manir Feitosa L, Palomares ML, Schiller L & Bradley D, (2024). Global shark fishing mortality still rising despite widespread regulatory change. *Science* **383**, 225-230.

Zachos J, Pagani M, Sloan L, Thomas E & Billups K, (2001). Trends, rhythms, and aberrations in global climate 65 Ma to present. *Science* **292**, 686-693.

Zelinka MD, Myers TA, McCoy DT, Po-Chedley S, Caldwell PM, Ceppi P, Klein SA & Taylor KE, (2020). Causes of higher climate sensitivity in CMIP6 models. *Geophysical Research Letters* **47**, e2019GL085782.

Zhu L, Fu B, Zhu H, Wang C, Jiao L & Zhou J, (2017). Trait choice profoundly affected the ecological conclusions drawn from functional diversity measures. *Scientific Reports* **7**, 3643.

Appendix 1 | Supplementary materials for chapter 2

Supporting Information

Are shark teeth proxies for functional traits? A framework to infer ecology from the fossil record

Contents

Other supporting information for this chapter can be found with the online version of the published manuscript (https://doi.org/10.1111/jfb.15326) and includes the following:

Data S1. Data collected from the literature. For individual tooth positions, NR = not recorded; S = symphysial; A = anterior; L = lateral; P = posterior. Upper-case letters represent upper jaw teeth and lower-case letters represent lower jaw teeth. Numbers are also used for individual jaw positions (i.e., A2 = Upper 2nd anterior tooth).

Data S2. Literature dataset recording each singular link between dental character and functional trait (N = 590). This dataset records individual links for each species and study, identifies how each link is established, if each link is independent and why, and notes study limitations and contradictions against other literature.

Data S3. All dental character data used for PCA and CART analyses. Catalogue numbers of all museums are provided; and corresponding images for each specimen are identified. Specimens catalogued as Inv.nr and GHC are deposited in the collections of the Haimuseum und Sammlung R. Kindlimann and Jaws International (Gainesville, FL) respectively, both of which are private collections with public access. The GHC is being gradually acquisitioned into the Florida Museum vertebrate paleontology collection and thus catalogue numbers of "GHC x" are used as placeholders until receiving an official museum catalogue number. All maximum size estimates and prey preferences come from literature, primarily Ebert et al. (2021). Feeding mechanism assignments follow Kent (1994).

1 | SUPPORTING FIGURES
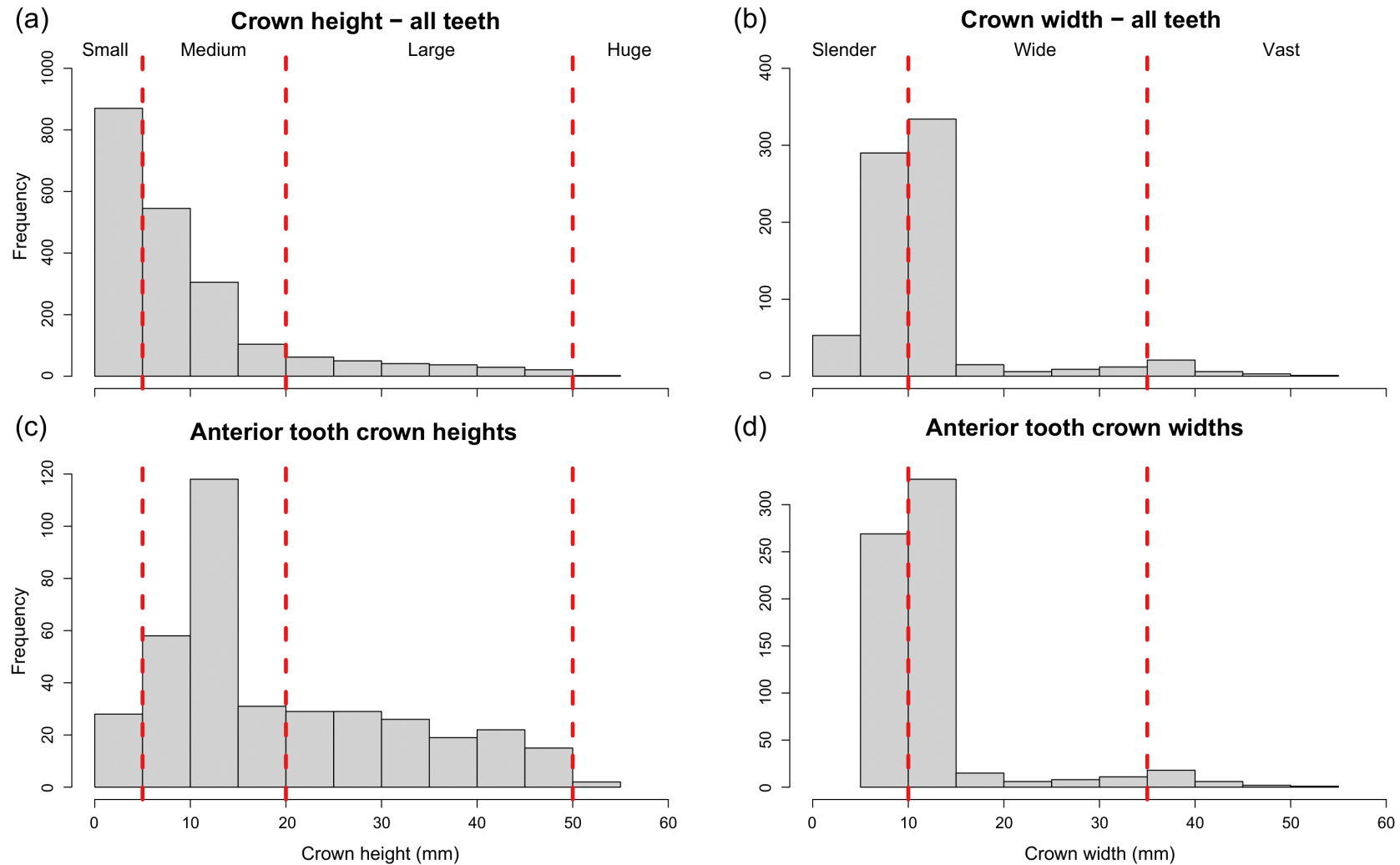
Figure S1.1. Distribution of crown height and width sizes in teeth studied in literature as proxies for body size (a, b) across all tooth positions; and (c, d) in anterior teeth only. Red vertical lines show cut-offs for size categorisations, which are labelled accordingly.
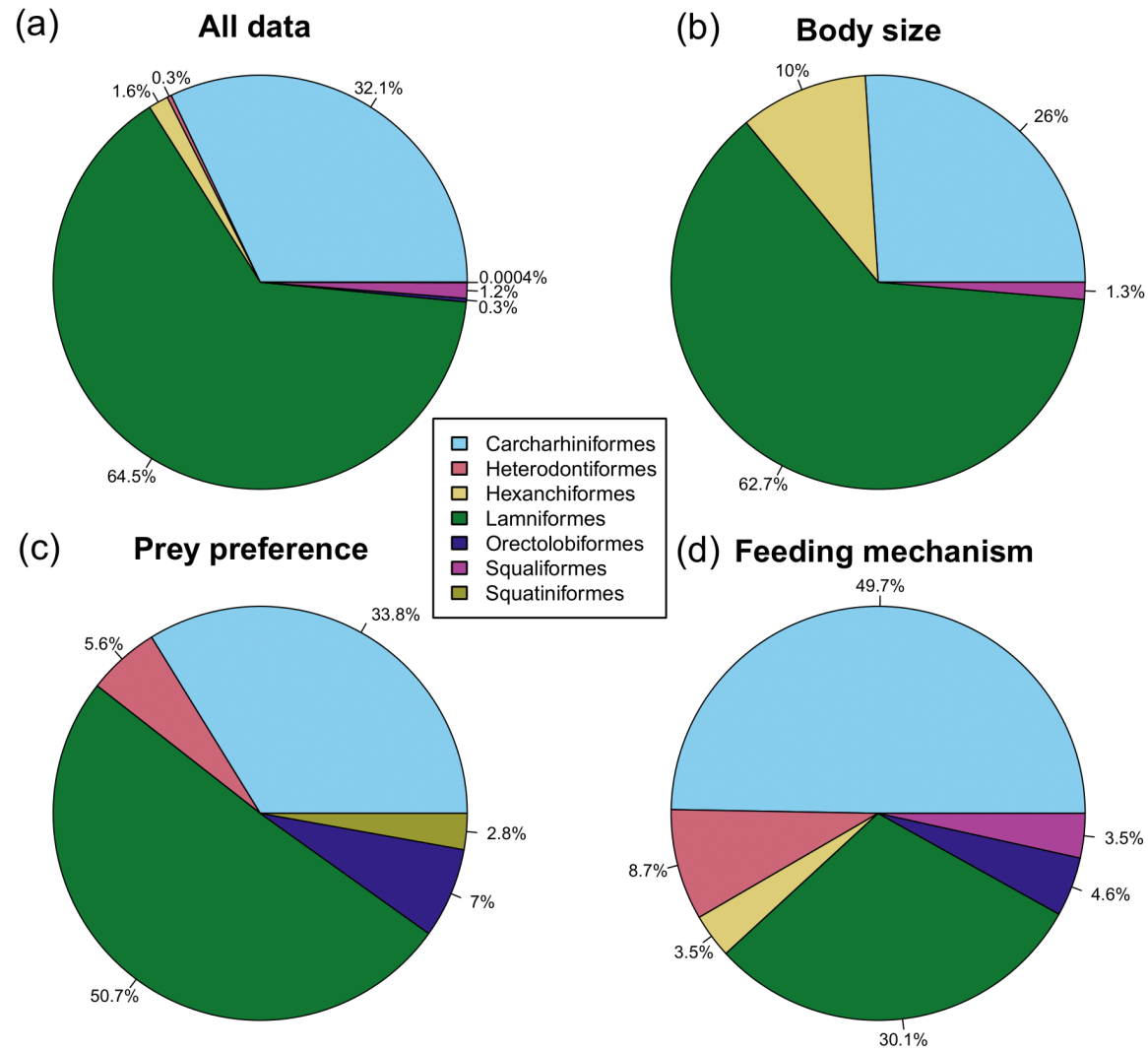
Figure S1.2. Representation of shark orders. (a) representation of shark orders across the entire literature review; and across the recovered data for each functional trait: (b) body size; (c) prey preference; and (d) feeding mechanism.

Functional diversity of sharks through time: past, present and future
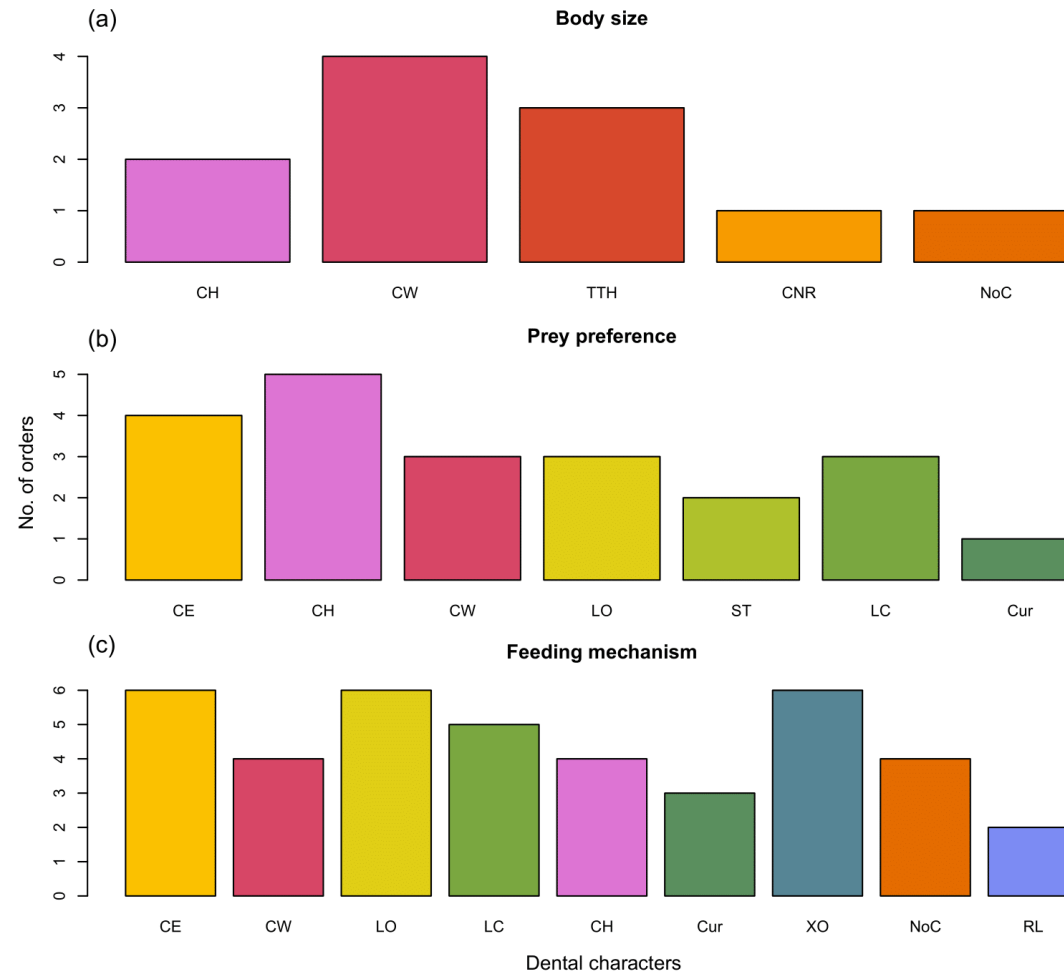
Figure S1.3. Dental character representation across shark orders from the data related to (a) body size; (b) prey preference; and (c) feeding mechanism. Abbreviations for each dental character are as follows: CH = crown height; CW = crown width; TTH = total tooth height; CNR = cusp number ratio; NoC = number of cusps; CE = cutting edge; LO = longitudinal outline; ST = serration type; LC = lateral cusplets; Cur = curvature; XO = cross-section outline; and RL = root lobes. See **Figure 2.2** for illustrations of each dental character.
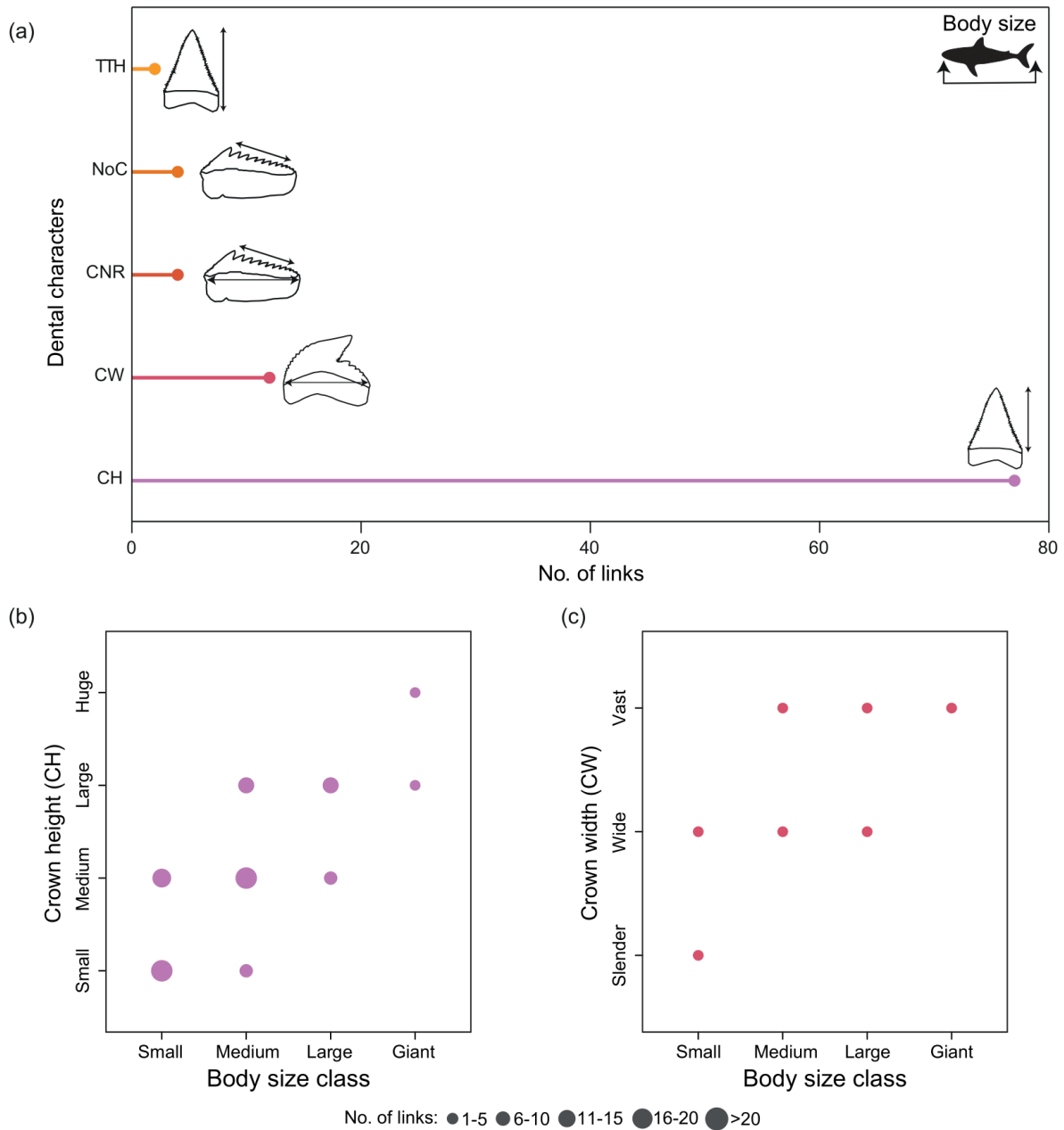
Figure S1.4. Dental characters used as proxies for body size in the literature when only anterior teeth are considered: (a) the number of links for each of the five identified dental characters: total tooth height (TTH); number of cusps (NoC); cusp number ratio (CNR); crown width (CW) and crown height (CH). Illustrations of each dental character are adapted from **Figure 2.2**. (b, c) Links between dental character states and body size classes in anterior tooth (b) crown heights; and (c) crown widths. Both characters are categorised following **Table 2.1** and **Appendix Figure S1.1**.
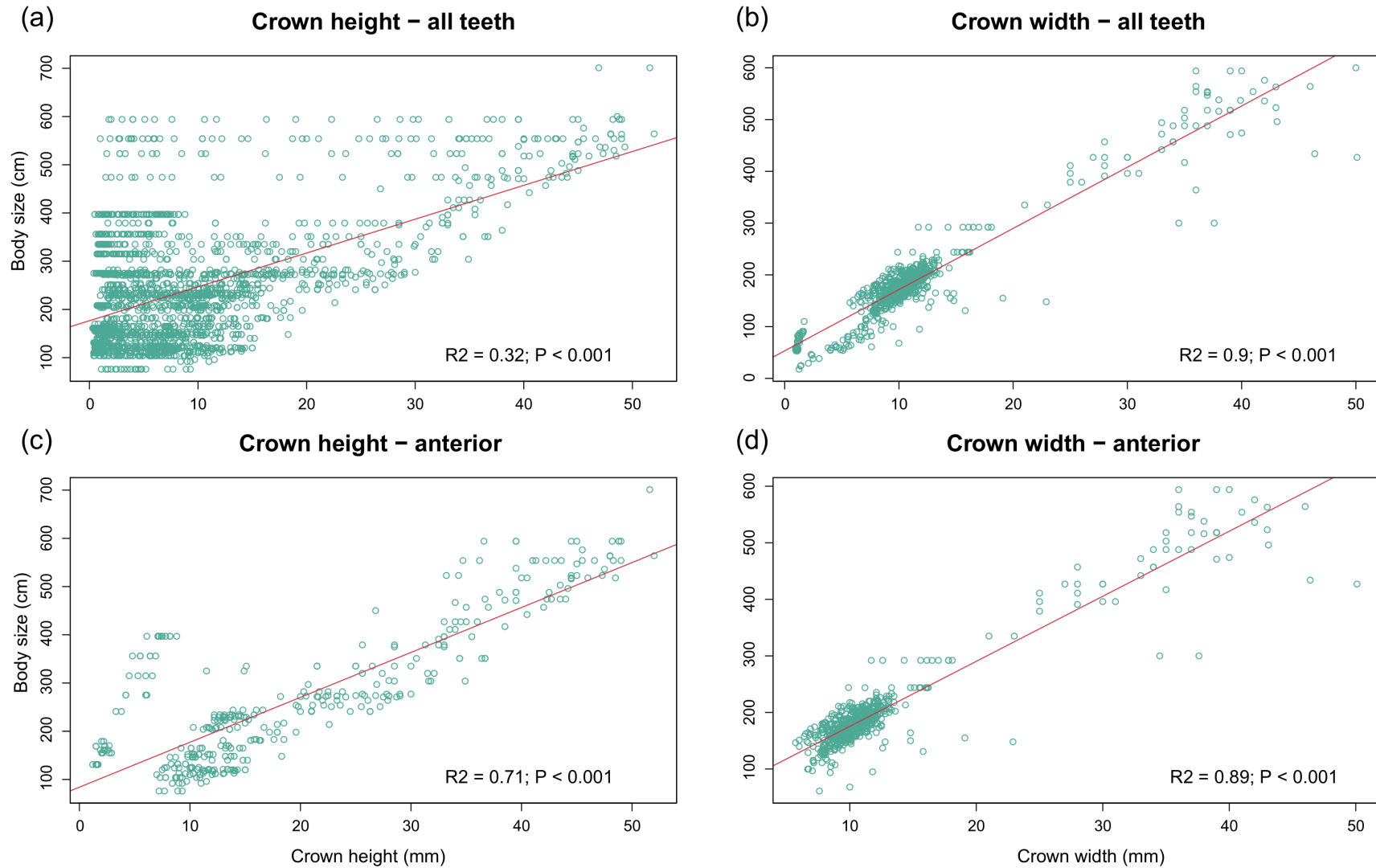
Figure S1.5. Linear regressions of crown height and crown width against body size considering (a, b) all tooth positions; and (c, d) only anterior teeth. Summary statistics are included for each regression.
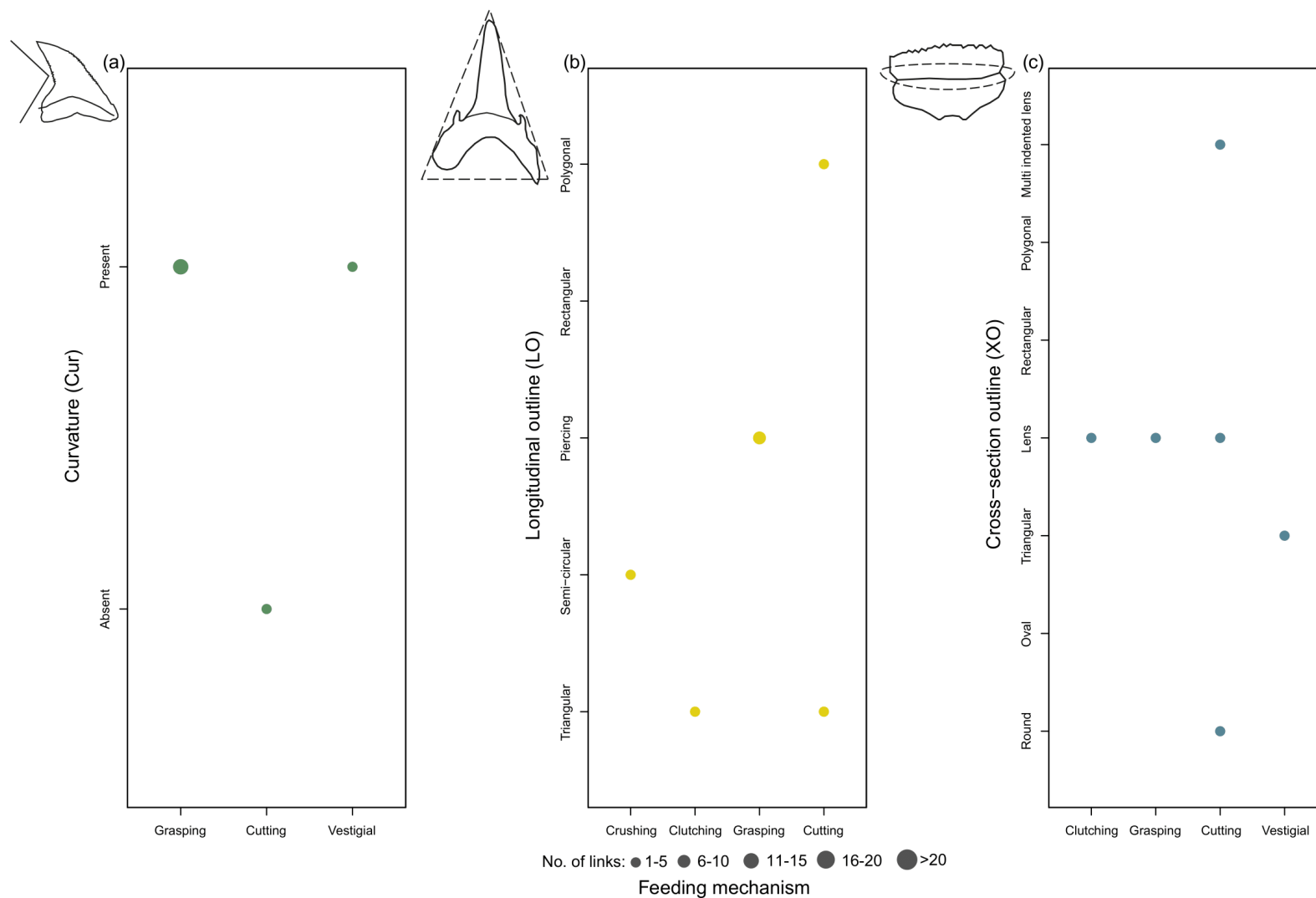
Figure S1.6. Visualisations of links between (a) curvature; (b) longitudinal outline; and (c) cross-section outline to feeding mechanism in extant sharks, as captured by the literature data. Each character and feeding mechanism modality are illustrated.
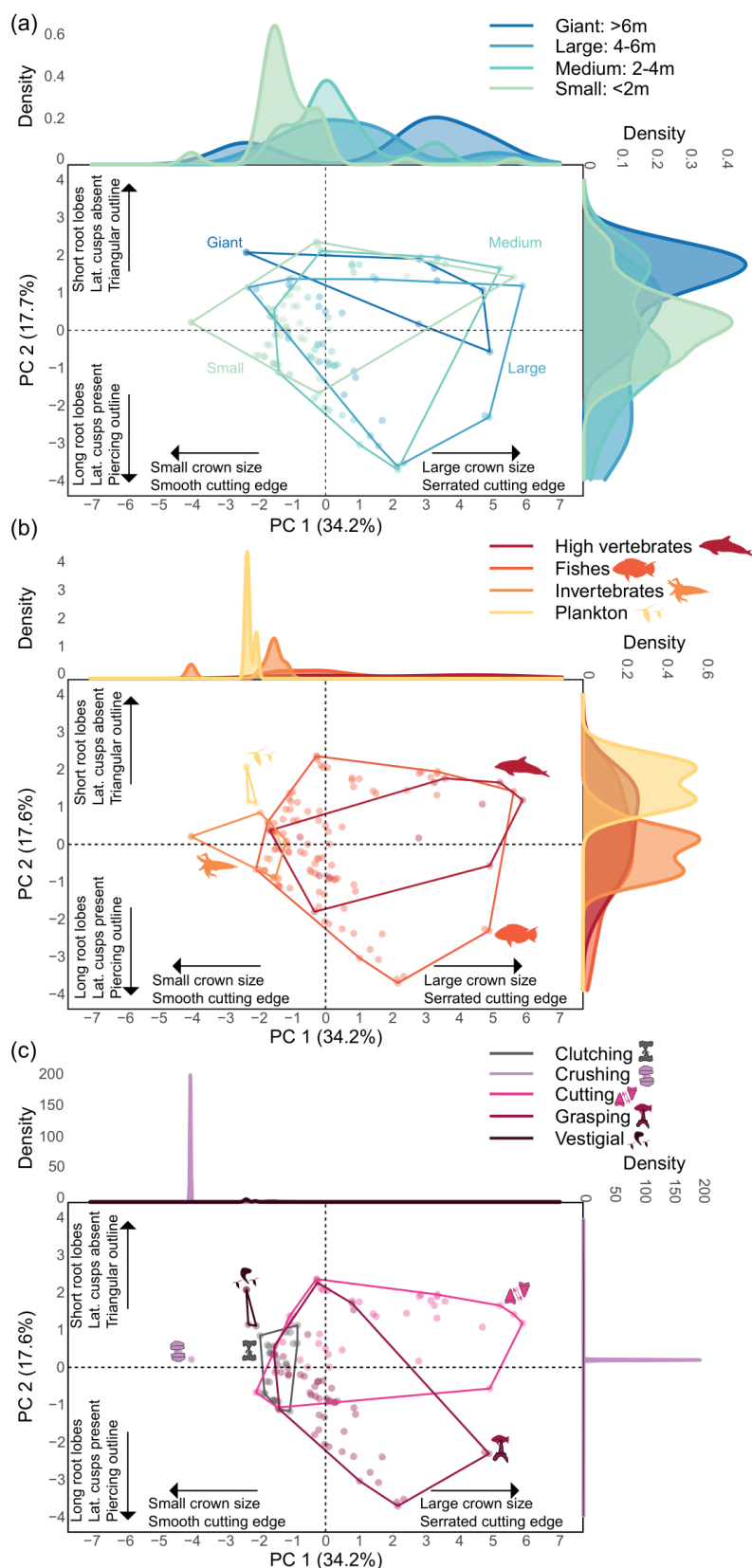
Figure S1.7. PCA of dental characters across functional traits based on the subset of anterior teeth from the museum dataset. Each set of analysis is linked to a single functional trait as follows: (a) body size; (b) prey preference; and (c) feeding mechanism, with values for each trait defining convex hulls. Arrows summarise how dental characters are correlated to each axis, based on their contributions recorded in **Appendix Table S1.3**. Density plots show the distribution of trait values along each axis.
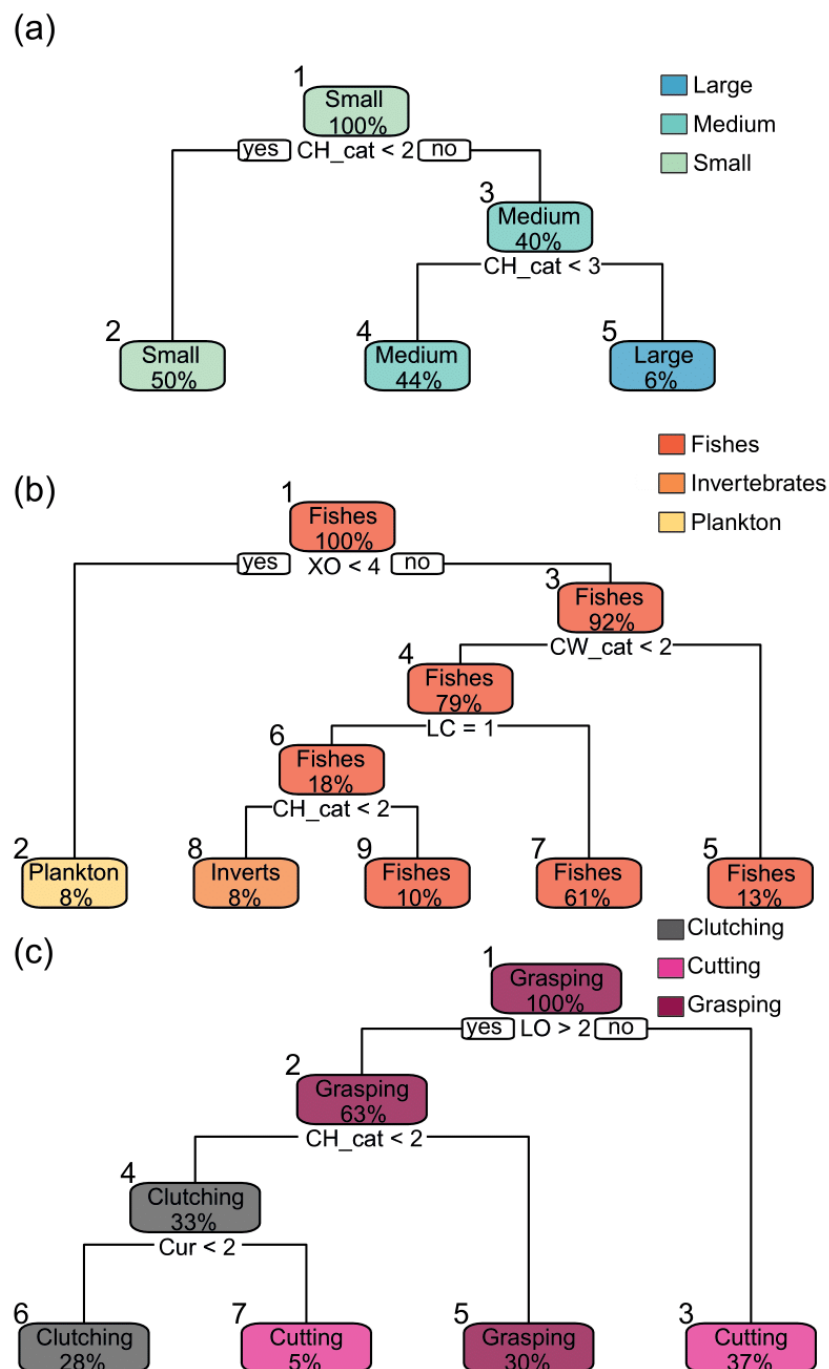
Figure S1.8. Classification tree analyses on the subset of the museum dataset of only anterior teeth. Each tree is related to a single functional trait as follows: (a) body size; (b) prey preference; and (c) feeding mechanism. Nodes are produced by splitting the data based on the presence of the dental character states recorded as predictors. The proportion of data each node contributes to the entire museum dataset is included alongside the most common trait value making up each node (see also **Appendix Table S1.4-S1.6**). Abbreviations are as follows: CH_cat = categorical crown height; XO = cross-section outline; CW_cat = categorical crown width; LC = lateral cusplets; LO = longitudinal outline; and Cur = curvature.

2 | SUPPORTING TABLES

Table S1.1. A summary of four different schemes that use tooth morphology to assign different feeding mechanisms to sharks, as identified in the literature review. In all schemes, the different teeth are referred to as dentition types, with each type being named after its proposed feeding mechanism. Homodont example species for each feeding mechanism are noted, as are the sources of each scheme. It should be noted that these schemes also consider heterodont dentition types due to many sharks exhibiting dignathic heterodonty (e.g., Kent (1994) assigns "Cutting-Grasping" dentitions to many *Carcharhinus* species – "Cutting" upper teeth and "Grasping" lower teeth); however, I focus on homodont dentition types here due to feeding mechanisms being inferred from isolated teeth in my analyses.

Tooth description	Example species	Kent, 1994	Motta, 2004	Ciampaglio et al. 2005	Cappetta, 2012
Low semi-circular teeth with no cusp. Used to crush (usually armoured) invertebrates	*Mustelus canis*	Crushing	Crushing/ Grinding	Crushing/ Grinding	Crushing/ Grinding
Small, smooth, robust teeth typically with multiple lateral cusplets. Used to restrain/grip lightly armoured invertebrates	*Chiloscyllium plagiosum*	Clutching	Seizing/ Grasping	Clutching	Clutching
Slender, elongate teeth with smooth cutting edges and sometimes lateral cusplets. Used to restrain small active prey	*Carcharias taurus*	Grasping	Tearing	Piercing	Tearing
Large, wide, blade-like teeth that are labiolingually flattened, often with serrations. Used to gouge large chunks of prey flesh	*Carcharodon carcharias*	Cutting	Cutting	Slicing/ Gouging	Cutting
Tiny, greatly reduced teeth, often with curvature. No functional role in food gathering and thus seen in filter feeders	*Rhincodon typus*	Vestigial	Not described	Not described	Clutching

Table S1.2. Shark taxa recovered from the literature review; at the order (n = 7), family (n = 25), genus (n = 39) and species levels (n = 63). Note that five taxa were recorded only to genus level. Nomenclature follows Weigmann (2016); with taxonomic corrections since that paper's publication then applied following Ebert *et al*. (2021). Abbreviations are as follows: BS = Body size; PP = prey preference; FM = feeding mechanism; LS = life stage; CW = crown width; NoC = number of cusps; CNR = cusp number ratio; CE = cutting edge; AS = acrocone serrations; CH = crown height; XO = cross-section outline; LO = longitudinal outline; LC = lateral cusplets; TTH = total tooth height; Cur = curvature; RL = root lobes; SC = serrational cusplets; ST = serration type.

Order	Family	Genus	Species	Traits	Dental Characters used
Hexanchiformes	Hexanchidae	*Heptranchias*	*perlo*	BS	CW; NoC; CNR
		Hexanchus	*griseus*	BS; FM; LS	CW; NoC; CNR; CE; AS
			nakamurai	BS; LS	CW; NoC; CNR; AS
		Notorynchus	*cepedianus*	BS	CW; NoC; CNR
Squaliformes	Squalidae	*Cirrihigaleus*	sp.	FM	CE
		Squalus	*acanthias*	FM	CH; CE; XO; LO
	Centrophoridae	*Centrophorus*	sp.	FM	CW; CE
	Etmopteridae	*Centroscyllium*	sp.	FM	LC
		Etmopterus	*spinax*	BS	TTH
	Somniosidae	*Scymnodon*	*ringens*	FM	CW; CE
	Dalatiidae	*Isistius*	*brasiliensis*	BS	CW
Squatiniformes	Squatinidae	*Squatina*	sp.	PP	CH; CE
Heterodontiformes	Heterodontidae	*Heterodontus*	*francisci*	PP; FM	CH; CW; CE; LC; XO; LO; NoC
Orectolobiformes	Hemiscylliidae	*Chiloscyllium*	*plagiosum*	FM	LC
	Ginglymostomatidae	*Ginglymostoma*	*cirratum*	PP; FM	CH; LC
	Rhincodontidae	*Rhincodon*	*typus*	PP; FM	CH; CW; CE; LC; Cur; XO; LO
Lamniformes	Mitsukurinidae	*Mitsukurina*	*owstoni*	BS	CH
	Carchariidae	*Carcharias*	*taurus*	BS; PP; FM	CH; CW; CE; LC; Cur; XO; LO; NoC; TTH
	Odontaspididae	*Odontaspis*	*ferox*	BS; FM	CH; CE; LC
			noronhai	BS	CH
	Pseudocarchariidae	*Pseudocarchari*	*kamoharai*	BS	CH
	Megachasmidae	*Megachasma*	*pelagios*	PP; FM	CH; CE; LC
	Cetorhinidae	*Cetorhinus*	*maximus*	PP; FM	CH; CW; CE; LC; Cur
	Alopiidae	*Alopias*	*pelagicus*	BS	CH
			superciliosus	BS; PP; FM	CH; CW; CE; LC; RL

Functional diversity of sharks through time: past, present and future

Order	Family	Genus	Species	Traits	Dental Characters used
			vulpinus	BS; PP	CH; CW; CE; LC; LO
	Lamnidae	*Carcharodon*	*carcharias*	BS; PP; FM; LS	CH; CW; CE; LC; Cur; XO; LO; NoC; RL; SC; ST
		Isurus	*oxyrinchus*	BS; PP; FM	CH; CW; CE; LC; Cur; LO
			paucus	BS	CH
		Lamna	*ditropis*	BS	CH
			nasus	BS; PP; FM	CH; CW; CE; LC
Carcharhiniformes	Pentanchidae	*Galeus*	*melastomus*	BS	CH
	Scyliorhinidae	*Scyliorhinus*	*canicular*	BS	TTH
			retifer	FM	CH; CE; LC
	Triakidae	*Galeorhinus*	*galeus*	BS; FM	CH; CE; XO; LO; NoC
		Iago	sp.	FM	CH
		Mustelus	*canis*	BS; PP; FM	CH; CW; CE; LO
		Triakis	*semifasciata*	BS	CH
	Carcharhinidae	*Carcharhinus*	*acronotus*	BS; FM	CH; CW; CE; Cur
			albimarginatus	BS	CH
			altimus	BS; FM	CH; CW; CE; Cur
			brachyurus	BS	CH; CW; TTH
			brevipinna	BS	CH; CW
			falciformis	BS; PP; FM	CH; CW; CE; Cur; XO
			galapagensis	BS	CH
			leucas	BS; PP; FM	CH; CW; CE; Cur
			limbatus	BS; PP; FM	CH; CW; CE; Cur
			longimanus	BS; FM	CH; CW; CE; LC; Cur; XO; LO; NoC
			macloti	BS; PP; FM	CH; CW; CE; LC; XO; LO; NoC; RL
			obscurus	BS; PP; FM	CH; CW; CE; LC; Cur; LO
			perezi	BS; PP	CH; CW; CE
			plumbeus	BS; PP; FM	CH; CW; CE; Cur; LO
			porosus	BS	CH
			sealei	BS	CH
			signatus	BS; FM	CH; CW; CE; Cur

Order	Family	Genus	Species	Traits	Dental Characters used
		Nasolamia	*velox*	BS	CH
		Negaprion	*brevirostris*	BS; PP; FM	CH; CW; CE; LC; Cur; LO
		Prionace	*glauca*	BS; PP; FM	CH; CW; CE; Cur; ST
		Rhizoprionodon	*acutus*	BS	CH
			longurio	BS	CH
			terraenovae	PP; FM	CH; CW; CE
		Scoliodon	*laticaudus*	BS	CH
	Galeocerdonidae	*Galeocerdo*	*cuvier*	BS; PP; FM	CH; CW; CE; LC; XO; LO; RL; ST
	Sphyrnidae	*Sphyrna*	*lewini*	BS	CH; CW
			media	BS	CH
			mokarran	BS	CH; CW
			tiburo	BS; PP	CH; CW
			zygaena	FM	CW; CE

Table S1.3. Contribution of shark dental characters to variance in the first two axes of the PCA when only anterior teeth are considered. All results are accurate to three decimal places. Bold values denote highest contributions.

Character	Abbreviation	PC1 contribution	PC2 contribution
Crown height (numerical)	CH_num	**0.395**	-0.292
Crown height (categorical)	CH_cat	**0.387**	-0.284
Crown width (numerical)	CW_num	**0.477**	0.055
Crown width (categorical)	CW_cat	**0.409**	0.179
Cutting edge	CE	**0.342**	**0.402**
Lateral cusplets	LC	-0.038	**-0.441**
Curvature	Cur	-0.107	0.151
Cross-section outline	XO	0.293	0.076
Longitudinal outline	LO	-0.131	**-0.479**
Root lobes	RL	0.184	**-0.412**
Number of cusps	NoC	0.180	-0.123

Table S1.4. Summaries of the root, decision, and terminal nodes of the classification trees to model body size from the recorded dental characters in the museum dataset. An upper and lower anterior, lateral and posterior tooth are analysed for each species, producing a total of 378 observations (6 observations for each of the 63 collated taxa). The number of observations for each character state are recorded for each node, with proportional values demonstrated in brackets, accurate to two decimal places. See **Figure 2.6a** and **Appendix Figure S1.8a** for graphical comparisons.

Tree data			Body size class observations			
All teeth						
Node	**Node type**	**Observations**	**Small**	**Medium**	**Large**	**Giant**
1	Root	378	156 (0.41)	126 (0.33)	72 (0.19)	24 (0.06)
2	Terminal	237	139 (0.59)	57 (0.24)	32 (0.13)	9 (0.04)
3	Decision	141	17 (0.12)	69 (0.49)	40 (0.28)	15 (0.11)
4	Terminal	131	17 (0.13)	68 (0.52)	34 (0.26)	12 (0.09)
5	Terminal	10	0	1 (0.1)	6 (0.6)	3 (0.3)
Anterior teeth						
1	Root	126	52 (0.41)	42 (0.33)	24 (0.19)	8 (0.06)
2	Terminal	63	44 (0.7)	11 (0.18)	6 (0.1)	2 (0.03)
3	Decision	63	8 (0.13)	31 (0.49)	18 (0.29)	6 (0.1)
4	Terminal	55	8 (0.14)	30 (0.54)	13 (0.24)	4 (0.07)
5	Terminal	8	0	1 (0.12)	5 (0.63)	2 (0.25)

Table S1.5. Summaries of the root, decision, and terminal nodes of the classification trees to model prey preference from the recorded dental characters in the museum dataset. An upper and lower anterior, lateral and posterior tooth are analysed for each species, producing a total of 378 observations (6 observations for each of the 63 collated taxa). The number of observations for each character state are recorded for each node, with proportional values demonstrated in brackets, accurate to two decimal places. See **Figure 2.6b** and **Appendix Figure S1.8b** for graphical comparisons.

Tree data			Prey preference observations			
All teeth						
Node	**Node type**	**Observations**	**Plankton**	**Invertebrates**	**Fishes**	**High vertebrates**
1	Root	378	12 (0.03)	36 (0.09)	294 (0.78)	36 (0.09)
2	Terminal	12	0	12 (1.00)	0	0
3	Decision	366	12 (0.03)	24 (0.07)	294 (0.81)	36 (0.1)
4	Decision	48	12 (0.25)	3 (0.06)	27 (0.56)	6 (0.13)
5	Terminal	318	0	21 (0.07)	267 (0.84)	30 (0.09)
6	Decision	40	12 (0.3)	3 (0.07)	25 (0.63)	0
7	Terminal	8	0	0	2 (0.25)	6 (0.75)
8	Decision	28	12 (0.43)	3 (0.11)	13 (0.46)	0
9	Terminal	12	0	0	12 (1.00)	0
10	Terminal	13	6 (0.46)	3 (0.23)	4 (0.31)	0
11	Terminal	15	6 (0.4)	0	9 (0.6)	0
Anterior teeth						
1	Root	126	4 (0.03)	12 (0.09)	98 (0.78)	12 (0.09)
2	Terminal	10	4 (0.4)	2 (0.2)	4 (0.4)	0
3	Decision	116	0	10 (0.09)	94 (0.81)	12 (0.1)
4	Decision	100	0	10 (0.1)	85 (0.85)	5 (0.05)
5	Terminal	16	0	0	9 (0.56)	7 (0.44)
6	Decision	23	0	6 (0.26)	15 (0.65)	2 (0.09)
7	Terminal	77	0	4 (0.05)	70 (0.91)	3 (0.04)
8	Terminal	10	0	6 (0.6)	4 (0.4)	0
9	Terminal	13	0	0	11 (0.85)	2 (0.15)

Table S1.6. Summaries of the root, decision, and terminal nodes of the classification trees to model feeding mechanism from the recorded dental characters in the museum dataset. An upper and lower anterior, lateral and posterior tooth are analysed for each species, producing a total of 378 observations (6 observations for each of the 63 collated taxa). The number of observations for each character state are recorded for each node, with proportional values demonstrated in brackets. See **Figure 2.6c** and **Appendix Figure S1.8c** for graphical comparisons.

Tree data			Feeding mechanism observations				
All teeth							
Node	**Node type**	**Observations**	**Crushing**	**Clutching**	**Grasping**	**Cutting**	**Vestigial**
1	Root	378	12 (0.03)	76 (0.2)	140 (0.37)	138 (0.36)	12 (0.03)
2	Decision	229	6 (0.03)	63 (0.27)	129 (0.56)	25 (0.11)	6 (0.03)
3	Decision	149	6 (0.04)	13 (0.09)	11 (0.07)	113 (0.76)	6 (0.04)
4	Decision	205	6 (0.03)	57 (0.28)	129 (0.63)	7 (0.03)	6 (0.03)
5	Decision	24	0	6 (0.25)	0	18 (0.75)	0
6	Terminal	12	6 (0.5)	0	0	0	6 (0.5)
7	Terminal	137	0	19 (0.09)	11 (0.08)	113 (0.82)	0
8	Decision	135	6 (0.04)	57 (0.42)	65 (0.48)	4 (0.03)	3 (0.02)
9	Terminal	70	0	0	64 (0.91)	3 (0.04)	3 (0.04)
10	Terminal	9	0	6 (0.67)	0	3 (0.33)	0
11	Terminal	15	0	0	0	15 (1.00)	0
12	Terminal	9	6 (0.67)	0	0	0	3 (0.33)
13	Decision	126	0	57 (0.45)	65 (0.52)	4 (0.03)	0
14	Terminal	37	0	23 (0.62)	14 (0.38)	0	0
15	Terminal	89	0	34 (0.38)	51 (0.57)	4 (0.04)	0
Anterior teeth							
1	Root	126	2 (0.02)	28 (0.22)	50 (0.4)	42 (0.33)	4 (0.03)
2	Decision	80	2 (0.02)	23 (0.29)	45 (0.56)	8 (0.1)	2 (0.02)
3	Terminal	46	0	5 (0.11)	5 (0.11)	34 (0.74)	2 (0.02)
4	Decision	42	2 (0.05)	23 (0.55)	10 (0.24)	5 (0.12)	2 (0.05)
5	Terminal	38	0	0	35 (0.92)	3 (0.08)	0
6	Terminal	35	2 (0.06)	22 (0.63)	10 (0.29)	1 (0.03)	0
7	Terminal	7	0	1 (0.14)	0	4 (0.57)	2 (0.29)

3 | SUPPORTING REFERENCES – REFERENCES RETURNED BY LITERATURE REVIEW

Abler, W.L. (1992). The serrated teeth of tyrannosaurid dinosaurs, and biting structures in other animals. *Paleobiology*, **18**, 161-183.

Adnet, S. (2006). Biometric analysis of the teeth of fossil and Recent hexanchid sharks and its taxonomic implications. *Acta Palaeontologica Polonica*, **51**, 477-488.

Adnet, S., Balbino, A.C., Antunes, M.T. & Marín-Ferrer, J.M. (2010). New fossil teeth of the White Shark (*Carcharodon carcharias*) from the Early Pliocene of Spain. Implication for its paleoecology in the Mediterranean. *Neues Jahrbuch fur Geologie und Palaontologie-Abhandlungen*, **256**, 7-16.

Adnet, S. & Martin, R.A. (2007). Increase of body size in sixgill sharks with change in diet as a possible background of their evolution. *Historical Biology*, **19**, 279-289.

Applegate, S.P. (1965). Tooth terminology and variation in sharks with special reference to the sand shark, *Carcharias taurus* Rafinesque. *Contributions in Science, Los Angeles County Museum*, **86**, 3-18.

Belben, R.A., Underwood, C.J., Johanson, Z. & Twitchett, R.J. (2017). Ecological impact of the end-Cretaceous extinction on lamniform sharks. *PLoS One*, **12**, e0178294.

Bemis, W.E., Moyer, J.K. & Riccio, M.L. (2015). Homology of lateral cusplets in the teeth of lamnid sharks (Lamniformes: Lamnidae). *Copeia*, **103**, 961-972.

Bor, T.J. & Peters, W. (2015). The Pliocene locality Balgoy (province of Gelderland, The Netherlands) and a new record of the great white shark, *Carcharodon carcharias* (Linnaeus, 1758). *Cainozoic Research*, **15**, 59-73.

Cappetta, H. (2012). Chondrichthyes. Mesozoic and Cenozoic Elasmobranchii: Teeth. In H.-P. Schultze (Ed.), *Handbook of paleoichthyology. Volume 3E* (pp. 1–512). Munich: Verlag Dr. Friedrich Pfeil.

Cappo, M. (1988). Size and age of the white pointer shark *Carcharodon carcharias* (Linnaeus): was Peter Riseley's white pointer a world record? *Safish*, **13**, 11–13.

Chavez, S., Zufan, S., Kim, S.H. & Shimada, K. (2012). Tooth sizes as a proxy for estimating body lengths in the porbeagle shark, *Lamna nasus*. *Journal of Fossil Research*, **45**, 1-5.

Ciampaglio, C.N., Wray, G.A. & Corliss, B.H. (2005). A toothy tale of evolution: convergence in tooth morphology among marine Mesozoic–Cenozoic sharks, reptiles, and mammals. *The Sedimentary Record*, **3**, 4-8.

Cione, A.L., Cabrera, D.A. & Barla, M.J. (2012). Oldest record of the great white shark (Lamnidae, *Carcharodon*; Miocene) in the Southern Atlantic. *Geobios*, **45**, 167-172.

Condamine, F.L., Romieu, J. & Guinot, G. (2019). Climate cooling and clade competition likely drove the decline of lamniform sharks. *Proceedings of the National Academy of Sciences*, **116**, 20584-20590.

Corn, K.A., Farina, S.C., Brash, J. & Summers, A.P. (2016). Modelling tooth–prey interactions in sharks: the importance of dynamic testing. *Royal Society Open Science*, **3**, 160141.

Cullen, J.A. & Marshall, C.D. (2019). Do sharks exhibit heterodonty by tooth position and over ontogeny? A comparison using elliptic Fourier analysis. *Journal of Morphology*, **280**, 687-700.

Ellis, J.R. & Shackley, S.E. (1995). Ontogenic changes and sexual dimorphism in the head, mouth and teeth of the lesser spotted dogfish. *Journal of Fish Biology*, **47**, 155-164.

Frazzetta, T.H. (1988). The mechanics of cutting and the form of shark teeth (Chondrichthyes, Elasmobranchii). *Zoomorphology*, **108**, 93-107.

Frazzetta, T.H. (1994). Feeding mechanisms in sharks and other elasmobranchs. In *Biomechanics of feeding in vertebrates* (pp. 31-57). Springer: Berlin, Heidelberg.

Hubbell, G. (1996). Using tooth structure to determine the evolutionary history of the white shark. In A.P. Klimley & D.G. Ainley (Eds.), *Great white sharks: the biology of Carcharodon carcharias*, (pp. 9-18), Academic Press: San Diego.

Kent, B.W. (1994) *Fossil sharks of the Chesapeake Bay region*. (pp. 1-146), Egan Rees & Boyer, Inc., Columbia.

Kent, B.W. (2018). The cartilaginous fishes (chimaeras, sharks, and rays) of Calvert Cliffs, Maryland, USA. In Godfrey, S.J. (ed.), *The Geology and Vertebrate Paleontology of Calvert Cliffs, Maryland, USA*, (pp. 45-157), Smithsonian Institution Scholarly Press.

Kenyon, K.W. (1959). A 15-foot maneater from San Miguel Island, California. *California Fish Game*, **45**, 58–59.

Landini, W., Collareta, A., Pesci, F., Di Celma, C., Urbina, M. & Bianucci, G. (2017). A secondary nursery area for the copper shark *Carcharhinus brachyurus* from the late Miocene of Peru. *Journal of South American Earth Sciences*, **78**, 164-174.

Litvinov, F.F., Agapov, S.N., Katalimov, V.G. & Mironov, S.G. (1983). Rate of tooth replacement in blue shark, *Prionace glauca* (Carcharhinidae), in relation to feeding. *Journal of Ichthyology*, **23**, 143-145.

Long, D.J. & Waggoner, B.M. (1996). Evolutionary relationships of the white shark: a phylogeny of lamniform sharks based on dental morphology. In A.P. Klimley & A.G. Dinley (Eds.), *Great white sharks: the biology of Carcharodon carcharias*, (pp. 37-47), Academic Press: San Diego.

Lucifora, L.O., Menni, R.C. & Escalante, A.H. (2001). Analysis of dental insertion angles in the sand tiger shark, *Carcharias taurus* (Chondrichthyes: Lamniformes). *Cybium*, **25**, 23-31.

Mollet, H.F., Cailliet, G.M., Klimley, A.P., Ebert, D.A., Testi, A.D. & Compagno, L.J.V. (1996). A review of length validation methods and protocols to measure large white sharks. In A.P. Klimley & A.G. Dinley (Eds.), *Great White Sharks: the biology of Carcharodon carcharias*, (pp.91-108), Academic Press: San Diego.

Moss, S.A. (1967). Tooth replacement in the lemon shark, *Negaprion brevirostris*. In P.W. Gilbert, R.F. Mathewson & D.P. Rall (Eds.), *Sharks, skates and rays*, (pp. 319-329), Johns Hopkins Press: Baltimore.

Moss, S.A. (1972). Tooth replacement and body growth rates in the smooth dogfish, *Mustelus canis* (Mitchill). *Copeia*, **1972**, 808-811.

Motta, P.J. (2004). Prey capture behavior and feeding mechanics of elasmobranchs. In J.C. Carrier, J.A. Musick, & M.R. Heithaus (Eds.), *Biology of sharks and their relatives*, (pp. 165-202), CRC Press: New York.

Moyer, J.K. & Bemis, W.E. (2017). Shark teeth as edged weapons: serrated teeth of three species of selachians. *Zoology*, **120**, 101-109.

Moyer, J.K., Hamilton, N.D., Seeley, R.H., Riccio, M.L. & Bemis, W.E. (2015). Identification of shark teeth (Elasmobranchii: Lamnidae) from a historic fishing station on Smuttynose Island, Maine, using computed tomography imaging. *Northeastern Naturalist*, **22**, 585-597.

Nambiar, P., Brown, K.A. & Bridges, T.E. (1996). Forensic implications of the variation in morphology of marginal serrations on the teeth of the great white shark. *The Journal of Forensic Odonto-stomatology*, **14**, 2-8.

Perez, V.J., Pimiento, C., Hendy, A., González-Barba, G., Hubbell, G. & MacFadden, B.J. (2017). Late Miocene chondrichthyans from Lago Bayano, Panama: functional diversity, environment and biogeography. *Journal of Paleontology*, **91**, 512-547.

Pollerspöck, J. & Straube, N. (2020). An identification key to elasmobranch species based on dental morphological characters. Part B: extant Lamniform sharks (Superorder Galeomorphii: Order Lamniformes). *Bulletin of Fish Biology*, **19**, 27-64.

Portell, R.W., Hubbell, G., Donovan, S.K., Green, J.L., Harper, D.A. & Pickerill, R. (2008). Miocene sharks in the Kendeace and Grand Bay formations of Carriacou, The Grenadines, Lesser Antilles. *Caribbean Journal of Science*, **44**, 279-286.

Ramsay, J.B. & Wilga, C.D. (2007). Morphology and mechanics of the teeth and jaws of white-spotted bamboo sharks (*Chiloscyllium plagiosum*). *Journal of Morphology*, **268**, 664-682.

Randall, J.E. (1973). Size of the great white shark (*Carcharodon*). *Science*, **181**, 169-170.

Royce, W.F. (1963). First record of white shark *Carcharondon carcharias* from southeastern Alaska. *Copeia*, **1**, 179.

Šanda, R. & De Maddalena, A. (2004). Collection of the sharks of the National Museum in Prague-Part 2. Skeletal preservations. *Journal of the National Museum (Praha), Natural History Series*, **173**, 51-58.

Shimada, K. (2002). The relationship between the tooth size and total body length in the shortfin mako, *Isurus oxyrinchus* (Lamniformes: Laminidae). *Journal of Fossil Research*, **35**, 6-9.

Shimada, K. (2003). The relationship between the tooth size and total body length in the white shark. *Journal of Fossil Research*, **35**, 28-33.

Shimada, K. (2004). The relationship between the tooth size and total body length in the sandtiger shark, *Carcharias taurus* (Lamniformes: Odontaspididae). *Journal of Fossil Research*, **37**, 76-81.

Shimada, K. (2006). The relationship between the tooth size and total body length in the common thresher shark, *Alopias vulpinus* (Lamniformes: Alopiidae). *Journal of Fossil Research*, **39**, 7-11.

Shimada, K., Becker, M.A. & Griffiths, M.L. (2020). Body, jaw, and dentition lengths of macrophagous lamniform sharks, and body size evolution in Lamniformes with special reference to 'off-the-scale' gigantism of the megatooth shark, *Otodus megalodon*. *Historical Biology*, **33**, 2543-2559.

Shimada, K. & Seigel, J.A. (2005). The relationship between the tooth size and total body length in the goblin shark, *Mitsukurina owstoni* (Lamniformes: Mitsukurinidae). *Journal of Fossil Research*, **38**, 49-56.

Siccardi, E., Gosztomy, A.E. & Menni, R.C. (1981). La presencia de *Carcharodon carcharias* e *Isurus oxyrinchus* en el mar Argentino. Chondrichthyes, Lamniformes. *Physis*, **A**, 39, 55–62.

Springer, S. (1961). Dynamics of the feeding mechanism of large galeoid sharks. *American Zoologist,* **1**, 183-185.

Strasburg, D.W. (1963). The diet and dentition of *Isistius brasiliensis*, with remarks on tooth replacement in other sharks. *Copeia*, 33-40.

Straube, N. & Pollerspöck, J. (2020). Intraspecific dental variations in the deep-sea shark *Etmopterus spinax* and their significance in the fossil record. *Zoomorphology*, **139**, 483-491.

Villafaña, J.A., Hernandez, S., Alvarado, A., Shimada, K., Pimiento, C., Rivadeneira, M.M. & Kriwet, J. (2020). First evidence of a palaeo-nursery area of the great white shark. *Scientific Reports*, **10**, 8502.

Whitenack, L.B. & Motta, P.J. (2010). Performance of shark teeth during puncture and draw: implications for the mechanics of cutting. *Biological Journal of the Linnean Society*, **100**, 271-286.

Whitenack, L.B., Simkins Jr, D.C. & Motta, P.J. (2011). Biology meets engineering: the structural mechanics of fossil and extant shark teeth. *Journal of Morphology*, **272**, 169-179.

Wilga, C.D. & Motta, P.J. (1998). Conservation and variation in the feeding mechanism of the spiny dogfish *Squalus acanthias*. *Journal of Experimental Biology*, **201**, 1345-1358.

Wilga, C.D. & Motta, P.J. (2000). Durophagy in sharks: feeding mechanics of the hammerhead *Sphyrna tiburo*. *Journal of Experimental Biology*, **203**, 2781-2796.

Appendix 2 | Supplementary materials for chapter 3

Supporting Information

The rise and fall of shark functional diversity over the last 66 million years

Contents

Other supplementary materials for this chapter can be found in the online version of the published manuscript (https://doi.org/10.1111/geb.13881) and include:

Data S1. Dataset of specimens collected. Data include taxonomy, status (i.e., extinct or extant), museum, geological information, tooth position and dental characters. *Taxon_corrected* refers to the corrected taxonomic information following Shark-References. *Age_ref* refers to the source where the geological age was obtained or refined. *Reference* provides the full reference for sources of all data obtained from literature. *Image_folder* and *Image* source the folder and image name of all tooth pictures, accessible in the Zenodo Repository (https://doi.org/10.5281/zenodo.10076354). Dental character abbreviations are as follows: CH = crown height; CW = crown width; CE = cutting edge; LC = lateral cusplets; XO = cross-section outline; LO = longitudinal outline.

Data S2. Trait data used for complementary analyses to assess how much the degraded Recent sample is representative of a functional space containing the total diversity of living sharks. Prey preference ('diet') and body size ('size') are extracted from Pimiento et al. (2023), specifically, the modal values across imputations (see supplementary methods). Feeding mechanism was extracted from (Kent 1994, 2018, Cappetta 2012). Rationale for feeding mechanism assignments is provided in the *notes* column.

Codes. All R code used to conduct the analyses is available via GitHub at https://github.com/Pimiento-Research-Group/Shark-FD-through-time.

1 | SUPPLEMENTARY METHODS

Data collection

Data were collected in three ways. Firstly, I collated images of teeth from the following online museum image repositories: iDigBio (https://www.idigbio.org/), the Vertebrate Paleontology collection database from the Florida Museum of Natural History (UF; Gainesville, FL, USA; https://www.floridamuseum.ufl.edu); and the paleontology collections database of the Smithsonian Institution National Museum of Natural History (USNM; Washington DC, USA; https://collections.nmnh.si.edu). Secondly, I visited the following museums to access specimens in their collections: the British Natural History Museum (NHM; London, UK); the Naturhistorisches Museum Wien (NHMW; Vienna, Austria); the Paleontological Museum, University of Zurich (PIMUZ; Zurich, Switzerland); the collection of Haimuseum und Sammlung R. Kindlimann (RKC; Aathal-Seegraben, Switzerland; a private collection with public access); the Royal Belgian Institute of Natural Sciences (RBINS; Brussels, Belgium); the Calvert Marine Museum (CMM; Solomons, MD, USA); the Florida Museum of Natural History (UF; Gainesville, FL, USA); the Gordon Hubbell Collection (GHC; Gainesville, FL, USA; a private collection with public access); and the Museo de Historia Natural, Universidad Nacional Mayor de San Marcos (MUSM; Lima, Peru). Thirdly, additional images of teeth were collected from figures in 208 scientific publications.

All specimens collected from museums were photographed, with teeth positioned on a flat surface, and photographed from above (i.e., at a 90° angle) to mitigate any possible parallax error. Scale bars were included alongside all photographed specimens to ensure replication of measurements. For sharks from the Recent, teeth were recorded from jaw specimens from which we used the first anterior, third lateral and last posterior tooth of upper and lower jaws following Cooper et al. (2023). Additionally, any visibly reworked or transported fossil specimens were not included in our data.

Specimens collected digitally from online museum image repositories and figures in literature were only considered if a scale bar was present in the image to allow for measurements. Links to online museum repository images and full references for the 208 scientific publications are included in Data S1 under the *Image* and *Reference* columns respectively. All tooth images from figures are deposited in the Zenodo Repository (https://doi.org/10.5281/zenodo.10076354) to facilitate replication.

Dental character treatment

To ensure the quantification of functional entities in our functional diversity analyses, crown height and crown width were converted into previously established categories (**Table S2.1**; Cooper et al. 2023). As such, they were both treated as ordinal variables throughout analyses. Cutting edge was treated as a nominal variable and categorised based on the absence of a cutting edge, or if a present cutting edge was smooth or serrated. Lateral cusplets is a binary variable measured based on presence or absence. However, as the *mFD* package used for analyses only computes ordinal, nominal and quantitative (i.e., numerical) variables (Magneville et al. 2022), this dental character was treated as a nominal variable. Finally, cross-section outline and longitudinal outline were both treated as nominal variables, with their categorisations being based on previous works (Ciampaglio et al. 2005, Cooper et al. 2023). Although curvature was also found to be a proxy for prey preference and feeding mechanism, it was excluded from our measurements because its association with trait values was weak compared to other dental characters (Cooper et al. 2023).

Complementary functional space of Recent sharks

I performed a complementary analysis to assess how much of the Recent sample was representative of a functional space comprising the total diversity of all Recent sharks, as well as to determine if the most functionally specialised species in such a space (i.e., the species with the most extreme trait values) were represented within our Recent sample.

Species selection

A list of all Recent elasmobranch species was obtained from Pimiento et al. (2023). I removed batoids, resulting in a dataset of 501 species (Data S2).

Trait selection

As body size, prey preference and feeding mechanism were the traits found to be related to dental characters used in my previous analyses (Cooper et al. 2023), only these three traits were considered in these complementary analyses. Body size (total length in cm, and then grouped into categories as in my main analyses) and prey preference (four distinct categories or combinations of these) were extracted from Pimiento et al. (2023). These traits underwent a comprehensive revision based on literature and did not include missing values as they were inferred via multiple imputations (Pimiento et al. 2023).

Feeding mechanism was extracted from Kent (1994, 2018) and Cappetta (2012), standardised to the "dentition type" scheme by Kent (1994) following Table S1 of Cooper et al. (2023). As our dental character proxies come from isolated teeth, which can vary in morphology based on jaw position (Kent 1994), we quantified feeding mechanism based on upper teeth-lower teeth. This can be either homodont (i.e., "Grasping" where both teeth are associated with a grasping feeding mechanism) or heterodont (i.e., "Cutting-Grasping" where upper teeth and lower teeth are associated with cutting and grasping mechanisms respectively). We were able to assign feeding mechanism to 438 species (~87% of the total list of species). The missing data (~13%) were not imputed as the *mFD* package allowed us to incorporate NA values into subsequent analyses.

All extracted trait values per species can be found in Data S2.

Functional diversity analyses

I followed the same analytical approach as in my main analyses quantifying functional diversity, specifically the functional space approach (see Methods in main manuscript; Mouillot et al. 2013). Accordingly, I computed a trait distance matrix and retrieved the axes of a Principal Coordinate Analysis (herein, PCoA). Contrary to my main analyses, I did not weight any trait as I did not have *a priori* expectations regarding the relative importance of traits. Using the "quality.fspaces" function allowed me to determine that our data was best represented using five dimensions. However, I used four axes to build the functional space given that (1) the difference in mean absolute deviation values between five and four dimensions was small (<0.002); and (2) four axes represented 73.25% of the total inertia. Based on this four-dimensional space, I: (1) quantified the functional richness of the Recent sample used in my main analyses to assess the extent of the functional space of all Recent species is occupied by our sample; and (2) calculated species-specific functional specialisation to assess if the Recent sample included the most specialised Recent species.

2 | SUPPLEMENTARY TABLES

Table S2.1. Dental characters measured from shark teeth and used as traits in functional diversity analyses. Definitions and states are modified from Table 1 of Cooper et al. (2023). Note that state 6 of cross-section outline ("polygonal") was not found to occur in shark teeth by Ciampaglio et al. (2005); which we also observed in our data. As such, just six states of this dental character are listed here.

Dental character	Definition	Variable type	States
Crown height	Maximum vertical enamel height	Ordinal	1 – <5 mm 2 – 5-20 mm 3 – 20-50 mm 4 – >50 mm
Crown width	Width of the tooth crown	Ordinal	1 – <10 mm 2 – 10-35 mm 3 – >35 mm
Cutting edge	The mesial and distal edge of the main cusp, which can be smooth or serrated in a typical cusp	Nominal	0 – None 1 – Smooth 2 – Serrated
Lateral cusplets	Small secondary cusps found on either side of the tooth's main cusp	Nominal	0 – Absent 1 – Present
Cross-section outline	The shape profile of the tooth in a cross-section (Ciampaglio et al. 2005)	Nominal	1 – Round 2 – Oval 3 – Triangular 4 – Lens 5 – Rectangular 7 – Multi-indented lens
Longitudinal outline	The shape profile of the whole tooth (Ciampaglio et al. 2005)	Nominal	1 – Triangular 2 – Semi-circular 3 – Piercing 4 – Rectangular 5 – Polygonal

Table S2.2. Summary of the relationships between dental characters and functional traits, based on Cooper et al. (2023). "Fig. 3-6" refer to figures from that study. The top three predicting dental characters are ranked accordingly. Abbreviations are as follows: PCA = principal component analysis; CART = classification and regression tree.

Trait	Best predicting dental character (s)					
	Most common (# links; Fig. 3)	**Linear regression (Fig. 3a)**	**Distinct links (Fig. 4)**	**PCA (ranked by variation contribution; Fig. 5)**	**CART (% accuracy; Fig 6)**	**Overall (ranked)**
Body size	Crown height (112)	Crown width ($R^2 = 0.9$; P < 0.001)	Crown height, Crown width	Crown width, Crown height	Crown height (53.1%)	1. Crown width 2. Crown height
Prey preference	Cutting edge (20), Crown height (18), Crown width (18)	NA	Cutting edge	Crown width, Crown height, Cutting edge	Cutting edge (83.9%)	1. Cutting edge 2. Crown width 3. Crown height
Feeding mechanism	Cutting edge (51), Crown width (32)	NA	Lateral cusplets, Cutting edge	Crown width, Crown height, Cutting edge (all PC1), Lateral cusplets (PC2), Longitudinal outline (PC2; anterior teeth)	Longitudinal outline (74.4%)	1. Longitudinal outline 2. Lateral cusplets 3. Cutting edge

Table S2.3. Polychoric correlations between tooth position and individual dental characters. All values are accurate to three decimal places.

Correlation	Rho
Tooth position ~ crown height	0.317
Tooth position ~ crown width	0.334
Tooth position ~ cutting edge	-0.210
Tooth position ~ lateral cusplets	-0.052
Tooth position ~ cross-section outline	-0.147
Tooth position ~ longitudinal outline	0.245

Table S2.4. Correlation between dental characters and coordinates of Cenozoic shark functional space (i.e., eta^2 statistics from Kruskal-Wallis tests) both in my main analyses with weighted dental characters, and in an alternative analysis where dental characters were not weighted. All correlation tests were statistically significant ($P < 0.05$). Bold values denote the dental characters explaining the highest variance in each axis. See **Appendix Figure S2.3** for a visualisation of the dental character-axes relationships of our main analyses (i.e., weighted dental characters).

Dental character	PCoA1	PCoA2	PCoA3
Weighted dental characters (weight)			
Crown height (0.5)	0.059	**0.302**	**0.325**
Crown width (0.5)	0.084	0.222	0.180
Cutting edge (1)	0.424	**0.359**	0.060
Lateral cusplets (1)	**0.671**	0.245	0.075
Cross-section outline (0.33)	0.132	0.149	0.153
Longitudinal outline (0.67)	**0.608**	0.254	0.219
Unweighted dental characters			
Crown height	0.062	**0.483**	0.134
Crown width	0.104	**0.339**	0.052
Cutting edge	0.424	**0.323**	0.023
Lateral cusplets	**0.658**	0.153	0.163
Cross-section outline	0.150	0.232	0.102
Longitudinal outline	**0.620**	0.234	**0.276**

Table S2.5. Bootstrap hypothesis tests comparing the net changes in successive epochs between empirical taxonomic richness and resampled taxonomic richness, including the central tendency (mean) and uncertainty (min and max) of the bootstrapped differences; and the test for significance (P-value). All results are accurate to three decimal places.

Net change	Mean	Min	Max	P-value
Paleocene-Eocene	-113.504	-114.023	-112.985	0.837
Eocene-Oligocene	94.906	94.418	95.394	0.709
Oligocene-Miocene	-78.798	-79.283	-78.313	0.999
Miocene-Pliocene	64.636	64.213	65.509	0.824
Pliocene-Pleistocene	15.280	15.043	15.517	1.000
Pleistocene-Recent	2.600	2.494	2.706	0.943

Table S2.6. Absolute and proportional differences of the empirical analysis results compared to the null model for each functional diversity metric per time bin ("Epoch", consisting of six Cenozoic epochs and the Recent). Differences are between median values for each metric across 1,000 iterations of both the empirical analyses and the null model. Percentage differences are included in brackets, accurate to one decimal place. Statistically significant deviations are highlighted in bold (see **Table 3.2** in the main text for *Z*-scores). Abbreviations are as follows: FEs = functional entities; FRed = functional redundancy; FOred = functional over-redundancy; FRic = functional richness; FOri = functional originality; FSpe = functional specialisation.

Epoch	FEs	FRed	FOred	FRic	FOri	FSpe
Paleocene	-4	+0.36	**+0.06**	**+0.23**	+0.008	-0.01
	(-11.1%)	(+12.5%)	**(+6%)**	**(+23%)**	(+56.2%)	(-3.5%)
Eocene	-2	+0.17	+0.004	+0.1	+0.0007	**-0.02**
	(-3.5%)	(+3.6%)	(+0.4%)	(+10%)	(+5.2%)	**(-5.4%)**
Oligocene	**+6**	**-0.43**	-0.03	**+0.32**	+0.005	-0.02
	(+16.2%)	**(-14%)**	(-3%)	**(+32%)**	(+34%)	(-5.4%)
Miocene	+2	-0.15	**-0.03**	**+0.17**	+0.005	-0.02
	(+3.7%)	(-3.6%)	**(-3%)**	**(+17%)**	(+33.9%)	(-5.3%)
Pliocene	**+7**	**-0.49**	**-0.04**	+0.16	+0.008	-0.009
	(+16.7%)	**(-14.3%)**	**(-4%)**	(+16%)	(+60.1%)	(-3%)
Pleistocene	+3	-0.22	-0.02	+0.09	+0.005	-0.02
	(+7.3%)	(7.3%)	(-2%)	(+9%)	(+33.7%)	(-5.6%)
Recent	-2	+0.17	+0.003	-0.02	-0.002	**-0.03**
	(-5.3%)	(+5.6%)	(+0.1%)	(-2%)	(-13.1%)	**(-7.9%)**

Table S2.7. Functional diversity metrics per geological stage. All metric values are medians calculated from 1,000 iterations of analyses, accurate to three decimal places for FOri and FSpe, and up to two decimal places for all other metrics. Age ranges of stages follow Gradstein et al. (2012). Proportional changes from one stage to the other are in parentheses. Abbreviations are as follows: Ma = million years ago; FEs = functional entities; FRed = functional redundancy; FOred = functional over-redundancy; FRic = functional richness; FOri = functional originality; FSpe = functional specialisation.

Epoch	Stage	Time (Ma)	FEs	FRed	FOred (%)	FRic (%)	FOri	FSpe
Paleocene	Danian	66-61.6	20	2.5	41	49	0.028	0.311
	Selandian	61.6-59.2	20 (+0%)	1.95 (-22%)	32 (-8%)	49 (+0%)	0.038 (+36%)	0.325 (+5%)
	Thanetian	59.2-66	27 (+35%)	2.48 (+27%)	42 (+10%)	52 (+3%)	0.023 (-39%)	0.314 (-3%)
Eocene	Ypresian	56-47.8	43 (+59%)	3.09 (+25%)	42 (+0%)	76 (+24%)	0.020 (-13%)	0.317 (+1%)
	Lutetian	47.8-41.2	47 (+9%)	3.66 (+18%)	46 (+4%)	78 (+2%)	0.016 (-20%)	0.297 (-6%)
	Bartonian	41.2-37.71	43 (-9%)	3.16 (-14%)	41 (-5%)	76 (-2%)	0.018 (+13%)	0.312 (+5%)
	Priabonian	37.71-33.9	46 (+7%)	2.98 (-6%)	42 (+1%)	85 (+9%)	0.024 (+33%)	0.317 (+2%)
Oligocene	Rupelian	33.9-27.82	42 (+9%)	2.52 (-15%)	38 (-4%)	80 (-5%)	0.022 (-8%)	0.308 (-3%)
	Chattian	27.82-23.03	39 (-7%)	2.46 (-2%)	37 (-1%)	70 (-10%)	0.022 (+0%)	0.287 (-7%)
Miocene	Aquitanian	23.03-20.44	50 (+28%)	3.18 (+29%)	42 (+5%)	85 (+15%)	0.024 (+9%)	0.301 (+5%)
	Burdigalian	20.44-15.97	52 (+4%)	3.54 (+11%)	43 (+1%)	86 (+1%)	0.022 (-8%)	0.300 (-1%)
	Langhian	15.97-13.82	52 (+0%)	3.06 (-14%)	40 (-3%)	86 (+0%)	0.024 (+9%)	0.307 (+2%)
	Serravallian	13.82-11.63	51 (-2%)	2.98 (-3%)	41 (-2%)	86 (+0%)	0.025 (+4%)	0.305 (-1%)
	Tortonian	11.63-7.25	50 (-2%)	3.18 (+7%)	42 (+1%)	83 (-3%)	0.023 (-8%)	0.311 (+2%)
	Messinian	7.25-5.33	50 (+0%)	3.14 (-1%)	42 (+0%)	83 (+0%)	0.023 (+0%)	0.310 (-1%)
Pliocene	Zanclean	5.33-3.6	50 (+0%)	2.92 (-7%)	41 (-1%)	70 (-13%)	0.023 (+0%)	0.309 (-1%)
	Piacenzian	3.6-2.58	47 (-6%)	2.85 (-2%)	41 (+0%)	70 (+0%)	0.022 (-4%)	0.309 (+0%)
Pleistocene	Gelasian	2.58-1.8	43 (-9%)	3.02 (+6%)	42 (+1%)	59 (-11%)	0.018 (-18%)	0.300 (-3%)
	Calabrian	1.8-0.77	43 (+0%)	3.07 (+2%)	42 (+0%)	59 (+0%)	0.018 (+0%)	0.300 (+0%)
	Chibanian	0.77-0.13	42 (-2%)	3.07 (+0%)	42 (+0%)	59 (+0%)	0.018 (+0%)	0.300 (+0%)
	Late/Upper	0.13-0.01	42 (+0%)	3.02 (-2%)	42 (+0%)	59 (+0%)	0.019 (+6%)	0.301 (+1%)
Recent	Recent	0	36 (-14%)	3.17 (+5%)	43 (+1%)	43 (-16%)	0.012 (-37%)	0.292 (-3%)

Table S2.8. Absolute and proportional differences of the empirical analysis results compared to the null model for each functional diversity metric per geological stage. Differences are between median values for each metric across 1,000 iterations of both the empirical analyses and the null model. Percentage differences are included in brackets, accurate to one decimal place. Statistically significant deviations are highlighted in bold. Abbreviations are as follows: FEs = functional entities; FRed = functional redundancy; FOred = functional over-redundancy; FRic = functional richness; FOri = functional originality; FSpe = functional specialisation.

| Epoch	Stage	FEs	FRed	FOred	FRic	FOri	FSpe
Paleocene	Danian	-3	+0.33	**+0.06**	+0.11	+0.013	+0.008
		(-13%)	(+15.2%)	**(+6%)**	(+11%)	(+86.7%)	(+2.6%)
	Selandian	+1	-0.1	-0.01	**+0.19**	+0.024	+0.023
		(+5.3%)	(-4.9%)	(-1%)	**(+19%)**	(+171.4%)	(+7.6%)
	Thanetian	-1	+0.09	+0.03	+0.02	+0.007	+0.011
		(-3.7%)	(+3.8%)	(+3%)	(+2%)	(+43.8%)	(+3.6%)
Eocene	Ypresian	+2	-0.15	-0.03	+0.05	+0.003	+0.013
		(+4.9%)	(-4.6%)	(-3%)	(+5%)	(+17.6%)	(+4.3%)
	Lutetian	+1	-0.08	+0.00	+0.02	-0.001	-0.007
		(+2.2%)	(-2.1%)	(+0%)	(+2%)	(-5.9%)	(-2.3%)
	Bartonian	+2	-0.16	-0.03	+0.05	+0.001	+0.008
		(+4.9%)	(-4.8%)	(-3%)	(5%)	(+5.9%)	(+2.6%)
	Priabonian	**+5**	**-0.36**	-0.02	+0.14	+0.008	+0.013
		(+12.2%)	**(-10.8%)**	(-2%)	(+14%)	(+50%)	(+4.3%)
Oligocene	Rupelian	**+6**	**-0.42**	**-0.05**	**+0.16**	+0.005	+0.004
		(+16.7%)	**(-14.3%)**	**(-5%)**	**(+16%)**	(+29.4%)	(1.3%)
	Chattian	**+5**	**-0.36**	**-0.05**	+0.08	+0.005	-0.017
		(+14.7%)	**(-12.8%)**	**(-5%)**	(+8%)	(+29.4%)	(-5.6%)
Miocene	Aquitanian	**+5**	**-0.35**	**-0.04**	+0.1	+0.007	-0.003
		(+11.1%)	**(-9.9%)**	**(-4%)**	(+10%)	(+41.2%)	(-1%)
	Burdigalian	+4	-0.29	**-0.04**	+0.07	+0.005	-0.003
		(+8.3%)	(-7.6%)	**(-4%)**	(+7%)	(+29.4%)	(-1%)
	Langhian	**+7**	**-0.47**	**-0.06**	+0.11	+0.007	+0.004
		(+15.6%)	**(-13.3%)**	**(-6%)**	(+11%)	(+41.2%)	(+1.3%)
	Serravallian	**+7**	**-0.47**	**-0.04**	+0.12	+0.008	+0.002
		(+15.9%)	**(-13.6%)**	**(-4%)**	(+12%)	(+47.1%)	(+0.6%)
	Tortonian	**+5**	**-0.35**	**-0.04**	+0.07	+0.006	+0.007
		(+11.1%)	**(-9.9%)**	**(-4%)**	(+7%)	(+35.3%)	(+2.3%)
	Messinian	**+5**	**-0.35**	**-0.04**	+0.07	+0.006	+0.006
		(+11.1%)	**(-10%)**	**(-4%)**	(+7%)	(+35.3%)	(+2%)
Pliocene	Zanclean	**+7**	**-0.48**	**-0.04**	-0.04	+0.006	+0.004
		(+16.3%)	**(-14.1%)**	**(-4%)**	(-4%)	(+35.3%)	(+1.3%)
	Piacenzian	**+6**	**-0.42**	**-0.03**	-0.02	+0.005	+0.005
		(+14.6%)	**(-12.8%)**	**(-3%)**	(-2%)	(+29.4%)	(+1.6%)
Pleistocene	Gelasian	+3	-0.23	-0.02	-0.11	+0.001	-0.004
		(+7.5%)	(-7.1%)	(-2%)	(-11%)	(+5.9%)	(-1.3%)
	Calabrian	+2	-0.15	-0.02	-0.12	+0.001	-0.004
		(+4.9%)	(-4.7%)	(-2%)	(-12%)	(+5.9%)	(-1.3%)
	Chibanian	+2	-0.16	-0.02	-0.12	+0.001	-0.004
		(+5%)	(-5%)	(-2%)	(-12%)	(+5.9%)	(-1.3%)
	Late/Upper	+2	-0.16	-0.02	-0.11	+0.002	-0.001
		(+5%)	(-5%)	(-2%)	(-11%)	(+11.8%)	(-1%)
Recent	Recent	-2	+0.17	+0.00	**-0.23**	-0.005	-0.012
		(-5.3%)	(+5.7%)	(+0%)	**(-23%)**	(-29.4%)	(-3.9%)

Table S2.9. *Z*-scores for all functional diversity metrics calculated at geological stage level, indicating how the empirical result of each metric differs from random chance expectations based on the number of taxa. All values are accurate to two decimal places. *Z*-scores marked in bold are considered statistically significant ($Z > |1.96|$), marking a value that falls outside of 95% of the null distribution. Abbreviations are as follows: FE = functional entities; FRed = functional redundancy; FOred = functional over-redundancy; FRic = functional richness; FOri = functional originality; FSpe = functional specialisation.

Epoch	Stage	FE	FRed	FOred	FRic	FOri	FSpe
Paleocene	Danian	-1.91	1.84	**2.25**	1.11	1.15	0.65
	Selandian	0.67	-0.61	-0.29	**2.06**	1.74	1.51
	Thanetian	-0.58	0.57	1.35	0.25	0.76	0.84
Eocene	Ypresian	0.96	-1.00	-1.30	0.74	0.50	1.32
	Lutetian	0.23	-0.23	0.21	0.17	0.01	-0.75
	Bartonian	0.96	-0.91	-1.79	0.65	0.26	0.86
	Priabonian	**2.38**	**-2.19**	-1.74	1.90	1.09	1.30
Oligocene	Rupelian	**2.90**	**-2.60**	**-2.51**	**2.02**	0.77	0.44
	Chattian	**2.49**	**-2.31**	**-2.32**	1.09	0.69	-1.47
Miocene	Aquitanian	**2.48**	**-2.27**	**-2.77**	1.41	1.08	-0.17
	Burdigalian	1.81	-1.80	**-2.57**	1.11	0.72	-0.37
	Langhian	**3.12**	**-2.95**	**-3.99**	1.52	1.07	0.32
	Serravallian	**3.22**	**-3.04**	**-2.84**	1.64	1.15	0.11
	Tortonian	**2.32**	**-2.12**	**-2.20**	0.92	0.84	0.72
	Messinian	**2.31**	**-2.24**	**-2.13**	0.87	0.91	0.63
Pliocene	Zanclean	**3.15**	**-2.84**	**-2.43**	-0.42	0.92	0.44
	Piacenzian	**2.73**	**-2.47**	**-1.98**	-0.18	0.75	0.51
Pleistocene	Gelasian	1.16	-1.14	-1.10	-1.34	0.26	-0.40
	Calabrian	0.93	-0.92	-1.22	-1.43	0.23	-0.39
	Chibanian	0.92	-0.89	-1.11	-1.41	0.17	-0.42
	Late/Upper	0.92	-0.88	-0.86	-1.35	0.35	-0.28
Recent	Recent	-0.97	0.91	0.04	**-3.31**	-0.66	-1.14

Table S2.10. P-values of Mann-Whitney U-tests between pairwise epochs. Comparisons are made between the median values of each functional diversity metric distribution across 1,000 iterations. All results are in bold and <0.05, indicating statistical significance. Abbreviations are as follows: FEs = functional entities; FRed = functional redundancy; FOred = functional over-redundancy; FRic = functional richness; FOri = functional originality; FSpe = functional specialisation.

Pairwise epochs	FEs	FRed	FOred	FRic	FOri	FSpe
Paleocene-Eocene	**<0.001**	**<0.001**	**<0.001**	**<0.001**	**<0.001**	**<0.001**
Eocene-Oligocene	**<0.001**	**<0.001**	**<0.001**	**<0.001**	**<0.001**	**<0.001**
Oligocene-Miocene	**<0.001**	**<0.001**	**<0.001**	**<0.001**	**0.016**	**0.003**
Miocene-Pliocene	**<0.001**	**<0.001**	**<0.001**	**<0.001**	**<0.001**	**<0.001**
Pliocene-Pleistocene	**<0.001**	**<0.001**	**<0.001**	**<0.001**	**<0.001**	**<0.001**
Pleistocene-Recent	**<0.001**	**<0.001**	**<0.001**	**<0.001**	**<0.001**	**<0.001**

3 | SUPPLEMENTARY FIGURES
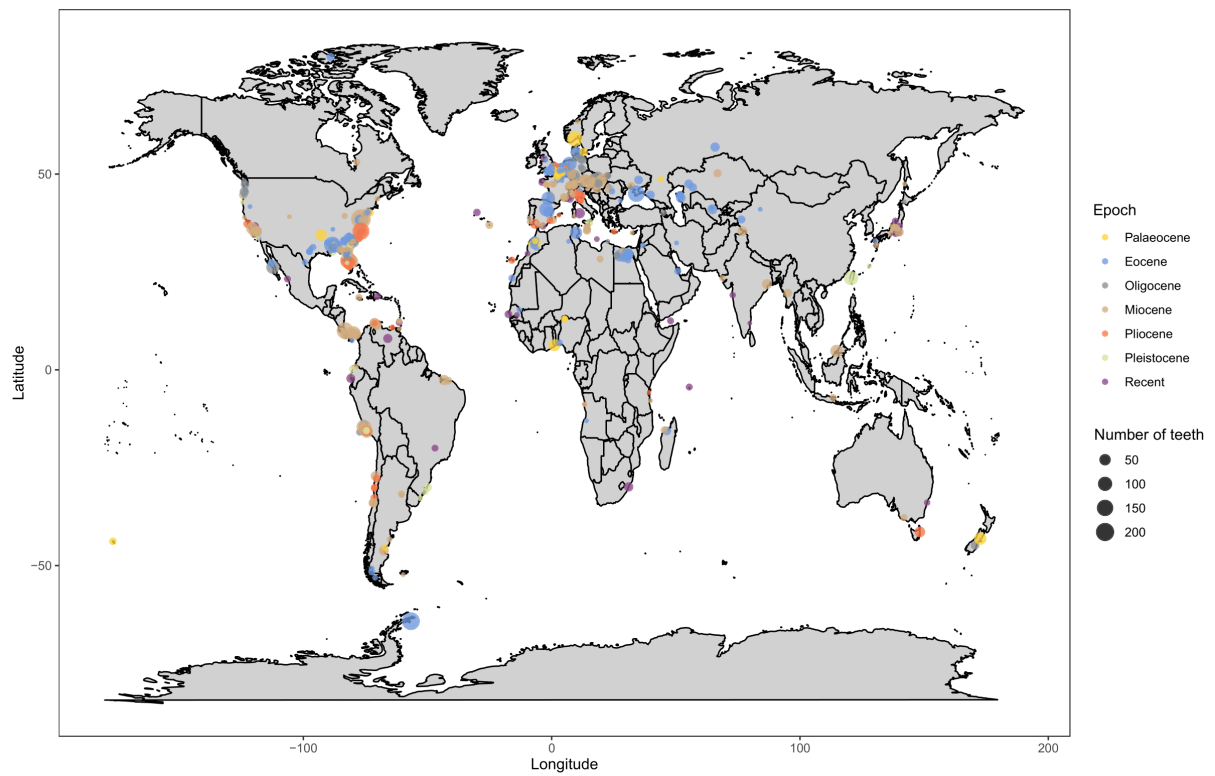
Figure S2.1. Map of localities, categorised by time bin ("Epoch", consisting of six Cenozoic epochs and the Recent), from which shark teeth were collected. Circle width denotes approximate number of teeth sampled from a locality.
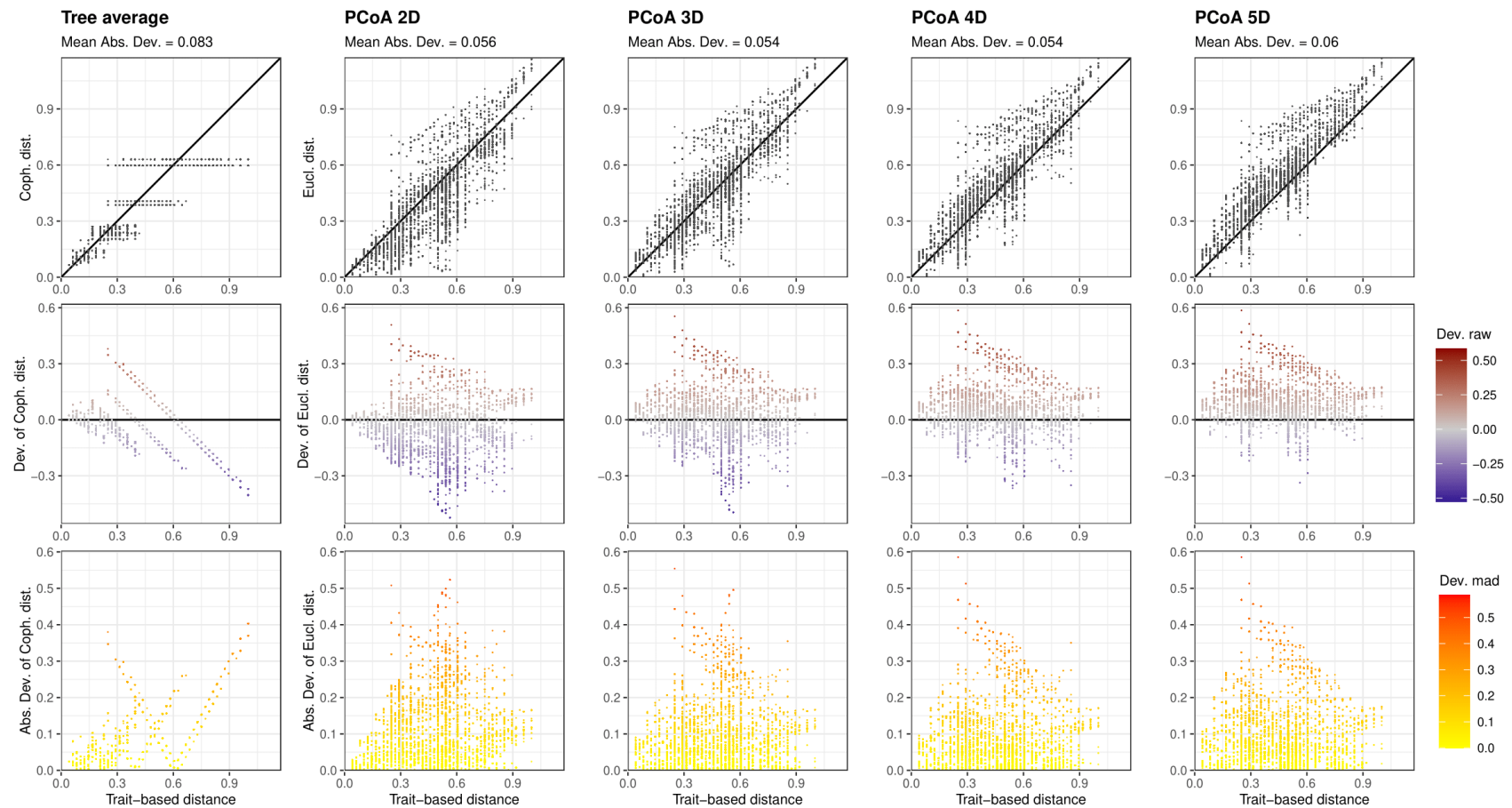
Figure S2.2. Quality of the functional space. Ten dimensions were included in these analyses and averaged to produce a dendrogram ("Tree Average"; leftmost column); but only the spaces from two to five dimensions are shown here, with each column from left to right representing a difference space. Mean absolute deviation values (Mean Abs. Dev.) show that my data are best represented by four dimensions; but are negligibly different from a three-dimensional space (by <0.0001). The top row depicts species functional distances in the multidimensional space, the middle row displays the raw deviation of species distances in the functional space compared to trait-based distances, and the bottom row showcases the absolute deviation of the distance in the functional space.
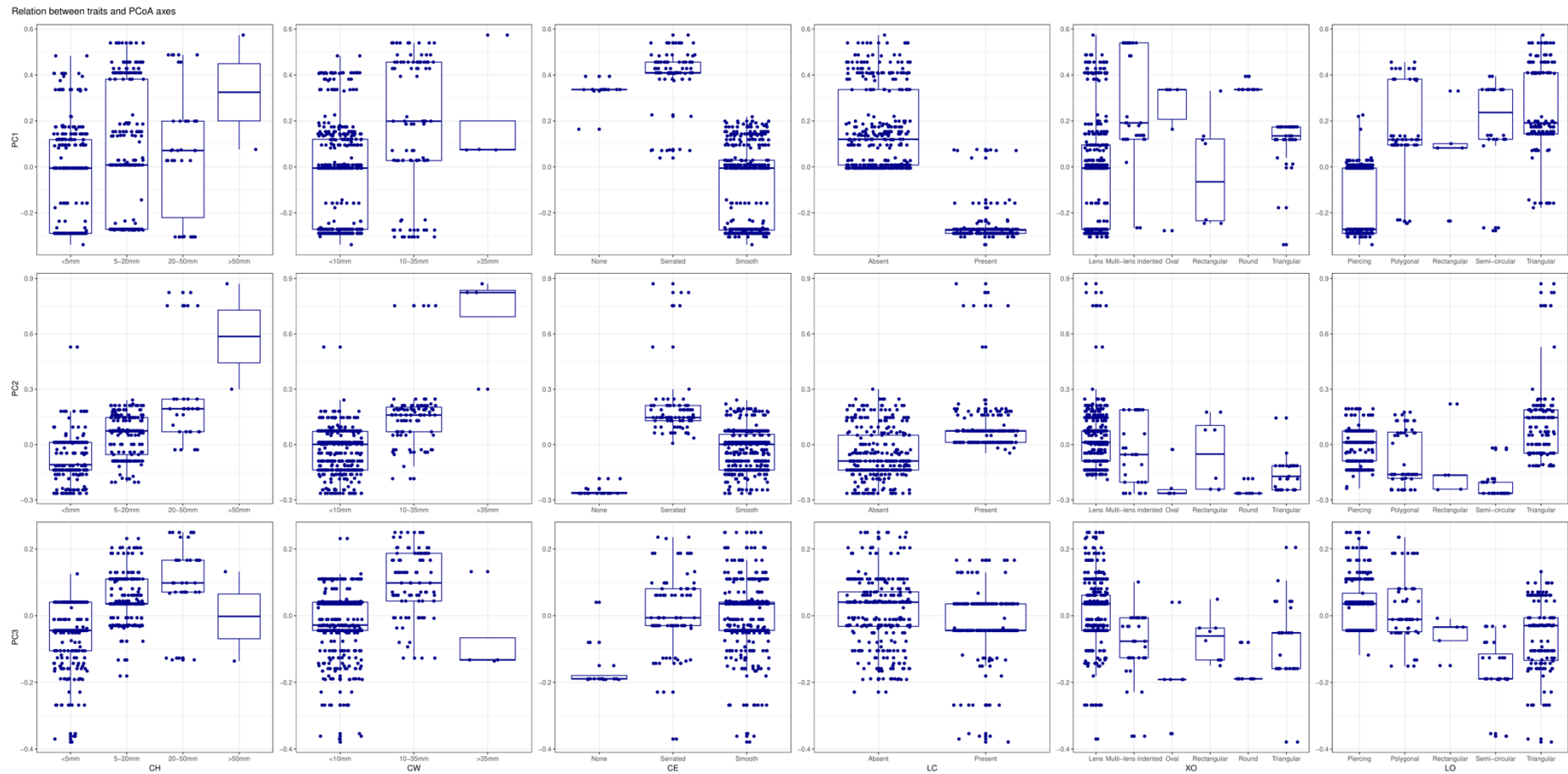
Figure S2.3. Visualised correlations between dental characters and the three PCoA axes used to form the functional space. See **Appendix Table S2.4** for correlation values from the returned Kruskal-Wallis tests. Abbreviations are as follows: PC = principal coordinate; CH = crown height; CW = crown width; CE = cutting edge; LC = lateral cusplets; XO = cross-section outline; LO = longitudinal outline.
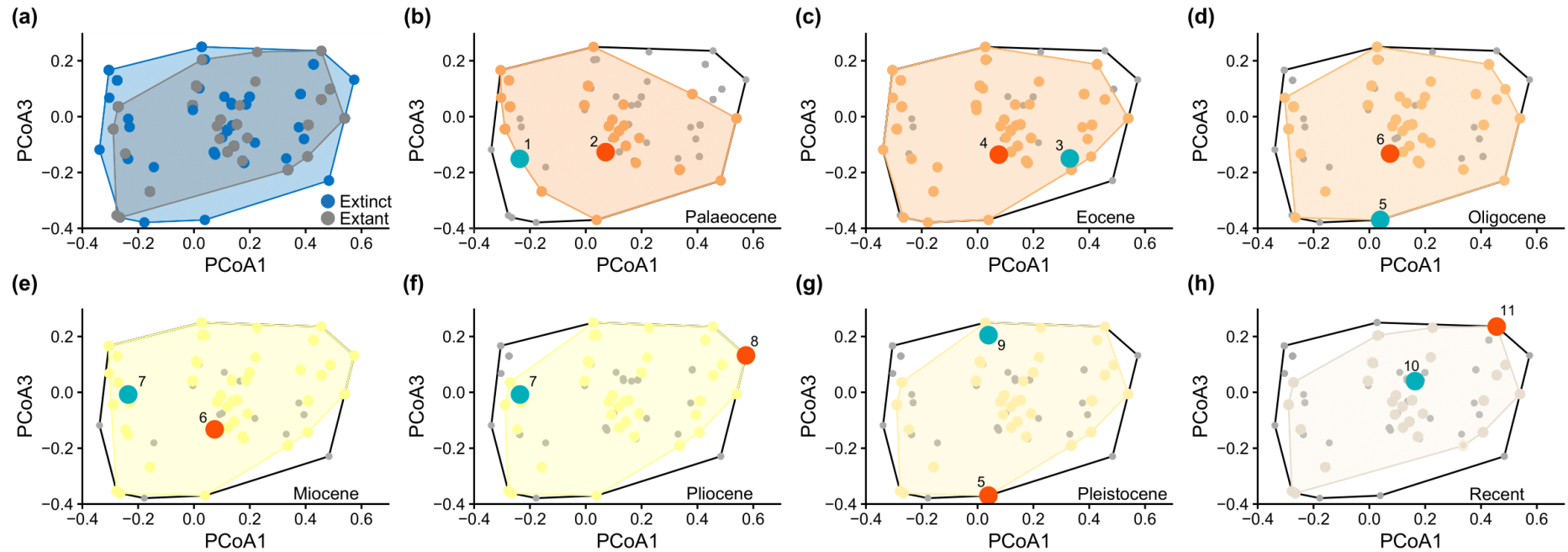
Figure S2.4. Functional space of Cenozoic sharks on the first and third axes. (a) Functional space of all Cenozoic sharks, where the blue and grey convex hulls mark space occupied by extinct and extant sharks respectively. (b-h) Functional space of sharks through time, with space occupied by each time bin represented by coloured convex hulls. Coloured dots denote species present in each space while grey dots represent absent species. Turquoise and orange dots in (b-h) respectively denote taxa with the highest functional originality (FOri) and functional specialisation (FSpe). Numbered taxa are as follows: (1) †*Squalodalatias* sp.; (2) †*Palaeocarcharodon orientalis*; (3) †*Heterodontus woodwardi*; (4) †*Otodus nodai*; (5) †*Dalatias* sp.; (6) †*Otodus angustidens*; (7) †*Echinorhinus blakei*; (8) †*Otodus megalodon*; (9) †*Megachasma* sp.; (10) *Sphyrna tiburo*; (11) *Galeocerdo cuvier*.
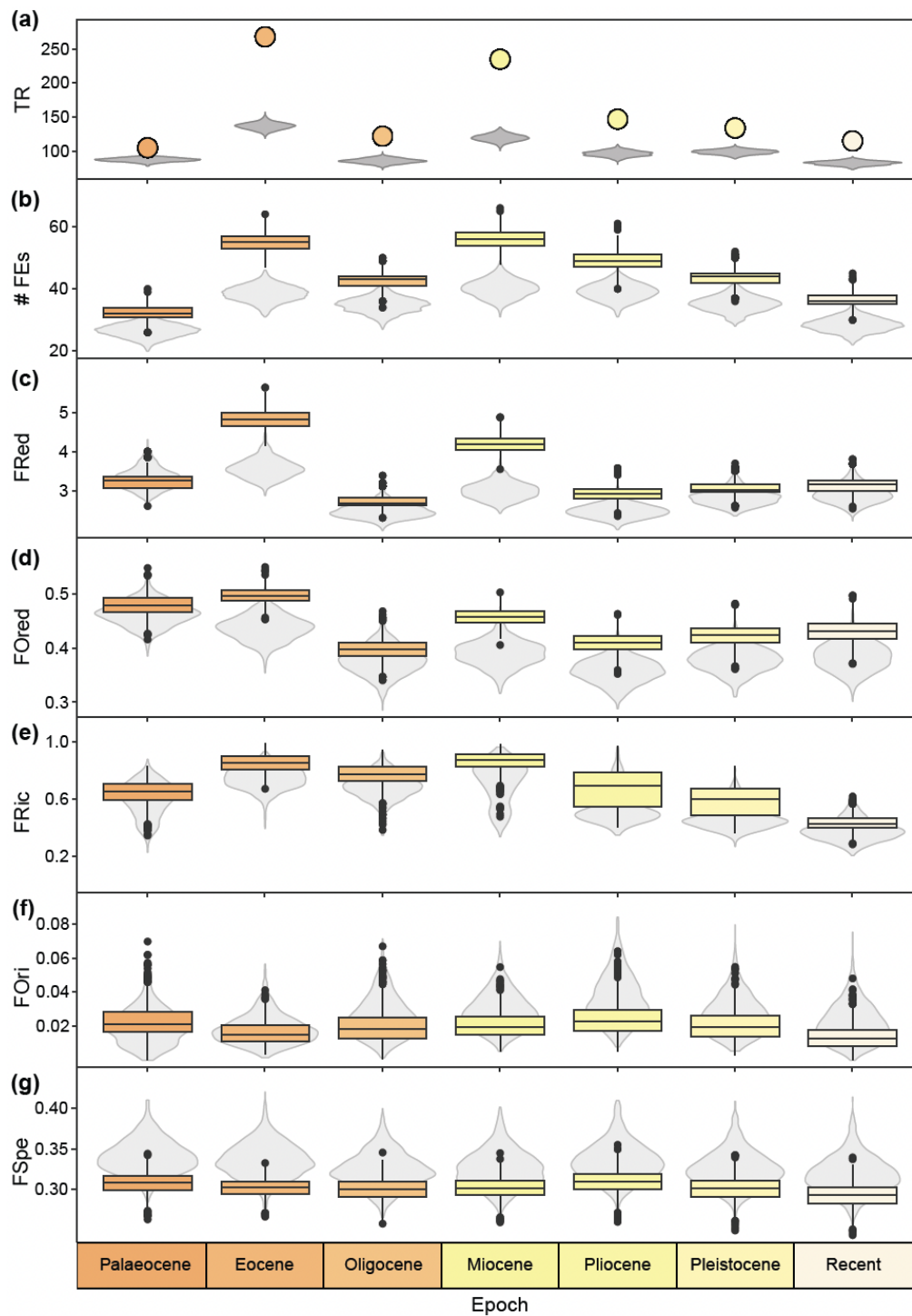
Figure S2.5. Changes in functional diversity compared to randomised resampling in which all epochs were equally sampled to 309 teeth to match the lowest sampled time bin. (a) taxonomic richness (TR); (b) functional entities (# FEs); (c) functional redundancy (FRed); (d) functional over-redundancy (FOred); (e) functional richness (FRic); (f) functional originality (FOri); (g) functional specialisation (FSpe). In (a), coloured dots represent empirical taxonomic richness while in (b-g) boxplots represent range of empirical results across 1,000 empirical iterations. The range of resampled metrics over 1,000 iterations are represented by the grey violin plots.
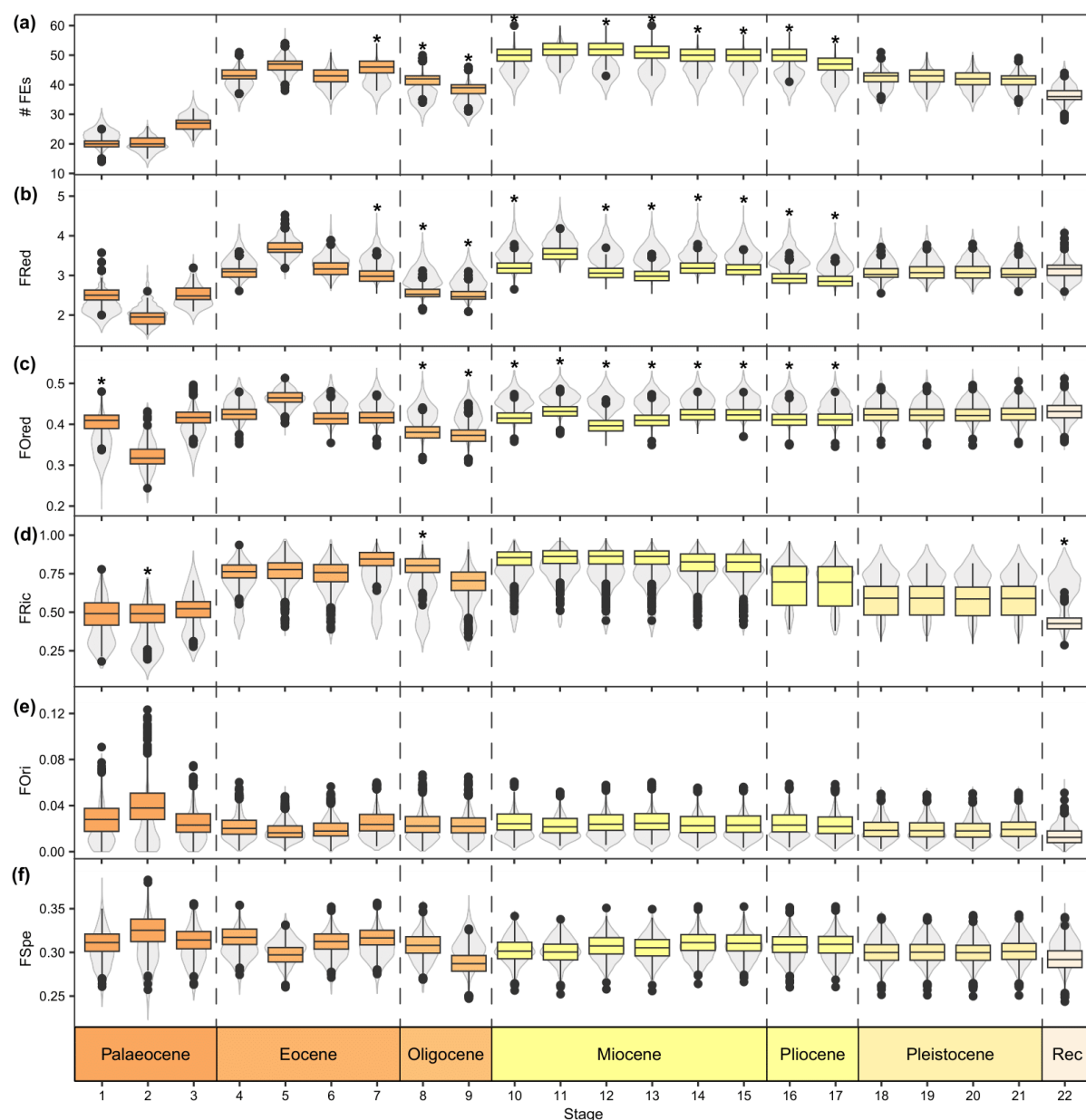
Figure S2.6. Changes in functional diversity (values in boxplots over 1,000 empirical iterations) at the geological stage level. (a) functional entities (# FEs); (b) functional redundancy (FRed); (c) functional over-redundancy (FOred); (d) functional richness (FRic); (e) functional originality (FOri); (f) functional specialisation (FSpe). The stages are grouped together within epochs, where Rec = Recent, and are numbered as follows: 1 = Danian (66-61.6 Ma); 2 = Selandian (61.6-59.2 Ma); 3 = Thanetian (59.2-56 Ma); 4 = Ypresian (56-47.8 Ma); 5 = Lutetian (47.8-41.2 Ma); 6 = Bartonian (41.2-37.71 Ma); 7 = Priabonian (37.71-33.9 Ma); 8 = Rupelian (33.9-27.82 Ma); 9 = Chattian (27.82-23.03 Ma); 10 = Aquitanian (23.03-20.44 Ma); 11 = Burdigalian (20.44-15.97 Ma); 12 = Langhian (15.97-13.82 Ma); 13 = Serravallian (13.82-11.62 Ma); 14 = Tortonian (11.62-7.246 Ma); 15 = Messinian (7.247-5.333 Ma); 16 = Zanclean (5.333-3.6 Ma); 17 = Piacenzian (3.6-2.58 Ma); 18 = Gelasian (2.58-1.8 Ma); 19 = Calabrian (1.8-0.774 Ma); 20 = Chibanian (0.774-0.129 Ma); 21 = Late/Upper (0.129-0.0117 Ma); 22 = Recent (0 Ma). Age ranges of stages follow (Gradstein et al. 2012). Asterisks are used to mark metrics that significantly deviate from null distribution, which is represented over 1,000 iterations by grey violin plots.
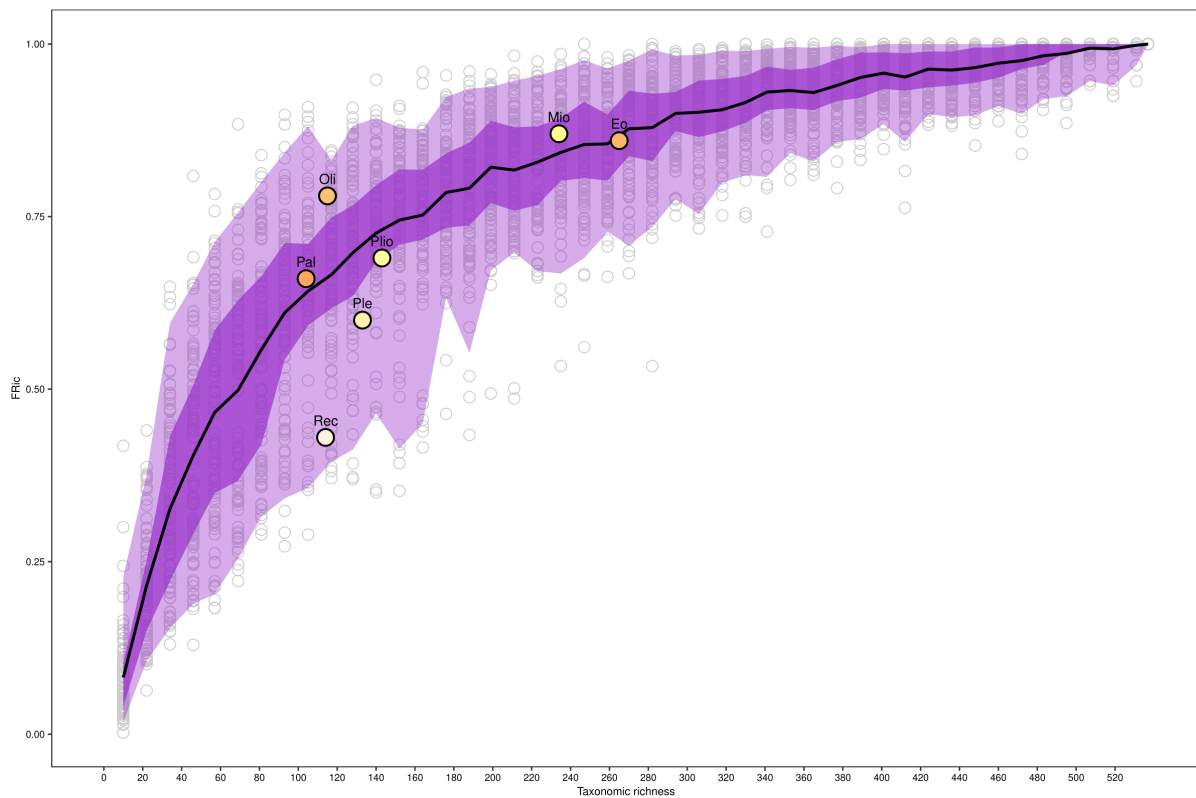
Figure S2.7. Changes in functional richness (FRic) in response to randomising a sequence of taxon loss, from 10 to 537 (100% taxonomic richness). Grey circles represent calculated FRic along the sequence, run through 100 randomisations, while coloured dots are median empirical values of FRic per time bin. Abbreviated labels associated with these dots are as follows: Pal = Paleocene; Eo = Eocene; Oli = Oligocene; Mio = Miocene; Plio = Pliocene; Ple = Pleistocene; Rec = Recent. The black line marks the mean value of the 100 randomisations while the dark and light purple shadings represent the range of the 50% and 95% confidence intervals respectively.

Functional diversity of sharks through time: past, present and future
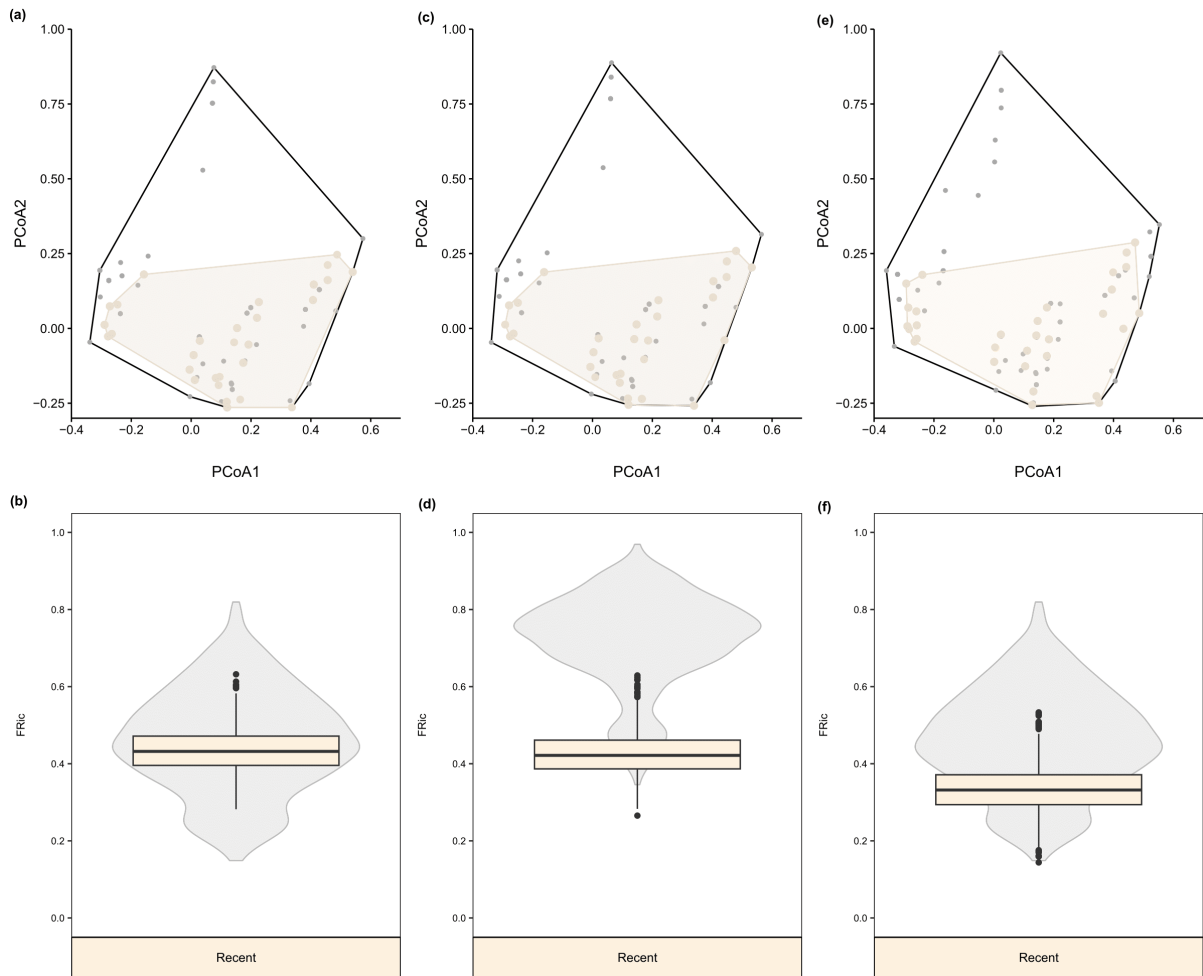
Figure S2.8. Functional richness (FRic) of sharks from the Recent based on (a, b) Recent taxa with a fossil record (n = 114); (c, d) all Recent taxa collected from present-day shark teeth with and without a fossil record ("Recent-plus" in the main text; n = 162); and (e, f) random resampling of all Recent taxa based on the number of taxa with a fossil record ("Resampled Recent-plus" in the main text; n = 114). The top panels (a, c, e) illustrate functional space occupation. In (b, d, f), the boxplots represent a range of results based on functional taxonomic unit randomisations, while the grey violin plots represent ranges of a null model based on respective taxonomic richness. Both ranges were recorded across 1,000 iterations. Only (d) showcases a result that significantly deviates from null expectations (*Z* = -4.56).
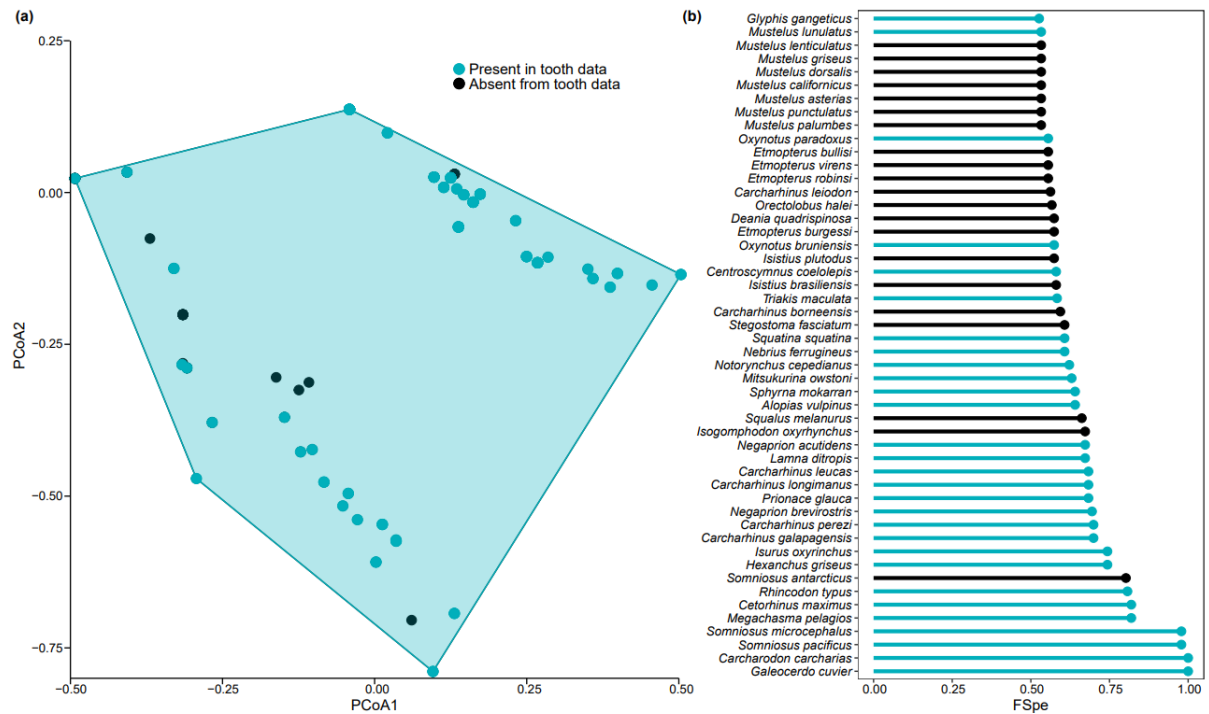
Figure S2.9. Functional structure of all Recent shark species from Pimiento et al. (2023) based on body size, prey preference and feeding mechanism (i.e., the three traits our dental characters are related to), presented on the first two axes. (a) Functional space of all species (i.e., one dot may represent multiple species occupying the same functional entity), with the light blue convex hull denoting the space occupied by species in the Recent sample of our tooth data; (b) Top 10% ranked functionally specialised species. In both plots, light blue marks species present within the Recent sample of our tooth data, while black denotes absent species.
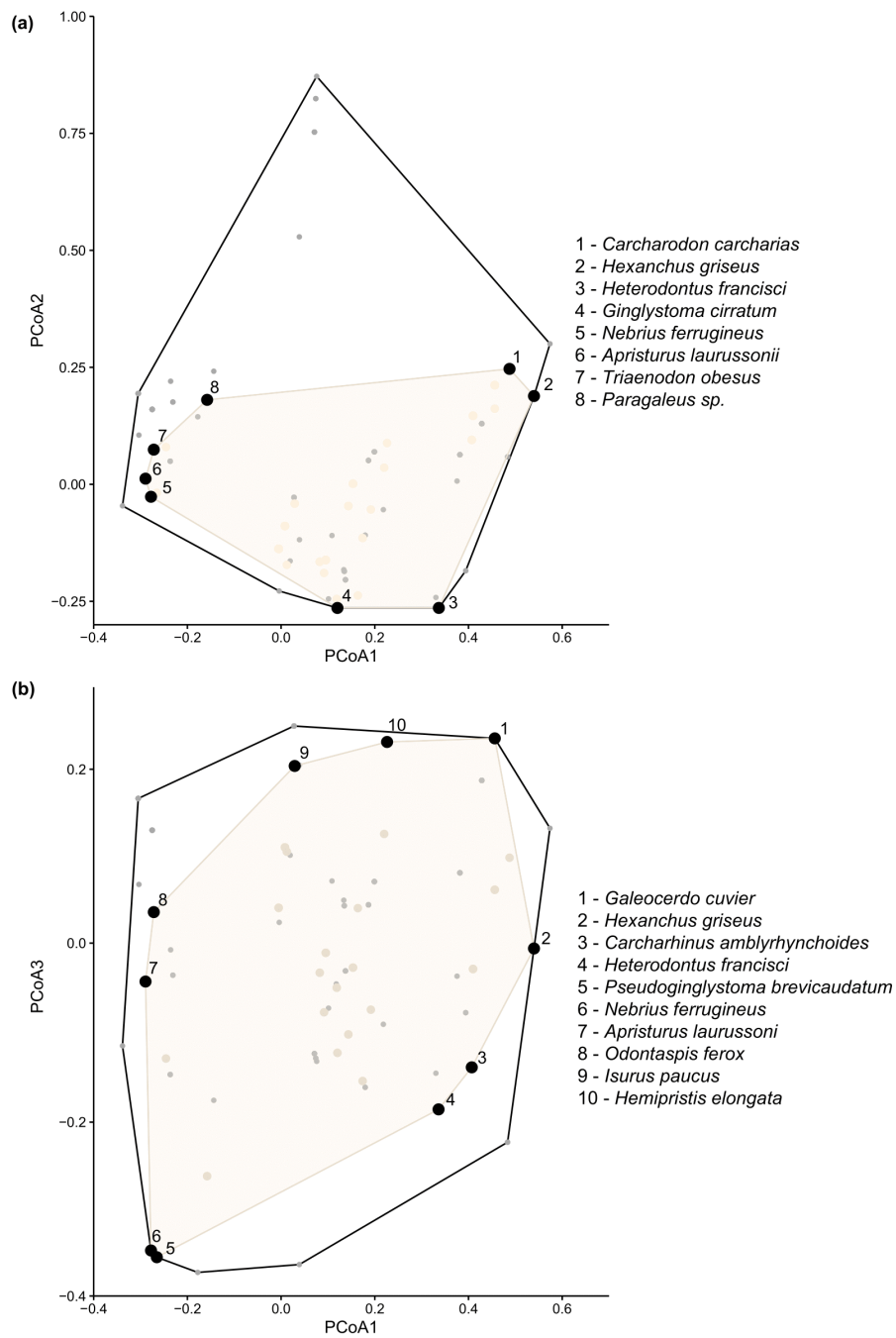
Figure S2.10. Functional space of Recent shark species in relation to the rest of the Cenozoic on (a) the first and second functional axis; and (b) the first and third functional axis. Coloured dots denote taxa present in the Recent, while grey dots represent all other taxa absent from the Recent. All taxa identified as vertices of the Recent space (i.e., found at the edges of the occupied space) are marked in large black dots and are labelled in the corresponding legends.

167
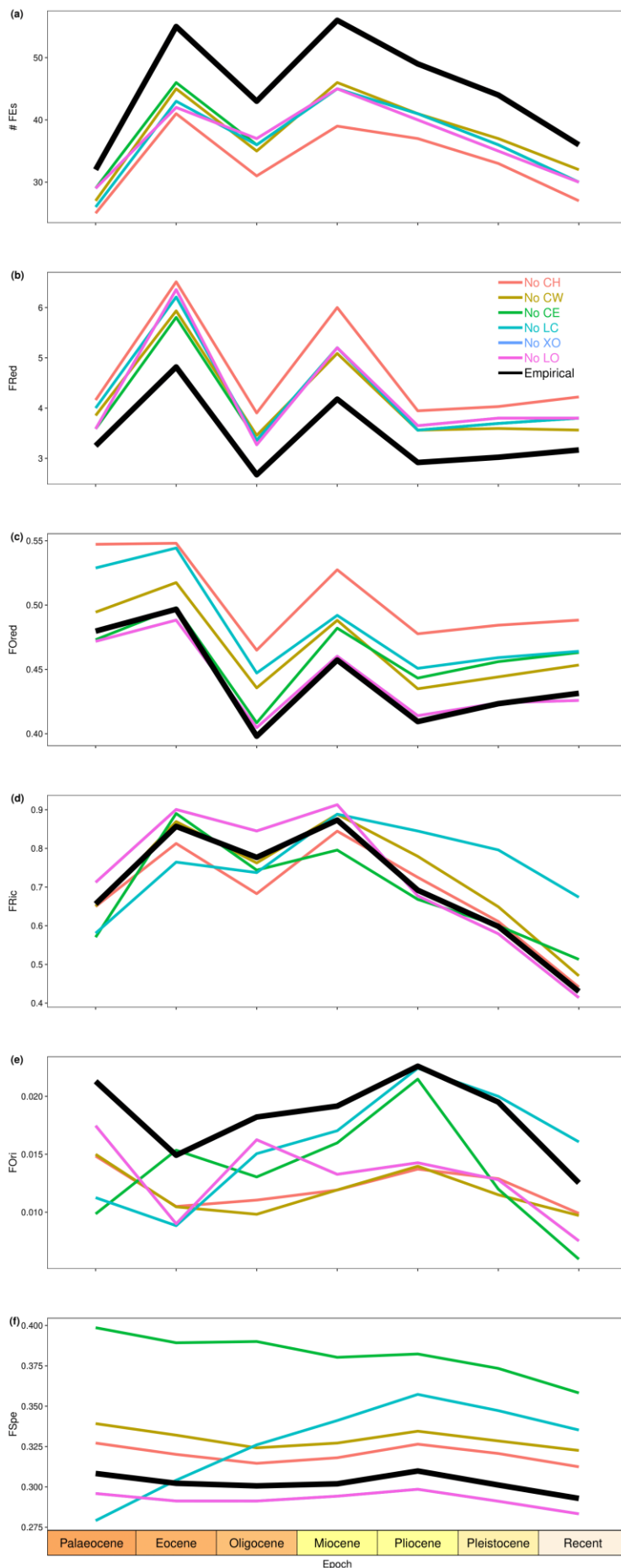
Figure S2.11. Sensitivity tests in which each dental character was removed from repeated functional diversity analyses. All metric values per time bin are medians based on 1,000 iterations to account for variation in shark tooth morphology. Results of all tests are presented as lines for the purpose of visualising multiple patterns through time. The thick black line marks the empirical analysis, while coloured lines denote each sensitivity test in which a specified dental character is removed. Abbreviations from the legend are therefore as follows: CH = crown height; CW = crown width; CE = cutting edge; LC = lateral cusplets; XO = cross-section outline; LO = longitudinal outline. Metrics being analysed are as follows: (a) functional entities (# FEs); (b) functional redundancy (FRed); (c) functional over-redundancy (FOred); (d) functional richness (FRic); (e) functional originality (FOri); and (f) functional specialisation (FSpe).
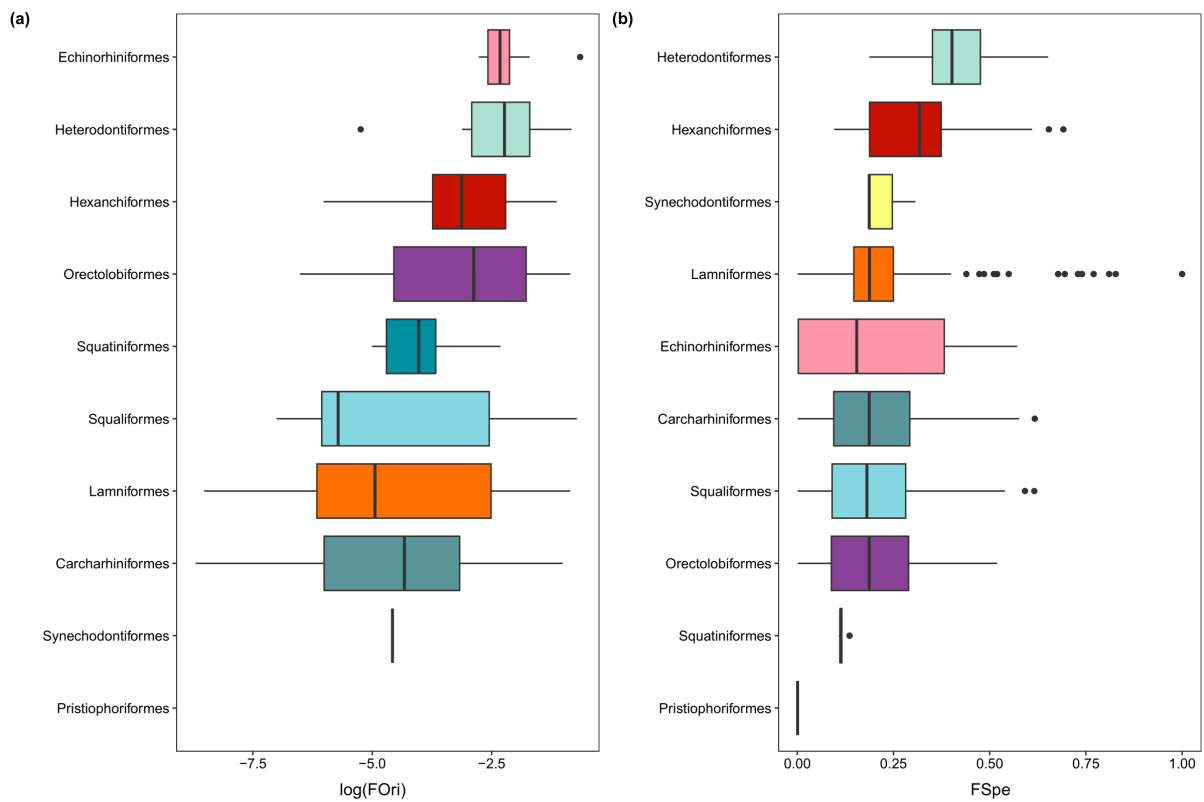
Figure S2.12. (a) Functional originality (FOri) and (b) specialisation (FSpe) of Cenozoic sharks at the order level. Values are calculated based on mean values per taxon across 1,000 empirical iterations. FOri values are log transformed for visualisation, though this resulted in the absence of Pristiophoriformes given its untransformed FOri value of 0, denoting teeth with identical dental character combinations (i.e., all species occupy the same functional entity), meaning that all species occupy the same trait space.

4 | SUPPLEMENTARY REFERENCES

Cappetta, H. (2012). Handbook of Paleoichthyology—Chondrichthyes—Mesozoic and Cenozoic Elasmobranchii: Teeth. In H.-P. Schultze (Ed.), *Handbook of paleoichthyology.* Volume 3E (pp. 1-512). Munich: Verlag Dr. Friedrich Pfiel.

Ciampaglio, C. N., Wray, G. A. & Corliss, B. H. (2005). A toothy tale of evolution: convergence in tooth morphology among marine Mesozoic–Cenozoic sharks, reptiles, and mammals. *The Sedimentary Record* **3**:4-8.

Cooper, J. A., Griffin, J. N., Kindlimann, R., & Pimiento, C. (2023). Are shark teeth proxies for functional traits? A framework to infer ecology from the fossil record. *Journal of Fish Biology* **103**:798-814.

Gradstein, F. M., Ogg, J. G., Schmitz, M. D., & Ogg, G. M. (2012). *The geologic time scale 2012.* Elsevier.

Kent, B. W. (1994). *Fossil sharks of the Chesapeake Bay region.* Egan Rees & Boyer, Inc., Columbia, Maryland.

Kent, B. W. (2018). The cartilaginous fishes (chimaeras, sharks and rays) of Calvert Cliffs, Maryland, USA. Pages 45-157. In S. J. Godfrey, (Ed.), *The Geology and Vertebrate Paleontology of Calvert Cliffs, Maryland, USA.* Smithsonian Institution Scholarly Press, Washington D.C.

Magneville, C., Loiseau, N., Albouy, C., Casajus, N., Claverie, T., Escalas, A., Leprieur, F., Maire, E., Mouillot, D., & Villéger, S. (2022). mFD: an R package to compute and illustrate the multiple facets of functional diversity. *Ecography* **2022**:e05904.

Mouillot, D., Graham, N. A., Villéger, S., Mason, N. W., & Bellwood, D. R. (2013). A functional approach reveals community responses to disturbances. *Trends in Ecology and Evolution* **28**:167-177.

Pimiento, C., Albouy, C., Silvestro, D., Mouton, T. L., Velez, L., Mouillot, D., Judah, A. B., Griffin, J. N., & Leprieur, F. (2023). Functional diversity of sharks and rays is highly vulnerable and supported by unique species and locations worldwide. *Nature Communications* **14**:7691.

Appendix 3 | Supplementary materials for chapter 4

Supporting Information

Poleward shift and functional decline of sharks and rays under future extinctions

Contents

Data used in this chapter are available open access in the following repositories:

- The functional trait dataset used in this work is available as Data S1 from Pimiento et al. (2023).

- Occurrence and environmental data from AquaMaps are freely available online at https://www.aquamaps.org.

1 | SUPPLEMENTARY TABLES

Table S3.1. Quality of the functional space built on an increasing number of axes. MAD refers to the value of mean absolute deviation. RMSD refers to the value of the root of the mean square deviation. Both values are given by the *mFD* R package's "quality.fspaces" function (Magneville et al. 2022). In both cases, the lowest value, accurate to five decimal places, marks the highest quality space, based on Maire et al. (2015). The total explained inertia per space is also given, accurate to two decimal places. Bold values denote the number of axes used in subsequent analyses with the lowest MAD and RMSD.

Axis	MAD	RMSD	Total inertia (%)
PCoA1	0.12064	0.16770	27.04
PCoA2	0.06716	0.10804	48.68
PCoA3	0.04841	0.07243	65.73
PCoA4	**0.03909**	**0.05316**	**75.54**
PCoA5	0.04330	0.05559	84.94
PCoA6	0.05060	0.06263	90.70
PCoA7	0.05495	0.06682	94.12
PCoA8	0.05761	0.06955	96.57
PCoA9	0.06013	0.07106	98.44
PCoA10	0.06250	0.07328	99.99

Table S3.2. Correlation between traits and coordinates of the functional space (i.e., R^2 statistics from linear regressions between maximum length and coordinates; eta^2 statistics from Kruskal-Wallis tests between coordinates and all other traits). Apart from relationships between PCoA2 coordinates and thermoregulation and feeding mechanism (marked as NA), all correlation tests were statistically significant ($P < 0.05$). Bold values mark the traits explaining the highest variance in each axis. See **Appendix Figure S3.2** for a visualisation of trait-axes relationships.

Trait	PCoA1	PCoA2	PCoA3	PCoA4
Habitat	0.333	**0.682**	0.108	**0.471**
Vertical position	**0.419**	0.208	0.187	0.323
Terrestriality	0.042	0.305	0.080	0.006
Thermoregulation	0.016	NA	0.008	0.020
Feeding mechanism	0.011	NA	0.032	0.034
Diet	**0.485**	0.024	**0.544**	0.095
Maximum body size	0.079	0.059	0.031	0.142

Table S3.3. The representation of highest ranked FUSE (functionally unique, specialised and endangered) species present in the AquaMaps data, indicated by absolute and proportional (i.e., %) values. See **Appendix Figure S3.5** for a visual representation of the top 25.

Top # FUSE species	# in AquaMaps	% in AquaMaps
Top 20	18	90
Top 25	21	84
Top 50	41	82
Top 100	72	72

Table S3.4. P-values for all Wilcoxon signed-rank tests comparing the "buffered" empirical changes in functional diversity (see methods in the main text) to those obtained from a null model where species present in each extinction scenario were randomised. All values highlighted in bold indicate statistical significance (P < 0.05).

Future scenario	FRic	FUn	FSp
2100 (i.e., 77 years)	0.17	0.50	**<0.001**
100 years	**0.002**	0.34	**<0.001**
200 years	**<0.001**	**<0.001**	**<0.001**
300 years	**<0.001**	**<0.001**	**<0.001**
400 years	**<0.001**	0.92	**<0.001**
500 years	**<0.001**	0.23	**<0.001**

Table S3.5. Results of binomial generalised linear mixed effect models using ranked FUS (functionally unique and specialised) scores as predictors of extinction probability for all future extinction scenarios. Based on a random trend model, with taxonomic order used as a random effect. For simplicity, fixed effect results are reported here. See **Figure 4.2b** of the main text and **Appendix Figure S3.6** for order-specific results based on partial pooling and raw data respectively. Bold p-values denote statistical significance. Std. Error = Standard error.

Scenario	Estimate	Std. Error	Z value	Pr(>|z|)
2100 (i.e., 77 years)	-0.0009	0.0004	-2.109	**0.035**
100 years	-0.0006	0.0008	-0.719	0.472
200 years	-0.0006	0.0003	-1.874	0.061
300 years	0.0003	0.0005	0.616	0.538
400 years	-0.0005	0.0007	-0.698	0.485
500 years	0.0007	0.0011	0.625	0.532

Table S3.6. Top ten highest ranked functionally unique and specialised (FUS) species and their presence or absence in the extinction scenario of 2100, as well as 100 (Y100) and 200 years in the future (Y200). In extinction scenarios, 1 marks survival while 0 denotes absence due to extinction. Abbreviations of IUCN Red List statuses are as follows: LC = Least Concern; VU = Vulnerable; EN = Endangered.

Species	Order	IUCN	FUS score	FUS rank	2100	Y100	Y200
Cetorhinus maximus	Lamniformes	EN	1.5	1	1	1	0
Carcharodon carcharias	Lamniformes	VU	1.32	2	1	1	0
Lamna ditropis	Lamniformes	LC	1.27	3	1	1	1
Mobula japonica	Myliobatiformes	EN	1.21	4	1	1	1
Manta alfredi	Myliobatiformes	VU	1.11	5	1	1	1
Mobula munkiana	Myliobatiformes	VU	1.08	6	1	1	1
Rhincodon typus	Orectolobiformes	EN	1.04	7	0	0	0
Isurus paucus	Lamniformes	EN	1.04	8	1	1	0
Somnious microcephalus	Squaliformes	VU	1.04	9	0	0	0
Isurus oxyrinchus	Lamniformes	EN	0.99	10	1	1	0

Table S3.7. Comparison of GLMs with binomial error examining species richness in 2100 (i.e., in grid cells from AquaMaps data) in response to environmental drivers used to model AquaMaps under each representative concentration pathway (RCP). In all models, extinctions projected by *iucn_sim* have been accounted for. Reported results are degrees of freedom (Df), deviance, Akaike Information Criterion (AIC), Likelihood Ratio Test (LRT) and the p-value based on a chi-squared test (Pr(>Chi)). Contribution of environmental parameters to the complete model was established by dropping each individual (i.e., drop1 in R). Asterisks are used to mark the best three predictors per RCP, denoted by the highest LRT value combined with statistical significance.

Environmental parameter	Df	Deviance	AIC	LRT	Pr(>Chi)
RCP 2.6					
Mean depth	1	1,447,109	2,008,607	483,762*	<0.001
Minimum depth	1	1,447,109	2,008,607	536,738*	<0.001
Maximum depth	1	1,447,109	2,008,607	369,089	<0.001
Sea surface temperature	1	1,447,109	2,008,607	235,256	<0.001
Sea bottom temperature	1	1,447,109	2,008,607	566,138*	<0.001
Salinity	1	1,447,109	2,008,607	4,225.4	<0.001
Bottom salinity	1	1,447,109	2,008,607	7,249.9	<0.001
Primary productivity	1	1,447,109	2,008,607	104,138	<0.001
Ice concentration	1	1,447,109	2,008,607	12,166	<0.001
Dissolved oxygen concentration	1	1,447,109	2,008,607	246,721	<0.001
Bottom oxygen concentration	1	1,447,109	2,008,607	59,825	<0.001
RCP 4.5					
Mean depth	1	1,440,802	2,004,663	466,408*	<0.001
Minimum depth	1	1,440,802	2,004,663	513,814*	<0.001
Maximum depth	1	1,440,802	2,004,663	356,742	<0.001
Sea surface temperature	1	1,440,802	2,004,663	198,646	<0.001
Sea bottom temperature	1	1,440,802	2,004,663	539,760*	<0.001
Salinity	1	1,440,802	2,004,663	1,864.2	<0.001
Bottom salinity	1	1,440,802	2,004,663	6,322.3	<0.001
Primary productivity	1	1,440,802	2,004,663	122,988	<0.001
Ice concentration	1	1,440,802	2,004,663	13,486	<0.001
Dissolved oxygen concentration	1	1,440,802	2,004,663	208,011	<0.001
Bottom oxygen concentration	1	1,440,802	2,004,663	50,181	<0.001
RCP 8.5					
Mean depth	1	1,106,335	1,603,481	275,732*	<0.001
Minimum depth	1	1,106,335	1,603,481	287,169*	<0.001
Maximum depth	1	1,106,335	1,603,481	220,292	<0.001
Sea surface temperature	1	1,106,335	1,603,481	66,823	<0.001
Sea bottom temperature	1	1,106,335	1,603,481	307,897*	<0.001
Salinity	1	1,106,335	1,603,481	3,990.4	<0.001
Bottom salinity	1	1,106,335	1,603,481	9,158.9	<0.001
Primary productivity	1	1,106,335	1,603,481	109,191	<0.001
Ice concentration	1	1,106,335	1,603,481	9,270.2	<0.001
Dissolved oxygen concentration	1	1,106,335	1,603,481	81,752	<0.001
Bottom oxygen concentration	1	1,106,335	1,603,481	14,290	<0.001

Table S3.8. Comparison of GLMs with binomial error examining functional richness in 2100 (i.e., in grid cells from AquaMaps data) in response to environmental drivers used to model AquaMaps under each representative concentration pathway (RCP). In all models, extinctions projected by *iucn_sim* have been accounted for. Reported results are degrees of freedom (Df), deviance, Akaike Information Criterion (AIC), Likelihood Ratio Test (LRT) and the p-value based on a chi-squared test (Pr(>Chi)). Contribution of environmental parameters to the complete model was established by dropping each individual (i.e., drop1 in R). Asterisks are used to mark the best three predictors per RCP, denoted by the highest LRT value combined with statistical significance.

| Environmental parameter	Df	Deviance	AIC	LRT	Pr(>Chi)
RCP 2.6					
Mean depth	1	19,461.9	41,921	11,326*	<0.001
Minimum depth	1	19,461.9	41,415	12,220*	<0.001
Maximum depth	1	19,462	42,934	9,247.5	<0.001
Sea surface temperature	1	19,462	42,136	939.07	<0.001
Sea bottom temperature	1	19,461.9	40,525	10,137*	<0.001
Salinity	1	19,462	43,310	354.66	<0.001
Bottom salinity	1	19,462	43,340	142.95	<0.001
Primary productivity	1	19,462	43,765	2,013.7	<0.001
Ice concentration	1	19,462	43,416	106.25	<0.001
Dissolved oxygen concentration	1	19,462	42,185	944.75	<0.001
Bottom oxygen concentration	1	19,462	42,976	158.34	<0.001
RCP 4.5					
Mean depth	1	19,072.8	40,493	11,095*	<0.001
Minimum depth	1	19,072.8	39,984	11,942*	<0.001
Maximum depth	1	19,073	41,288	9,061	<0.001
Sea surface temperature	1	19,073	39,536	711.42	<0.001
Sea bottom temperature	1	19,072.8	39,606	9,550.3*	<0.001
Salinity	1	19,073	40,529	301.28	<0.001
Bottom salinity	1	19,073	40,205	86.661	<0.001
Primary productivity	1	19,073	40,813	2,230.8	<0.001
Ice concentration	1	19,073	40,404	115.86	<0.001
Dissolved oxygen concentration	1	19,703	39,554	692.15	<0.001
Bottom oxygen concentration	1	19,703	40,131	90.66	<0.001
RCP 8.5					
Mean depth	1	15,252.4	29,522	8,279.6*	<0.001
Minimum depth	1	15,252.4	29,655	8,645.3*	<0.001
Maximum depth	1	15,252.4	29,272	6,937.9*	<0.001
Sea surface temperature	1	15,252	27,057	143.21	<0.001
Sea bottom temperature	1	15,252.4	28,355	6,104.3	<0.001
Salinity	1	15,252	27,380	106.74	<0.001
Bottom salinity	1	15,252	27,047	26.97	<0.001
Primary productivity	1	15,252	27,877	2,039.1	<0.001
Ice concentration	1	15,252	27,206	63.2	<0.001
Dissolved oxygen concentration	1	15,252	27,020	163.5	<0.001
Bottom oxygen concentration	1	15,252	27,179	0.01	0.9

Table S3.9. Comparison of GLMs with binomial error examining functional uniqueness in 2100 (i.e., in grid cells from AquaMaps data) in response to environmental drivers used to model AquaMaps under each representative concentration pathway (RCP). In all models, extinctions projected by *iucn_sim* have been accounted for. Reported results are degrees of freedom (Df), deviance, Akaike Information Criterion (AIC), Likelihood Ratio Test (LRT) and the p-value based on a chi-squared test (Pr(>Chi)). Contribution of environmental parameters to the complete model was established by dropping each individual (i.e., drop1 in R). Asterisks are used to mark the best three predictors per RCP, denoted by the highest LRT value combined with statistical significance.

Environmental parameter	Df	Deviance	AIC	LRT	Pr(>Chi)
RCP 2.6					
Mean depth	1	18.45	149.34	2.95	0.086
Minimum depth	1	18.45	149.68	3.29	0.07
Maximum depth	1	18.45	148.59	2.2	0.138
Sea surface temperature	1	18.45	151.29	4.89*	0.027
Sea bottom temperature	1	18.45	152.04	5.64*	0.018
Salinity	1	18.45	146.43	0.04	0.84
Bottom salinity	1	18.45	146.68	0.29	0.59
Primary productivity	1	18.45	147.21	0.82	0.365
Ice concentration	1	18.45	146.59	0.2	0.657
Dissolved oxygen concentration	1	18.45	151.76	5.36*	0.02
Bottom oxygen concentration	1	18.45	147.29	0.9	0.34
RCP 4.5					
Mean depth	1	18.65	149.03	2.72	0.099
Minimum depth	1	18.65	149.35	3.04	0.08
Maximum depth	1	18.65	148.31	2	0.157
Sea surface temperature	1	18.65	150.88	4.58*	0.03
Sea bottom temperature	1	18.65	151.58	5.27*	0.02
Salinity	1	18.65	146.36	0.055	0.81
Bottom salinity	1	18.65	146.56	0.26	0.61
Primary productivity	1	18.65	147.28	0.97	0.32
Ice concentration	1	18.65	146.5	0.198	0.66
Dissolved oxygen concentration	1	18.65	151.31	5.01*	0.025
Bottom oxygen concentration	1	18.65	147.17	0.87	0.35
RCP 8.5					
Mean depth	1	16.54	121.56	0.9	0.34
Minimum depth	1	16.54	121.58	0.927	0.336
Maximum depth	1	16.54	121.36	0.7	0.4
Sea surface temperature	1	16.54	122.12	1.47*	0.23
Sea bottom temperature	1	16.54	122.63	1.97*	0.16
Salinity	1	16.54	121.26	0.6	0.44
Bottom salinity	1	16.54	121.14	0.48	0.49
Primary productivity	1	16.54	121.52	0.86	0.35
Ice concentration	1	16.54	120.79	0.13	0.72
Dissolved oxygen concentration	1	16.54	122.56	1.9*	0.168
Bottom oxygen concentration	1	16.54	120.95	0.29	0.59

Table S3.10. Comparison of GLMs with binomial error examining functional specialisation in 2100 (i.e., in grid cells from AquaMaps data) in response to environmental drivers used to model AquaMaps under each representative concentration pathway (RCP). In all models, extinctions projected by *iucn_sim* have been accounted for. Reported results are degrees of freedom (Df), deviance, Akaike Information Criterion (AIC), Likelihood Ratio Test (LRT) and the p-value based on a chi-squared test (Pr(>Chi)). Contribution of environmental parameters to the complete model was established by dropping each individual (i.e., drop1 in R). Asterisks are used to mark the best three predictors per RCP, denoted by the highest LRT value combined with statistical significance.

Environmental parameter	Df	Deviance	AIC	LRT	Pr(>Chi)
RCP 2.6					
Mean depth	1	2,720.8	156,772	913.51*	<0.001
Minimum depth	1	2,720.8	155,552	1,013*	<0.001
Maximum depth	1	2,720.8	158,345	728.46*	<0.001
Sea surface temperature	1	2,720.8	162,327	154.98	<0.001
Sea bottom temperature	1	2,720.8	159,604	534.55	<0.001
Salinity	1	2,720.8	163,600	0.0039	0.95
Bottom salinity	1	2,720.8	163,598	0.02	0.88
Primary productivity	1	2,720.8	163,495	56.41	<0.001
Ice concentration	1	2,720.8	163,288	74.09	<0.001
Dissolved oxygen concentration	1	2,720.8	162,638	124.86	<0.001
Bottom oxygen concentration	1	2,720.8	163,623	0.36	0.547
RCP 4.5					
Mean depth	1	2,759.2	158,989	880.83*	<0.001
Minimum depth	1	2,759.2	157,749	980.79*	<0.001
Maximum depth	1	2,759.2	160,544	700.22*	<0.001
Sea surface temperature	1	2,759.2	163,896	202.88	<0.001
Sea bottom temperature	1	2,759.2	161,644	538.41	<0.001
Salinity	1	2,759.2	165,587	1.31	0.25
Bottom salinity	1	2,759.2	165,549	0.0001	0.99
Primary productivity	1	2,759.2	165,415	58.99	<0.001
Ice concentration	1	2,759.2	165,204	80.78	<0.001
Dissolved oxygen concentration	1	2,759.2	164,381	155.47	<0.001
Bottom oxygen concentration	1	2,759.2	165.591	3.46	0.06
RCP 8.5					
Mean depth	1	2,771.3	142,100	899.83*	<0.001
Minimum depth	1	2,771.3	141,004	1,002.7*	<0.001
Maximum depth	1	2,771.3	143,570	719.38*	<0.001
Sea surface temperature	1	2,771.3	147,918	236.33	<0.001
Sea bottom temperature	1	2,771.3	144,715	607.33	<0.001
Salinity	1	2,771.3	149,016	0.72	0.396
Bottom salinity	1	2,771.3	148,954	2.16	0.14
Primary productivity	1	2,771.3	148,748	65.26	<0.001
Ice concentration	1	2,771.3	148,711	51.98	<0.001
Dissolved oxygen concentration	1	2,771.3	148,314	173.8	<0.001
Bottom oxygen concentration	1	2,771.3	148,990	0.65	0.42

2 | SUPPLEMENTARY FIGURES
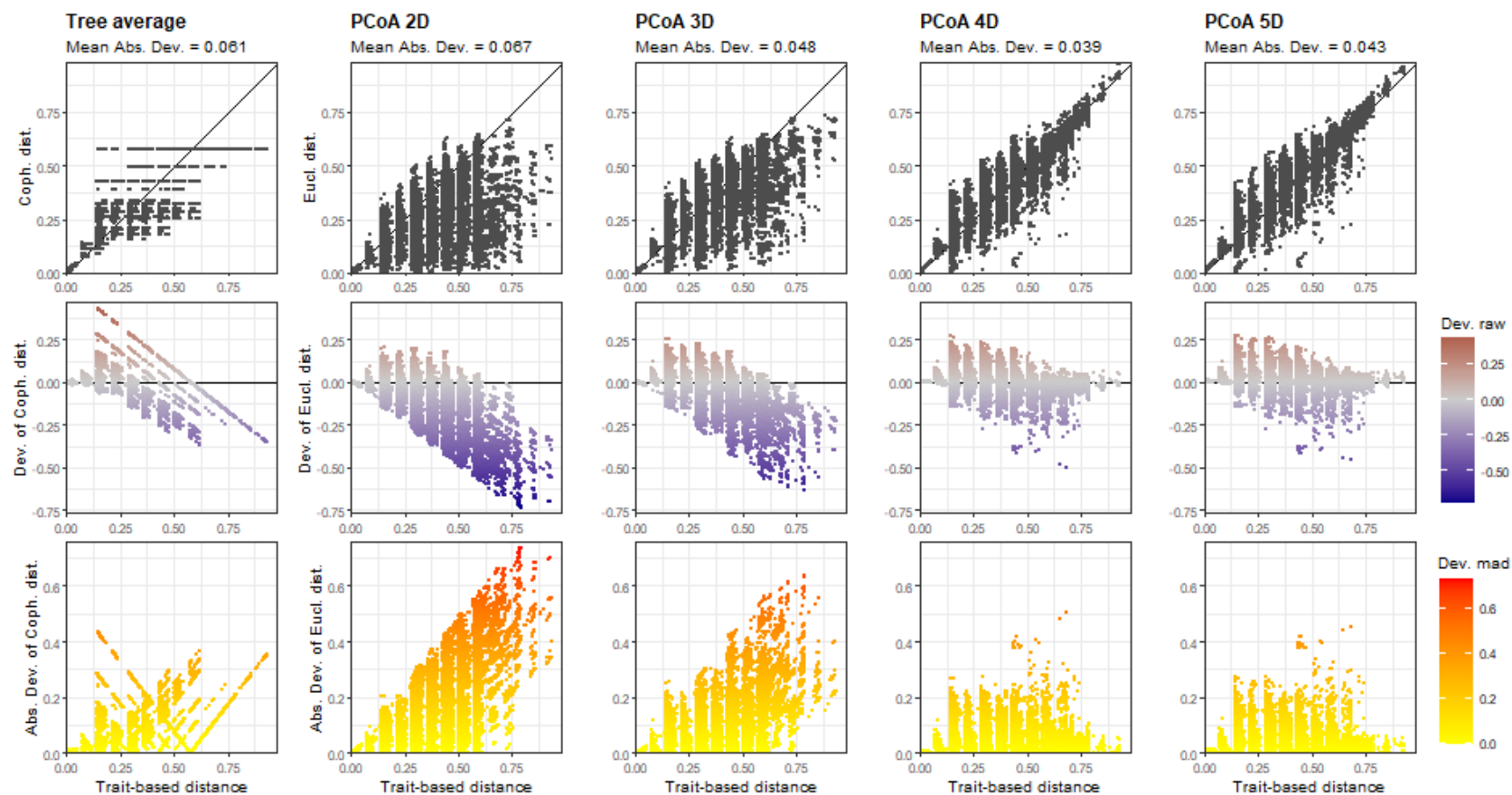
Figure S3.1. Quality of the functional space. Ten dimensions were included in analyses and averaged to produce a dendrogram (Tree average; leftmost column). From left to right onwards, only the spaces from two (PCoA 2D) to five dimensions (PCoA 5D) are shown here. Mean absolute deviation values (Mean Abs. Dev.) clearly indicate that my data are best represented by four dimensions. The top row depicts species functional distances in the multidimensional space, the middle row represents the raw deviation of species distances in the functional space compared to trait-based distances, and the bottom row denotes the absolute deviation of the distance in the functional space.
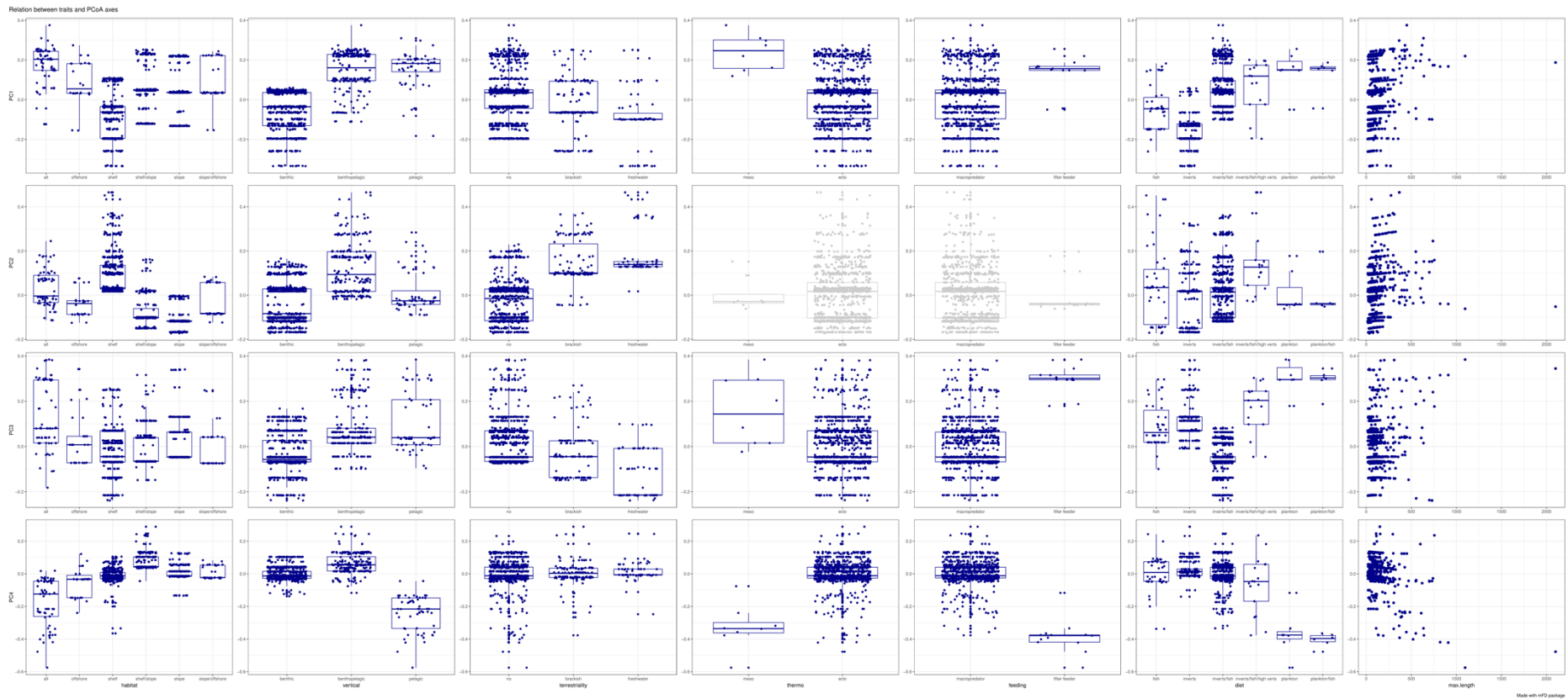
Figure S3.2. Visualised correlations between traits and the four PCoA axes used to form the functional space. See **Appendix Table S3.2** for correlation values from returned tests. Plots marked in blue denote tests with statistical significance while plots without statistical significance are marked in grey.
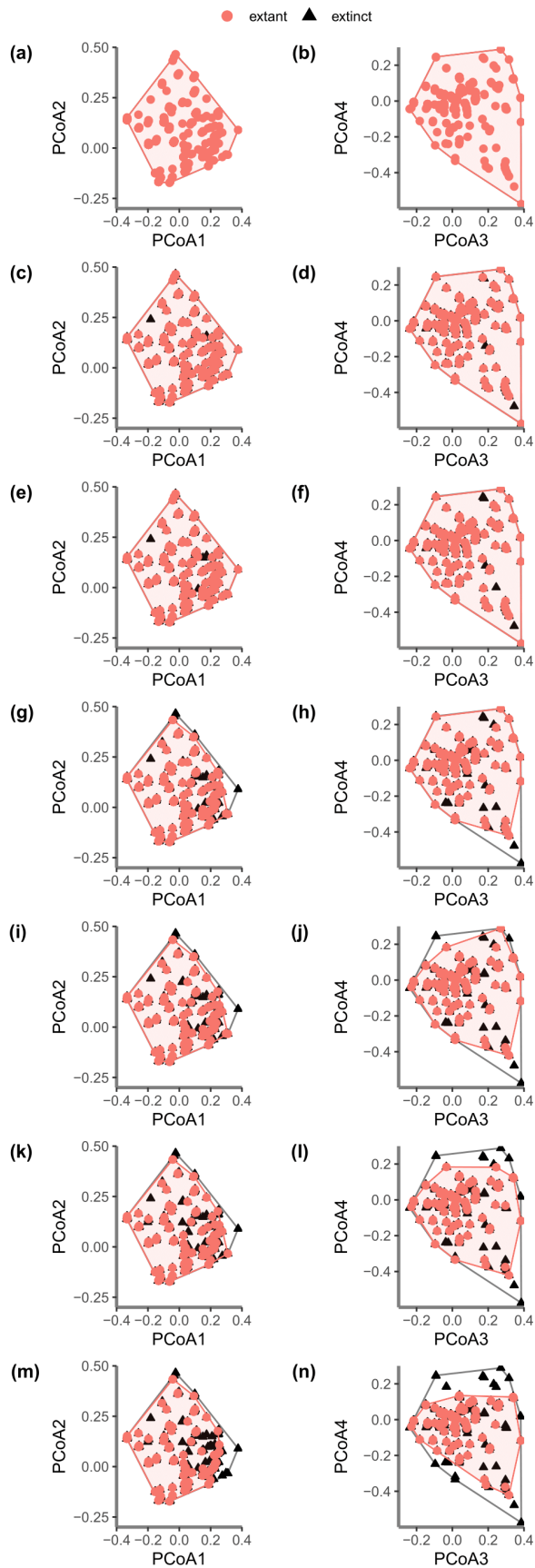
Figure S3.3. Elasmobranch functional occupation over time, on the first and second (left column) and third and fourth (right column) axes. Scenarios are as follows: (a, b) the present day; (c, d) the year 2100; (e, f) 100 years in the future; (g, h) 200 years in the future; (i, j) 300 years in the future; (k, l) 400 years in the future; and (m, n) 500 years in the future. The red convex hull represents the range of occupied space per scenario (i.e., functional richness). Red dots denote species present within the occupied space, while black triangles represent species absent from the occupied space; i.e., species that have become extinct by each point in the future.

Functional diversity of sharks through time: past, present and future
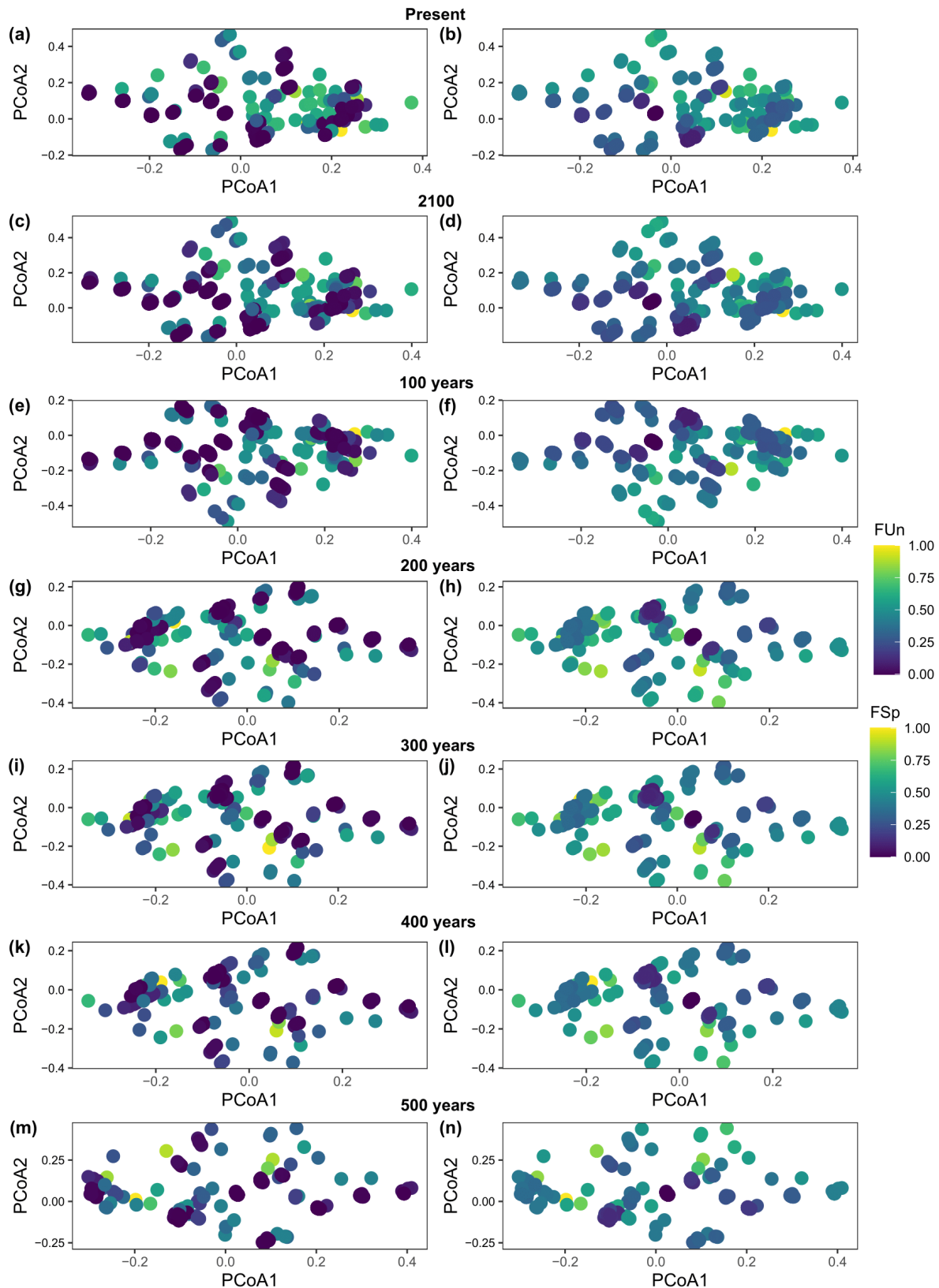
Figure S3.4. Species-specific functional uniqueness (FUn; left column) and specialisation (FSp; right column) scores in the occupied functional space per scenario, shown here on the first two functional axes. Scenarios are as follows: (a, b) the present day; (c, d) the year 2100; (e, f) 100 years in the future; (g, h) 200 years in the future; (i, j) 300 years in the future; (k, l) 400 years in the future; and (m, n) 500 years in the future. In all plots, yellow-green colours represent the highest scores.

Functional diversity of sharks through time: past, present and future
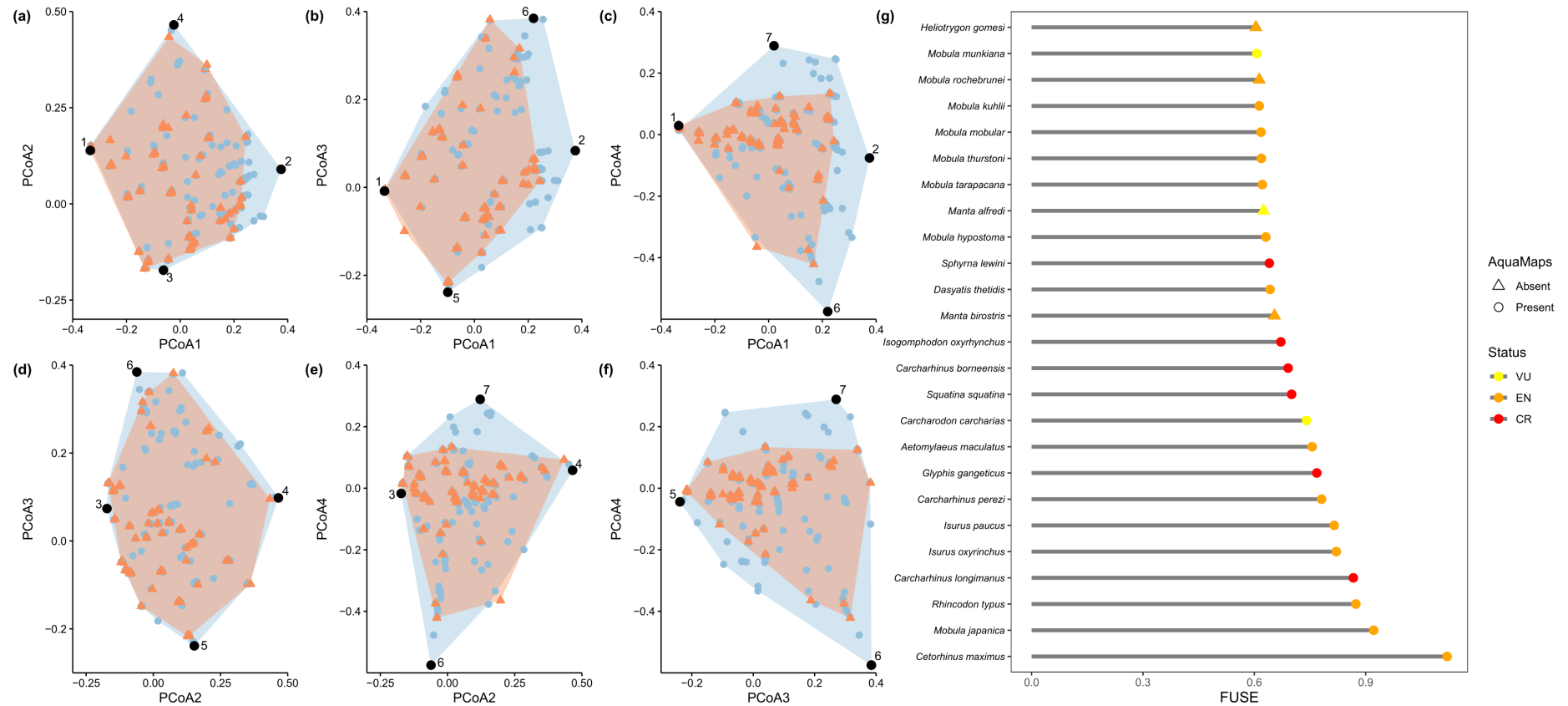
Figure S3.5. Functional range of AquaMaps data. (a-f) Functional space occupation of AquaMaps data on all axes pairs, shown with blue convex hulls and dots per axis-pairing. Orange convex hulls and triangles mark species absent from the AquaMaps data. Vertices species on the lowest and highest ends of each axis are all present in AquaMaps, marked in black, their circular shape denoting their presence in AquaMaps, and labelled as follows: 1 = *Himantura signifier*; 2 = *Odontaspis ferox*; 3 = *Sinobatis borneensis;* 4 = *Negaprion brevirostris*; 5 = *Pristis zijsron*; 6 = *Cetorhinus maximus*; 7 = *Mustelus lenticulatus*. (g) Top 25 ranked FUSE species based on and colourised by IUCN Red List status (VU = vulnerable; EN = endangered; CR = critically endangered). Like in (a-f), triangled lollipop shapes mark species absent from AquaMaps data while circular lollipop shapes denote species present within AquaMaps.
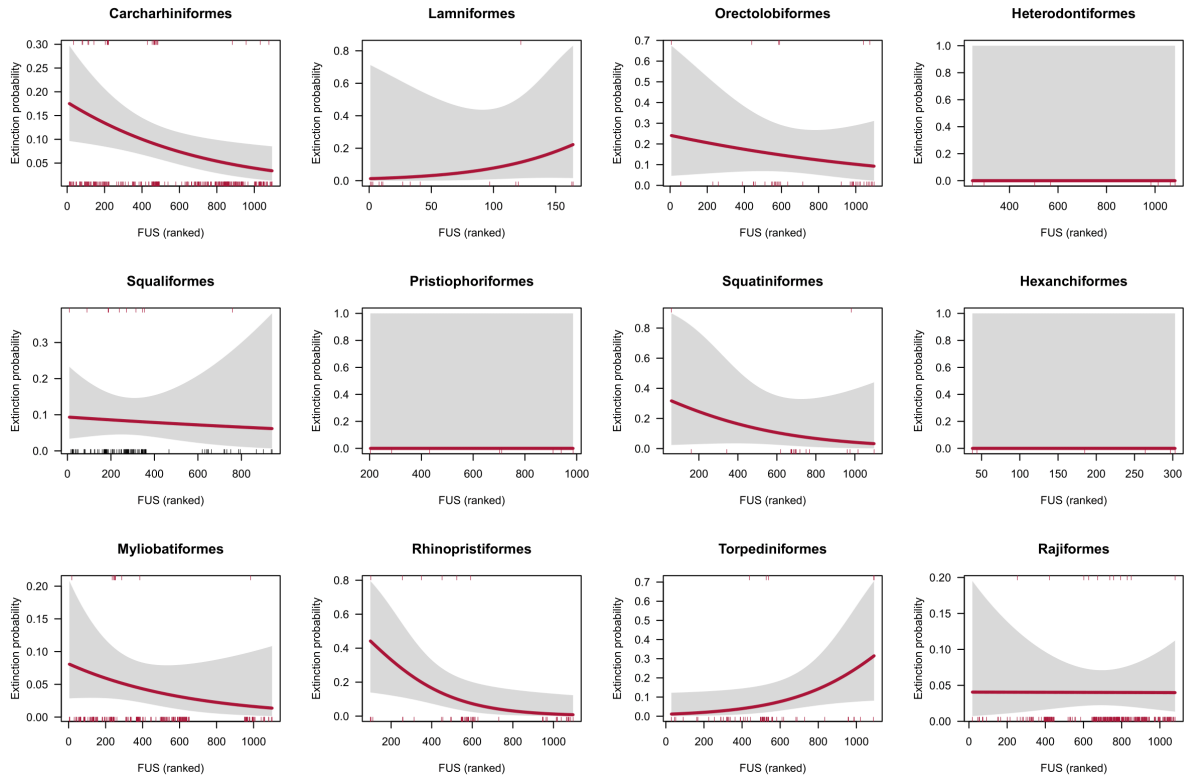
Figure S3.6. The relationships between extinction probability in 2100 and species ranked by their FUS scores per taxonomic order, based on raw data and provided by binomial generalised linear models.

Extinction~Ranked FUS in 100 years

Extinction probability

FUS (ranking)

Extinction~Ranked FUS in 200 years

Extinction probability

FUS (ranking)

Extinction~Ranked FUS in 300 years

Extinction probability

FUS (ranking)

Extinction~Ranked FUS in 400 years

Extinction probability

FUS (ranking)

Extinction~Ranked FUS in 500 years

Extinction probability

FUS (ranking)
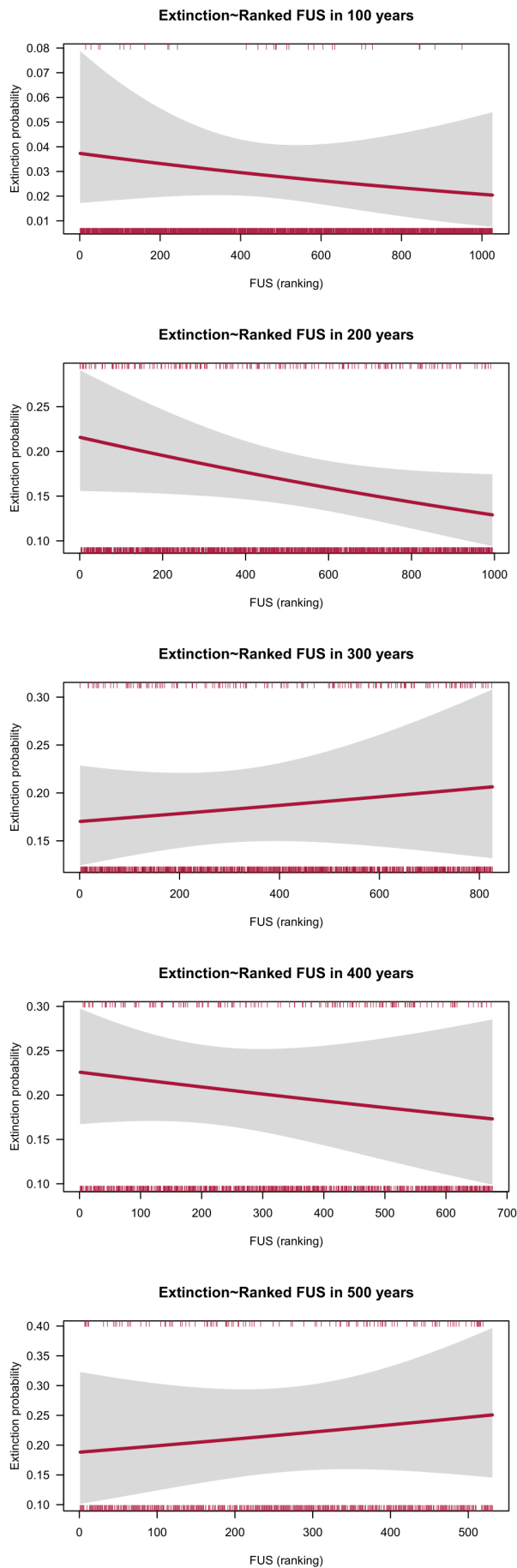
Figure S3.7. The relationship between extinction probability and FUS score rankings of elasmobranchs in 100-500 years as provided by binomial generalised linear mixed effect models. FUS score rankings are reset in each scenario based on surviving species from the previous scenario (i.e., all species that survive by 2100 make up the data pool in the model for 100 years).
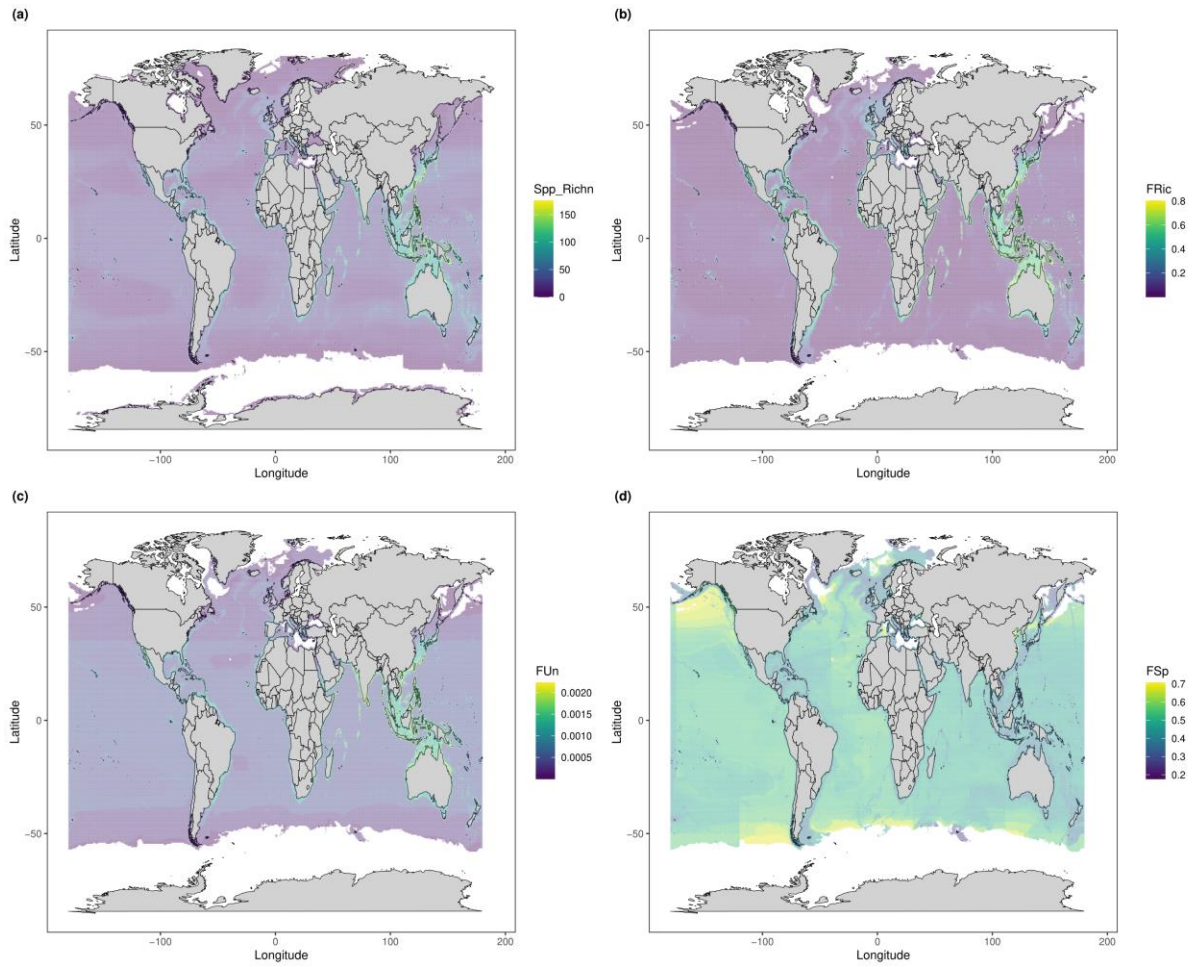
Figure S3.8. Geographic patterns of elasmobranch species richness and functional diversity in the present-day based on the AquaMaps model. (a) Species richness (Spp_Richn); (b) functional richness (FRic); (c) functional uniqueness (FUn); (d) functional specialisation (FSp). In all plots, purple-blue colours represent the lowest values while yellow-green colours denote the highest values.
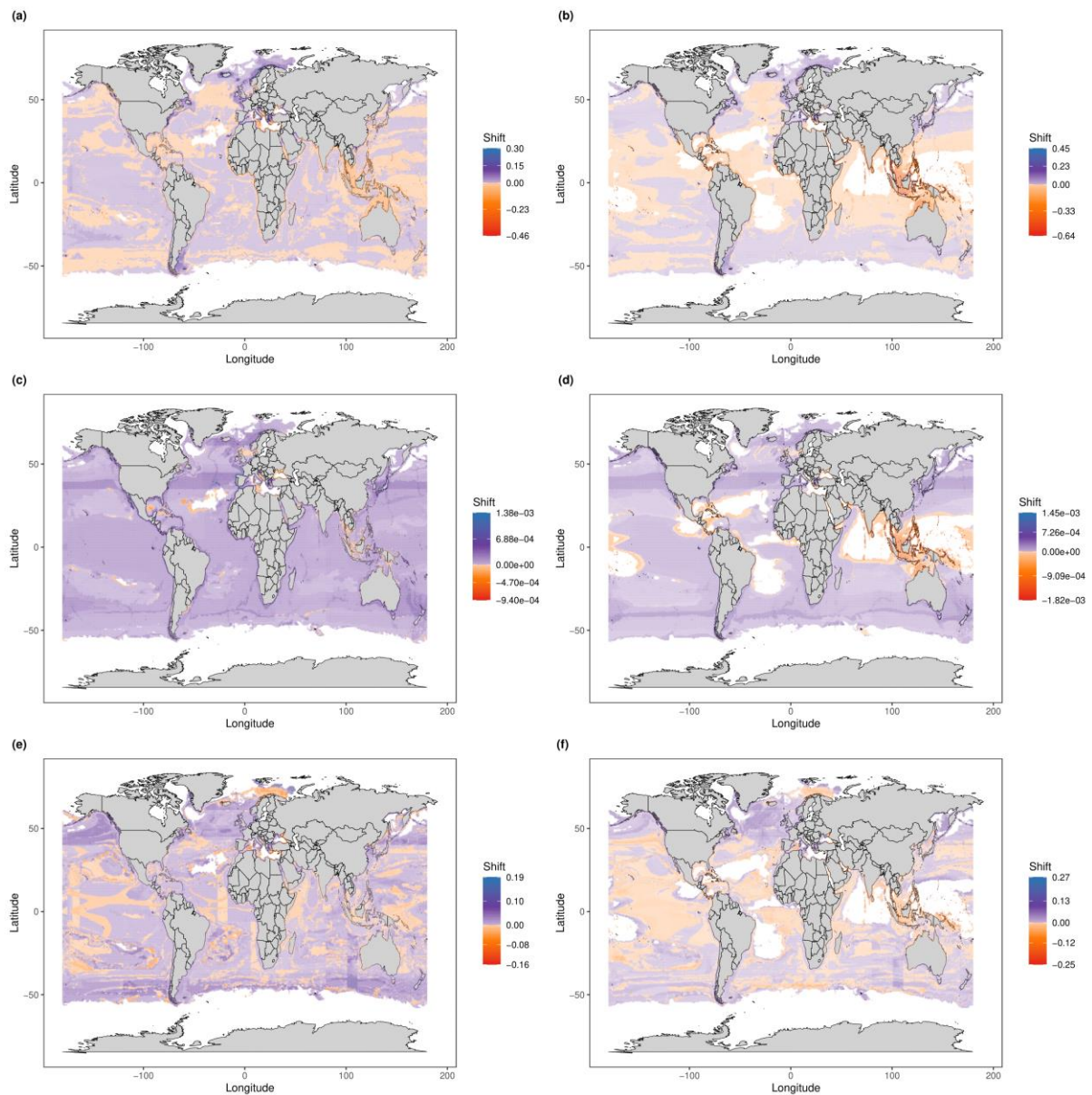
Figure S3.9. Geographic shifts in elasmobranch functional diversity by 2100. Each row of maps visualises shifts in (a, b) functional richness; (c, d) functional uniqueness; (e, f) functional specialisation. Each column marks shifts under a different climate change pathway; with the leftmost column denoting RCP 2.6; and the rightmost column RCP 8.5. In all plots, blue and purple represent gains in functional diversity, and orange and red mark losses in functional diversity; with the largest gains and losses respectively denoted by blue and red.

3 | SUPPLEMENTARY REFERENCES

Magneville, C., Loiseau, N., Albouy, C., Casajus, N., Claverie, T., Escalas, A., Leprieur, F., Maire, E., Mouillot, D., & Villéger, S. (2022). mFD: an R package to compute and illustrate the multiple facets of functional diversity. *Ecography* **2022**:e05904.

Maire, E., Grenouillet, G., Brosse, S., & Villéger, S. (2015). How many dimensions are needed to accurately assess functional diversity? A pragmatic approach for assessing the quality of functional spaces. *Global Ecology and Biogeography* **24**:728-740.

Pimiento, C., Albouy, C., Silvestro, D., Mouton, T. L., Velez, L., Mouillot, D., Judah, A. B., Griffin, J. N., & Leprieur, F. (2023). Functional diversity of sharks and rays is highly vulnerable and supported by unique species and locations worldwide. *Nature Communications* **14**:7691.

Appendix 4 | Additional paper co-authored by the candidate and published during his PhD: The extinct giant shark *Otodus megalodon* was an apex superpredator: inferences from 3D modelling

Title: The extinct shark *Otodus megalodon* was a transoceanic super-predator: Inferences from 3D modelling

Short title: Megalodon ecological inferences from new 3D model

Jack A. Cooper[1], John R. Hutchinson[2*], David C. Bernvi[3], Geremy Cliff[3,4], Rory P. Wilson[1], Matt L. Dicken[3,5], Jan Menzel[6], Stephen Wroe[7], Jeanette Pirlo[8] and Catalina Pimiento[1,9,10*]

[1]Department of Biosciences, Swansea University, Swansea SA2 8PP, UK

[2]Structure and Motion Laboratory, Department of Comparative Biomedical Sciences, Royal Veterinary College, Hawkshead Lane, Hatfield, Hertfordshire, AL9 7TA, UK

[3]KwaZulu-Natal Sharks Board, Umhlanga Rocks 4320, South Africa

[4]School of Life Sciences, University of KwaZulu-Natal, Durban, KZN, South Africa

[5]Department of Development Studies, School of Economics, Development and Tourism, Nelson Mandela University, PO Box 77000, Port Elizabeth 6031, South Africa

[6]janmenzelart, Stellenbosch 7600, South Africa

[7]Function, Evolution and Anatomy Research Lab, School of Environmental and Rural Science, University of New England, Armidale, NSW 2351, Australia

[8]Department of Biology, University of Florida, Gainesville, FL 32611, USA

[9]Paleontological Institute and Museum, University of Zurich, Zurich CH-8006, Switzerland

[10]Smithsonian Tropical Research Institution, Balboa, Panama

*Corresponding authors. Emails: ███████████████████████████████;
████████████████

Abstract

Although shark teeth are abundant in the fossil record, their bodies are rarely preserved. Thus, our understanding of the anatomy of the extinct *Otodus megalodon* remains rudimentary. We used an exceptionally well-preserved fossil to create the first 3D model of the body of this giant shark and used it to infer its movement and feeding ecology. We estimate that an adult *O. megalodon* could cruise at faster absolute speeds than any shark species today, and fully consume prey the size of modern apex predators. A dietary preference for large prey potentially enabled *O. megalodon* to minimize competition and provided a constant source of energy to fuel prolonged migrations without further feeding. When taken together, our results suggest that *O. megalodon* played an important ecological role as a transoceanic super-predator. As such, its extinction likely had large impacts on global nutrient transfer and trophic food webs.

Teaser: *O. megalodon* 3D model suggests unprecedented swimming and prey intake abilities, and potential global ecological impacts.

Functional diversity of sharks through time: past, present and future

Introduction

Computer modelling has given palaeontologists the unprecedented ability to use exceptionally well-preserved fossils to reconstruct the entire body of extinct animals, which in turn allows estimations of biological traits from the resulting geometry (*1-4*). For example, complete skeletons of *Tyrannosaurus rex* have been used to estimate an adult mass of ~5,000-10,000 kg (*1, 3, 4*). This task is, however, considerably harder for extinct sharks, whose cartilaginous skeletons have poor preservation potential in the fossil record and usually only leave behind teeth and occasionally vertebrae (*5*). Therefore, biological traits of extinct sharks are typically inferred based on extrapolations from close relatives and ecological analogues.

Otodus megalodon, a member of the extinct family Otodontidae (Order: Lamniformes), was the largest known macropredatory shark (*6*). Fossil remains of this extinct giant consist mainly of teeth. Based on the age, morphology and worldwide distribution of these teeth, it has been proposed that this species was a cosmopolitan predator that lived from the Miocene to the Pliocene (23-2.6 Ma; *6-10*). Its extinction has been attributed to a reduction of productive coastal habitats in the late Pliocene, which likely caused the loss of other marine megafaunal species, many of which could have been *O. megalodon* prey; and the appearance of potential competitors (*9, 11*).

The body length of the iconic *O. megalodon* has been inferred based on tooth measurements and comparisons with the extant great white shark (*Carcharodon carcharias,* Order: Lamniformes; Family: Lamnidae), which is regarded as the best available ecological analogue, despite belonging to a different family (*12, 13*). For instance, extrapolations of the relationship between tooth crown height and total length (i.e., length from the snout to the tip of the tail; herein TL) in *C. carcharias* (*12*) have suggested a maximum TL of 14-18 m for *O. megalodon* (*6, 7, 13*). More recently, however, a maximum TL of 20 m has been calculated based on the tooth crown width of associated dentitions of other lamniform sharks (*14*). The dimensions of *O. megalodon* body parts have also been estimated using multiple lamniform analogues, suggesting that an adult ~16 m *O. megalodon* would have had a head 4.7 m long, a dorsal fin 1.6 m tall and a tail about 4 m high (*15*).

The body mass of *O. megalodon* at different life stages (e.g., ~48,000 kg for a ~16 m individual) has also been estimated based on vertebral centra and extrapolations from *C. carcharias* (*7*). Vertebral columns hardly ever preserve, with only two specimens to our knowledge reported from Miocene deposits of Belgium and Denmark (*7, 16*). The column from Belgium consists

of 141 centra (IRSNB P 9893; formerly labelled IRSNB 3121) and was previously examined by Gottfried *et al*. (*7*), who concluded that it belonged to a single individual; undoubtedly an exceptional fossil due to the sheer number of centra preserved. Although a recent study examined the growth bands of three of the centra and concluded that IRSNB P 9893 died at age 46 (*17*), no study, prior or since, has attempted to reconstruct this specimen in detail based on its vertebral column.

Fossil evidence of bite marks on bones has shed some light on the autoecology of *O. megalodon* (*18-21*). For instance, it has been hypothesised that *O. megalodon* preferentially preyed on small- to medium-size cetaceans (e.g., 2.5 to 7 m; *19, 20*) such as the extinct *Piscobalaena nana* (*19*) and *Xiphiacetus bossi* (*20*). Larger prey includes taxa related to the modern humpback (*Megaptera novaeangliae*) or blue whales (*Balaenoptera musculus*; *18*). Evidence from calcium isotopes has further suggested that *O. megalodon* occupied a higher trophic level than *C. carcharias* (*22*), which typically consumes comparatively small prey in their entirety (e.g., sharks: *Carcharhinus obscurus* and *Prionace glauca*, and dolphins: *Tursiops truncatus* and *Delphinus delphis*; *23, 24*) and travels great distances across oceans (*25*). Finally, it has been proposed that an adult *O. megalodon* could reach cruising speeds of 1.3-1.4 m/s (*26, 27*) and burst speeds of 10.3 m/s (*26*), and that such an ability was enhanced by mesothermy (*26*), a thermoregulatory adaptation that elevates the temperature of locomotory muscles (*28*). The purported mesothermic physiology of *O. megalodon* has been supported by multiple lines of evidence, including comparative analyses, stable isotopes, and species distribution models (*9, 26, 29*).

Notwithstanding these advances in the understanding of *O. megalodon*, its full body anatomy and critical aspects of its ecology remain unclear or outdated. For instance, its body mass, a key trait to infer other eco-physiological properties, was last estimated in the early 1990s based on the assumption that *C. carcharias* is a direct descendant of *O. megalodon* (*7*), which has since been disfavoured (*30*). Given the most recent advances in computer modelling, it is now possible to make a more comprehensive and up-to-date reconstruction of *O. megalodon* to estimate various biological traits of this extinct shark.

Here, we create the first 3D model of the body of *O. megalodon* and use it to infer its movement and feeding ecology. We first reconstructed the axial skeleton using 3D scans of the exceptional vertebral column IRSNB P 9893 from Belgium, an associated dentition from the United States, and a *C. carcharias* chondrocranium (Fig. 1, fig. S1, S2). We completed the model by adding "flesh" around the skeleton using a full-body scan of *C. carcharias* (Fig. 1) and adjusted it

based on a 2D reconstruction of *O. megalodon* that accounts for other analogues (i.e., *Isurus* and *Lamna* spp.; see Methods; *15*). We quantified total length, volume, and gape size from the complete 3D model. Volume was then used to calculate body mass. Finally, we estimated the model's swimming speed, stomach volume, daily energetic demands and prey encounter rates based on their mathematical relationships with mass in extant sharks. Our results reveal the potentially distinctive ecological role that *O. megalodon* played in the global oceans, advancing our knowledge of the impacts of megafaunal species on marine ecosystems in deep time, and the potential ecological consequences of their extinctions.

Results

Anatomical reconstruction

We used a hoop-based approach to build a 3D model of the full body of *O. megalodon* in Blender 2.80 (http://www.blender.org). We adjusted the initial model based on a previous 2D reconstruction (*15*) to account for phylogenetic uncertainties and the intraspecific variation amongst lamniforms (see Methods). The complete model (Fig. 1) was first measured directly in Blender, rendering a total length (TL) of 15.9 m (Table 1). Then, it was imported into MeshLab (*31*) where a volume of 58.1 m^3 was computed. We used this volume and its relationship with the density of pelagic sharks relative to seawater (*32*) to calculate a body mass of 61,560 kg (Table 1). Although our methodology (*1-4*) is considered to provide precise mass estimates in extant and extinct taxa (*2, 3*), we tested its best-case validity based on a *C. carcharias* specimen of known size. To do so, we measured the volume of our *C. carcharias* full body scan (Fig. 1G; see Methods), estimated its mass, and compared it with the mass empirically measured (164 kg; see Methods). We found the mass estimated from the volumetric 3D scan to be 17.5% lower than that the mass reported from the specimen when it was weighed *in situ*.

Swimming speed estimations

We calculated the absolute cruising speed (meters per second, herein m/s) of the modelled *O. megalodon* using a previously established relationship between speed and body mass, based on 391 individuals across 28 extant shark species (*33*). We also converted this calculation to relative cruising speed (body lengths per second, herein BL/sec). Our results suggest a mean absolute speed of 1.4 m/s (5 km/hr), with a 95% confidence interval (herein, CI) of 0.5–4.1 m/s. Mean relative cruising speed was 0.09 BL/s (95% CI = 0.03-0.26 BL/s; Table 1). The wide CI values of these calculations reflect the size variation in extant sharks and the inherent

uncertainties of estimating biological properties for extinct animals, especially one of such enormous size compared to its living relatives. Considering that the upper CIs are particularly implausible for such a large shark (*34*), our inferences and interpretations are based on the *mean* cruising speed which, although not assumed to be accurate, agrees with previous estimates (*26, 27*).

We contrasted the estimated mean absolute cruising speed of the model against the mean values of the 28 species mentioned above (see Methods; *33*) and found that a ~16 m *O. megalodon* was able to cruise faster than all living species considered (data S1), including the mesothermic salmon shark (*Lamna ditropis*), porbeagle shark (*Lamna nasus*) and great white shark (*C. carcharias*; Fig. 2A). We also compared the mean absolute cruising speed of the model with the 391 individuals belonging to the 28 species and found that a ~16 m *O. megalodon* (#1 in Fig. 2B) could swim seven times faster than the largest individual in the dataset, an 18 m TL, 24,800 kg whale shark (*Rhincodon typus*; an ectothermic filter feeder; #2 in Fig. 2B), and 60 times faster than the slowest individual, a 4 m TL, 215 kg *R. typus* (#3 in Fig. 2B). Conversely, the model's estimated absolute cruising speed was two times slower than that of four mesothermic macropredators: three *C. carcharias* of 428, 874 and 750 kg (3.6, 4.6 and 4.4 m TL and #4-6 in Fig. 2B respectively); and a 16 kg (1.1 m TL) *Isurus oxyrinchus* (#7 in Fig. 2B). Furthermore, the absolute cruising speed of the model was similar to that of a 3,800 kg (8 m TL) *Cetorhinus maximus* (an ectothermic filter feeder; #8 in Fig. 2B), a 494 kg (3.8 m TL) *C. carcharias* (#9 in Fig. 2B) and a 23 kg (1.42 m TL) *I. oxyrinchus* (#10 in Fig. 2B). We repeated these comparisons using relative cruising speed, which is adjusted to body size (see Methods). As expected, given the nature of the metric, at 0.09 BL/s, the ~16 m *O. megalodon* model was found to be slower than almost all macropredatory sharks (fig. S3A), but remained considerably faster than filter feeders of similar size (i.e., an 18 m *R. typus* swimming at 0.01 BL/s; #2 in fig. S3B).

Prey intake estimations

We estimated the model's gape size and stomach volume in order to infer maximum prey size. Gape size was quantified in Blender at different angles (fig. S4). Our calculations indicated a gape height of 1.2 m at a 35º angle and of 1.8 m at 75º. Gape width measured 1.7 m at both 35º and 75º angles (Table 1). To estimate stomach volume, we determined the relationship between body mass and stomach volume in *C. carcharias* by dissecting and examining the stomachs of 12 individuals (see Methods). We used *C. carcharias* as the sole proxy for this and subsequent prey intake analyses because of their inferred similarities in diet and metabolism (*19, 20, 26,*

35). Our results suggest that the model *O. megalodon* had a stomach of 9,605 L (95% CI = 8,487-10,722 L; Table 1). We compared our results against the size of potential contemporaneous prey, as well as their modern relatives (Table 2; see Methods) and found that medium-size prey between 3 and 6 m (Table 2) could have been ingested in very few bites, assuming a gape angle of 75º (*7*). For example, a 5 m *P. nana*, a proposed prey of *O. megalodon* based on bite marks (*19*), could have been eaten in just three bites according to our estimates. Larger prey of 7-8 m would then have had to be severed into five or more chunks. Furthermore, assuming a limit of 70% stomach fullness (*36*), we found that while complete hypothetical prey of 8 m (e.g., the size of a modern *O. orca*) or less could be completely ingested, larger prey (e.g., the size of the modern humpback whale, *M. novaeangliae*) could not. These results were also found when using the upper and lower CIs of the stomach volume estimations (Table 2); thus, subsequent interpretations were based on the *mean* estimate of 9,605 L.

We estimated the model's energetic demands using the previously established relationship between body mass and daily energy requirement based on 16 *C. carcharias* individuals (see Methods; *37*). We found that the *O. megalodon* model required 98,175 kcal per day (95% CI = 78,085-123,067 kcal/day; Table 1), which is 20 times higher than that of an adult *C. carcharias* (4,871 kcal for a ~900 kg individual; *37, 38*). We contrasted this result against calorie-rich substances of potential prey (Table 2) to estimate the caloric contributions from prey-intake, while assuming 70% assimilation efficiency (*39*). Given that 30 kg of cetacean blubber contains ~200,000 kcal (*38*) based on a value of 6,667 kcal/kg (*37*), a ~16 m *O. megalodon* could have met its energy demands by consuming ~21 kg of blubber per day (95% CI = 16.73-26.37 kg). Because 15-33% of a marine mammal's body is blubber (*40, 41*), approximately 81.3% of a 123 kg *X. bossi* and as little as 0.01% of a 6,000 kg *O. orca* (Table 2) would have satisfied the daily calorific demands of an adult *O. megalodon*. Similarly, shark liver has been estimated to have an energy density of 8,150 kcal/kg (*42*). Hence, an adult *O. megalodon* might also have met its daily energetic demands by consuming ~17.2 kg of shark liver (95% CI = 13.69-21.57 kg). Given that up to 28% of the body mass of *C. carcharias* is liver (*43*), an adult *O. megalodon* may have met its daily energetic demands by consuming ~1.4% of the liver of a 7 m *C. carcharias* [3,271 kg body mass (*44*); 915.8 kg liver (*43*)]. Finally, shark muscle has been estimated to have energy density of ~4,400 kcal/kg in *C. carcharias* (*42*). As such, *O. megalodon* could have met its daily energetic demands by consuming ~31.9 kg of shark muscle (95% CI = 25.35-39.96 kg).

We further used a random process to calculate the accumulation of net energy (*45*) in order to model the prey encounter rates that *O. megalodon* would have needed to sustain its population. To do so we used 1) the 3D model's properties (Table 1), including the rate of energy expenditure, 2) the total energy contained in the whole body of each putative prey (Table 2) and 3) the relative abundance of such prey (table S1) (*46*). Our results indicate that if *O. megalodon* hypothetically fed exclusively on the smallest prey (e.g., 2 – 3 m; Table 2) it would have to eat, on average, once every 1.3 days to sustain its population (Fig. 3). In contrast, *O. megalodon* could have eaten only every 145 days (i.e., 5 months) if it fed exclusively on the largest prey (e.g., >12 m) while the most abundant of the putative prey (i.e., *Metaxytherium;* table S1) would have sustained *O. megalodon* for 15.5 days. Finally, if it exclusively fed on the largest prey that could be completely consumed (i.e., 8 m; Table 2), the ingested energy would sustain *O. megalodon* for 63 days (2 months). This result for mean rates of prey encounter based on our probabilistic model is largely mirrored when using the ratio between energy ingested and energy expended per day.

Discussion

Body size

The calculated TL (15.9 m) for the IRSNB P 9893-based 3D model is markedly longer than previously estimated for this specimen (9.2 m; *7*). Indeed, when scaled to real size in Blender (155 mm diameter in centrum 4; see Methods), the complete column alone was 11.1 m. Size differences likely stem from the fact that the previous estimation was based on the relationship between largest centrum diameter and TL in *C. carcharias* and thus, based only on centrum 4 (*7*). Nevertheless, there are some problems with the latter approach. First, it implicitly assumed that *O. megalodon* was a direct ancestor of *C. carcharias*, which is now disfavoured (*30*). Second, it assumed that both species have similar vertebrae numbers and column structure (i.e., similar proportions of caudal and precaudal centra); however, the number of vertebrae varies, even within members of the same family (*47*). Finally, although the centrum used to estimate TL comes from an exceptionally well-preserved fossil, it is still not an entirely complete specimen (*7*); hence it is unknown if that was in fact the largest centrum. Indeed, larger *O. megalodon* centra have been reported elsewhere, with the largest measuring 230 mm in diameter (*16*). Our *O. megalodon* 3D reconstruction is also larger than a maximum size of 14.2-15.3 m previously proposed based on upper anterior teeth (*13*). The model's large size combined with the existence of known vertebral centra ~50% larger than those of IRSNB P

9893 (*16*) supports a more recent suggestion that *O. megalodon* may have reached a maximum TL of 20 m (*14*).

Our estimated body mass (61,560 kg; Table 1) was also ~23% higher than that previously inferred for a 16 m *O. megalodon* based on the relationship between TL and mass in *C. carcharias* (47,690 kg; *7*). This mass difference could be due to the reliance on *C. carcharias* in previous estimates, whereas we adjusted our model to account for multiple analogues, namely all members of the family Lamnidae (Order Lamniformes; see Methods). Indeed, it has been shown that incorporating multiple lamnids results in stockier *O. megalodon* body reconstructions (*15*). The use of multiple analogues to reconstruct the body of *O. megalodon* has recently been questioned based on a supposed lack of a relationship between body form and thermophysiology in lamniforms, when analysing drawings of all 15 extant species (*48*). Nevertheless, justification for the use of multiple analogues to reconstruct the body of *O. megalodon* is based on the combination of ecology with thermophysiology, as both ultimately determine swimming strategy and consequently, body form in sharks (*29, 49*). Accordingly, the analogues used to inform the reconstruction of *O. megalodon* encompass only the lamniforms that share similar diet, feeding strategy and thermoregulatory physiologies (*15*). These include the family Lamnidae (*49-52*) but exclude ectothermic filter feeders (families Cetorhinidae and Megachasmidae) and the family Alopiidae, which includes a mesothermic species, but displays anatomical adaptations (i.e., enlarged caudal fins) for a specialised hunting behaviour (*53*) unlikely to be analogous to *O. megalodon* (*18-21*). Hence, the purported lack of a relationship between body form and thermophysiology in extant lamniforms based on the inclusion of species not analogous to *O. megalodon (48)* is not only irrelevant to the reconstruction of the extinct species as proposed in (*15*), but at odds with previous studies demonstrating body form convergence amongst mesothermic taxa, including lamnid sharks, tunas (*49, 50*) and ichthyosaurs (*54, 55*). We therefore contend that, although *C. carcharias* is the best available ecological analogue of *O. megalodon*, the use of multiple lamnids to inform our 3D reconstruction is appropriate given the uncertainties regarding the interrelationships between extinct and extant Lamniformes (see Methods). Most importantly, given that our best-case validity test suggests that our volumetric approach does not result in overestimations (see Methods), we consider a mass of 61,560 kg to be conservative to infer ecological parameters based on extant sharks. When taken together, our body size results suggest that the IRSNB P 9893 specimen is bigger than hitherto proposed, and larger than the maximum size estimated for *O. megalodon* based on anterior teeth only (*13*). These results highlight the importance of

using body parts other than anterior teeth and multiple analogues to infer the size of this extinct shark.

Movement ecology

Absolute cruising speed (m/s) estimations and species-level comparisons (Fig. 2A) suggest that the reconstructed ~16 m individual was able to cruise faster than all extant species analysed (*33*), including its closest mesothermic, macropredatory, extant relatives. Notably, the model was also much faster than the largest extant shark species, which is the filter-feeding, ectothermic whale shark (*R. typus*; maximum size = ~18 m; Fig. 2A; *35*). A faster cruising speed than *R. typus* was also found when considering relative speed (BL/s), a metric inversely correlated with body size (fig. S3A). It is well-supported that mesothermy allows all mackerel sharks (family Lamnidae: *C. carcharias*, *Isurus* spp. and *Lamna* spp. (*49, 50*)) and the common thresher (*Alopias vulpinus*; *56*) to reach faster speeds than their ectothermic counterparts (*51, 52*). Different lines of evidence have suggested that *O. megalodon* also had this thermoregulatory adaptation (*26, 35*). Given that our estimated cruising speed for *O. megalodon* was based mostly on ectothermic, hence slower, species (see Methods; *51, 52*), we consider it to be conservative.

The potential ability of *O. megalodon* to cruise at faster absolute speeds than other species (Fig. 2A), would enable it to move greater distances, thus increasing prey encounter rates (*51*). Fossils of marine mammals with multiple bites from the Miocene Pisco Formation of Peru have been used to hypothesise that *O. megalodon* may have exploited pinniped colonies for foraging (*19*). As such, the ecological benefits of a faster cruising speed likely allowed *O. megalodon* to move between distant feeding sites, a predation tactic also used by *C. carcharias* to find abundant, calorie-rich prey (*57*). Overall, our species-level comparisons of absolute cruising speed suggest that *O. megalodon* was, in general, an adept swimmer capable of undertaking long migrations, perhaps even farther than extant species. In modern oceans, a *C. carcharias* swimming at a mean cruising speed of 1.3 m/s (0.1 m/s slower than *O. megalodon*) can travel as far as 11,110 km across the entire Indian Ocean (*25*). Considering that large, highly mobile animals disproportionately drive nutrient movement between marine regions today (*58*), we propose that *O. megalodon* likely played an important ecological role transporting nutrients across oceans. As such, the extinction of this species may have negatively impacted global nutrient transfer, potentially compromising ecosystem diversity, productivity, and stability (e.g., *58, 59*).

Individual-level comparisons between *O. megalodon* absolute (m/s) cruising speed with that of the 391 sharks analysed, combined with relative cruising estimations (BL/s), provide additional clues about the biotic interactions of this extinct species. Interestingly, a few smaller macropredatory individuals can exceed the absolute cruising speed of a ~16 m *O. megalodon*, [i.e., two adult (#5-6 in Fig. 2B) and one sub-adult (#4 in Fig. 2B) *C. carcharias,* and a juvenile *I. oxyrinchus* (#7 in Fig. 2B; data S1).] Similarly, the relative cruising speed (BL/s) of the *O. megalodon* model (Table 1) was found to be slower than almost all other macropredatory sharks (fig. S3). This finding is not surprising given the size of the model (Fig. 1) relative to extant species. Nevertheless, when taken together, these results suggest that despite *O. megalodon*'s potential ability to move greater distances than any other species today, its gigantic size likely imposed constraints on its swimming abilities when compared to smaller macropredatory individuals. For instance, the fact that the absolute speed of a 16 m *O. megalodon* could hypothetically be exceeded by an adult *C. carcharias,* which would share a similar diet (*60*), suggests that ancient white sharks [e.g., *C. hubbelli*; a 5 m species (*14*) that overlaps with *O. megalodon* in the Pisco Formation (*30*)], could also cruise faster*,* potentially outcompeting it. Although this is highly speculative given that we only estimated cruising speed and not burst speed, which is directly related with prey capture (*61, 62*), it has been observed that small *C. carcharias* outcompete larger individuals using swift burst speeds when ambushing prey (*61*). Moreover, it has been previously proposed that an 18 m *O. megalodon* could reach burst speeds of 10 m/s (*26*) whereas a 3.4 m *C. carcharias* can reach at least 12 m/s (*62*). Given that body mass is curvilinearly correlated with absolute burst speed across both terrestrial and marine taxa (*34*), *O. megalodon*'s burst speed was most likely limited by the drag produced by its gigantic size (*32*). Therefore, *O. megalodon*'s maximum speed would have been attained by younger individuals, while those approaching 16 m [which is close to maximum size (*6, 14*)] would have been less agile hunters. The appearance of potential competitors in the late Miocene has already been proposed to have contributed to the extinction of *O. megalodon* in the Pliocene, in addition to habitat loss driven by sea level oscillations and the decline of potential prey (*9-11*). Although our absolute cruising speed comparisons do not provide enough evidence to propose that ancient white sharks were able to reach faster burst speeds for swifter and more effective predatory attacks*,* they do imply that if *O. megalodon* faced competition, it would have been with smaller, yet adult homeothermic macropredators. Future studies considering burst speeds could shed more light on the competitive interactions between *O. megalodon* and other sharks.

Feeding ecology

Our prey size and intake results suggest that a ~16 m *O. megalodon* could completely ingest, and in as few as five bites, prey as large as *O. orca* (i.e., 8 m), a top consumer in modern marine food webs (*63*). The macroraptorial sperm whale *Zygophyseter varolei* occupied a similar ecological niche to modern orcas in the Miocene and likely overlapped with *O. megalodon* (*64, 65*). *Z. varolei* is only known from a holotype specimen from Italy and has been estimated to reach 7 m of length (*64, 65*). Accordingly, *O. megalodon* could potentially have fully consumed this large predator. Such a predatory behaviour would be similar to that of large extant predators such as *C. carcharias*, which can fully consume dolphins in two pieces (*24*). The potential ability of *O. megalodon* to fully consume large predators has two main ecological implications. First, it supports previous findings of *O. megalodon* sitting at a higher trophic level than apex predators today based on calcium isotopes (*22*), further implying an important ecological function as an apex super-predator. Second, when also considering the potential competitive interactions from our swimming speed analyses, it further suggests the possibility of a dietary preference for large prey. Although it has been previously hypothesised that *O. megalodon* preferred prey of 2-7 m (*19, 20*), empiric studies have shown that large sharks prey upon a broader range of sizes than their smaller counterparts (*66*). Moreover, one of the benefits of gigantism in macropredatory marine taxa is the ability to exploit less competitive niches by consuming large prey (*29, 35, 67*). For example, while toothed whales tend to feed on large patches of small prey, the largest sperm whales can acquire similar amounts of energy from eating just a few large, high-energy items (*67*). Similar energetic gains from frequent but small prey relative to less frequent but large prey were also found in our *O. megalodon* prey encounter analysis (Fig. 3). As such, it is possible that large *O. megalodon* individuals may have minimized competition by targeting large prey.

Our results further suggest that large prey would have provided *O. megalodon* calories well beyond its energetic demands and would have been found frequently enough to support adult populations (Fig. 3; table S1). Although frequent predation on smaller prey such as *X. bossi* or *Metaxytherium* (Table 2) would have also sufficed *O. megalodon*'s caloric needs (Fig. 3; table S1), it is common for large macropredatory sharks to consume far more than their required daily energy intake at a time, particularly ram-ventilating mesotherms that need to swim continuously to acquire oxygen and power metabolism (*32, 33, 57*). For example, adult *C. carcharias* can consume more than 30 kg of blubber from scavenging a large cetacean carcass without filling their stomachs, which is hypothesised to sustain them for up to 1.5 months,

assuming continuous cruising speed (*38*). Moreover, they have been observed eating entire dolphins (*24*), which would provide up to 60 times their daily energy requirement [44 kg of blubber in a 200 kg dolphin = ~293,000 kcal (*41*)]. Prey intake beyond daily energetic demands is also common in other aquatic top predators, like polar bears (*Ursus maritimus*), which can obtain enough calories to live for up to 60 days from fully consuming an adult seal (*68*). In sharks like *C. carcharias,* excess energy from consuming calories beyond their daily requirements is stored in liver lipids, sustaining them during prolonged migrations (*57*). This fits an established hypothesis that large mesothermic taxa have higher mass-specific metabolic limits (e.g., *29*), which notably lowers the cost of transport and enhances fasting capabilities (*69*). The hypothetical full consumption of a cetacean of the size of a modern *O. orca* (8 m), might have sustained a ~16 m *O. megalodon* for 63 days without jeopardizing population survival, which would have allowed it to travel over 7,500 km, assuming a continuous cruising speed of 1.4 m/s. Although this suggestion is inherently inferential, it fits observations of extant species, specifically its ecological analogue *C. carcharias* (*25, 37*). Taken together, our results indicate that a preference for, and the full consumption of large prey, would have not only allowed *O. megalodon* to exploit less competitive niches, but also potentially enabled transoceanic movements. The extinction of *O. megalodon* therefore may have released large cetaceans from a strong predatory pressure (*8*), likely impacting global trophic webs (e.g., *59*).

The exceptionally preserved vertebral column of the extinct giant shark *Otodus megalodon* from Belgium (IRSNB P 9893; Fig. 1A-B; fig. S1) provided a unique opportunity to reconstruct its entire body using 3D computer modelling, which in turn enabled novel inferences on its movement and feeding ecology. It is important to acknowledge, however, that there are inherent uncertainties associated with any estimations of biological properties in extinct animals, which magnify when they are used as the basis for further inferences. Our conservative estimates and cautious interpretations suggest that *O. megalodon* was likely able to swim great distances and to feed on prey as large as modern apex predators, implying an ecological function as a transoceanic, super-predator. A potential preference for large prey would not only have allowed adult individuals to obtain enough calories to undertake prolonged migrations, much like its modern ecological analogues (*25, 37*), but to exploit less competitive niches. The extinction of this purported highly migratory super-predator likely had large-scale impacts, from releasing large cetaceans from a strong predatory pressure, thus affecting global food webs (*8*); to altering global nutrient transport, ocean productivity and ecosystem stability (*58*).

Materials and Methods

Fossil specimens

Vertebral column: Based on identical colouring and surface texture, the degree of preservation, and a gradual decrease in centrum diameter, IRSNB P 9893 is a vertebral column belonging to a single *O. megalodon* individual (*7*). This exceptional fossil specimen is stored at the Royal Belgian Institute of Natural Sciences (RBINS) in Brussels, Belgium. It was recovered from around the Antwerp Basin in the 1860s (*7*); however, neither the locality nor an age has been specified beyond a Miocene range (23-5.3 Ma). The 141 centra vary in degrees of preservation from fragmentary to near-complete. These centra were labelled by museum curatorial staff as '1-150' (Fig. 1A; fig. S1), although duplicated labelling or missing centra deserve consideration. Namely, there are two centra each labelled as centrum 33, 100 and 115. Moreover, centra 30, 35-37, 45, 105, 131, 136, 141, 146, 147 and 149 are missing from the column. These issues were accounted for during model reconstruction (see "3D scans" below).

We measured the preserved diameter of all centra using digital callipers (data S1). As in previous studies (*7, 17*), we observed that centrum 4 was the largest (155 mm in diameter; Fig. 1A; fig. S1) and that there is a gradual decrease in diameter towards the posterior-most section of the column, with centrum 150 being the smallest (57 mm; Fig. 1A; fig. S1). Because the largest centrum in *C. carcharias* vertebral columns is typically immediately behind the chondrocranium, Gottfried *et al*. (*7*) considered the possibility that the centra were not in the correct order. However, given the gradual decrease in centrum diameter observed in IRSNB P 9893, which has also been reported in exceptionally well-preserved columns of other extinct lamniforms (*70*), we consider it more likely that IRSNB P 9893 centra are labelled in the correct order, but the anterior-most centra are missing; an alternative also considered by Gottfried *et al*. (*7*). Despite missing anterior and caudal centra, IRSNB P 9893 is by far the most complete *O. megalodon* vertebral column known in the fossil record and serves as the basis for our 3D reconstruction.

Dentition: Teeth of *O. megalodon* are often discovered as isolated fossils. As such, associated dentitions [i.e., where all preserved teeth belong to a single individual (*14*)] are rare. Nevertheless, there are a few such *O. megalodon* dentitions in the public record (*14*). For our reconstruction, we used a dentition (UF 311000; fig. S2) from the early Pliocene Yorktown Formation of the Lee Creek Mine in Aurora, North Carolina, United States, which is housed in

the Vertebrate Paleontology Collection of the Florida Museum of Natural History (FLMNH) at the University of Florida (*14*).

3D scans

O. megalodon vertebral column: Individual centra of IRSNB P 9893 were scanned at the RBINS. Surface scans of all fossils were conducted using an HDI advanced scanner (HDI Advance R3X, LMI Technologies, Brussels, Belgium). Following scanning, the individual centrum scans were then imported into Meshmixer (http://www.meshmixer.com) and arranged based on column position labelling. Intercentrum distances in this column were distributed uniformly following descriptions of known shark vertebral columns in the literature (e.g., *70*). Missing centra were accommodated by temporarily filling the space with a near-complete neighbouring centrum, scaled according to its column position to ensure uniform intercentrum distances, and then removing this placeholder centrum. This was also done for fragmented centra to ensure their correct positioning. Once the column was complete, it was exported as an STL file (Fig. 1B).

O. megalodon jaws: 3D scans of the UF 311000 dentition were downloaded from Morphosource (www.morphosource.org; accessed May 2015). Each tooth (Fig. 1C) was imported into Meshmixer and arranged based on their known position in the jaw, as recorded by the FLMNH. Distance between teeth was inferred based on known inter-tooth distance in jaws of *C. carcharias* (*5*). Given that the preservation of UF 311000 is limited almost entirely to the left side of the jaw (fig. S2; see also (*14*)), these teeth were mirrored around the x axis (anteroposterior) to recreate the right side of the jaw. The complete 3D dentition was exported as an STL file (Fig. 1D) and later used to reconstruct the jaw of the *O. megalodon* model.

C. carcharias specimens

We used 3D scans of two *C. carcharias* specimens to digitally reconstruct the body outline of *O. megalodon*. Although other lamnids can be considered as closely related to *O. megalodon* as *C. carcharias* (*15*), the latter is the largest, most well-studied species, and has the most similar dentition to *O. megalodon*. Moreover, *C. carcharias* was the one large-bodied species with an available full-body 3D scan that could be used.

The first specimen was a 3D mesh of the chondrocranium of a 2.5 m TL (240 kg) juvenile (NSWDPI-WS2006/4; Fig. 1E), which was previously modelled from CT scan data to calculate the shark's bite force (*71*). The second was a 3D scan of the entire body of a 2.56 m TL (164 kg) juvenile female (Fig. 1F). It was retrieved by the Kwa-Zulu Natal Sharks Board (KZNSB)

in November 2018 as part of its bather protection programme (*23*). This individual was scanned on site at the KZNSB research laboratory, Umhlanga, South Africa, with a *Creaform Go!Scan 3D* scanner using an accuracy of 0.5 mm. Following 8 hours of digital assembly, the resulting 3D mesh was sculpted to a neutral swimming position using Rhino (http://www.rhino3d.com), Rapidform XOR (http://www.rapidform.com) and zbrush (http://www.Pixologic.com) software.

Model reconstruction

Skeletal model: The completed vertebral column STL file (Fig. 1B) was imported into Blender and scaled to real size based on the measured diameter of the largest centrum (centrum 4; Fig. 1A) so that the model could be recreated at the approximate size of the shark. In parallel, the scan of the *C. carcharias* chondrocranium (Fig. 1E) was imported into Meshmixer and scaled to match the size of the articulated dentition from UF 311000 (Fig. 1D). Then, the dentition was placed over the chondrocranium's teeth. The resulting mesh was exported as a single STL file and then imported into Blender, where it was scaled to fit with IRSNB P 9893 at the first vertebra. Together, the *C. carcharias* chondrocranium, UF 311000 teeth and IRSNB P 9893 comprised the skeletal base model of the *O. megalodon* reconstruction (Fig. 1B*, D-E*).

Full body construction: The skeletal base model was used to first recreate the head. This was done in Blender by tightly fitting octagonal hoops onto the chondrocranium and lofting them to create the final watertight mesh (Fig. 1F) using a previously established methodology (*1-4*). Then, the body of *C. carcharias* was used for the flesh reconstruction. To do so, we imported the full-body scan of *C. carcharias* (Fig. 1G) into Blender and scaled it so that IRSNB P 9893 ended at the base of the caudal fin. This is because the smallest centrum (#150) was proposed as being among the last of the precaudal centra (*7*). The octagonal hooping method used in the head was then repeated to fit tightly along the body and around each fin (Fig. 1H-L). The skeletal base model (particularly the chondrocranium), rather than the full-body scan of the *C. carcharias,* was used to reconstruct the *O. megalodon′*s head because a watertight mesh requires symmetry for more accurate mass estimates (*2*), which the full-body *C. carcharias* head did not have. Consequently, our reconstruction of the head is slightly undersized. The resulting hoops around the chondrocranium, vertebral column and full-body *C. carcharias* produced the outline of our *O. megalodon* model and all were lofted together to form the shark's flesh (Fig. 1M).

Model adjustment: We adjusted the dimensions of the initial *O. megalodon* model based on a previous 2D reconstruction that was built using all lamnid species as analogues (*15*). The selection of analogues was based on both ecological and thermophysiological similarities amongst extant relatives (*15*). The use of these analogues was further justified based on quantitative evidence for isometry between body parts (n = 24) with respect to TL within and among laminds using photographic data from 41 individuals at different life stages (*15*). This was done for three reasons: 1) despite *C. carcharias* being considered the best modern analogue of *O. megalodon* (*7, 13*), there are uncertainties regarding the interrelationships between extinct and extant Lamniformes and therefore, *O. megalodon* could be as closely related to *C. carcharias* as to any other lamniform (*35*); 2) the previous 2D reconstruction of *O. megalodon* showed that relying solely on *C. carcharias* results in a more slender body (i.e., narrower vertical dimensions) than when also using similarly related lamniform analogues (*15*); and 3) the *C. carcharias* scans used to complete the model were juveniles and our skeletal model based on IRSNB P 9893 was an adult. Only two vertical dimensions (dorsal tip to abdomen [DTA] and dorsal posterior to abdomen [DPA]; table S2) required adjusting, as they were initially close to the minimum estimated values. Finally, we used this 2D model (*15*) to aid the reconstruction of the anal fin, which was the only fin not captured in the scan of *C. carcharias*, likely due to how the shark was positioned during scanning. To recreate this fin, we duplicated the *O. megalodon* model's dorsal fin, mirrored it around the z axis (mediolateral) and scaled it down to match the size, shape and positioning of this fin in the 2D reconstruction (*15*). These steps concluded the reconstruction of the model, which once completed was used for all subsequent analyses (Fig. 1N-Q). A detailed guide of the model reconstruction procedure can be found in the Dryad Data Repository.

Model measurements

The total length (TL) of the completed model was measured in Blender (Table 1). Then, the model mesh (Fig. 1N-O; data S2) was exported as an STL file and imported into MeshLab (*31*), where it was cleaned and simplified. Then, the "Compute Geometrics Measures" filter was applied, which produced mesh surface area, volume (*V*) and centre of mass (*COM*). To calculate the model polygonal mesh's body mass (*M*), we combined *V* with density (*D*), as performed in previous studies (*1, 3, 4*). The density of sharks is widely accepted as being only slightly higher than that of seawater (*43, 72*). In pelagic sharks, this has been found to be an average of around 1,060 kg/m^3 (*32*). We therefore applied this same density value to the *O. megalodon* model. The resulting equation used to calculate mass is as follows:

$$M\ (kg) = V\ (m^3) * D\ (\frac{kg}{m^3})$$

(1)

We measured the gape height (maximum distance between upper and lower jaws) and width (distance between left and right edges of the mouth) of the model in Blender at 35º and 75º angles (fig. S4). The 35º gape angle was assumed because it has been previously used to calculate bite force in *C. carcharias* and subsequently *O. megalodon* (*71*). Similarly, the 75º gape angle was used because it is among the largest gape sizes observed in *C. carcharias* and was used in a previous reconstruction of *O. megalodon* based on IRSNB P 9893 (*7*). We therefore consider 75º to be a conservative gape angle because large sharks typically exhibit wider gapes than small sharks as they consume larger prey (*73*). Nevertheless, we do not propose 75º as a maximum gape angle considering that estimating maximum gape size or precise kinematics (*74*) without a preserved chondrocranium would be highly speculative. We recreated the model *O. megalodon* exhibiting these open gapes (Fig. 1P, Q) by using the same hoop-based methodology (*1-4*) as in the original model (Fig. 1F-M, movie S1).

Best-case validity test

To test the validity of the method used to calculate the model's body mass, we imported the full-body *C. carcharias* 3D scan (Fig. 1G) into MeshLab (*31*) and calculated its volume (0.13 m^3), surface area (2.5 m^2) and centre of mass (*COM;* x = 0.59; y = 0.03; x = 0.57). We then applied equation 1 and compared this result against the mass measured empirically of this individual (=164 kg). We found that the mass resulting from the 3D scan was 135.4 kg, which is ~18% lower than the individual's empirically calculated mass. This underestimation might be due to the fact that the anal fin was not captured by the scan and/or by *post mortem* processes taking place between capture and measurements in the laboratory.

Ecological estimations

Cruising speed: We used the calculated *M* to estimate the model's mean cruising speed (*S*). We did so by using the equation proposed in (*33*):

$$S\ (m/s) = 0.266\ M\ (kg)^{0.15}$$

(2)

Equation 2 was based on empirical data from 26 mesothermic, but mostly ectothermic extant shark species from 64 studies (*33*). The exponent of 0.15 is derived from a theoretical model

that incorporates metabolism into the scaling relationship, while correcting for phylogeny (at the order level). The 0.266 constant comes from fitting the power equation to the untransformed data from the 26 species, while accounting for trophic level, habitat type and temperature (table S3; data S1; *33*). To estimate a possible range of cruising speeds for *O. megalodon*, we applied equation 2 using the lower and upper limit of the 95% CIs of the 0.15 exponent (95% CI = 0.053–0.249; *33*). To calculate the model's relative cruising speed, we divided its absolute cruising speed by its TL (recorded in m; note that TL is used here as BL). Once the cruising speed of *O. megalodon* was estimated, we included it in the dataset from (*33*) in order to compare it with other shark species. We did so by searching the 64 studies comprising this dataset to gather the TL, body mass and mean cruising speed (both absolute and relative) of each individual recorded. For studies where only body length measurements were reported, we determined body mass using length-weight power equations from FishBase (*75*). We added two additional extant species to the species dataset: the Greenland shark (*Somniosus microcephalus*), due to its large size, and the spinner shark (*Carcharhinus brevipinna*) as it is larger than many of its relatives included in the dataset (*53*). In total, we collated the mean cruising speeds of 391 individuals representing 28 extant shark species.

Stomach volume: Twelve *C. carcharias* individuals from the KZNSB bather protection programme (*23*) were weighed and then dissected and their stomachs removed with the duodenum and oesophagus attached. Stomach contents were removed, and cable ties were used to close the pyloric sphincter. Each stomach was suspended by the oesophagus and filled with water up to the cardia; with the resulting volume being measured to the nearest centilitre (table S4). The linear relationship between M and SV ($R^2 = 0.974$) was recorded as follows:

$$SV\ (L) = 0.15613\ M\ (kg) - 6.54137$$

(3)

Of the 12 *C. carcharias* individuals examined, 11 were juveniles and the other was a sub-adult. However, the relationship between SV and M in this species has been found to be isometric (*37*), indicating that they grow at similar rates throughout ontogeny. The presence of entire prey items, not necessarily fully intact, such as small sharks or dolphins, within *C. carcharias* stomachs (*23, 24*) has been previously used to justify the accuracy of this relationship (*37*). Given that isometric scaling relationships between body parts have been found in different lamnid species and used to infer the dimensions of *O. megalodon* (*15*), we used equation 3 to estimate the mesh model's SV. To account for the uncertainties that arise from estimating

properties of an extinct species; 95% CIs were calculated for each of equation 3's components (table S5) to obtain a lower and upper limit of *SV*.

Prey size: To further infer the size of prey items that *O. megalodon* could consume, we collected from the literature the body length and mass of various potential and hypothetical prey, encompassing a wide range of body sizes. These included: 1) extinct taxa that have likely been preyed on by *O. megalodon* based on fossil evidence (e.g., *Xiphiacetus bossi* and *Piscobalaena nana*; *19, 20*); 2) taxa that could have overlapped in time (Miocene and/or Pliocene epochs) with *O. megalodon* at genus level (e.g., *Carcharodon*, *Orcinus* and *Megaptera*; *11*); and 3) extant species belonging to these genera (Table 2). We compared the length of each putative prey against the calculated gape width. We also calculated the volume of each prey by dividing its body mass (kg) by the approximate density of water (1000 kg/m^3) and converting from m^3 to litres (*L*). This volume was then multiplied by 1.025 to account for the specific gravity of sea water (*72*). The results were compared against the stomach volume calculated for the *O. megalodon* model to determine if this shark could have entirely consumed each taxon. Given that *O. megalodon* stomach is unlikely to have ever been completely full because stomach acids, digestive enzymes and accidently-ingested seawater occupy stomach space (*76*), we limited the maximum mass/volume of prey to 70% of *O. megalodon* stomach volume based on data from extant sharks (*36*).

Daily energy requirement: Body mass, thermoregulation and energetic requirements are closely associated with metabolism (*49*). Notably, it has been proposed that *C. carcharias* has a similar metabolic rate to endothermic mammals and birds (*37*). This is a result of its mesothermy (*49*), an ability assumed to have also evolved in *O. megalodon* (*26, 29, 35*). One of the proposed advantages of this physiological adaptation, in addition to elevated cruising speeds, is niche expansion, as it allows sharks to tolerate a greater range of temperatures (*51*;but see *52*). This is apparent in *C. carcharias*, which has a worldwide distribution across both temperate and tropical waters (*53*), and has been recorded migrating across entire oceans (*25*). Biogeographic analyses of fossil occurrences have suggested that *O. megalodon* also occupied a worldwide geographical range, supporting similar metabolic demands and thermoregulation (*9*).

Our calculation of the model's daily energetic requirement (*DER*) was based on a previous work that used the body mass and cruising speeds of 16 *C. carcharias* individuals of different sizes, to estimate their daily red muscle heat production (*37*). As ram ventilators must continuously swim, it is generally assumed that the heat produced from a day's average cruising

speed matches resting metabolic rate (*37, 38, 77*). Heat production is then transformed into energy production (in kcal), with the energy produced in a day assumed to be the minimum requirement (*37*). Heat production estimates from this study (*37*) coincide closely with the temperature of the tissue adjacent to red muscles of adult *C. carcharias* observed in the field (*38, 78*), as well as metabolic rates calculated from oxygen consumption in both captive neonates (*77*) and a field-observed adult individual (*38*). Given that *O. megalodon* was likely mesothermic (*26, 35*), it would have had a metabolic rate comparable with that of other mesothermic sharks such as *C. carcharias* (*38, 77*). As such, in order to calculate *O. megalodon*'s *DER,* we applied the following equation based on the *C. carcharias* heat production model as proposed in (*37*):

$$DER\left(\frac{kcal}{day}\right) = 37.405\ M\ (kg)^{0.7139}$$

(4)

As in both *S* and *SV*, we utilised 95% CIs to account for uncertainties. Previous work on *C. carcharias* provided standard errors for equation 4's constant and exponent (±1.04 and ±0.008 respectively) (*37*). We thus calculated CIs from those standard errors (1.96*SE; CI = ±2.0384 and ±0.01568 respectively) and applied them to equation 4 to provide lower and upper limits of *O. megalodon* daily energy requirement.

Prey encounter rate: The ability of *O. megalodon* to meet its *DER* likely depended not only on prey size and energy content, but also on how frequently it encountered such prey. We modelled *O. megalodon* food encounter rates for a hypothetical population, which followed each individual over an extended time period. Our model used a constant probability that animals would find food for any time spent foraging but incorporated a rate of decline of energy reserves for both foraging and non-foraging periods. Thus, our model, which was based on a random process to calculate the net energy accumulated (*45*), estimated the mean encounter rates necessary for a population to survive, while accounting for the variability that scarce food sources engender in feeding frequency across populations, and therefore, the nutritional state of all individuals within that population (*79*). To populate this model, we used energy densities and mean mass of putative prey from literature (Table 2) to calculate the total energy available from each prey. We then subjected total energy figures to an assimilation efficiency of 70% (*39*) to derive a final value for available energy per prey item. We also assumed that the shark foraged for 50% of the time, spending its calculated daily energy requirement (equation 4). To access the necessary mean encounter rate, for any given prey, we iteratively changed the

probability of prey encounter per hour spent foraging until a population of 10,000 *O. megalodon* sharks: (1) maintained their average body mass over a complete year (see *46* for an extended time-based analysis of the consequences of probabilistic prey encounter) while (2) no more than 5% of the population lost more than 30% of their body mass [because maximum body mass loss in sharks before death is ca. 35% (*80*)]. We also determined which putative prey would have been most abundant based on fossil occurrence data gathered from the Palaeobiology Database (http://paleodb.org, accessed April 2021; table S1) to assess the probabilities of encountering such prey. Probabilities, normally defined as a number between 0 and 1 per unit time (*79*), were, for convenience, expressed as the mean number of days over which all sharks had to forage for the survival criteria listed above to be fulfilled.

Figures
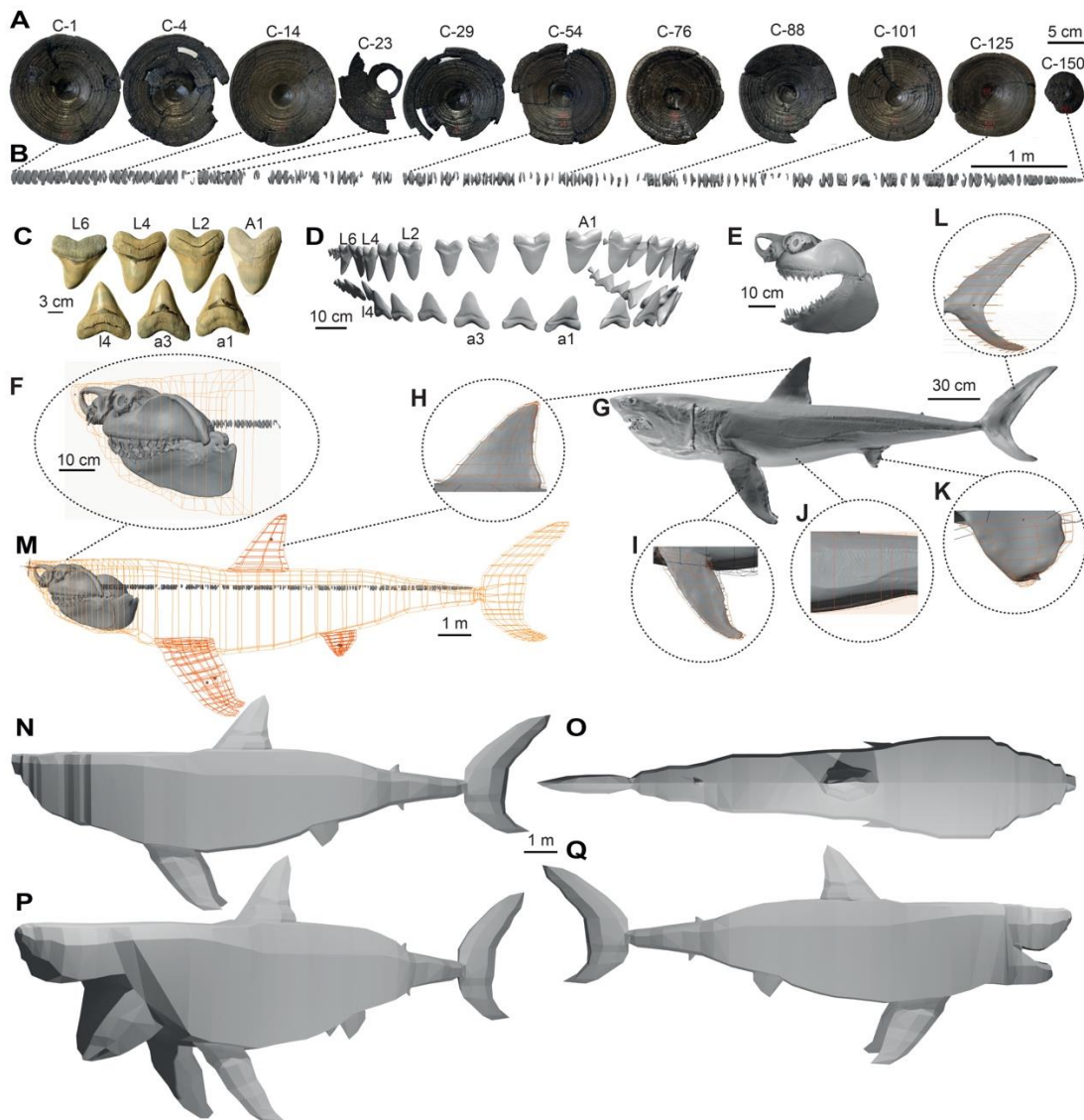
Fig. 1. Modelling procedure. (**A**) Sample of 11 of the 141 vertebral centra in the *Otodus megalodon* column (IRSNB P 9893); (**B**) 3D scan and reconstruction of the *O. megalodon* vertebral column, with centra from **A** linked to their corresponding position; (**C**) sample of seven *O. megalodon* teeth from the UF 311000 dentition (lingual view) with their respective positions (upper case denotes upper teeth; lower case refers to lower teeth; "A" denotes anterior teeth and "L" lateral); (**D**) 3D scan and reconstruction of the UF 311000 dentition (labial view) with the corresponding labels from **C**; (**E**) 3D scan of *Carcharodon carcharias* chondrocranium used to model *O. megalodon*'s head; (**F**) *C. carcharias* chondrocranium with UF 311000 dentition and IRSNB P 9893 column attached, and hoops outlining the model's head; (**G**) 3D scan of the full-body of the *C. carcharias* specimen used for flesh reconstruction with elliptical hooping methodology indicated for the (**H**) dorsal fin; (**I**) pectoral fins; (**J**) abdomen; (**K**) pelvic fins and (**L**) caudal fin; (**M**) base skeletal model with octagonal hoops that mark flesh boundaries; (**N**) the final lofted polygon mesh of *O. megalodon* used for analyses at lateral view and (**O**) dorsal view; (**P**) visualisation of open gape at 75° angle at oblique view and (**Q**) 35° gape angle at lateral view.
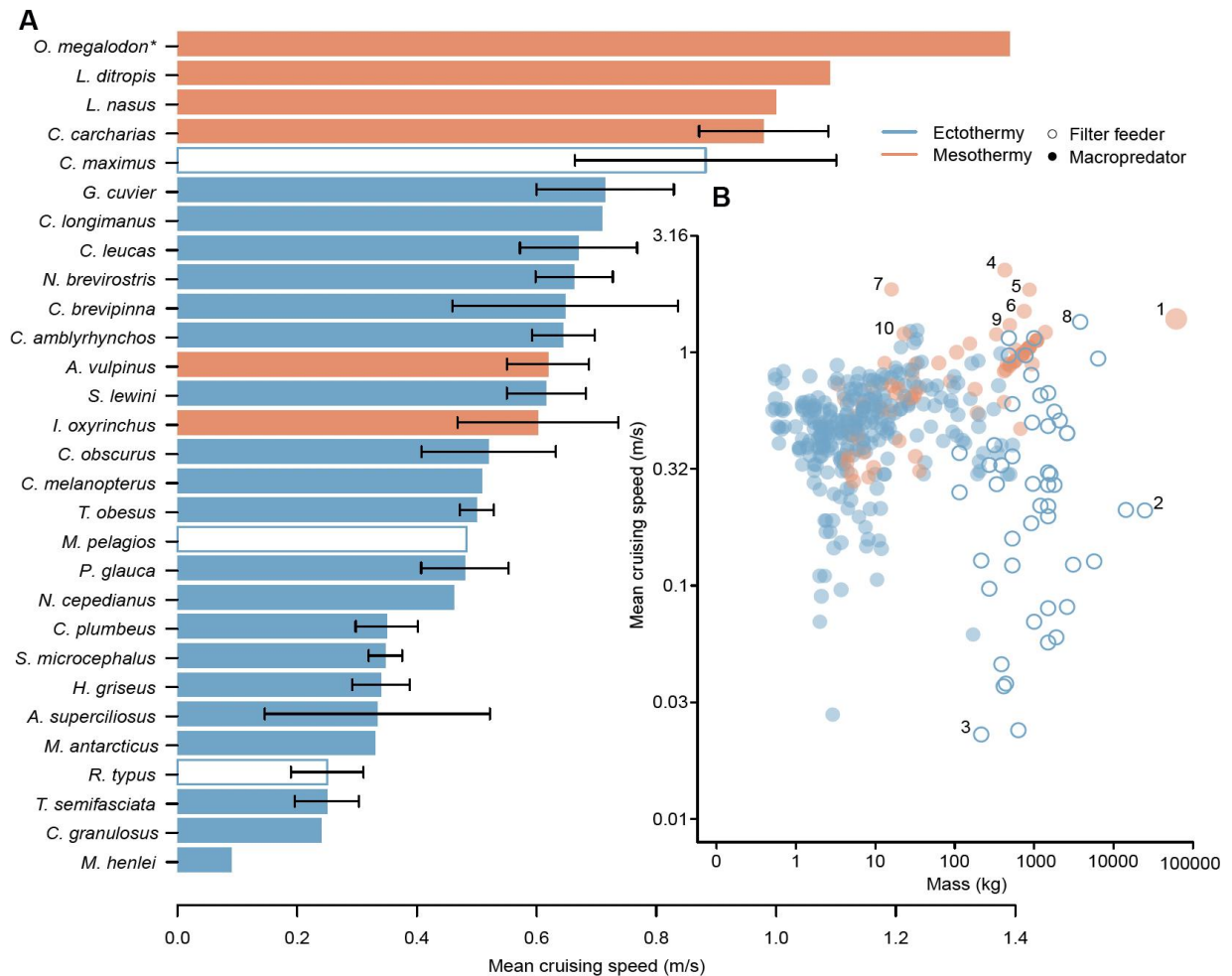
Fig. 2. Sharks absolute cruising speeds. (**A**) Mean cruising speeds of all shark species gathered in data S1 (n = 28 plus the *O. megalodon* model) with error bars drawn from multiple individuals per species. An asterisk (*) indicates that *O. megalodon*'s speed estimate was made from equation 2 rather than from the mean of multiple speeds. Species without error bars are those from which only one individual was recorded. (**B**) Mass and mean cruising speed of *all* individual sharks in data S1 (n = 392) plotted on a log scale. Species marked in **B** are as follows: (1) *Otodus megalodon*; (2, 3) the whale shark (*Rhincodon typus*); (4-6) the great white shark (*Carcharodon carcharias*); (7) the shortfin mako shark (*Isurus oxyrinchus*); (8) the basking shark (*Cetorhinus maximus*); (9) *C. carcharias*; and (10) *I. oxyrinchus* (see text for details of specific individuals).
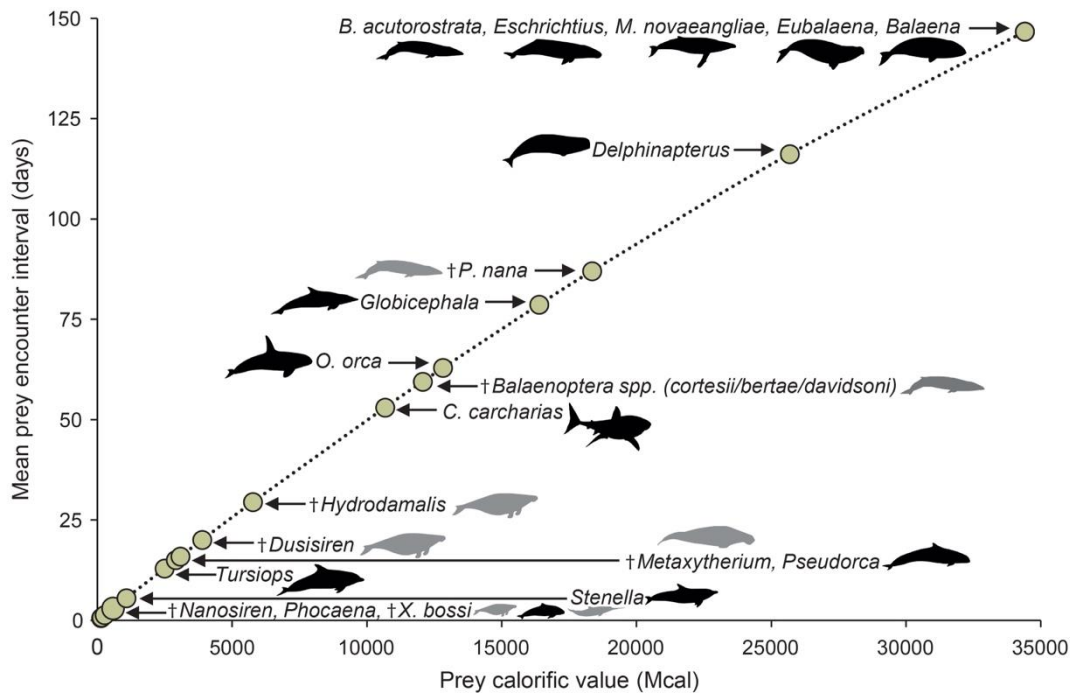
Fig. 3. Prey encounter rates. Mean required predation rate of various putative *O. megalodon* prey assuming that they are the sole food source and assuming 70% assimilation efficiency for the simulated population to be maintained (see text for details). Body mass and energy densities of all prey items are recorded in Table 2. Note that the connecting line is not linear. Dagger symbols and grey animal shapes denote extinct taxa. Black animal shapes denote extant species.

Artistic cover: Life reconstruction of *Otodus megalodon* based on 3D model. An artistic depiction of a 16 m *O. megalodon* predating on an ~8 m *Balaenoptera* sp. in the Pliocene. In the distance, a 4 m *Carcharodon* sp. seizes a juvenile of the Balaenoptera pod. Illustration by J. J. Giraldo.

Tables

Table 1. Calculated properties of the completed *O. megalodon* reconstruction. *COM* represents centre of mass, *DER* refers to daily energetic requirement, *TL* refers to total length. *COM* axes directions are as follows: x) lateral; y) posterior; z) dorsal. CI = 95% confidence intervals from equations.

Property (units)	Source	Measurement	CI
TL (m)	Blender	15.9	NA
Surface area (m^2)	MeshLab (*31*)	131.2	NA
Volume (m^3)	MeshLab (*31*)	58.1	NA
COM x (m)	MeshLab (*31*)	0.2	NA
COM y (m)	MeshLab (*31*)	-3.3	NA
COM z (m)	MeshLab (*31*)	0.8	NA
Density (kg/m^3)	Literature (*32*)	1,060	NA
Body mass (kg)	Equation 1	61,560	NA
Absolute cruising speed (m/s)	Equation 2 (*33*)	1.4	0.5-4.1
Relative cruising speed (BL/s)	Absolute speed/TL	0.09	0.03-0.26
Stomach volume (L)	Equation 3	9,605	8,487-10,722
Gape height 35°	Blender	1.2	NA
Gape height 75°	Blender	1.8	NA
Gape width 35°	Blender	1.7	NA
Gape width 75°	Blender	1.7	NA
DER (kcal/day)	Equation 4 (*37*)	98,175	78,085-123,067

Table 2. Body mass and volume of putative *O. megalodon* prey. Volume of each taxon is compared against the estimated stomach volume of the *O. megalodon* model (9,605 L) to determine if it could have been completely consumed ("Complete ingestion?"). We set a limit of 70% stomach volume for full prey consumption (*36*). Energy densities for marine mammal taxa come from whole body estimates for sirenians (1,257 kcal/kg), dolphins (3,052 kcal/kg) and baleen whales (7,314 kcal/kg), and muscle estimates for *C. carcharias* (*42*). All literature sources for body length, body mass and energy density can be found in table S6. Extinct taxa are denoted by daggers (†).

Taxa	Body length (m)	Body mass (kg)	Volume (L)	Energy density (kcal/kg)	Complete ingestion?
Phocoena	2	70	71.75	3,052	Yes
†*Nanosiren*	2	150	153.75	1,257	Yes
Stenella	3	235	240.46	3,052	Yes
†*Xiphiacetus bossi*	<3.5	123	126.08	3,052	Yes
Tursiops	3.5	500	512.5	3,052	Yes
†*Orcinus* sp.	3.5	2,049	2,100.22	3,052	Yes
†*Piscobalaena nana*	<5	3,584	3,672.96	7,314	Yes
†*Carcharodon* sp.	5	1,154	1,183.02	4,400	Yes
†*Dioplotherium*	5.3	2,827	2,897.68	1,257	Yes
†*Metaxytherium*	5.7	3,492	3,579.3	1,257	Yes
Pseudorca	6	1,360	1394	3,052	Yes
†*Balaenoptera* spp. (*cortesii/bertae/davidsoni*)	6	2,357	2,415.83	7,314	Yes
Globicephala	6	3,200	3,280	7,314	Yes
Delphinapterus	6	5,016	5,141.8	7,314	Yes
†*Dusisiren*	6.2	4,411	4,521.28	1,257	Yes
†*Hydrodamalis*	7	6,553	6,716.83	1,257	Yes
Carcharodon carcharias	7	3,271	3,352.54	4,400	Yes
Orcinus orca	8	6,000	6,150	3,052	Yes
Balaenoptera acutorostrata	9	8,498	8,710.51	7,314	No
Eschrichtius	>12	20,000	20,500	7,314	No
Eubalaena	>12	31,700	32,492.5	7,314	No
Balaena	>12	75,000	76,875	7,314	No
Megaptera novaeangliae	16	30,000	30,750	7,314	No

References

1. J. R. Hutchinson, V. Ng-Thow-Hing, F. C. Anderson, A 3D interactive method for estimating body segmental parameters in animals: application to the turning and running performance of *Tyrannosaurus rex*. *J. Theor. Biol.* **246**, 660-680 (2007).
2. V. Allen, H. Paxton, J. R. Hutchinson, Variation in center of mass estimates for extant sauropsids and its importance for reconstructing inertial properties of extinct archosaurs. *Anat. Rec.* **292**, 1442-1461 (2009).
3. K. T. Bates, P. L. Manning, D. Hodgetts, W. I. Sellers, Estimating mass properties of dinosaurs using laser imaging and 3D computer modelling. *PLoS One* **4**, e4532 (2009).
4. J. R. Hutchinson, K. T. Bates, J. Molnar, V. Allen, P. J. Makovicky, A computational analysis of limb and body dimensions in *Tyrannosaurus rex* with implications for locomotion, ontogeny, and growth. *PLoS One* **6**, e26037 (2011).
5. G. Hubbell, "Using tooth structure to determine the evolutionary history of the white shark" in *Great white sharks: the biology of Carcharodon carcharias*, A. P. Klimley, and Ainley, D.G, Ed. (Academic Press, San Diego, 1996), pp. 9-18.
6. C. Pimiento, M. A. Balk, Body-size trends of the extinct giant shark *Carcharocles megalodon*: a deep-time perspective on marine apex predators. *Paleobiology* **41**, 479-490 (2015).
7. M. D. Gottfried, L. J. V. Compagno, S. C. Bowman, "Size and skeletal anatomy of the giant "megatooth" shark *Carcharodon megalodon*" in *Great white sharks: the biology of Carcharodon carcharias,* A. P. Klimley, and Ainley, D.G, Ed. (Academic Press, San Diego, 1996), pp. 55-66.
8. C. Pimiento, C. F. Clements, When did *Carcharocles megalodon* become extinct? A new analysis of the fossil record. *PLoS One* **9**, e111086 (2014).
9. C. Pimiento, B. J. MacFadden, C. F. Clements, S. Varela, C. Jaramillo, J. Velez-Juarbe, B. R. Silliman, Geographical distribution patterns of *Carcharocles megalodon* over time reveal clues about extinction mechanisms. *J. Biogeogr.* **43**, 1645-1655 (2016).
10. R. W. Boessenecker, D. J. Ehret, D. J. Long, M. Churchill, E. Martin, S. J. Boessenecker, The Early Pliocene extinction of the mega-toothed shark *Otodus megalodon*: a view from the eastern North Pacific. *PeerJ* **7**, e6088 (2019).
11. C. Pimiento, J. N. Griffin, C. F. Clements, D. Silvestro, S. Varela, M. D. Uhen, C. Jaramillo, The Pliocene marine megafauna extinction and its impact on functional diversity. *Nat. Ecol. Evol.* **1**, 1100-1106 (2017).
12. K. Shimada, The relationship between the tooth size and total body length in the white shark. *J. Fossil Res.* **35**, 28-33 (2003).
13. K. Shimada, The size of the megatooth shark, *Otodus megalodon* (Lamniformes: Otodontidae), revisited. *Hist. Biol.* **33**, 904-911 (2019).
14. V. J. Perez, R. M. Leder, T. Badaut, Body length estimations of Neogene lamniform sharks (*Carcharodon* and *Otodus*) derived from associated dentitions. *Palaeontol. Electron.* **24**, a09 (2021).
15. J. A. Cooper, C. Pimiento, H. G. Ferrón, M. J. Benton, Body dimensions of the extinct giant shark *Otodus megalodon*: a 2D reconstruction. *Sci. Rep.* **10**, 14596 (2020).
16. S. E. Bendix-Almgreen, *Carcharodon megalodon* from the Upper Miocene of Denmark, with comments on elasmobranch tooth enameloid: coronoïn. *Bull. Geol. Soc. Denmark* **32**, 1-32 (1983).
17. K. Shimada, M. F. Bonnan, M. A. Becker, M. L. Griffiths, Ontogenetic growth pattern of the extinct megatooth shark *Otodus megalodon* – implications for its reproductive biology, development, and life expectancy. *Hist. Biol.* **33**, 3254-3259 (2021).
18. R. J. Kallal, S. J. Godfrey, D. J. Ortner, Bone reactions on a Pliocene cetacean rib indicate short-term survival of predation event. *Int. J. Osteoarchaeol.* **22**, 253-260 (2010).

19. A. Collareta, O. Lambert, W. Landini, C. Di Celma, E. Malinverno, R. Varas-Malca, M. Urbina, G. Bianucci, Did the giant extinct shark *Carcharocles megalodon* target small prey? Bite marks on marine mammal remains from the late Miocene of Peru. *Palaeogeogr. Palaeoclimatol. Palaeoecol.* **469**, 84-91 (2017).

20. S. J. Godfrey, M. Ellwood, S. Groff, M. Verdin, *Carcharocles*-bitten Odontocete caudal vertebrae from the Coastal Eastern United States. *Acta Palaeontol. Pol.* **63**, 463-468 (2018).

21. S. J. Godfrey, J. R. Nance, N. L. Riker, *Otodus*-bitten sperm whale tooth from the Neogene of the Coastal Eastern United States. *Acta Palaeontol. Pol.* **66**, 599-603 (2021).

22. J. E. Martin, T. Tacail, S. Adnet, C. Girard, V. Balter, Calcium isotopes reveal the trophic position of extant and fossil elasmobranchs. *Chem. Geol.* **415**, 118-125 (2015).

23. G. Cliff, S. F. J. Dudley, B. Davis, Sharks caught in the protective gill nets off Natal, South Africa. 2. The great white shark *Carcharodon carcharias* (Linnaeus). *S. Afr. J. Mar. Sci.* **8**, 131-144 (1989).

24. I. K. Fergusson, "Distribution and autoecology of the white shark in the Eastern North Atlantic and the Mediterranean Sea" in *Great white sharks: the biology of Carcharodon carcharias,* A. P. Klimley, and Ainley, D.G, Ed. (Academic Press, San Diego, 1996), pp. 321-345.

25. R. Bonfil, M. Meÿer, M. C. Scholl, R. Johnson, S. O'Brien, H. Oosthuizen, S. Swanson, D. Kotze, M. Paterson, Transoceanic migration, spatial dynamics, and population linkages of white sharks. *Science* **310**, 100-103 (2005).

26. H. G. Ferrón, Regional endothermy as a trigger for gigantism in some extinct macropredatory sharks. *PLoS One* **12**, e0185185 (2017).

27. D. M. Jacoby, P. Siriwat, R. Freeman, C. Carbone, Correction to 'Is the scaling of swim speed in sharks driven by metabolism?'. *Biol. Lett.* **12**, 20160775 (2016).

28. K. A. Dickson, J. B. Graham, Evolution and consequences of endothermy in fishes. *Physiol. Biochem. Zool.* **77**, 998-1018 (2004).

29. H. G. Ferrón, C. Martínez-Pérez, H. Botella, The evolution of gigantism in active marine predators. *Hist. Biol.* **30**, 712-716 (2017).

30. D. J. Ehret, B. J. MacFadden, D. S. Jones, T. J. Devries, D. A. Foster, R. Salas-Gismondi, Origin of the white shark *Carcharodon* (Lamniformes: Lamnidae) based on recalibration of the Upper Neogene Pisco Formation of Peru. *Palaeontology* **55**, 1139-1153 (2012).

31. P. Cignoni, M. Callieri, M. Corsini, M. Dellepiane, F. Ganovelli, G. Ranzuglia, "Meshlab: an open-source mesh processing tool" in *Eurographics Italian chapter conference* (Salerno, 2008), pp. 129-136.

32. A. C. Gleiss, J. Potvin, J. A. Goldbogen, Physical trade-offs shape the evolution of buoyancy control in sharks. *Proc. Roy. Soc. B* **284**, 20171345 (2017).

33. D. M. Jacoby, P. Siriwat, R. Freeman, C. Carbone, Is the scaling of swim speed in sharks driven by metabolism? *Biol. Lett.* **11**, 20150781 (2015).

34. M. R. Hirt, W. Jetz, B. C. Rall, U. Brose, A general scaling law reveals why the largest animals are not the fastest. *Nat. Ecol. Evol.* **1**, 1116-1122 (2017).

35. C. Pimiento, J. L. Cantalapiedra, K. Shimada, D. J. Field, J. B. Smaers, Evolutionary pathways toward gigantism in sharks and rays. *Evolution* **73**, 588-599 (2019).

36. W. N. Joyce, S. E. Campana, L. J. Natanson, N. E. Kohler, H. L. Pratt Jr, C. F. Jensen, Analysis of stomach contents of the porbeagle shark (*Lamna nasus* Bonnaterre) in the northwest Atlantic. *ICES J. Mar. Sci.* **59**, 1263-1269 (2002).

37. D. C. Bernvi, "Ontogenetic influences on endothermy in the great white shark (*Carcharodon carcharias*)", MSc thesis, Stockholm University (2016).

38. F. G. Carey, J. W. Kanwisher, O. Brazier, G. Gabrielson, J. G. Casey, H. L. Pratt Jr, Temperature and activities of a white shark, *Carcharodon carcharias*. *Copeia* **2**, 254-260 (1982).

39. S. C. Leigh, Y. Papastamatiou, D. P. German, The nutritional physiology of sharks. *Rev. Fish Biol. Fish.* **27**, 561-585 (2017).

40. C. Lockyer, Body weights of some species of large whales. *ICES J. Mar. Sci.* **36**, 259-273 (1976).

41. D. Struntz, W. A. McLellan, R. Dillaman, J. E. Blum, J. R. Kucklick, D. A. Pabst, Blubber development in bottlenose dolphins (*Tursiops truncatus*). *J. Morphol.* **259**, 7-20 (2004).

42. H. R. Pethybridge, C. C. Parrish, B. D. Bruce, J. W. Young, P. D. Nichols, Lipid, fatty acid and energy density profiles of white sharks: insights into the feeding ecology and ecophysiology of a complex top predator. *PLoS One* **9**, e97877 (2014).

43. T. Lingham-Soliar, Caudal fin allometry in the white shark *Carcharodon carcharias*: implications for locomotory performance and ecology. *Naturwissenschaften* **92**, 231-236 (2005).

44. H. F. Mollet, G. M. Cailliet, "Using allometry to predict body mass from linear measurements of the white shark" in *Great white sharks: the biology of Carcharodon carcharias,* A. P. Klimley, and Ainley, D.G, Ed. (Academic Press, San Diego, 1996), pp. 81-89.

45. D. W. Stephens, E. L. Charnov, Optimal foraging: some simple stochastic models. *Behav. Ecol. Sociobiol.* **10**, 251-263 (1982).

46. R. P. Wilson, M. D. Holton, A. Neate, M. Del'Caño, F. Quintana, K. Yoda, A. Gómez-Laich, Luck and tactics in foraging success: the case of the imperial shag. *Mar. Ecol. Prog. Ser.* **682**, 1-12 (2022).

47. B. W. Kent, "The cartilaginous fishes (chimaeras, sharks and rays) of Calvert Cliffs, Maryland, USA" in *The Geology and Vertebrate Paleontology of Calvert Cliffs, Maryland, USA,* S. J. Godfrey, Ed. (Smithsonian Institution Scholarly Press, Washington D.C., 2018), pp. 45-157.

48. P. C. Sternes, J. J. Wood, K. Shimada, Body forms of extant lamniform sharks (Elasmobranchii: Lamniformes), and comments on the morphology of the extinct megatooth shark, *Otodus megalodon*, and the evolution of lamniform thermophysiology. *Hist. Biol.* 1-13 (2022).

49. D. Bernal, K. A. Dickson, R. E. Shadwick, J. B. Graham, Analysis of the evolutionary convergence for high performance swimming in lamnid sharks and tunas. *Comp. Biochem. Physiol. A* **129**, 695-726 (2001).

50. J. M. Donley, C. A. Sepulveda, P. Konstantinidis, S. Gemballa, R. E. Shadwick, Convergent evolution in mechanical design of lamnid sharks and tunas. *Nature* **429**, 61-65 (2004).

51. Y. Y. Watanabe, K. J. Goldman, J. E. Caselle, D. D. Chapman, Y. P. Papastamatiou, Comparative analyses of animal-tracking data reveal ecological significance of endothermy in fishes. *Proc. Nat. Acad. Sci. U.S.A.* **112**, 6104-6109 (2015).

52. L. Harding, A. Jackson, A. Barnett, I. Donohue, L. Halsey, C. Huveneers, C. Meyer, Y. Papastamatiou, J. M. Semmens, E. Spencer, Y. Watanabe, N. Payne, Endothermy makes fishes faster but does not expand their thermal niche. *Funct. Ecol.* **00**, 1-9 (2021).

53. D. A. Ebert, S. L. Fowler, L. J. V. Compagno, *Sharks of the world: a fully illustrated guide* (Wild Nature Press, Plymouth, 2013).

54. T. Lingham-Soliar, Convergence in thunniform anatomy in lamnid sharks and Jurassic ichthyosaurs. *Integr. Comp. Biol.* **56**, 1323-1336 (2016).

55. A. Bernard, C. Lécuyer, P. Vincent, R. Amiot, N. Bardet, E. Buffetaut, G. Cuny, F. Fourel, F. Martineau, J. Mazin, A. Prieur, Regulation of body temperature by some Mesozoic marine reptiles. *Science* **328**, 1379-1382 (2010).

56. D. Bernal, C. A. Sepulveda, Evidence for temperature elevation in the aerobic swimming musculature of the common thresher shark, *Alopias vulpinus*. *Copeia* **2005**, 146-151 (2005).

57. G. Del Raye, S. J. Jorgensen, K. Krumhansl, J. M. Ezcurra, B. A. Block, Travelling light: white sharks (*Carcharodon carcharias*) rely on body lipid stores to power ocean-basin scale migration. *Proc. Roy. Soc. B* **280**, 20130836 (2013).

58. C. E. Doughty, J. Roman, S. Faurby, A. Wolf, A. Haque, E. S. Bakker, Y. Malhi, J. B. Dunning, Jr., J. C. Svenning, Global nutrient transport in a world of giants. *Proc. Nat. Acad. Sci. U.S.A.* **113**, 868-873 (2016).

59. R. A. Myers, J. K. Baum, T. D. Shepherd, S. P. Powers, C. H. Peterson, Cascading effects of the loss of apex predatory sharks from a coastal ocean. *Science* **315**, 1846-1850 (2007).

60. C. G. Diedrich, Evolution of white and megatooth sharks, and evidence for early predation on seals, sirenians, and whales. *Nat. Sci.* **05**, 1203-1218 (2013).

61. R. A. Martin, N. Hammerschlag, R. S. Collier, C. Fallows, Predatory behaviour of white sharks (*Carcharodon carcharias*) at Seal Island, South Africa. *J. Mar. Biol. Assoc. U.K.* **85**, 1121-1136 (2005).

62. R. A. Martin, N. Hammerschlag, Marine predator–prey contests: Ambush and speed versus vigilance and agility. *Mar. Biol. Res.* **8**, 90-94 (2012).

63. S. J. Jorgensen, S. Anderson, F. Ferretti, J. R. Tietz, T. Chapple, P. Kanive, R. W. Bradley, J. H. Moxley, B. A. Block, Killer whales redistribute white shark foraging pressure on seals. *Sci. Rep.* **9**, 6153 (2019).

64. G. Bianucci, W. Landini, Killer sperm whale: a new basal physteroid (Mammalia, Cetacea) from the Late Miocene of Italy. *Zool. J. Linn. Soc.* 148, 103-131 (2006).

65. E. Peri, P. L. Falkingham, A. Collareta, G. Bianucci, Biting in the Miocene seas: Estimation of the bite force of the macroraptorial sperm whale *Zygophyseter varolai* using finite element analysis. *Hist. Biol.* 1-12 (2021).

66. L. O. Lucifora, V. B. García, R. C. Menni, A. H. Escalante, N. M. Hozbor, Effects of body size, age and maturity stage on diet in a large shark: ecological and applied implications. *Ecol. Res.* **24**, 109-118 (2009).

67. J. A. Goldbogen, D. E. Cade, D. M. Wisniewska, J. Potvin, P. S. Segre, M. S. Savoca, E. L. Hazen, M. F. Czapanskiy, S. R. Kahane-Rapport, S. L. DeRuiter, S. Gero, P. Tønnesen, W. T. Gough, M. B. Hanson, M. M. Holt, F. H. Jensen, M. Simon, A. K. Stimpert, P. Arranz, D. W. Johnston, D. P. Nowacek, S. E. Parks, F. Visser, A. S. Friedlaender, P. L. Tyack, P. T. Madsen, N. D. Pyenson, Why whales are big but not bigger: Physiological drivers and ecological limits in the age of ocean giants. *Science* **366**, 1367-1372 (2019).

68. A. M. Pagano, T. M. Williams, Physiological consequences of Arctic sea ice loss on large marine carnivores: unique responses by polar bears and narwhals. *J. Exp. Biol.* **224**, jeb228049 (2021).

69. J. A. Goldbogen, Physiological constraints on marine mammal body size. *Proc. Nat. Acad. Sci. U.S.A.* **115**, 3995-3997 (2018).

70. J. Kriwet, H. Mewis, O. Hampe, A partial skeleton of a new lamniform mackerel shark from the Miocene of Europe. *Acta Palaeontol. Pol.* **60**, 857-875 (2014).

71. S. Wroe, D. R. Huber, M. Lowry, C. McHenry, K. Moreno, P. Clausen, T. L. Ferrara, E. Cunningham, M. N. Dean, A. P. Summers, Three-dimensional computer analysis of white shark jaw mechanics: how hard can a great white bite? *J. Zool.* **276**, 336-342 (2008).

72. A. Larramendi, G. S. Paul, S. Y. Hsu, A review and reappraisal of the specific gravities of present and past multicellular organisms, with an emphasis on tetrapods. *Anat. Rec.* **304**, 1833-1888 (2020).

73. T. L. Ferrara, P. Clausen, D. R. Huber, C. R. McHenry, V. Peddemors, S. Wroe, Mechanics of biting in great white and sandtiger sharks. *J. Biomech.* **44**, 430-435 (2011).

74. C. D. Wilga, P. J. Motta, C. P. Sanford, Evolution and ecology of feeding in elasmobranchs. *Integr. Comp. Biol.* **47**, 55-69 (2007).

75. R. Froese, D. Pauly, FishBase World wide web electronic publication, version (01/2017); www.fishbase.org [accessed June 2020].

76. T. Kubodera, H. Watanabe, T. Ichii, Feeding habits of the blue shark, *Prionace glauca*, and salmon shark, *Lamna ditropis*, in the transition region of the Western North Pacific. *Rev. Fish Biol. Fish.* **17**, 111-124 (2006).

77. J. M. Ezcurra, C. G. Lowe, H. F. Mollet, L. A. Ferry, J. B. O'Sullivan, "Oxygen consumption rate of young-of-the-year white sharks, *Carcharodon carcharias*, during transport to the Monterey Bay aquarium" in *Global Perspectives on the Biology and Life History of the Great White Shark,* M. L. Domeier, Ed. (CRC Press, Boca Raton, 2012), pp. 17-25.

78. T. C. Tricas, J. E. McCosker, Predatory behavior of the white shark (*Carcharodon carcharias*), with notes on its biology. *Proc. Calif. Acad. Sci.* **43**, 221-238 (1984).

79. R. P. Wilson, A. Neate, M. D. Holton, E. L. C. Shepard, D. M. Scantlebury, S. A. Lambertucci, A. di Virgilio, E. Crooks, C. Mulvenna, N. Marks, Luck in food finding affects individual performance and population trajectories. *Curr. Biol.* **28**, 3871-3877 (2018).

80. K. O. Lear, D. L. Morgan, J. M. Whitty, N. M. Whitney, E. E. Byrnes, S. J. Beatty, A. C. Gleiss, Divergent field metabolic rates highlight the challenges of increasing temperatures and energy limitation in aquatic ectotherms. *Oecologia* **193**, 311-323 (2020).

81. E. Nordøy, L. Folkow, P.-E. Mtensson, A. Blix, "Food requirements of Northeast Atlantic minke whales" in *Developments in Marine Biology* (Elsevier, 1995), pp. 307-317.

82. P. C. Valery, T. Ibiebele, M. Harris, A. C. Green, A. Cotterill, A. Moloney, A. K. Sinha, G. Garvey, Diet, physical activity, and obesity in school-aged indigenous youths in northern Australia. *J. Obes.* **2012**, 1-12 (2012).

83. B. Davidson, G. Cliff, Comparison of pinniped and cetacean prey tissue lipids with lipids of their elasmobranch predator. *In Vivo* **28**, 223-228 (2014).

84. W. A. McLellan, H. N. Koopman, S. A. Rommel, A. J. Read, C. W. Potter, J. R. Nicolas, A. J. Westgate, D. A. Pabst, Ontogenetic allometry and body composition of harbour porpoises (*Phocoena phocoena*, L.) from the western North Atlantic. *J. Zool.* **257**, 457-471 (2002).

85. D. P. Domning, O. A. Aguilera, Fossil Sirenia of the West Atlantic and Caribbean region. VIII.*Nanosiren garciae*, gen. et sp. nov. and *Nanosiren sanchezi*, sp. nov. *J. Vertebr. Paleontol.* **28**, 479-500 (2008).

86. W. F. Perrin, M. L. L. Dolar, C. M. Chan, S. J. Chivers, Length-weight relationships in the spinner dolphin (*Stenella longirostris*). *Mar. Mammal Sci.* **21**, 765-778 (2005).

87. S. H. Montgomery, J. H. Geisler, M. R. McGowen, C. Fox, L. Marino, J. Gatesy, The evolutionary history of cetacean brain and body size. *Evolution* **67**, 3339-3353 (2013).

88. H. Shirihai, B. Jarrett, G. M. Kirwan, *Whales, dolphins, and other marine mammals of the world* (Princeton University Press, 2006).

89. V. Bouetel, C. de Muizon, The anatomy and relationships of *Piscobalaena nana* (Cetacea, Mysticeti), a Cetotheriidae s.s. from the early Pliocene of Peru. *Geodiversitas* **28**, 319-395 (2006).

90. D. K. Sarko, D. P. Domning, L. Marino, R. L. Reep, Estimating body size of fossil sirenians. *Mar. Mammal Sci.* **26**, 937-959 (2010).
91. P. J. Stacey, R. W. Baird, S. Leatherwood, *Pseudorca crassidens*. *Mar. Mammal Sci.* **456**, 1-6 (1994).
92. L. Folkow, A. Blix, Metabolic rates of minke whales (*Balaenoptera acutorostrata*) in cold water. *Acta Physiol. Scand.* **146**, 141-150 (1992).
93. T. A. Jefferson, M. A. Webber, R. L. Pitman, *Marine mammals of the world: a comprehensive guide to their identification* (Elsevier, Oxford, UK, 2008).
94. D. Sergeant, P. Brodie, Body size in white whales, *Delphinapterus leucas*. *J. Fish. Board Can.* **26**, 2561-2580 (1969).
95. R. W. Baird, R. W. Baird, *Killer whales of the world: natural history and conservation* (Voyageur Press, 2006).
96. S. Agbayani, S. M. E. Fortune, A. W. Trites, Growth and development of North Pacific gray whales (*Eschrichtius robustus*). *J. Mammal.* **101**, 742-754 (2020).
97. S. M. E. Fortune, M. J. Moore, W. L. Perryman, A. W. Trites, Body growth of North Atlantic right whales (*Eubalaena glacialis*) revisited. *Mar. Mammal Sci.* **37**, 433-447 (2020).
98. R. M. Nowak, *Walker's Mammals of the World* (John Hopkins University Press, Baltimore, Maryland, 1999).
99. L. Riekkola, V. Andrews-Goff, A. Friedlaender, A. N. Zerbini, R. Constantine, Longer migration not necessarily the costliest strategy for migrating humpback whales. *Aquat. Conserv.* **30**, 937-948 (2020).
100. M. R. McCurry, F. G. Marx, A. R. Evans, T. Park, N. D. Pyenson, N. Kohno, S. Castiglione, E. M. G. Fitzgerald, Brain size evolution in whales and dolphins: new data from fossil mysticetes. *Biol. J. Linn. Soc.* **133**, 990-998 (2021).
101. C. R. McClain, M. A. Balk, M. C. Benfield, T. A. Branch, C. Chen, J. Cosgrove, A. D. Dove, L. C. Gaskins, R. R. Helm, F. G. Hochberg, F. B. Lee, A. Marshall, S. E. McMurray, C. Schanche, S. N. Stone, A. D. Thaler, Sizing ocean giants: patterns of intraspecific size variation in marine megafauna. *PeerJ* **3**, e715 (2015).

Appendix 5 | Supplementary material for Appendix 4

Supplementary Materials for

The extinct shark *Otodus megalodon* was a transoceanic super-predator: Inferences based on 3D modelling

Jack A. Cooper, John R. Hutchinson[*], David C. Bernvi, Geremy Cliff, Rory P. Wilson, Matt L. Dicken, Jan Menzel, Stephen Wroe, Jeanette Pirlo, Catalina Pimiento[*]

*Corresponding authors. Email: ██████████████████████; ██████████████████

This appendix includes:
>   Figs. S1 to S4
>   Tables S1 to S6

Other Supplementary Materials for this manuscript
(https://www.science.org/doi/full/10.1126/sciadv.abm9424) include:
>   Movie S1

Materials included in the Dryad Data Repository include:
>   Step by step guide on how to make a giant shark in Blender
>   Data S1 to S5
>   Available here: https://doi.org/10.5061/dryad.7h44j0zvw

Figure S1. All 141 vertebral centra in the *Otodus megalodon* column (IRNSB P 9893). Labelling refers to position of the centra in the column, and the former labelling of the specimen (IRSNB 3121) (*7*). Centra labelled 30, 35-37, 45, 105, 131, 136, 141, 146, 147 and 149 are missing from the column and there are two centra labelled as 33, 100 and 115 (see main text).
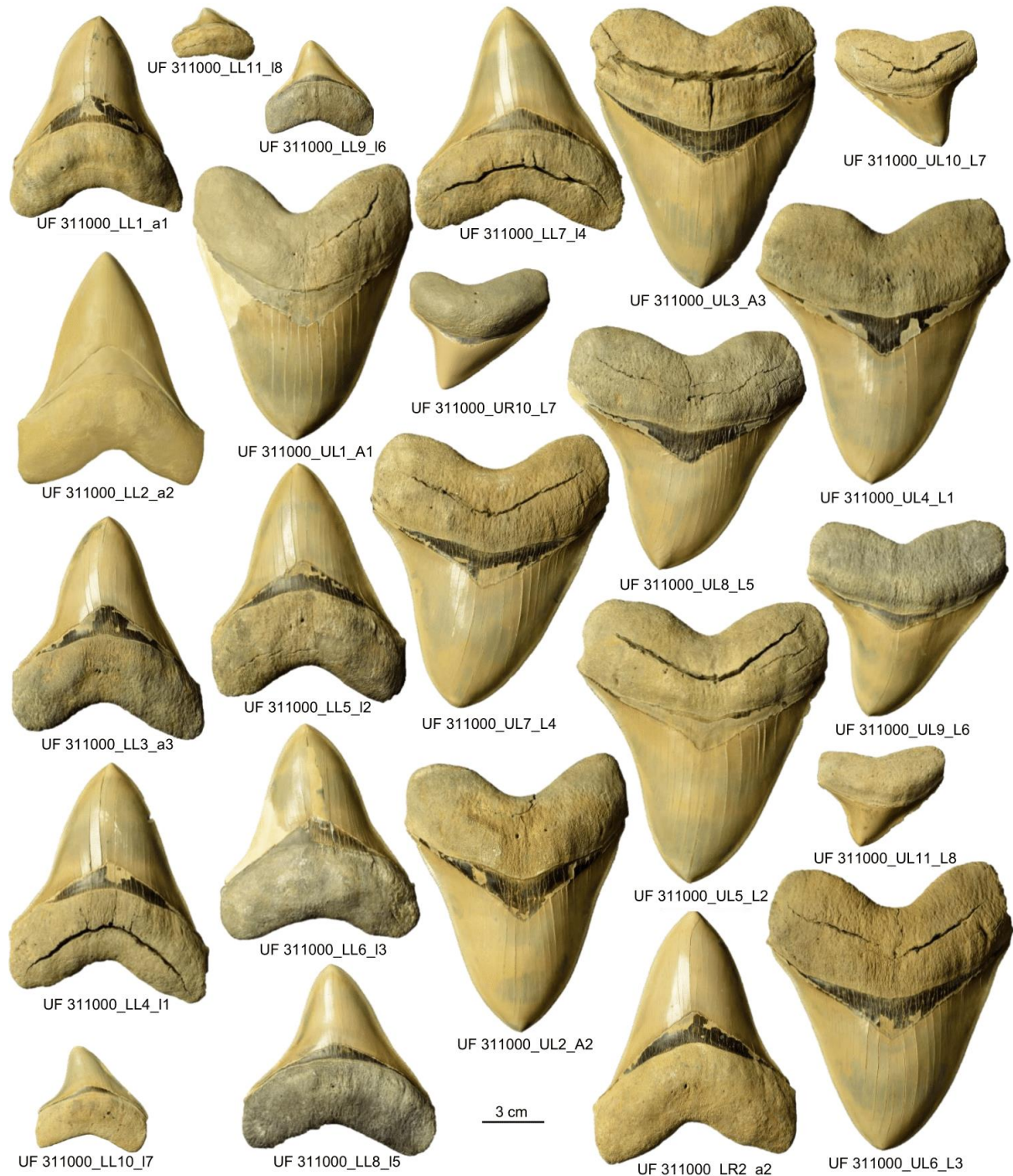
Figure S2. All *Otodus megalodon* teeth (n = 24) from specimen UF 311000, which formed the basis of our model's jaws. Labelling refers to specimen name, tooth position recorded by the Florida Museum of Natural History (LL = lower left; UL = upper left; LR = lower right; UR = upper right), and the tooth position following standard nomenclature, where A/a refers to anterior teeth and L/l represents lateral teeth. In the latter case, upper-case and lower-case letters indicate upper and lower teeth respectively. Photographs taken from the Florida Museum of Natural History online catalogue.
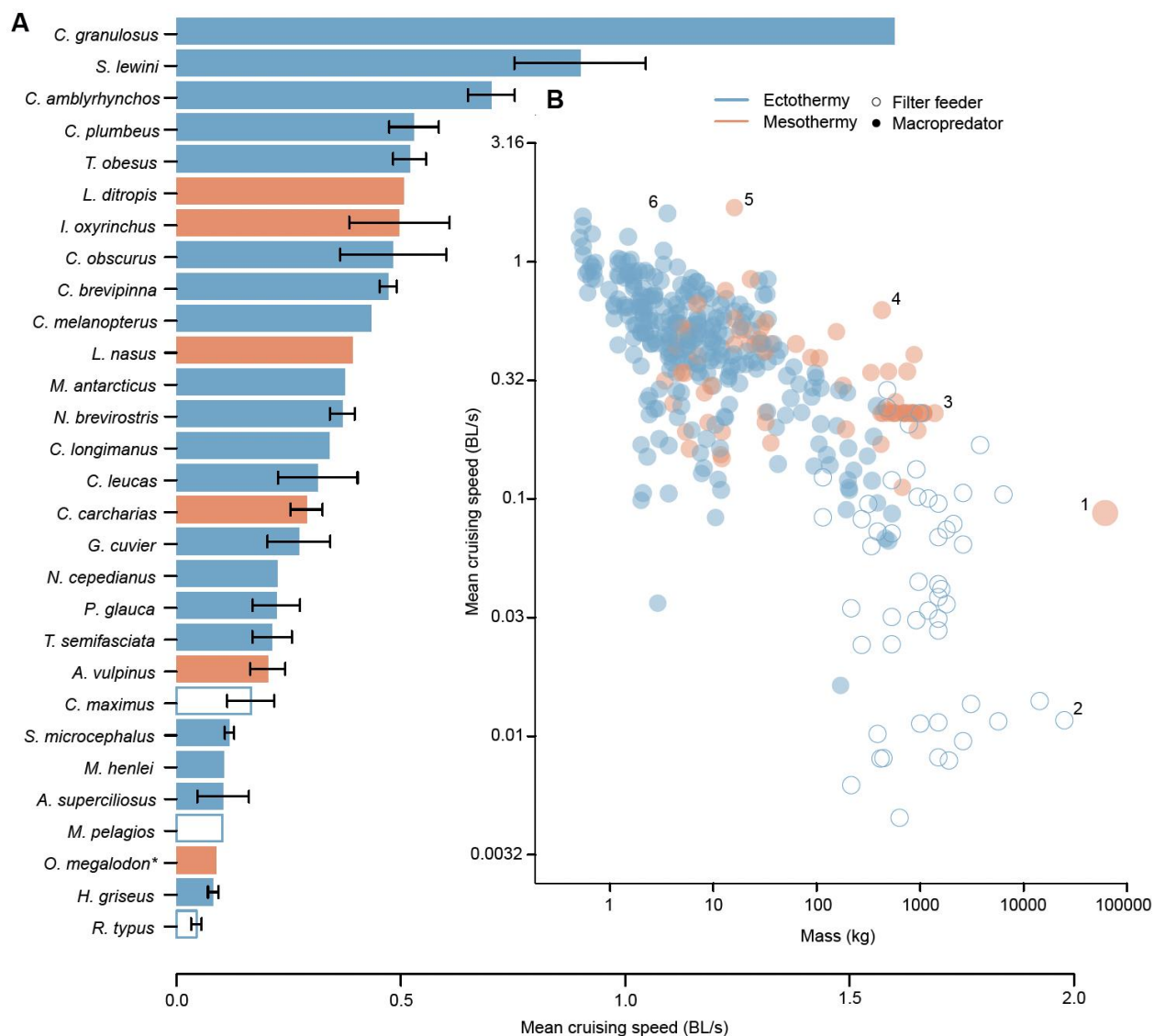
Figure S3. Shark mean relative cruising speeds. (**A**) Mean relative cruising speeds of all shark species from data S1 (n = 28 plus the model *Otodus megalodon*) with error bars drawn from multiple individuals per species. Species without error bars are those where only one individual is represented. An asterisk (*) indicates that *O. megalodon*'s speed estimate was made from equation 2 rather than from the mean of multiple speeds. (**B**) Mass and mean relative cruising speed of all individual sharks recorded in data S1 (n = 391 plus the model *O. megalodon*), plotted on a log scale. Numbered individuals are as follows: 1) the 15.9 m, 61,560 kg model individual of *Otodus megalodon*; 2) an 18 m, 24,800 kg individual of the whale shark (*Rhincodon typus*); 3) a 5.3 m, 1,382 kg great white shark (*Carcharodon carcharias*); 4) a 3.6 m, 427.5 kg *C. carcharias*; 5) a 1.1 m, 16 kg shortfin mako shark (*Isurus oxyrinchus*); and 6) a 0.15 m, 3.6 kg gulper shark (*Centrophorus granulosus*).
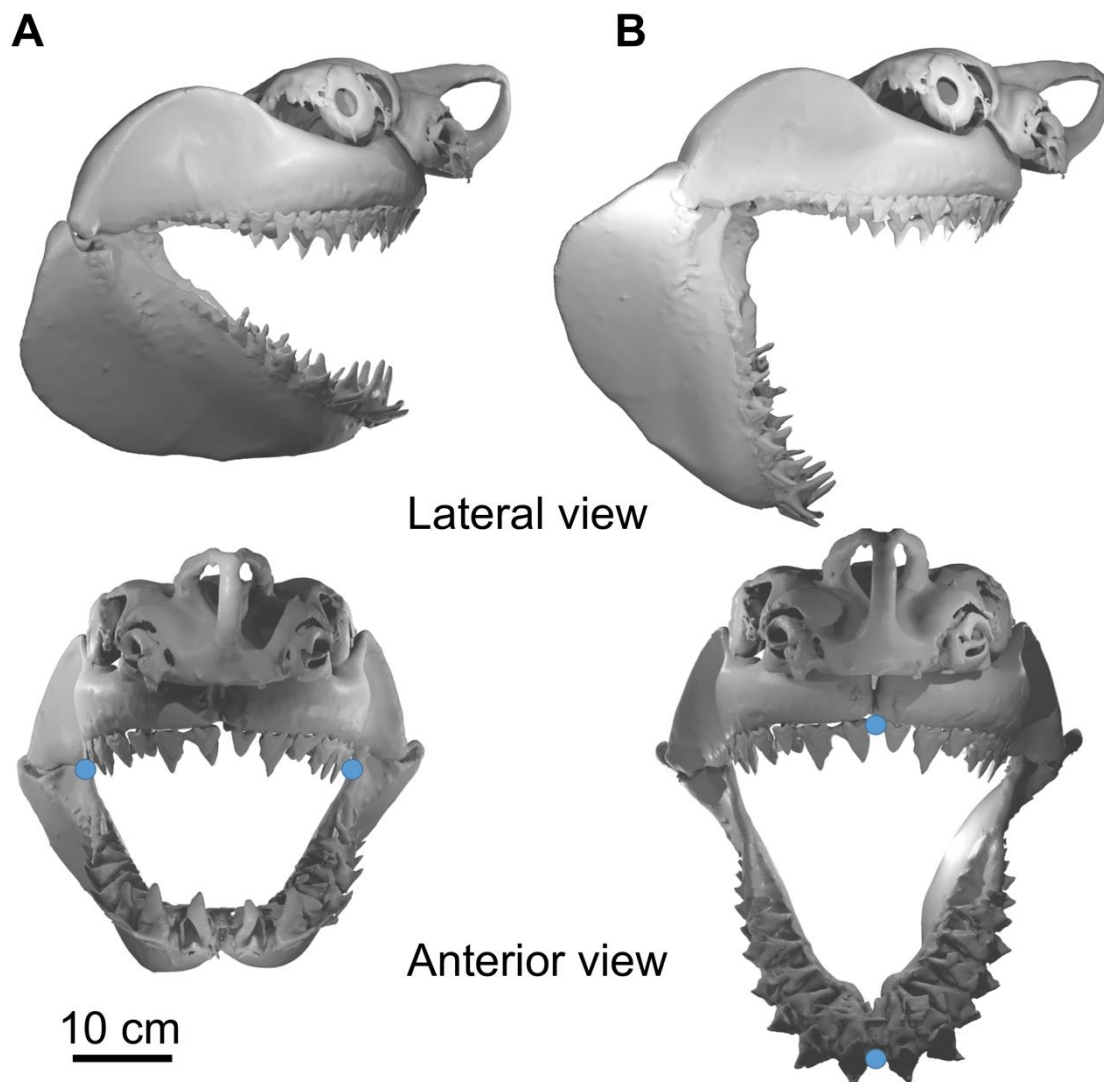
Figure S4. Gape angles used to estimate gape size of the *Otodus megalodon* model. This uses a *Carcharodon carcharias* chondrocranium containing the UF 311000 *O. megalodon* teeth at (**A**) 35º, and (**B**) 75º. The *C. carcharias* chondrocranium is scaled according to its original size here. Blue landmarks are used in the anterior views to denote the points between which (**A**) gape width and (**B**) height were measured.

Table S1. Summarised occurrence data of putative *Otodus megalodon* prey taxa. Abundance is categorised based on raw occurrences as: <10 = "Low"; 10-24 = "Medium"; ≥25 = "High". Daggers (†) denote extinct taxa. Data was downloaded from the Paleobiology Database (https://paleobiodb.org/). Max_ma and Min_ma represent the earliest and latest occurrence in the Paleobiology Database respectively.

Taxa	Occurrences	Abundance	Max_ma	Min_ma
Phocoena	3	Low	5.333	2.588
†Nanosiren	12	Medium	23.03	3.6
Stenella	10	Medium	7.246	2.588
†Xiphiacetus bossi	25	High	23.03	2.588
Tursiops	10	Medium	15.97	0.781
†Orcinus sp.	4	Low	15.97	0.781
†Piscobalaena nana	5	Low	13.82	5.333
†Carcharodon sp.	34	High	23.03	2.588
†Dioplotherium	15	Medium	23.03	3.6
†Metaxytherium	200	High	28.1	2.588
Pseudorca	5	Low	5.333	2.588
†Balaenoptera spp. *(cortesii/bertae/davidsoni)*	55	High	23.03	0.01
Globicephala	16	Medium	23.03	0.781
Delphinapterus	2	Low	15.97	0.781
†Dusisiren	20	Medium	15.97	3.6
†Hydrodamalis	27	High	11.62	2.588
Carcharodon carcharias	58	High	23.03	1.8
Orcinus orca	1	Low	5.333	3.6
Balaenoptera acutorostrata	10	Medium	23.03	2.588
Eschrichtius	1	Low	3.6	2.588
Eubalaena	11	Medium	23.03	2.588
Balaena	19	Medium	23.03	0.781
Megaptera novaeangliae	17	Medium	23.03	2.588

Table S2. Comparisons between body dimensions from a *Otodus megalodon* 2D model that accounts for multiple analogues (*15*) and those from the completed 3D model. The 19 body-part dimensions measured are as follows: Snout-eye distance (SE); snout-pectoral fin distance (SP); pectoral fin length (PecL) and width (PecW); snout-dorsal fin distance (SD): dorsal fin height (DH) and width (DW); dorsal tip-abdomen distance (DTA); dorsal posterior-abdomen distance (DPA); primary-secondary dorsal fin distance (DD); pectoral-pelvic fin distance (PP); pelvic fin length (PelL) and width (PelW); dorsal side-pelvic fin anterior distance (BPA); pelvic-anal fin distance (PA); secondary dorsal-anal fin distance (DA); dorsal-caudal fin distance (DC); fork height (FH) and tail height (TH). SE was measured using the *C. carcharias* chondrocranium CT scan (*71*) scaled to fit our model while all other measurements are taken from the completed model.

Variable	Predicted (*15*)		Empirical	
	Mean (cm)	Standard deviation (cm)	Model measurement (cm)	Fits mean ± SD? (Y/N)
SE	79.34	25.44	83.23	Y
SP	419.83	45.96	391.75	Y
PecL	307.07	76.88	301.03	Y
PecW	164.07	31.16	152.15	Y
SD	591.11	49.93	591.96	Y
DH	161.77	35.38	162.02	Y
DW	198.09	29.88	186.54	Y
DTA	451.12	55.51	447.76	Y
DPA	279.19	40.08	281.31	Y
DD	366.39	31.86	353.02	Y
PP	350.38	57.99	348.43	Y
PelL	73.24	18.13	74.83	Y
PelW	99.34	24.34	101.12	Y
BPA	195.11	19.41	194.71	Y
PA	143.37	31.86	158.74	Y
DA	95.58	15.93	96.56	Y
DC	804.9	46.84	831.09	Y
FH	43.5	4.84	43.14	Y
TH	383.68	69.47	355.66	Y

Table S3. Output of the geometric scaling model between body mass and cruising speed from Jacoby et al. (*33*). We independently re-collected and re-analysed the data from (*33*) to both replicate this model and perform our speed comparisons (see main text). Trophic level, temperature and habitat type, which are considered in the model, were gathered from the supplementary material of (*33*). Converting the intercept and mass coefficients to a power function generates the equation: $y = 0.266x^{0.082}$. Note that the exponent of 0.0823 falls within the CI range (0.053-0.249) and that this exponent was found to be 0.15 following correction for phylogeny (*33*). SE = standard error.

	Coefficients	SE	T value	P value
Intercept	-1.328	10.143	-0.131	0.898
Log mass	0.082	0.071	1.159	0.269
Log trophic level	-0.164	6.949	-0.024	0.982
Temperature – Mixed	-8.933	8.489	-1.052	0.313
Temperature – Warm	-4.447	3.582	-1.242	0.238
Habitat type – benthopelagic	0.794	0.516	1.538	0.15
Habitat type – demersal	-7.578	10.298	-0.736	0.476
Habitat type – pelagic-oceanic	0.79	10.51	0.075	0.941
Habitat type – reef-associated	16.728	13.157	1.271	0.228

lm(formula = log(Speed) ~ log(Mass) + log(Trophic level)*Temperature*Habitat type

$F_{(13,12)} = 3.534$, $R^2 = 0.79$, $P = 0.018$

Table S4. *C. carcharias* individuals dissected and analysed for stomach volume analysis.

Shark KZNSB-ID	Sex	Total length (cm)	Body mass (kg)	Stomach volume (L)
TRA15004	Male	196	67	7.49
RB15017	Male	263	156	10.86
RB15023	Female	255	126	12.2
MG15008	Female	271	188	18.45
GLN17003	Male	270	162	13
LEB17007	Female	220	106	12
RB17031	Female	224	105	18.55
BAL17003	Male	324	296	42
LEB18004	Female	310	282	31.8
SAL18004	Male	204	115	21.3
RB18037	Female	239	130	8.7
ZIN09016	Female	437	892	135

Table S5. Model outputs of the linear regression of body mass and stomach volume in *Carcharodon carcharias*. SE = Standard error; LCL = Lower limit of the 95% confidence interval; UCL = Upper limit of the 95% confidence interval. $R^2 = 0.97$.

	Coefficients	SE	LCL	UCL	t Stat	p-value
Intercept	-6.54	2.48	-12.07	-1.02	-2.64	0.02
Body mass	0.16	0.01	0.14	0.17	19.25	0.00

Table S6. Literature sources for body size and energy density of putative *Otodus megalodon* prey. Body mass estimates of each taxon are found in individual literature sources. Energy densities for marine mammal taxa come from estimates for different groups – specifically sirenians (1,257 kcal/kg), dolphins (3,052 kcal/kg), and baleen whales (7,314 kg/kcal) (*81-83*) – whereas the energy density for *Carcharodon carcharias* is based on the muscle energy density reported in (*42*). Extinct taxa are denoted by daggers (†).

Taxa	Group	Body mass reference	Energy density reference
Phocoena[a]	Dolphin	(*84*)	3,052 (*83*)
†*Nanosiren*[a]	Sirenian	(*85*)	1,257 (*82*)
Stenella[a]	Dolphin	(*86*)	3,052 (*83*)
†*Xiphiacetus bossi*[b]	Dolphin	(*87*)	3,052 (*83*)
Tursiops[a]	Dolphin	(*88*)	3,052 (*83*)
†*Orcinus* sp.[a]	Dolphin	(*87*)	3,052 (*83*)
†*Piscobalaena nana*[c,d]	Baleen whale	(*89*)	7,314 (*81*)
†*Carcharodon* sp.[e,f]	Shark	(*44*)	4,400 (*42*)
†*Dioplotherium*[a]	Sirenian	(*90*)	1,257 (*82*)
†*Metaxytherium*[a]	Sirenian	(*90*)	1,257 (*82*)
Pseudorca[a]	Dolphin	(*91*)	3,052 (*83*)
†*Balaenoptera* spp. (*cortesii/bertae/davidsoni*)[a]	Baleen whale	(*92*)	7,314 (*81*)
Globicephala[a]	Baleen whale	(*93*)	7,314 (*81*)
Delphinapterus[a]	Baleen whale	(*94*)	7,314 (*81*)
†*Dusisiren*[a]	Sirenian	(*90*)	1,257 (*82*)
†*Hydrodamalis*[a]	Sirenian	(*90*)	1,257 (*82*)
Carcharodon carcharias[f,g]	Shark	(*44*)	4,400 (*42*)
Orcinus orca[a,h]	Dolphin	(*95*)	3,052 (*83*)
Balaenoptera acutorostrata[a]	Baleen whale	(*92*)	7,314 (*81*)
Eschrichtius[a]	Baleen whale	(*96*)	7,314 (*81*)
Eubalaena[a]	Baleen whale	(*97*)	7,314 (*81*)
Balaena[a]	Baleen whale	(*98*)	7,314 (*81*)
Megaptera novaeangliae[a,i]	Baleen whale	(*99*)	7,314 (*81*)

[a]Genus-level taxa recorded in the Pliocene as reported in (*11*); [b]fossil evidence of *O. megalodon* bite mark (*20*); [c]fossil evidence of *O. megalodon* bite mark (*19*); [d]size estimated based on humerus, radius and ulna (*90*) and following (*100*); [e]size based on (*14*); [f]mass calculated from (*44*) (see Methods); [g]largest size based on (*23, 101*); [h]largest male size (*95*); [i]fossil rib specimen potentially bitten by *O. megalodon* not identified to species-level; however, similar to *M. novaeangliae* (*18*).

Movie S1. Rotation videos of all model components (separate file).
Included model components are as follows: IRSNB P 9893, UF 311000, NSWDPI-WS2006/4 with *O. megalodon* teeth (UF 311000) attached, the South African full-body 3D scan of *C. carcharias*, the final *O. megalodon* model, and the visualised open gape models of 35º and 75º gape angles.

Data S1. Datasets assembled for this study (Dryad Data Repository).
Divided into two sheets. *Vertebral column*: Measurement data of IRSNB P 9893 vertebral centra. Preservation state of all vertebrae are labelled as follows: 0) fragmentary; 1) partial preservation; 2) near-complete. *Species comparisons*: Feeding strategy, thermoregulatory ability, body mass and cruising speed for 28 extant species and the *Otodus megalodon* model used in swim speed analysis.

Data S2. Blender file of the completed *Otodus megalodon* model (Dryad Data Repository).

Data S3. Blender file of the 3D scanned *Carcharodon carcharias* used to aid flesh reconstruction (Dryad Data Repository).

Data S4. Blender file of the recreated fossil specimen UF 311000 (Dryad Data Repository)

Data S5. Blender file of the recreated fossil specimen IRSNB P 9893 (Dryad Data Repository).

Appendix 6 | Additional paper co-authored by the candidate and published during his PhD: The extinct marine megafauna of the Phanerozoic

The extinct marine megafauna of the Phanerozoic

Catalina Pimiento[a,b], Kristína Kocáková[a]*, Gregor H. Mathes[a]*, Thodoris Argyriou[c,d], Edwin-Alberto Cadena[e,f,g], Jack A. Cooper[b], Dirley Cortés[h,i,j,g], Daniel J. Field[k,l,m], Christian Klug[a], Torsten M. Scheyer[a], Ana M. Valenzuela-Toro[n,o], Timon Buess[p], Meike Günter[q], Amanda M. Gardiner[a], Pascale Hatt[p], Geraldine Holdener[p], Giulia Jacober[r], Sabrina Kobelt[p], Sheldon Masseraz[s], Ian Mehli[t], Sarah Reiff[u], Eva Rigendinger[v], Mimo Ruckstuhl[p], Santana Schneider[p], Clarissa Seige[p], Nathalie Senn[w], Valeria Staccoli[p], Jessica Baumann[s], Livio Flüeler, Lino J. Guevara[d], Esin Ickin[s], Kimberley C. Kissling[a], Janis Rogenmoser[x], Dominik Spitznagel[a], Jaime A. Villafaña[y,z], Chiara Zanatta[a]

[a]Department of Paleontology, University of Zurich, Zurich, Switzerland
[b]Department of Biosciences, Swansea University, Swansea, UK
[c]Department of Earth and Environmental Sciences, Ludwig-Maximilians-Universität München, Munich, Germany
[d]GeoBio-Center, Ludwig-Maximilians-Universität München, Munich, Germany
[e]Facultad de Ciencias Naturales and Grupo de Investigación Paleontología Neotropical Tradicional y Molecular (PaleoNeo), University of Rosario, Bogotá, Colombia
[f]Field Museum of Natural History, Chicago, Illinois, USA
[g]Smithsonian Tropical Research Institute, Balboa, Panama
[h]Redpath Museum, Biology Department, McGill University, Montréal, Canada
[i]Centro de Investigaciones Paleontológicas, Villa de Leyva, Boyacá, Colombia
[j]Grupo de Investigación Biología para la Conservación, Universidad Pedagógica y Tecnológica de Colombia, Boyacá, Colombia
[k]Department of Earth Sciences, University of Cambridge, Cambridge, UK
[l]Museum of Zoology, University of Cambridge, Cambridge, UK
[m]Fossil Reptiles, Amphibians and Birds Section, Natural History Museum, London, UK
[n]Centro de Investigación y Avance de la Historia Natural de Atacama (CIAHN), Caldera, Chile
[o]Department of Paleobiology, National Museum of Natural History, Smithsonian Institution, Washington, D.C., USA
[p]Faculty of Science, University of Zurich, Zurich, Switzerland
[q]Department of Evolutionary Anthropology, University of Zurich, Zurich, Switzerland
[r]Department of Evolutionary Medicine, Universiy of Zurich, Zurich, Switzerland
[s]Department of Evolutionary Biology and Environmental Studies, University of Zurich, Zurich, Switzerland
[t]Department of Environmental Systems Science, ETH, Zurich, Switzerland
[u]Department of Systematic and Evolutionary Botany, University of Zurich, Zurich, Switzerland
[v]Department of Biology, ETH, Zurich, Switzerland
[w]Tissue Biology Research Unit, Department of Surgery, University Children's Hospital, Zurich, Switzerland

Functional diversity of sharks through time: past, present and future

*Institute of Medical Microbiology, University of Zurich, Zurich, Switzerland
*Laboratorio de Paleobiología, Centro de Estudios Avanzados en Zonas Áridas (CEAZA), Coquimbo, Chile
*Centro de Investigación en Recursos Naturales y Sustentabilidad, Universidad Bernardo O'Higgins, Santiago, Chile

*These authors contributed equally

Corresponding author: Catalina Pimiento; ███████████████████████

Abstract

The modern marine megafauna is known to play important ecological roles and includes many charismatic species that have drawn the attention of both the scientific community and the public. However, the *extinct* marine megafauna has never been assessed as a whole, nor has it been defined in deep-time. Here, we review the literature to define and list the species that constitute the *extinct* marine megafauna, and to explore biological and ecological patterns throughout the Phanerozoic. We propose a size cut-off of 1 m of length to define the extinct marine megafauna. Based on this definition, we list 706 taxa belonging to eight main groups. We found that the extinct marine megafauna was conspicuous over the Phanerozoic and ubiquitous across all geological eras and periods, with the Mesozoic, especially the Cretaceous, having the greatest number of taxa. Marine reptiles include the largest size recorded (21 m; *Shonisaurus sikanniensis*) and contain the highest number of extinct marine megafaunal taxa. This contrasts with today's assemblage, where marine animals achieve sizes of over 30 m. The extinct marine megafaunal taxa were found to be well-represented in the Paleobiology Database, but not better sampled than their smaller counterparts. Among the extinct marine megafauna, there appears to be an overall increase in body size through time. Most extinct megafaunal taxa were inferred to be macropredators preferentially living in coastal environments. Across the Phanerozoic, megafaunal species had similar extinction risks as smaller species, in stark contrast to modern oceans where the large species are most affected by human perturbations. Our work represents a first step towards a better understanding of the marine megafauna that lived in the geological past. However, more work is required to expand our list of taxa and their traits so that we can obtain a more complete picture of their ecology and evolution.

Impact statement

Given their exceptional size, the marine megafauna plays key ecological roles in modern ecosystems. Although large animals are known from the fossil record, including many charismatic species, the marine megafauna of the past has never been defined or described before. Here, we propose a definition for the marine megafauna that can be applied to the fossil record. Based on this definition, we review the paleontological literature and list the taxa that constitute the *extinct* marine megafauna throughout the Phanerozoic, to then do a first exploration of their ecological and evolutionary patterns over time. Our findings reveal that the extinct marine megafauna is dominated by reptiles, in great contrast with today's assemblage in which reptiles are a minority. The Mesozoic stands out for hosting over 50% of the extinct marine megafauna, and the largest body size recorded in the past: 21 m. Like today's assemblage, most extinct marine megafauna are coastal macropredators. Our work represents a first step towards a better understanding of the extinct marine megafauna and a baseline to inspire further work on this remarkable group.

Introduction

Today, the global marine megafauna includes all freely moving animals of over 45 kg that inhabit coastal and ocean habitats, excluding colonial reef-forming scleractinian corals (Estes et al. 2016). They contain representatives of numerous taxonomic groups, including invertebrates, bony fishes, cartilaginous fishes (hereafter, chondrichthyans), reptiles, seabirds and mammals. Collectively, these animals play important roles in marine systems, including nutrient transportation and storage, top-down population control, biochemical cycling, connecting oceanic ecosystems, and shaping and altering habitats (Estes et al. 2016; Malhi et al. 2016; Tavares et al. 2019). This fauna largely comprises the survivors of a global extinction event that took place around 3 million years ago, which resulted in the loss of one third of megafauna genera, and around 17% of their functional diversity (Pimiento et al. 2017). At least 40% of the extant marine megafauna are currently under threat due to multiple human impacts (Pimiento et al. 2020).

Because the profound influence that the marine megafauna has on ecosystems is mostly due to their large size, the definition of 'marine megafauna' is size-based (Estes et al. 2016). The size cut-off to define this fauna is derived from the fossil record, particularly on elevated extinction rates among large terrestrial mammals (>45 kg) during the Pleistocene (Lyons et al. 2004). However, applying this 45 kg cut-off to extinct animals is problematic, as the body masses of many fossil taxa are unknown because of the inherent incompleteness of the geological record, especially over deep timescales. This problem is exacerbated by the polyphyletic nature of this marine faunal assemblage, whereby body size estimates are markedly different between body plans, resulting in heterogeneous size measures (e.g., total length, diameter, etc.). As a result, previous paleontological works on 'marine megafauna' have not used a body-size-based definition, and instead, have included available representatives of marine mammals, marine turtles, seabirds, and chondrichthyans (Dominici et al. 2018; Pimiento et al. 2017). Therefore, a definition of marine megafauna that can be applicable to the fossil record is not yet in use.

Why do we need to define the extinct marine megafauna? Large marine animals are prevalent in the fossil record and include many charismatic extinct species that draw the attention of the scientific community and the public. The fossils of many large extinct species suggest they likely played important roles in ancient marine ecosystems, with their extinctions having a considerable impact on the evolution of major marine clades. For example, the giant extinct

shark *Otodus megalodon* has been proposed to have transported nutrients across oceans, controlled the population of their prey, and potentially influenced the evolution of gigantism in cetaceans (Cooper et al. 2022; Pimiento and Clements 2014; Pyenson and Sponberg 2011). Hence, large-bodied extinct species likely play important ecological roles in ecosystems collectively and through deep timescales. However, to better understand the extinct marine megafauna, as well as their impact on maintaining ecosystems and evolutionary processes, it is fundamental to first distinguish them from other animal species. To do so, a body size definition applicable across clades is required.

Here, we propose a body size cut-off of 1 m of length to define the *extinct* marine megafauna. This definition is based on the fact that members of the extant marine megafauna are, in addition to being >45 kg, also ≥ 1 m when length is considered. For example, the smallest megafauna species today are the sea otter (*Enhydra lutris*), the emperor penguin (*Aptenodytes forsteri*) and the common ling (*Molva molva*), all of which can reach body lengths in excess of 1 m (Estes et al. 2016; Pimiento et al. 2020). Although this definition is arbitrary and might not be universally applicable, it allows us to focus on a set of extinct taxa as a first step towards reaching a better understanding of the marine megafauna that lived in the geological past. We use length instead of other measurements such as mass to ensure the inclusion of as many extinct species as possible from the available literature, while also avoiding the introduction of biases and uncertainties in body mass calculations for extinct taxa.

The purpose of this review is to describe the diversity of *extinct* marine megafauna over the Phanerozoic. To do so, we reviewed the scientific literature for all known records of extinct marine animals equal to or over 1 m in length. Following Estes et al. (2016), we exclude colonial-forming organisms and include taxa occurring in coastal and open oceans, which contain semi-aquatic animals (e.g. pinnipeds, sea turtles and sea birds). We use the data extracted from the literature to investigate patterns related to the ecology and extinction throughout the Phanerozoic.

Literature review

Data were gathered via a joint effort of experts on different taxonomic groups, and the students enrolled in the Marine Megafauna through Deep Time course (BIO 263) at the University of Zurich in autumn semester of 2022. A list of extinct animals considered to be exceptionally

large in their respective taxonomic groups was first compiled by experts (see author contributions). These lists were divided among student groups, each working on one of the following taxonomic groups: invertebrates; jawless fishes, placoderms, and bony fishes; chondrichthyans; reptiles (including birds); and marine mammals. The students were tasked with collecting relevant information for each animal on the list, which was then expanded by searching for additional taxa using Google Scholar (https://scholar.google.com) or specific journal websites using a variety of key words, such as "giant", "large", "fossil", "extinct", "marine" in addition to key words relevant to each taxonomic group.

Five categories of information were collected – taxonomy, age range, maximum size reported, type of size measurement, and ecology (see below). Any taxon identified to taxonomic ranks above genus, or for which body size was unknown, was excluded. All data gathered for taxa identified to genus-level was collected based on described specimens (e.g., the age of *Ptychodus* sp. is based on the specimen from which the maximum size was gathered). As such, genus-level taxa in our dataset do not represents entire genera but the specimen from which maximum size was gathered (e.g., the *Ptychodus* sp. entry does not represent the entire *Ptychodus* genus). Taxon age-ranges were obtained from literature and from the Paleobiology Database (https://paleobiodb.org, hereafter, PBDB), with the oldest and youngest record of each taxon entered to the best available resolution. All dataand sources are included in Data S1.

Body size data obtained from the literature were inferred from fossil specimens, with many of the values reported being estimates from scaling equations based on specific body parts, [e.g., hind limb bone length in birds, or tooth size in sharks (Jadwiszczak 2001; Perez et al. 2021)]. All body size data collected pertains to length, which in most cases, refers to the size from the tip of the head to the end of the body. However, length estimates were different for some taxonomic groups (Table 1). For example, in invertebrates and marine turtles, length was often directly measured from fossil remains representing the majority of the animal's body, such as column length, shell diameters, maximum shell size and carapace lengths (Ifrim et al. 2021; Weems and Sanders 2014). Fish body sizes were inferred using three types of length measurements– total length, standard length and fork length (see definitions in Table 1). In sea birds, length was inferred in terms of total swimming length or standing height (Table 1). In a few exceptional cases in marine reptiles, trunk length was used as a proxy (~ raw total length) of body size. Although these specific taxa likely reached sizes much larger than their relative

trunk length, we consider that including these data adds to the analysis despite the limited availability of total length data in published datasets. All the references used to collect size data are included in Data S1. The lack of standardisation across measurements likely introduces significant noise to our comparisons across taxonomic groups. Nevertheless, they provide a faithful representation of the literature and therefore, the current state of knowledge for the different taxa.

The ecological information collected follows previous works (Paillard et al. 2021; Pimiento et al. 2019; Pimiento et al. 2017; Pimiento et al. 2020) and includes:

1. Guild, i.e., most common feeding mechanism:

   - Macropredator, i.e., feeding mostly upon macroscopic organisms
   - Micropredator, i.e., planktivorous
   - Herbivore, i.e., feeding on plants

2. Vertical position, i.e., position in the water column where animals feed:

   - Benthic, i.e., bottom on the ocean
   - Pelagic, i.e., along the water column
   - Benthopelagic

3. Habitat, i.e., lateral position where they live:

   - Coastal, i.e., continental shelf, usually above 200 m of depth
   - Oceanic, i.e., open ocean, usually below 200 m of depth
   - Coastal and oceanic

We were able to collect inferred ecological data for most extinct megafaunal taxa. However, around 5% of taxa are missing guild data; 24% are missing data on vertical position, and 23% on habitat. Using a logistic regression approach to test for systematic missing values, we found no indication that missing data is non-randomly distributed (with $p < 0.01$ for all three traits). Invertebrates and birds are the only taxonomic groups without missing ecological data. Notably, among marine reptiles, 42% have unknown vertical positions and 35% lack habitat information. Unsurprisingly, Cenozoic taxa have more complete data overall than taxa from

older time intervals (Data S1). After data collection, the dataset was reviewed by experts to ensure validity of the data entries.

Our literature review reveals 706 extinct marine megafaunal taxa (defined here as extinct animals equal or exceeding 1 m of body length; Data S1) belonging to the following taxonomic groups: invertebrates (7% of the total megafauna diversity); jawless fishes (0.7%), placoderms (7%), bony fishes (17%), chondrichthyans (12%); marine reptiles (38%); seabirds (2%); and marine mammals (17%). Most of the extinct marine megafauna taxa are identified to species level (93%). The earliest marine megafauna species are the 1 m long *Anomalocaris canadensis* and *Amplectobelua symbrachiata* from the Cambrian (Cong et al. 2017; Daley and Budd 2010; Daley and Edgecombe 2014; Fig. 1). The largest size attained by any extinct marine megafauna sampled was 21 m by *Shonisaurus sikanniensis*, an oceanic, pelagic, macropredatory ichthyosaur from the Upper Triassic (Nicholls and Manabe 2004; Fig. 1). It is worth noting that this maximum size, despite being remarkable, remains at least 10 m smaller than the maximum size achieved by the largest marine animals in today's ocean, the 31 m blue whale and the 36.6 m Lion's Mane Jellyfish (McClain et al. 2015). The second largest size was found to be 20 m, reached by three species: *Otodus megalodon* (Perez et al. 2021), a coastal, macropredatory, pelagic shark from the Neogene (Pimiento et al. 2016); by *Basilosaurus cetoides*, a Paleogene archaeocete with pelagic, coastal/oceanic habits (Swift and Barnes 1996; Voss et al. 2019); and *Perucetus colossus*, a coastal, benthic and presumably macropredatory early whale from the Eocene (Fig. 1; Bianucci et al. 2023). The next largest size was 18 m, reached by the pelagic macroraptorial sperm whale *Livyatan melvillei* from the Miocene, by *Cymbospondylus youngorum,* a pelagic, oceanic macropredatory ichthyosaur from the Middle Triassic (Lambert et al. 2010; Sander et al. 2021; Voss et al. 2019), and by *Basilosaurus isis*, a pelagic macropredator with coastal/oceanic habits (Pyenson 2017; Voss et al. 2019). The largest bony fish was *Leedsichthys problematicus* (16.5 m; 4th largest size; a pelagic, oceanic micropredator) and the largest invertebrate was *Seirocrinus subangularis,* a 15 m crinoid (5th largest size; a coastal, pelagic micropredator), both from the Jurassic (Fig. 1; Friedman et al. 2010; Hagdorn 2016; Liston and Gendry 2015; Liston et al. 2013). The largest placoderm was the 8 m *Glyptaspis verrucosa* from the Devonian, a benthic macropredator (Fig. 1; Boylan and Murphy 1978; Sallan and Galimberti 2015). Birds and jawless fishes occupy the lowest spectrum of body size ranges, with the largest maximum size being 2 m, which is reached by three penguins from the Eocene: *Anthropornis* sp., *Palaeeudyptes klekowskii* and

Anthropornis nordenskjoeldi (Bargo and Reguero 1998; Hospitaleche 2014; Jadwiszczak 2001; Marples 1953; Reguero et al. 2012; Stilwell and Zinsmeister 1992); and two coastal micropredatory jawless fishes from the Devonian: *Pyconosteus* sp. and *Tartuosteus* sp. (Fig. 1; Blieck et al. 2002; Mark-Kurik 2000; Moloshnikov 2001; Sallan and Galimberti 2015). It is worth noting that potentially larger seabirds are known, for example, the 160 kg *Kumimanu fordycei*, which has been proposed to be the largest-known fossil penguin (Ksepka et al. 2023). However, given the lack of body length measurements available for this and potentially other birds, it was not included in our dataset.

Representation in the Paleobiology Database

We assessed the current state of knowledge of the extinct megafauna taxa in the PBDB. Specifically, we quantified the number of occurrences of each taxon, both at the species and genus levels. To do so, we downloaded all occurrences from the PBDB while accounting for synonyms. This was achieved by contrasting identified *vs.* accepted names in the PBDB, thereby identifying the instances when megafauna taxa had multiple occurrences under different taxonomic names.

More than half of megafaunal taxa (523 taxa; 74%) are represented in the PBDB. Those identified to the genus level have 77% representation, whereas those identified to the species level have 74%. Around 28% of the extinct megafauna species only have one occurrence in the PBDB (i.e., singletons; Fig. 2A). Placoderms are the least represented taxonomic group in the PBDB, with only 15% of their taxa having an occurrence. All birds, 91% of marine mammals, and 89% of marine reptiles have at least one occurrence in the PBDB. Over half of all chondrichthyan, jawless fish and bony fish megafauna have PBDB occurrences (66%, 60%, 56% of their taxa, respectively; Fig. 2B). Chondrichthyan megafauna exhibit the highest number total of occurrences in the PBDB overall (1,800 total occurrences), with *Otodus megalodon* having the highest number of occurrences (n = 289; Fig. 2A).

It could be argued that the relatively high representation of the marine megafauna in the PBDB is due to their large size, which can increase detectability (Payne and Heim 2020). To assess whether the extinct marine megafauna was better sampled than the smaller counterpart (i.e., extinct non-megafauna of < 1 m, hereafter "baseline"), we quantified sampling rates (i.e., probability for a taxon to be sampled when present in a given time bin) for both groups. The

baseline group was assessed by downloading from the PBDB all species-level occurrences belonging to the genus of each megafaunal taxon but excluding the megafaunal species (> 1 m). Therefore, each baseline species was extinct and assumed to have a body length < 1 m. We then used a capture–mark–recapture (CMR) approach, whereby each species was marked as either present or absent for each Phanerozoic stage using the Cormack-Jolly-Seber model (Cormack 1964; Jolly 1965; Seber 1965) with Markov Chain Monte Carlo sampling. We found that the fossil record of megafauna species is not better sampled than that of smaller body-sized species of the same genera, as baseline species showed an average sampling completeness of 0.06 per stage (95% Credible Interval [hereafter CI] = 0.03, 0.09) and the marine megafauna sampling completeness was, on average, 0.03 per Stage (95% CI =0.02, 0.05; Fig. 2C).

The extinct marine megafauna through the Phanerozoic

Representatives of the extinct marine megafauna are found in all geological eras and periods. The Palaeozoic encompasses 20% of the total diversity, the Mesozoic 52%, and the Cenozoic 28% (Fig. 3A). Invertebrates, bony fishes, and chondrichthyans have extinct marine megafauna representation in all three eras; jawless fishes and placoderms are restricted to the Palaeozoic; non-avian reptile megafauna is only present in the Mesozoic and Cenozoic, and megafaunal representatives of seabirds and mammals are only present in the Cenozoic (Table 2; Fig. 3A). Around half of the extinct marine megafauna occur in the Cretaceous (26%) or Neogene (15%; Fig. 3A; Table 2). First Appearance Datums (FADs) and Last Appearance Datums (FADs) occur mostly in the Upper Cretaceous (20% of FADs, 21% of LADs) and the Miocene (13% of FADs, 11% of LADs; Table 3; Fig. 3B). Invertebrates, bony fishes and chondrichthyans range through all geological eras. Jawless fish and placoderms only range through the Devonian. Birds and mammals rane only through the Cenozoic, especially during the Eocene for birds, and the Miocene for marine mammals (Fig. 3B-C). Most extinct marine megafauna (84%) have a LAD and FAD in the same Epoch (Fig. 3C; Table 3). The mean stratigraphic range of the extinct marine megafauna is 3.5 million years (hereafter, myrs), with longest ranges being that of the shark *Cretalamna appendiculata* [Lower Cretaceous to Eocene, 82.6 myrs; Fig. 3C; (Albert et al. 2009; Andrews et al. 2005; Sallan and Coates 2010)]. Chondrichthyans, bony fishes and invertebrates are the taxonomic groups within the top 2.5% of taxa with the longest ranges (41 – 82.6 myrs; Fig. 3C; Data S2).

The maximum body size recorded for most extinct marine megafauna range between 1 m and 3 m, with sizes over 10 m being rare among all taxonomic groups (Fig. 4A). While the Mesozoic and Cenozoic display the full range of extinct megafauna sizes (1 – 21 m in the Mesozoic; 1 – 20 m in the Cenozoic), the Palaeozoic only displays half of the range, with the maximum size at up to 9 m [*Endoceras giganteum*, a cephalopod from the Ordovician; Fig. 4B; (Klug et al. 2015)]. Overall, maximum size appears to increase over time across all extinct marine megafauna taxa, with a 1.8% increase, on average, every million-year (95% CI = 1.3%, 2.2%, p < 0.001; black line Fig. 4B).

Palaeozoic

During the Cambrian, only two taxa were found to be categorised as megafauna following our definition: *Anomalocaris canadensis* and *Amplectobelua symbrachiata,* both reaching 1 m (Figs. 1, 4B; Cong et al. 2017; Daley and Budd 2010; Daley and Edgecombe 2014). During the Ordovician, the maximum body size for the entire Palaeozoic is reached (Fig. 4B) with the possibly up to 9 m long nautiloid *Endoceras giganteum* (Klug et al. 2015). Both the Cambrian and the Ordovician have only invertebrate megafauna (Figs. 3B-C, 4B). Fish megafauna first appear in the Silurian, with the 1 m lobefinned fish *Megamastax amblyodus* (Figs. 3C, 4B; Choo et al. 2014). The Devonian is dominated by placoderms, jawless fish and lobe-finned fish megafauna. This is the period when the first chondrichthyan megafauna appear, the largest being the 3 m *Cladoselache clarki* (Figs. 4B-C; Albert et al. 2009). The marine megafauna of the Palaeozoic was composed mostly by coastal, benthic macropredators (Fig. 5).

Mesozoic

Non-avian reptilian megafauna first appeared in the Mesozoic and are the most common taxonomic group of this era (Fig. 3B-C, 4B). During the first and shortest period of the Mesozoic, the Triassic, a remarkably 21-meter-long ichthyosaur attains the largest known body size of the Phanerozoic (*Shonisaurus sikanniensis*; Figs. 1, 4B). The Cretaceous, a transitional time in Earth's history, is the interval with the greatest number of extinct marine megafauna taxa (n = 182; Figs. 3C, 4B; Table 2). The presence of such a significant volume of megafauna could be related to the extent of epicontinental seas during this time (Barron 1983; Lagomarcino and Miller 2012) and possibly the development of higher trophic levels at the Mesozoic Marine Revolution (Cortés and Larsson 2023; Vermeij 1977). Invertebrates, bony fishes, chondrichthyans, and marine reptiles all have megafauna representatives across the

Mesozoic (Figs. 3B, 4C). The marine megafauna of the Mesozoic was significantly rich, mostly oceanic, with a large presence of pelagic macropredators (Fig. 5).

Cenozoic

During the Cenozoic, megafaunal mammals and seabirds first appeared. Although marine mammals seem to have been the dominant group (Fig. 3B), all marine megafauna taxonomic groups occur in the Cenozoic, except for jawless fishes and placoderms (Figs. 3-4). Chondrichthyans and marine mammals display the largest sizes of the Cenozoic (20 m), peaking in the Neogene (Fig. 4B). The Quaternary is the most taxon-depauperated interval, with only three extinct marine megafauna taxa occurring in this period, all of which are mammals: the Steller's sea cow (*Hydrodamalis gigas*, 7 m)*,* the otariid *Proterozetes* (6 m) and the odobenid *Oriensarctos* (3 m; Domning 1978; Mitchell 1968; Poust and Boessenecker 2017; Sarko et al. 2010)*.* The low diversity of the Quaternary is likely a sampling and/or preservation artifact, despite the extinction event of the Plio-Pleistocene (Pimiento et al. 2017), given that the fossil record of marine vertebrates seems to be particularly scarce during this time period (Pimiento and Benton 2020; Valenzuela-Toro and Pyenson 2019). In addition, edge effects might have artificially reduced Quaternary diversity (Alroy 1998; Foote 2000). The marine megafauna of the Cenozoic was mostly composed of coastal, pelagic macropredators (Fig. 5), a continuing ecological trend since the Mesozoic.

The extinct marine megafaunal groups

Invertebrates

The invertebrate marine megafauna was more common in the geological past than in the present (48 extinct species *vs*. 5 extant species; Data S1; Estes et al. 2016) despite the fact that their diversity might be underestimated due to the poor preservation of soft-body organisms in the fossil record. The scarcity of invertebrates in the modern assemblage might be a result of the mass-based definition in Estes et al. (2016). The extinct invertebrate marine megafauna occurs in all geological eras and includes molluscs, echinoderms, arthropods, and segmented worms (phyla Mollusca, Echinodermata, Arthropoda, and Annelida; Fig. 6). The greatest diversity of invertebrate megafauna taxa occurs in the Palaeozoic (Fig. 3A). Invertebrate megafauna taxa have sizes between 1 and 3 m, with the largest size reached at 15 m by an echinoderm in the Mesozoic (*Seirocrinus subangularis*; Figs. 1, 4A-B, 6B; Hagdorn 2016). This size is significantly smaller than that or the extant Lion's mane

jellyfish, which has been proposed to be 36.6 m long. However, this enormous size has not been confirmed (McClain et al. 2015). Arthropod and annelid megafauna is only present in the Palaeozoic, echinoderm megafauna only in the Mesozoic, and mollusc megafauna in all three eras (Fig. 6B). In general, body size increases over the Phanerozoic amongst the extinct invertebrate marine megafauna, with a 2.2% average increase every million-years (95% CI = 0.6%, 3.8%, p = 0.007; Fig. 4C). The extinct invertebrate megafauna taxa are coastal, occupy both benthic and pelagic environments, and include micro- and macropredators (Table 4; Fig. 5). Invertebrates are the ony group that contains sessile taxa, which belong to Bivalvia and Crinoidea.

Bony fishes

Extinct marine megafaunal bony fishes include 122 taxa (Data S1), which is comparable with the number of megafauna species today: 133 species (Estes et al. 2016). Both in the past and today, bony fishes represent one of the most species-rich marine megafaunal group (Figs. 3A). The extinct marine bony fish megafauna includes ray-finned fish (Actinopterygii) and lobed-finned fish (Sarcopterygii), although it is mostly represented by Actinopterygii (Fig. 6). The earliest bony fish megafaunal species appeared in the Silurian [*Megamastax amblyodus* (1 m); Figs. 3B-C, 4B; (Choo et al. 2014)]. Interestingly, the coelacanth *Latimeria chalumnae* is part of today's marine megafauna (Estes et al. 2016), despite marine sarcopterygians being absent from the Cenozoic megafauna assemblage (Fig. 6B). The highest number of megafaunal bony fish taxa lived in the Mesozoic (Fig. 3A), with the Cenozoic only having actinopterygian representatives (Fig. 6B). Most of the extinct bony fish megafauna were between 1 and 2 m (Fig. 4A), with the maximum body size at 16.5 m, reached by an actinopterygian in the Mesozoic (*Leedsichthys problematicus;* Figs. 4A-B; Liston et al. 2013). Fish body size does not display a trend over time (0.6% on average per million-year, p = 0.12; Fig. 4C). Extinct bony fish megafauna taxa were coastal or oceanic, pelagic macropredators (Table 4).

Jawless fishes and placoderms

Extinct marine megafaunal jawless fishes ('Agnatha') include five species, and are restricted to the Palaeozoic era, specifically the Devonian (Fig. 3). Jawless megafaunal fish reached a maximum body size of 2 m (*Pycnosteus* sp. and *Tartuosteus* sp.) and are coastal, benthic micropredators (Table 4, Fig. 5). There are no extant representatives of jawless fishes amongst the modern megafauna (Estes et al. 2016). Indeed, surviving lampreys and hagfishes rarely exceed 1 m in length (Froese and Pauly 2017). Armoured fishes, the extinct placoderms,

include 48 megafaunal species, all restricted to the Palaeozoic era, specifically the Devonian (Fig. 3B). They include the clades Arthrodira, Ptyctodontida, Antiarchi, Phylloepida and Rhenanida, with Arthrodira having the highest number of taxa (Fig. 6). Megafaunal placoderms were mostly 1 m of size, coastal, benthic and macropredators (Figs. 5, 7, Table 4). They reached a maximum body size of 8 m (*Glyptaspis verrucosa*; Fig. 1; Sallan and Galimberti 2015) and do not display a significant trend in body size over time (8% on average per million-year, p = 0.21; Fig. 4C).

Chondrichthyans

The extinct chondrichthyan marine megafauna includes spiny sharks (†Acanthodii), chimaeras (Holocephali), rays and skates (Batoidea), and sharks (Selachimorpha; Fig. 6). Overall, there are 81 chondrichthyan megafaunal taxa, the vast majority being represented by sharks (67%; Fig 6). This diversity is higher than today, when 69 chondrichthyan species are part of the global marine megafauna (Estes et al. 2016). Chondrichthyan marine megafauna ranged through the entire Phanerozoic (Fig. 3). However, the stem-chondrichthyan †Acanthodii is exclusively present in the Palaeozoic, Holocephali is present in both the Palaeozoic and Mesozoic, Batoidea in both the Mesozoic and Cenozoic (Fig. 6), and Selachii occurs in all three eras (Figs. 3A, 6B). Within the chondrichthyan extinct megafauna, body size appears to increase over time, with increases of 2.8% per million-year on average (95% CI = 1.6%, 4%, p < 0.001; Fig. 4C). The earliest chondrichthyan megafauna taxa appear in the Lower Devonian [*Machaeracanthus bohemicus* (2 m), *Machaeracanthus hunsrueckianum* (1.5 m), and *Machaeracanthu sulcatus* (1 m); Figs. 3B-C] and are all acanthodians (Botella et al. 2012; Sallan and Galimberti 2015; Südkamp and Burrow 2007). The largest known chondrichthyan species is the 20 m *Otodus megalodon*, a gigantic megatooth shark from the Cenozoic (Figs. 4A-B; Perez et al. 2021). Extinct chondrichthyan megafauna occupy all vertical positions and habitats and are mostly coastal, pelagic macropredators (Table 4, Figs. 5, 7).

Marine reptiles

Among the extinct marine megafauna, reptiles include early branching Archosauromorpha, Paracrocodylomorpha, †Ichthyosauromorpha (ichthyosaurs), Pantestudines (e.g., marine turtles), †Sauropterygia (plesiosaurs, placodonts and relatives), and Lepidosauruomorpha (specifically Squamata, i.e., mosasaurs and sea snakes). Overall, there are 266 extinct marine megafauna taxa that are reptiles, which makes them the group with highest number of taxa, most of them occurring in the Mesozoic and none in the Palaeozoic (Fig. 2A). This diversity is

much higher than that of today, as only seven non-avian reptilian species are part of the modern marine megafauna (Estes et al. 2016). Indeed, most reptilian marine megafauna clades are entirely extinct today (Fig. 6A). †Sauropterygia hold the highest number of reptilian marine megafauna taxa (Fig. 6A). †Sauropterygia, †Ichthyosauromorpha and early branching Archosauromorpha are absent from the Cenozoic (Fig. 6B). The earliest reptilian megafauna species appears in the Lower Triassic [*Utatsusaurus hataii* (2.6 m); *Sclerocormus parviceps* (1.6 m); Parvinatator wapitiensis (1 m)*; Grippia longirostris* (1 m); *Eretmorhipis carroldongi* (1 m); and *Corosaurus alcovensis* (1.6 m)] and the maximum size is reached in the Upper Triassic by the 21 m *Shonisaurus sikanniensis* (Fig. 4B; Motani 1996; Nicholls and Manabe 2004; Scheyer et al. 2014). This remarkable size is extreme, as other large-bodied ichthyosaurs such as *Cymbospondylus youngorum*, *Himalayasaurus tibetensis, Shonisaurus populais* and *Temnodontosaurus* sp. are estimated to have reached 18 m (*Cymbospondylus youngorum*) and 15 m, respectively. Most extinct reptilian megafauna are between 1 and 5 m (Fig. 4A), with body size appearing to increase over time, specifically displaying 4.3% increases, on average, every million-year (95% CI = 2.9%, 5.7%, p < 0.001; Fig. 4C). Representatives of the extinct non-avian reptilian megafauna are mostly oceanic, pelagic macropredators, although this is the group with most missing ecological data (Table 4, Figs. 5, 7).

Birds

Seabirds are the least rich group of extinct marine megafauna, with only 17 species reaching ≥1 m. This group is represented by a single order, Sphenisciformes (total-clade penguins), which are only present in the Cenozoic (Figs. 3A, 6B). The number of extinct seabirds is likely to be underrepresented under our definition of megafauna, as body mass, and not length, is usually used to size extinct birds (Field et al. 2013). Nevertheless, the past diversity of avian marine megafauna largely surpasses that of today, when only one seabird is part of the global assemblage (*Aptenodytes forsteri*; Estes et al. 2016). The earliest bird megafauna appeared in the Paleocene [*Crossvallia unienwillia* (1.4 m)*, Kumimanu biceae* (1.7 m) and *Waimanu manneringi* (1.2 m); Figs. 4B (Giovanardi et al. 2021; Mayr et al. 2017; Slack et al. 2006; Tambussi et al. 2005)]. All extinct avian megafauna is between 1 and 2 m (Fig. 4A), and are coastal, pelagic macropredators (Fig. 5A).

Mammals

There are 119 mammals that are part of the extinct marine megafauna, a diversity coincidently identical to today's mammalian marine megafauna (119 species; Estes et al. 2016; Pimiento et al. 2020). As such, marine mammals, which only occur in the Cenozoic, are the third richest taxonomic group of extinct marine megafauna after reptiles and bony fishes (Fig. 3A). Extinct marine megafaunal mammals include carnivores (Carnivora), cetaceans (Cetacea), desmostylians (†Desmostylia), sea cows (Sirenia) and xenarthrans (Xenarthra). Cetaceans and carnivorans display the greatest number of taxa (Fig. 6A). Most marine mammals that are part of the extinct marine megafauna range between 1 and 3 m in maximum body size (Fig. 4A), with the largest species being *Perucetus colossus* and *Basilosaurus cetoides*, both reaching 20 m in the Eocene, which is the earliest recorded age when marine megafaunal mammals first appeared (Figs. 1, 3B, 4B; Bianucci et al. 2023; Blanckenhorn 1900; Voss et al. 2019). The mammalian extinct marine megafauna showed no significant trend in size over time (-10.3% on average per million-year, p = 0.93; Fig. 4C) and were mostly coastal, pelagic macropredators (Figs. 5, 7).

The ecological roles of the extinct marine megafauna

The vast majority of extinct marine megafauna (from which guild data was collected) are macropredators (i.e., consuming macroscopic organisms; 88%), with all six major megafaunal groups having macropredatory representatives distributed throughout the entire Phanerozoic (Fig. 7A). Notably, macropredators include the taxa with extreme sizes (Fig. 7B), including the 21-m-long *Shonisaurus sikanniensis,* which despite not having teeth as adults, it has been inferred to feed upon cephalopods and fish, and to lack of filter-feeding structures (Motani 1996; Nicholls and Manabe 2004). Herbivory is the least common guild among extinct marine megafauna (3%) and is occupied by mammals no larger than 10 m in the Cenozoic (sirenians, desmostylians and xenanthras), and by a single 3 m non-avian reptile (*Atopodentatus unicus*) from the Triassic (Cheng et al. 2014). Thus, this guild is absent from the Palaeozoic (Figs. 5A, 7). Micropredators (i.e., planktivorous) represent 9% of the extinctmarine megafauna diversity, include representatives from all taxonomic groups, except birds and reptiles, and are distributed throughout the entire Phanerozoic (Figs. 5A, 7). While micropredators are not common amongst the most extreme sizes, there are some large (>10 m) representatives, including the bony fish *Leedsichthys problematicus* (16.5 m; Jurassic Friedman et al. 2010; Liston et al. 2013), the crinoid *Seirocrinus subangularis* (15 m; Jurassic; Hagdorn 2016; Zmarzly 1985) and the cetacean *Pelocetus* sp. (12 m; Neogene; Fig.

7B; Bisconti et al. 2021; Coombs et al. 2022). Nevertheless, unlike the present time when the largest sizes are reached by micropredators (e.g., baleen whales; 30 m; Estes et al. 2016; Goldbogen et al. 2019), in the deep time, the largest sizes were reached by macropredators (20-21 m; *S. sikanninesis*, *Otodus megalodon*, *Perucetus colossus* and *Basilosaurus cetoides*; Nicolls and Manabe 2004; Perez et al. 2021; Voss et al. 2019].

Over 54% of the extinct marine megafauna (from which vertical position data was collected) is exclusively pelagic (i.e., feeding along the water column), with this vertical position being present throughout the Phanerozoic and across all sizes (Figs. 5B, 7). Exclusively benthic taxa (i.e., feeding on the bottom of the ocean) comprise 17% of the diversity, which is spread out across the Phanerozoic. The largest exclusively benthic representatives are the cetacean *Perucetus colossus* (20 m; Bianucci et al. 2023) and the placoderm *Glyptaspis verrucosa* (8 m; Boylan and Murphy 1978; Sallan and Galimberti 2015). Benthopelagic taxa comprise only 6% of the total diversity and are mostly represented by chondrichthyans and mammals, with reptiles and bony fishes having one benthopelagic taxon each (Fig. 7A). This vertical position is largely absent from the Palaeozoic assemblage, with only one taxon from the Devonian being benthopelagic (*Cladoselache clarki*; Fig. 5A).

Around half of the extinct marine megafauna (from which habitat data was collected) lived in coastal environments (i.e., along the continental shelf, usually < 200 m of depth; 44% exclusively coastal), with this habitat being represented in all taxonomic groups (Figs. 5C, 7A). Although this might be a result of near-shore environments being better preserved than oceanic habitats in the fossil record (Dominici et al. 2018), shallow-waters are also considered a cradle of evolution likely supporting great biodiversity both in deep time and today, especially for the marine megafauna (Pimiento 2018; Pimiento et al. 2017; Pimiento et al. 2020; Sallan et al. 2018). Oceanic megafauna (i.e., exclusively living in the open ocean; usually > 200 m of depth) represents 26% of the total diversity, includes all taxonomic groups but jawless fishes and birds, and the largest currently known extinct marine taxon of the Phanerozoic (*S. sikanniensis*, 21 m; Figs. 5, 7). However, the next largest sizes occur in other habitats (*O. megalodon,* 20 m, coastal; *B. cetoides* 20 m, coastal/oceanic; and *P. colossus* 20 m, coastal; Fig. 7B). Only 7% of the extinct marine megafauna lived in both coastal and oceanic habitats and include a variety of bony fishes, chondrichthyans, reptiles and mammals (Fig. 7A).

Overall, the extinct marine megafauna was mostly macropredatory, living in coastal habitats and feeding in the water column (i.e., 'pelagic'; Fig. 7A). This is similar to the modern assemblage, except that most modern megafaunal species are benthic (Pimiento et al. 2020). However, our results, especially the lack of benthopelagic and coastal/oceanic ecologies, likely represent an artifact given the number of missing ecological data, especially in marine reptiles which is the most species-rich group of the extinct assemblage.

Were marine megafaunal species more prone to extinction than smaller species?

Today, large-bodied marine species are more vulnerable to extinction than smaller species (Harnik et al. 2012; McCauley et al. 2015; Olden et al. 2007; Payne et al. 2016). Using the novel dataset collected for this study, we tested whether this was the case in the geological past by modelling extinction risk in marine megafauna and comparing it with that of baseline species. To do this, we used occurrences downloaded from the PBDB at the species level (see above). We identified the FADs and LADs for each megafauna and baseline taxon, which we then binned into geological stages (Gradstein et al. 2020). Taxa confined to a single stage were excluded as they tend to produce undesirable distortions of the fossil record (Foote 2000). We then modelled the extinction risk for each taxon using a hierarchical Bayesian generalized model with a binomial family link using the *brms* R package (Bürkner 2017). The LAD of each taxon was coded as "extinction" and occurrences in geologic stages between FADs and the LADs as "survival". As such, this approach assumes FADs and LADs are equivalent to species' origination and extinction times. We regressed this binomial extinction/survival response against the group identity (i.e., megafauna *vs.* baseline) allowing for a mixed effect trend, thereby estimating the average extinction risk for each group in every time interval. We also allowed this average extinction risk to vary between taxonomic groups by setting a random effect. We used flat priors on each parameter as the amount of data was high (3.055 extinction/ survival responses), allowing the likelihood to dominate the posterior samples.

We found the extinction risk of species belonging to megafauna to be similar to that of baseline species (Fig. 8A), in agreement with a previous study at genus level (Payne and Heim 2020). Specifically, the baseline group showed an average extinction risk of 36.8% (95% CI = 25%, 51%) across all geological stages, while megafauna species had an average extinction risk of 36.5% (95% CI = 17%, 56%). This result is robust across all studied taxonomic groups; however, baseline birds and chondrichthyans showed slightly higher extinction risk than

250

megafauna taxa (birds = 2.4% higher risk, 95% CI = 2%, 5%; chondrichthyans = 8% higher risk. 95% CI = 6%, 9%). We found this signal of equal risk for megafauna and baseline taxa to be robust across the whole Phanerozoic (Fig. 8B). Our findings are unlikely to be biased by size-based sampling differences (Payne and Heim 2020), as our capture-mark-recapture analyses indicate that the fossil record for megafauna species is not more complete compared to baseline species (Fig. 2C). Overall, our results from the geological past contrast with the present time where marine megafauna is particularly at risk (Dulvy et al. 2014; Dulvy et al. 2003; Dulvy et al. 2017; McCauley et al. 2015; Pacoureau et al. 2021; Payne et al. 2016), further supporting the idea that the extinction drivers acting over deep-time are different to those acting in the Anthropocene (Harnik et al. 2012; Payne et al. 2016).

It is worth noting, however, that our results are not conclusive because: a) the FADs and LADs do not necessarily indicate true times of origination and extinction (Silvestro et al. 2014a; Silvestro et al. 2014b), and b) our occurrence data from PBDB does not represent a comprehensive account of all known occurrences of the marine fauna of the Phanerozoic. Still, our work is the first to explicitly define marine megafauna in geological time and assemble a comprehensive dataset of megafauna taxa. While preliminary, our findings provide a first step towards elucidating the potential differences between the extinction mechanisms of megafauna and non-megafauna (baseline) species.

Concluding remarks and future directions

We defined the marine megafauna in deep time and listed 706 extinct taxa based on an exhaustive literature review. The extinct marine megafauna is fairly well-represented in the PBDB; however, our resampling analyses suggest that they are not better known in the paleontological literature than their smaller counterparts (Fig. 2). Overall, the extinct marine megafauna is dominated by reptiles, as they represent one quarter of total diversity and includes the largest species (Figs. 1-3). This finding contrasts with today's assemblage, in which marine reptiles are a minority and occupy the small end of the body size distribution (Estes et al. 2016; Pimiento et al. 2020). The Mesozoic era (a.k.a., the 'Age of Reptiles') stands out for hosting over 40% of the extinct megafaunal taxa, and the largest body size (*Shonisaurus sikanniensis,* 21 m; Figs. 1-4). However, body size among the extinct marine megafauna tends to increase over time across the Phanerozoic, with iconic gigantic sharks and cetaceans in the Neogene, including *Otodus megalodon*, *Perucetus colossus*, *Basilosaurus*

cetoides and *Livyatan melvillei* (Figs. 1, 4). Similar to the modern assemblage, most extinct marine megafauna are coastal macropredators (Figs 5, 7). Unlike today (Dulvy et al. 2003; Dulvy et al. 2014; Dulvy et al. 2017; McCauley et al. 2015; Pacoureau et al. 2021; Payne et al. 2016), the marine megafauna from the past does not seem to have higher extinction risk than their smaller counterparts (Fig. 8). However, these results are preliminary and more comprehensive examinations are warranted to assess shifts in extinction risk through geologic time.

Although our list of extinct marine megafaunal taxa is comprehensive for the most part, temnospondyl amphibians are yet to be included and, despite our efforts, the list of bony fishes is likely missing some species. To gain a better understanding of the extinction mechanisms influencing the marine megafauna throughout geological history, it is fundamental to compile a comprehensive occurrence dataset of all extinct marine megafauna taxa so that accurate times of origination and extinction can be estimated (Silvestro et al. 2014b). Importantly, to improve our knowledge regarding body-size patterns and the ecological roles of the extinct marine megafauna over the Phanerozoic, it is essential to fill the gaps in our current dataset, particularly in terms of the habitat and vertical position in the water column of many anatomically diverse taxa, such as marine reptiles (Fig. 5). Expanding our understanding of taphonomic processes and biases of the extinct marine megafauna is therefore critical to strengthening our ecological interpretations. Other life-history and ecological traits such as metabolism (e.g., thermoregulation capabilities) and reproductive strategies could further provide a more complete picture of the functional diversity of the marine megafauna through deep time. A better-informed picture of what constitutes megafauna in deep time and its macroevolutionary patterns can be achieved by the standardization of the array of measurements reported in the literature (e.g., biovolume (Payne et al. 2009), and by using and/or adopting methodologies that consider parameters such as lateral body surface area to provide better proxies for body size.

Author contributions Statement

CP designed the study, performed exploratory analyses and led the writing. KK coordinated the data gathering and collected data. GHM analysed the data and created figures with input from CP. TA, EAC, JAC, DC, DF, CK, KK, TMS and AVT (clade experts) collected the initial

set of data and checked student-collected data. KK, GHM, JAC, AMG, EI and DS collated ecological data. TB, MG, AMG, PH, GJ, SK, SM, IM, SR, ER, MR, SS, CS, NS, VS (the students) collected additional data from literature. JB, JR and JAV checked and harmonized the student-collected data. EI, KCK, JR, DS and CZ filled data gaps. LF and LJG curated and harmonized the references. KK, GHM, TA, EAC, DC, DF, CK, TMS and AVT provided input on different versions of this manuscript.

Conflict of Interest Statement

The authors declare no conflict of interest.

Data availability Statement

The data collected in this study is included as Supplementary Material (Data S1). All code used to conduct the analyses of this work are available at https://github.com/Pimiento-Research-Group/marine_megafauna_extinction. This is the Paleobiology Database publication number 489.

Table 1. Types of body size measurements in each taxonomic group.

Taxonomic group	Abbreviation	Size measurement	Explanation
Fishes	SL	Standard length	Length from the tip of the longest jaw to the end of the caudal peduncle (at the base of the caudal fin)
	TL	Total length	Length from the tip of the longest jaw to the tip of the caudal fin
	FL	Fork length	Length from the tip of the snout to the end of the posterior junction of the two caudal fin lobes
Invertebrates	BL	Body length	Length of the entire body, specifics might differ for different taxa
	MSL	Maximum shell length	Estimated from partially preserved shell fragments of cephalopods (see Klug et al. 2014)
	D	Diameter	Diameter of a bivalve or ammonoid shell
	CL	Column length	Length of the stalk of a crinoid
Birds	TL	Total length	Measured from the head to the distal edge of the ulnar condyle (See Table 1. in Ksepka and Clarke, 2010)
	SH	Standing height	Measured from the top of the head to the heel
	SL	Swimming length	Measured from the tip of the beak to the tip of the hind lib (see Fig 1. in Clarke et al. 2010)
Reptiles	TL	Total length	Length of the entire body, specifics might differ for different taxa
	CPL	Carapace length	Straight length of the carapace of a turtle measured from the anterior point at mid-line to the posterior tip of the carapace
	TKL	Trunk length	Length of the trunk, used in the absence of full body size measurement availability
Chondrichthyans	TL	Total length	Measured from the tip of the snout to tip of the caudal fin
Mammals	TL	Total length	Measured from the tip of the head to the tip of the tail or hind limbs

Table 2. Extinct marine megafauna across geological periods.

Functional diversity of sharks through time: past, present and future

Era	Period	Taxa count	Percentage (%)
Paleozoic	Cambrian	2	0.283
	Ordovician	7	0.990
	Silurian	12	1.697
Mesozoic	Devonian	92	13.013
	Carboniferous	18	2.546
	Permian	7	0.990
	Triassic	81	11.457
	Jurassic	104	14.710
	Cretaceous	182	25.743
Cenozoic	Paleogene	89	12.588
	Neogene	109	15.417
	Quaternary	3	0.424

Table 3. First appearance datums (FADs) and last appearance datums (LADs) of extinct marine megafauna per geological epoch.

Epoch	Proportion of FADs (%)	Proportion of LADs (%)
Upper Ediacaran	0	0
Terreneuvian	0	0
Series 2	0	0
Maolingian	0.3	0.3
Furongian	0	0
Lower Ordovician	0.1	0.1
Middle Ordovician	0.3	0.3
Upper Ordovician	0.6	0.6
Llandovery	0.1	0
Wenlock	0.6	0.6
Ludlow	0.4	0.4
Pridoli	0.6	0.6
Lower Devonian	3.5	2.9
Middle Devonian	4.7	3.8
Upper Devonian	4.8	5.9
Mississippian	2.3	1.9
Pennsylvanian	0.3	0.9
Cisuralian	0.6	0.3
Guadalupian	0	0
Lopingian	0.4	0.4
Lower Triassic	2.1	1.9
Middle Triassic	6.9	5.9
Upper Triassic	2.5	3.5
Lower Jurassic	6.9	7.1
Middle Jurassic	3.1	1.7
Upper Jurassic	4.7	5.7
Lower Cretaceous	5.4	4.4
Upper Cretaceous	20.4	21.4
Paleocene	2.8	2.4
Eocene	4.9	4.9
Oligocene	4.7	3.5
Miocene	12.4	10.6
Pliocene	3.1	6.1
Pleistocene	0.4	1.3
Holocene	0	0

Table 4. Ecological traits across the taxonomic groups of extinct marine megafauna. Bold denotes highest values per trait.

|	Invertebrates	Bony fishes	Jawless fishes	Placoderms	Chondrichthyans	Non-avian reptiles	Birds	Mammals
Macropredator	**34**	**102**	0	**35**	66	**254**	17	80
Micropredator	14	10	**4**	2	11	0	0	17
Herbivore	0	0	0	0	0	1	0	22
Missing	0	10	1	11	4	11	0	0
Pelagic	23	**79**	1	10	**46**	**145**	17	59
Benthic	**25**	21	**3**	16	10	9	0	34
Benthopelagic	0	1	0	0	15	1	0	22
Missing	0	21	1	**22**	10	111	0	4
Coastal	**42**	49	**4**	17	37	69	17	74
Coastal/Oceanic	0	2	0	0	14	2	0	34
Oceanic	6	**48**	0	2	19	**104**	0	5
Missing	0	23	1	**29**	11	91	0	6
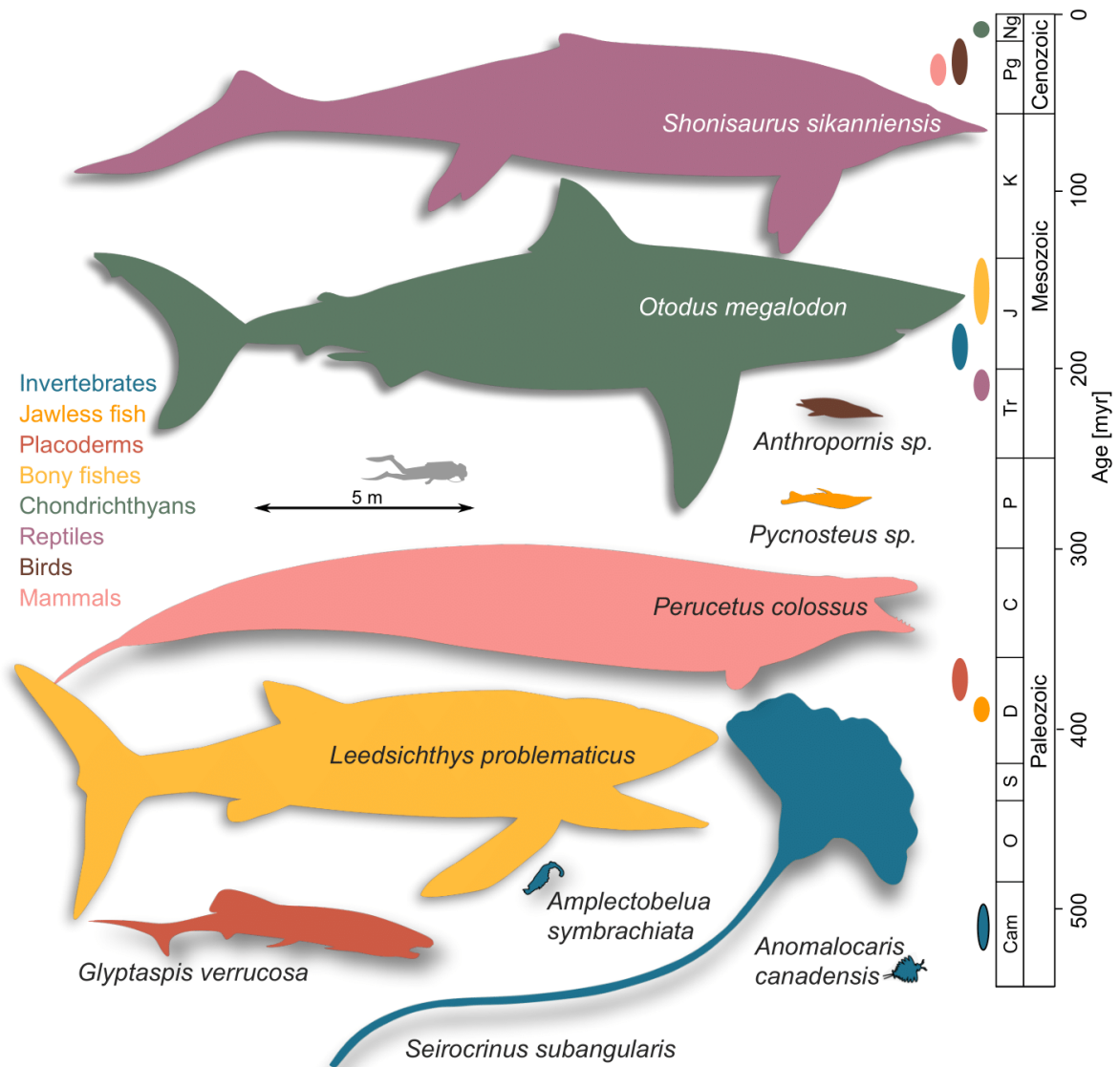
Figure 1. A graphical representation of the earliest and largest extinct marine megafaunal taxa. Colours denote the taxonomic group to which each taxon belongs to, which is also used in the geological timescale on the right to denote stratigraphic range. Animal shapes were downloaded from www.phylopic.org. Credits are as follows: *Shonisaurus sikanniensis* and *Leedsichthys problematicus*: Gareth Monger; *Otodus megalodon*: T. Michael Keesey; *Perucetus colossus*: Michael Tripoli. Remaining animal shapes have a Public Domain license without copyright (http://creativecommons.org/licenses/by/3.0).
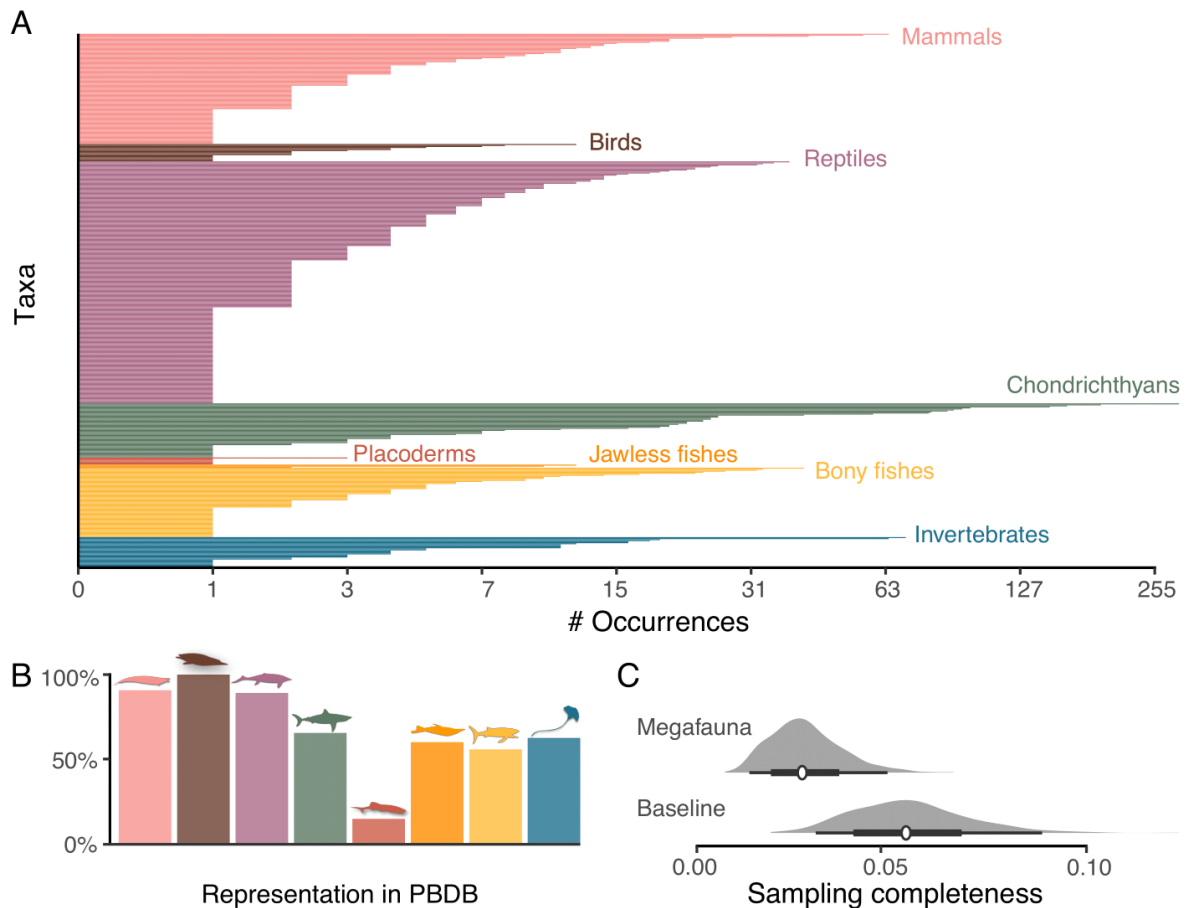
Figure 2. Representation of extinct marine megafauna in the Paleobiology Database (PBDB) to capture their current state of knowledge. (A) Number of occurrences of each taxon. Each horizontal line (n = 523) represents a taxon (see text). X-axis is log-transformed. (B) Representation of taxonomic groups in PBDB showed as percentages relative to total number of megafaunal taxa in each group. Colours denote the taxonomic group to which each taxon belongs to in A and B. Animal shapes in B are those from Fig. 1. (C) Sampling completeness rates for the extinct marine megafauna and the baseline dataset (extinct species with a body length < 1 m) as estimated using a capture-mark-recapture approach. Thick lines indicate the 55% credible interval for the sampling rate, whereas thin lines indicate the 95% interval.
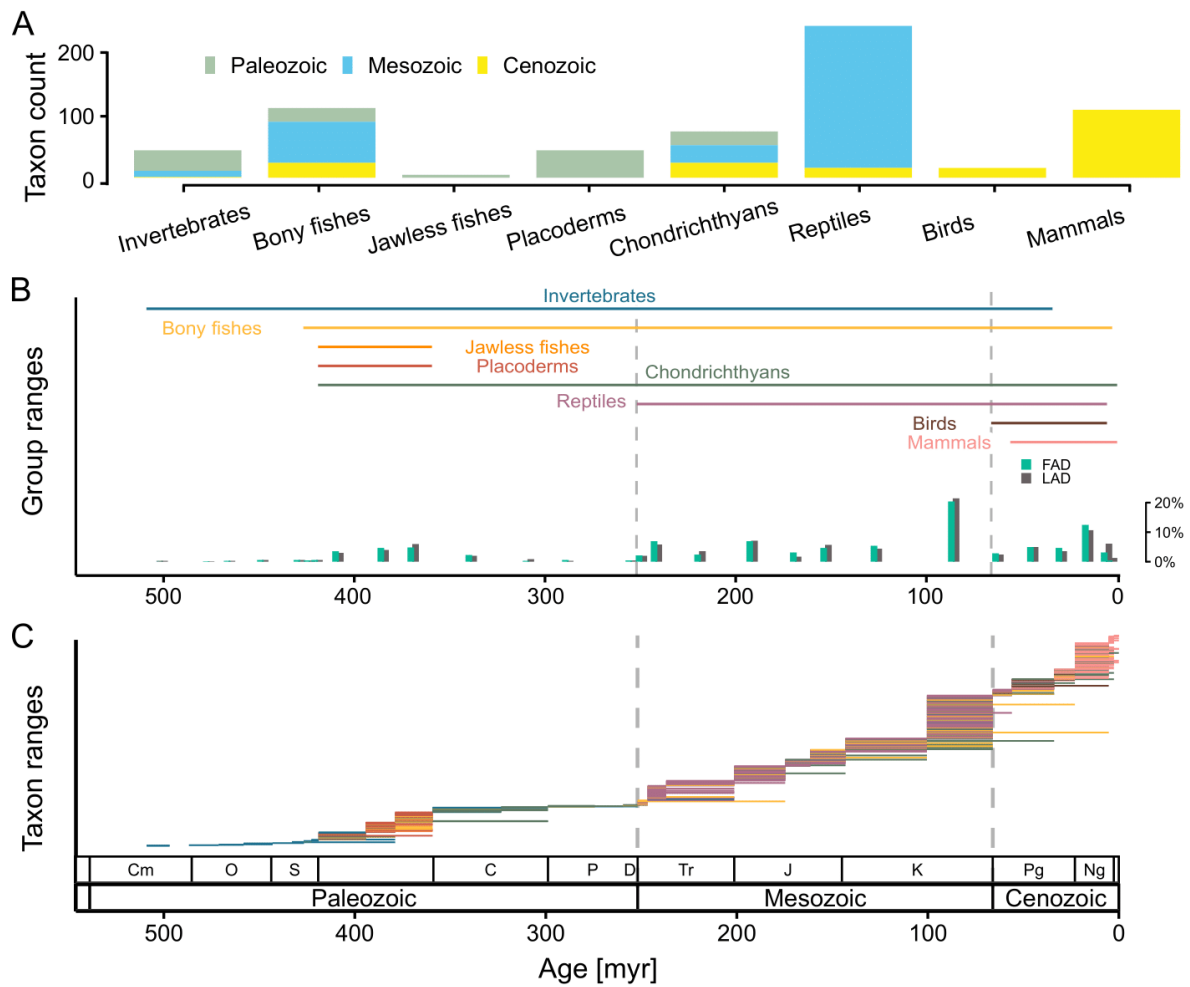
Figure 3. Extinct marine megafauna over time. (A) Number of taxa per taxonomic group and across geological eras. (B) Stratigraphic ranges of the different taxonomic groups (horizontal lines) and percentage of First Appearance Datums (FADs; green), Last Appearance Datums (LADs; grey) in each geological period shown in vertical bars. See Table 3 for details. (C) Stratigraphic ranges of individual taxa. Grey dashed lines delimit the geological eras. See Data S2 for details.
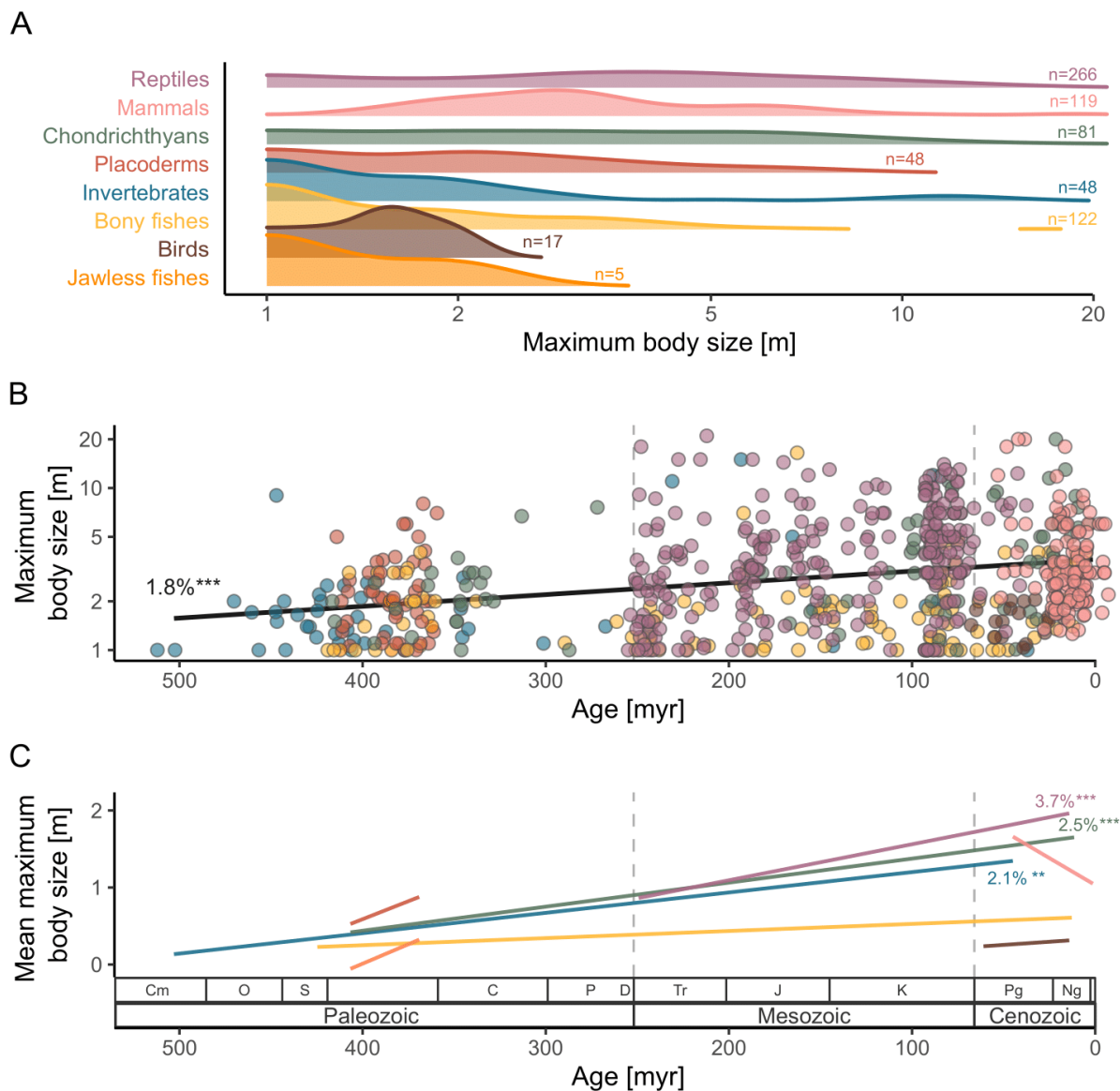
Figure 4. Body size patterns amongst the extinct marine megafauna. (A) Distribution of maximum body sizes per taxonomic group based on density estimates. Taxonomic groups are ordered by mean maximum body size, with the largest estimate at the top. Sample size (number of extinct megafaunal taxa per group) is shown at the right of each density curve. (B) Maximum body size of each taxon over time, whereby the mid-point of the stratigraphic range was used. The black line shows the average linear trend in maximum body size over time considering all taxonomic groups. (C) Average linear trends in body size per taxonomic group. In A and B, the asterisks indicate statistical significance; the numbers show the average increase in body size per every million-year; maximum body size is log-transformed and grey dashed lines delimit the geological eras.
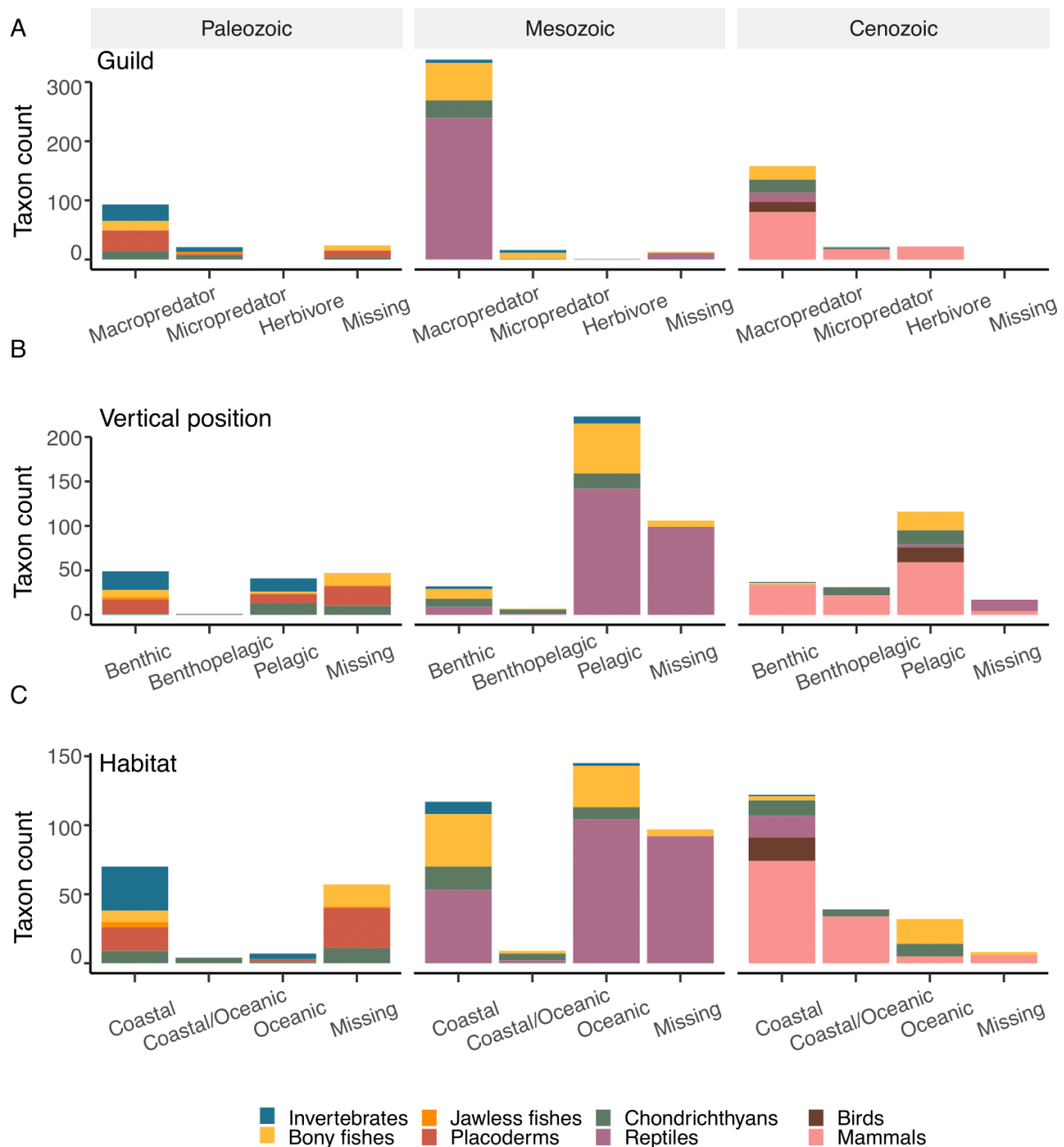
Figure 5. Ecological traits across geological eras. The number of taxa per taxonomic group and ecological trait, including counts where the ecological data is missing. (A) Guild, or most common feeding mechanism. (B) Vertical position, or distribution in the water column where animals feed. (C) Habitat, or lateral position where animals live.
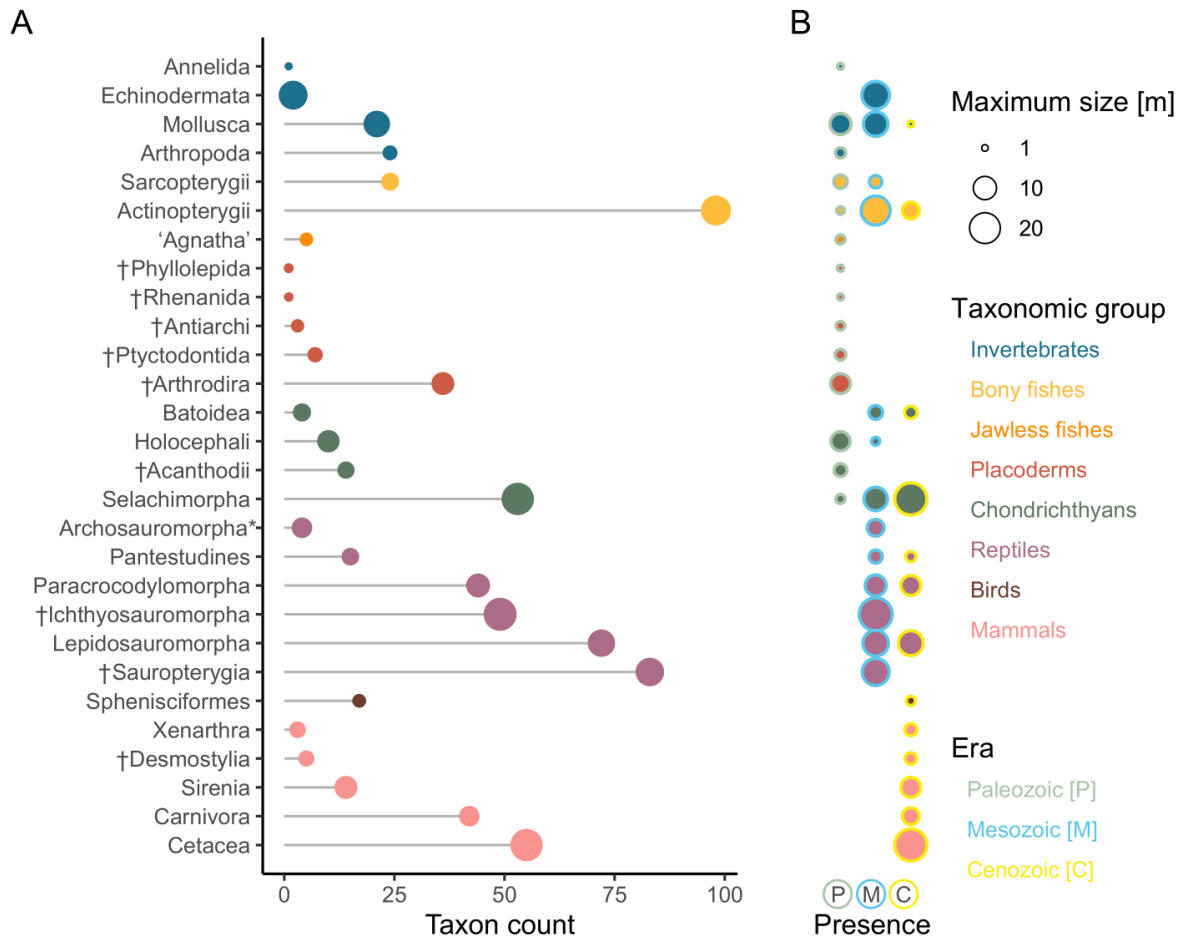
Figure 6. Major clades within the extinct marine megafauna taxonomic groups. (A) The number of taxa per clade within taxonomic groups, whereby the maximum body size of each clade is depicted by the point size. (B) Presence of each megafaunal clade across geological eras where the size of the points depicts the maximum body size, and the coloured surrounding ring represents the corresponding era. No point means that the clade is not occurring in that geological era. *Here, the clade Archosauromorpha only refers to early branching taxa and excludes Paracrocodylomorpha.
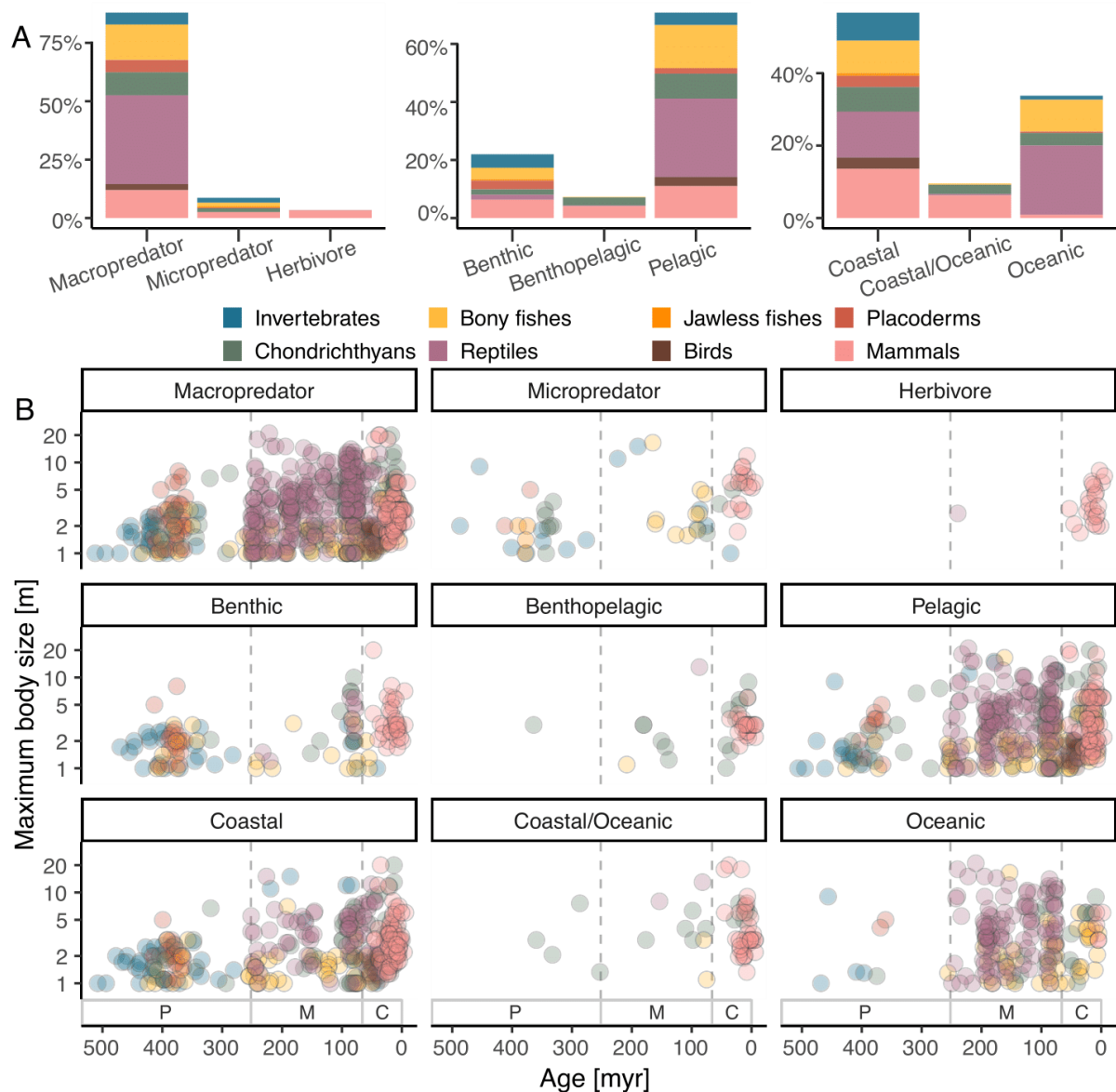
Figure 7. Distribution of ecological traits (guild, position in the water column, and habitat) for the extinct marine megafauna assemblage. (A) The relative frequency of each ecological trait per taxonomic group as percentage. (B) The log-transformed maximum body size in meter per taxon over time and per ecological trait. The mid-point of the stratigraphic range for each taxon was used to plot the maximum body size. Grey dashed lines depict boundaries between eras.
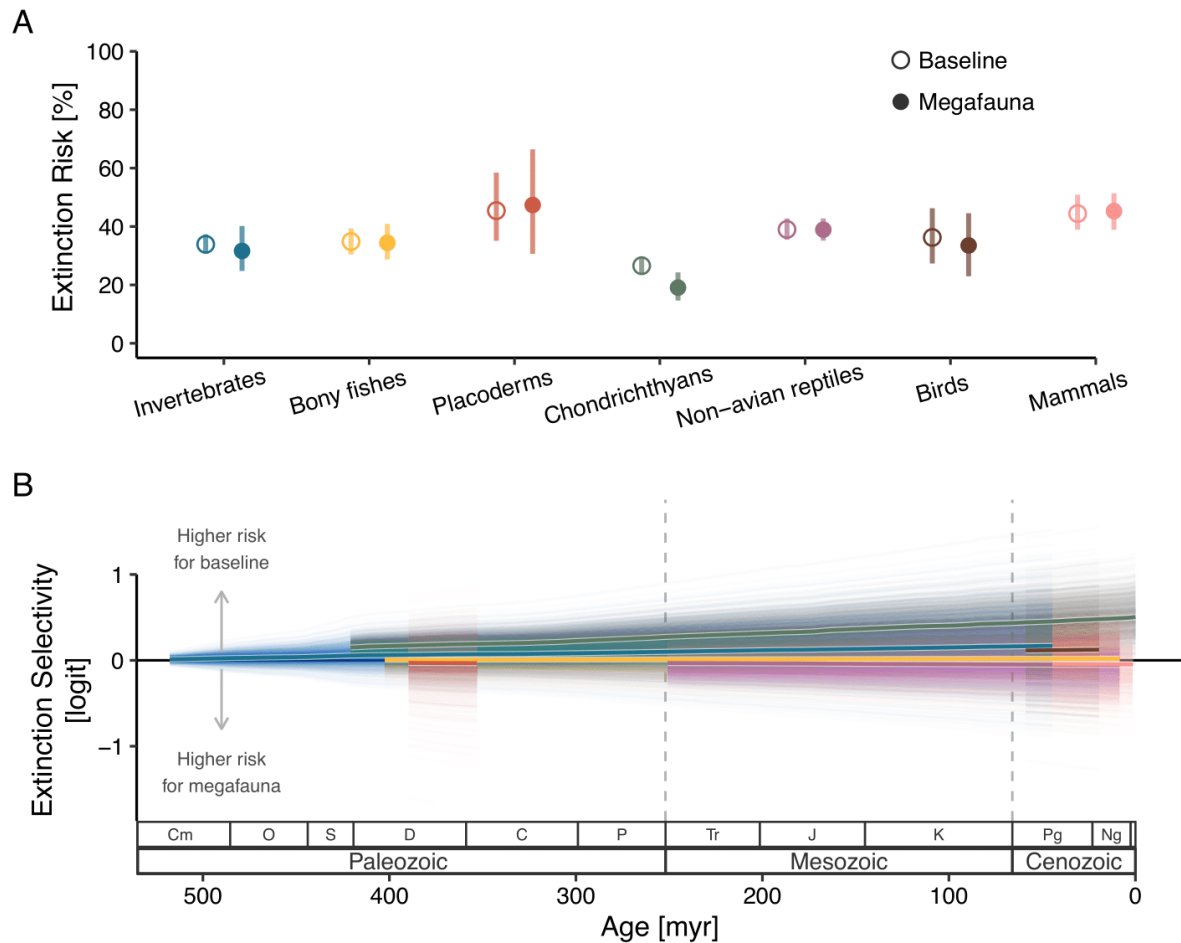
Figure 8. Extinction selectivity of marine megafauna compared with non-megafauna species (i.e., baseline, taxa that belong to the same genus as the extinct megafauna, but that are < 1 m). (A) The extinction risk for fossil taxa as estimated by a Bayesian generalized linear mixed effect model. Points show the average extinction risk for each taxonomic group, and lines the 95% Credible Interval. (B) Extinction selectivity over time on a logit scale for each megafauna group as estimated by the Bayesian model. Positive values indicate an extinction selectivity towards baseline taxa and negative values preferential extinction of megafauna taxa. Thick coloured lines depict the average trend per taxonomic group and the shaded area the corresponding 95% Credible Interval. Logit values are defined as the logarithm of the extinction probability for megafaunal taxa divided by the extinction probability for baseline taxa.

References

Albert J, Johnson D and Knouft J (2009) Fossils provide better estimates of ancestral body size than do extant taxa in fishes. *Acta Zoologica* **90,** 357-384. https://doi.org/10.1111/j.1463-6395.2008.00364.x.

Alroy J (1998) Cope's rule and the dynamics of body mass evolution in North American fossil mammals. *Science* **280**(5364). https://doi.org/10.1126/science.280.5364.731.

Andrews M, Long J, Ahlberg P, Barwick R and Campbell K (2005) The structure of the sarcopterygian *Onychodus jandemarrai* n. sp. from Gogo, Western Australia: with a functional interpretation of the skeleton. *Earth and Environmental Science Transactions of The Royal Society of Edinburgh* **96**(3)**,** 197-307.

Bargo MS and Reguero MA (1998) Annotated catalogue of the fossil vertebrates from Antarctica housed in the Museo de La Plata, Argentina. I. Birds and land mammals from La Meseta Formation (Eocene-? Early Oligocene). *Publicación Electrónica de la Asociación Paleontológica Argentina* **5**(1).

Barron EJ (1983) A warm, equable Cretaceous: The nature of the problem. *Earth-Science Reviews* **19**(4)**,** 305-338. https://doi.org/https://doi.org/10.1016/0012-8252(83)90001-6.

Bianucci G, Lambert O, Urbina M, Merella M, Collareta A, Bennion R, Salas-Gismondi R, Benites-Palomino A, Post K, de Muizon C, Bosio G, Di Celma C, Malinverno E, Pierantoni PP, Villa IM and Amson E (2023) A heavyweight early whale pushes the boundaries of vertebrate morphology. *Nature* **620**(7975)**,** 824-829. https://doi.org/10.1038/s41586-023-06381-1.

Bisconti M, Pellegrino L and Carnevale G (2021) Evolution of gigantism in right and bowhead whales (Cetacea: Mysticeti: Balaenidae). *Biological Journal of the Linnean Society* **134**(2)**,** 498-524.

Blanckenhorn M (1900) Neues zur Geologie und Paläontologie Aegyptens. *Zeitschrift der deutschen geologischen Gesellschaft***,** 21-47.

Blieck AR, Karatajute-Talimaa VN and Mark-Kurik E (2002) Upper Silurian and Devonian heterostracan pteraspidomorphs (Vertebrata) from Severnaya Zemlya (Russia): a preliminary report with biogeographical and biostratigraphical implications. *Geodiversitas* **24**(4)**,** 805-820.

Botella H, Martínez-Pérez C and Soler-Gijón R (2012) *Machaeracanthus goujeti* n. sp.(Acanthodii) from the Lower Devonian of Spain and northwest France, with special reference to spine histology. *Geodiversitas* **34**(4)**,** 761-783.

Boylan JC and Murphy PA (1978) The ventral armor and feeding biomechanics of *Glyptaspis verrucosa* Newberry, a placoderm from the Fammenian Cleveland Shale. *American Museum novitates*; no. 2655.

Bürkner P (2017) An R package for bayesian multilevel models using Stan. *Journal of Statistical Software*.

Cheng L, Chen X-H, Shang Q-H and Wu X-C (2014) A new marine reptile from the Triassic of China, with a highly specialized feeding adaptation. *Naturwissenschaften* **101,** 251-259.

Clarke JA, Ksepka DT, Salas-Gismondi R, Altamirano AJ, Shawkey MD, D'Alba L, Vinther J, DeVries TJ, and Baby P (2010) Fossil evidence for evolution of the shape and color of penguin feathers. Science **330**(6006), 954-957. https://doi.org/10.1126/science.1193604

Choo B, Zhu M, Zhao W, Jia L and Zhu Ya (2014) The largest Silurian vertebrate and its palaeoecological implications. *Scientific Reports* **4**(1)**,** 5242.

Cong P, Daley AC, Edgecombe GD and Hou X (2017) The functional head of the Cambrian radiodontan (stem-group Euarthropoda) *Amplectobelua symbrachiata*. *Bmc Evolutionary Biology* **17**(1)**,** 1-23.

Coombs EJ, Felice RN, Clavel J, Park T, Bennion RF, Churchill M, Geisler JH, Beatty B and Goswami A (2022) The tempo of cetacean cranial evolution. *Current Biology* **32**(10)**,** 2233-2247. e2234.

Cooper JA, Hutchinson JR, Bernvi DC, Cliff G, Wilson RP, Dicken ML, Menzel J, Wroe S, Pirlo J and Pimiento C (2022) The extinct shark *Otodus megalodon* was a transoceanic superpredator: Inferences from 3D modeling. *Science Advances* **8**(33)**,** eabm9424.

Cormack RM (1964) Estimates of survival from the sighting of marked animals. *Biometrika* **51**(3/4)**,** 429-438.

Cortés D and Larsson HCE (2023) Top of the food chains: an ecological network of the marine Paja Formation biota from the Early Cretaceous of Colombia reveals the highest trophic levels ever estimated. *Zoological Journal of the Linnean Society*. https://doi.org/10.1093/zoolinnean/zlad092.

Daley AC and Budd GE (2010) New anomalocaridid appendages from the Burgess Shale, Canada. *Palaeontology* **53**(4)**,** 721-738.

Daley AC and Edgecombe GD (2014) Morphology of Anomalocaris canadensis from the Burgess Shale. *Journal of Paleontology* **88**(1)**,** 68-91.

Dominici S, Danise S and Benvenuti M (2018) Pliocene stratigraphic paleobiology in Tuscany and the fossil record of marine megafauna. *Earth-Science Reviews* **176,** 277-310. https://doi.org/https://doi.org/10.1016/j.earscirev.2017.09.018.

Domning DP (1978) Sirenian evolution in the north Pacific Ocean. *University of California Publication in Geological Sciences* **118,** 1-176.

Dulvy NK, Fowler SL, Musick JA, Cavanagh RD, Kyne PM, Harrison LR, Carlson JK, Davidson LNK, Fordham SV, Francis MP, Pollock CM, Simpfendorfer CA, Burgess GH, Carpenter KE, Compagno LJV, Ebert DA, Gibson C, Heupel MR, Livingstone SR, Sanciangco JC, Stevens JD, Valenti S and White WT (2014) Extinction risk and conservation of the world's sharks and rays. *Elife* **3**. https://doi.org/10.7554/eLife.00590.

Dulvy NK, Sadovy Y and Reynolds JD (2003) Extinction vulnerability in marine populations. *Fish and Fisheries* **4**(1)**,** 25-64. https://doi.org/10.1046/j.1467-2979.2003.00105.x.

Dulvy NK, Simpfendorfer CA, Davidson LNK, Fordham SV, Bräutigam A, Sant G and Welch DJ (2017) Challenges and priorities in shark and ray conservation. *Current Biology* **27**(11)**,** R565-R572. https://doi.org/10.1016/j.cub.2017.04.038.

Estes JA, Heithaus M, McCauley DJ, Rasher DB and Worm B (2016) Megafaunal impacts on structure and function of ocean ecosystems. *Annual Review of Environment and Resources* **41**(1)**,** 83-116. https://doi.org/10.1146/annurev-environ-110615-085622.

Field DJ, Lynner C, Brown C and Darroch SA (2013) Skeletal correlates for body mass estimation in modern and fossil flying birds. *PLoS ONE* **8**(11)**,** e82000.

Foote M (2000) Origination and extinction components of taxonomic diversity: general problems. *Paleobiology* **26**(4)**,** 74-102. https://doi.org/10.1666/0094-8373(2000)26[74:oaecot]2.0.co;2.

Friedman M, Shimada K, Martin LD, Everhart MJ, Liston J, Maltese A and Triebold M (2010) 100-Million-Year Dynasty of Giant Planktivorous Bony Fishes in the Mesozoic Seas. *Science* **327**(5968)**,** 990-993. https://doi.org/10.1126/science.1184743.

Froese R and Pauly D (2017) FishBase World Wide Web electronic publication, Version (01/2017). *URL Www Fishbase Org* **1**.

Giovanardi S, Ksepka DT and Thomas DB (2021) A giant Oligocene fossil penguin from the North Island of New Zealand. *Journal of Vertebrate Paleontology* **41**(3)**,** e1953047.

Goldbogen JA, Cade DE, Wisniewska DM, Potvin J, Segre PS, Savoca MS, Hazen EL, Czapanskiy MF, Kahane-Rapport SR and DeRuiter SL (2019) Why whales are big but not bigger: physiological drivers and ecological limits in the age of ocean giants. *Science* **366**(6471)**,** 1367-1372.

Gradstein FM, Ogg JG, Schmitz MD and Ogg GM (2020) *Geologic time scale 2020*. Elsevier, 21-32. https://doi.org/10.1016/B978-0-12-824360-2.00002-4.

Hagdorn H (2016) From benthic to pseudoplanktonic life: morphological remodeling of the Triassic crinoid *Traumatocrinus* and the Jurassic Seirocrinus during habitat change. *PalZ* **90**(2)**,** 225-241.

Harnik PG, Lotze HK, Anderson SC, Finkel ZV, Finnegan S, Lindberg DR, Liow LH, Lockwood R, McClain CR, McGuire JL, O'Dea A, Pandolfi JM, Simpson C and Tittensor DP (2012) Extinctions in ancient and modern seas. *Trends in Ecology & Evolution* **27**(11)**,** 608-617. https://doi.org/10.1016/j.tree.2012.07.010.

Hospitaleche CA (2014) New giant penguin bones from Antarctica: systematic and paleobiological significance. *Comptes Rendus Palevol* **13**(7)**,** 555-560.

Ifrim C, Stinnesbeck W, González González AH, Schorndorf N and Gale AS (2021) Ontogeny, evolution and palaeogeographic distribution of the world's largest ammonite *Parapuzosia* (*P.*) *seppenradensis* (Landois, 1895). *PLoS ONE* **16**(11)**,** e0258510.

Jadwiszczak P (2001) Body size of Eocene Antarctic penguins. *Polish Polar Research* **22**(2).

Jolly GM (1965) Explicit estimates from capture-recapture data with both death and immigration-stochastic model. *Biometrika* **52**(1/2)**,** 225-247.

Klug C, De Baets K, Kröger B, Bell MA, Korn D and Payne JL (2015) Normal giants? Temporal and latitudinal shifts of Palaeozoic marine invertebrate gigantism and global change. *Lethaia* **48**(2)**,** 267-288.

Ksepka DT, Clarke, JA (2010) The Basal Penguin (Aves: Sphenisciformes) *Perudyptes devriesi* and a Phylogenetic Evaluation of the Penguin Fossil Record. *Bulletin of the American Museum of Natural History* **337,** 1-77. https://doi.org/10.1206/653.1.

Ksepka DT, Field DJ, Heath TA, Pett W, Thomas DB, Giovanardi S and Tennyson AJD (2023) Largest-known fossil penguin provides insight into the early evolution of sphenisciform body size and flipper anatomy. *Journal of Paleontology* **97**(2)**,** 434-453. https://doi.org/10.1017/jpa.2022.88.

Lagomarcino AJ and Miller AI (2012) The relationship between genus richness and geographic area in Late Cretaceous marine biotas: epicontinental sea versus open-ocean-facing settings.

Lambert O, Bianucci G, Post K, de Muizon C, Salas-Gismondi R, Urbina M and Reumer J (2010) The giant bite of a new raptorial sperm whale from the Miocene epoch of Peru. *Nature* **466**(7302). https://doi.org/10.1038/nature09067.

Liston J and Gendry D (2015) Le python de Caen, les algues géantes d'Amblie, et autres spécimens perdus de *Leedsichthys* d'Alexandre Bourienne, Jules Morière, Eugène Eudes-Deslongchamps et Alexandre Bigot. *L'Écho des Falaises* **19,** 17-33.

Liston J, Newbrey M, Challands T and Adams C (2013) Growth, age and size of the Jurassic pachycormid *Leedsichthys problematicus* (Osteichthyes: Actinopterygii).

Lyons SK, Smith FA and Brown JH (2004) Of mice, mastodons and men: human-mediated extinctions on four continents. *Evolutionary Ecology Research* **6**(3)**,** 339-358.

Malhi Y, Doughty CE, Galetti M, Smith FA, Svenning J-C and Terborgh JW (2016) Megafauna and ecosystem function from the Pleistocene to the Anthropocene. *Proceedings of the National Academy of Sciences of the United States of America* **113**(4)**,** 838-846. https://doi.org/10.1073/pnas.1502540113.

Mark-Kurik E (2000) The Middle Devonian fishes of the Baltic States (Estonia, Latvia) and Belarus. *Courier-Forschungsinstitut Sensckenberg***,** 309-324.

Marples BJ (1953) Fossil penguins from the mid-Tertiary of Seymour Island.

Mayr G, Scofield RP, De Pietri VL and Tennyson AJ (2017) A Paleocene penguin from New Zealand substantiates multiple origins of gigantism in fossil Sphenisciformes. *Nature Communications* **8**(1)**,** 1927.

McCauley DJ, Pinsky ML, Palumbi SR, Estes JA, Joyce FH and Warner RR (2015) Marine defaunation: animal loss in the global ocean. *Science (New York, N.Y.)* **347**(6219)**,** 1255641-1255641. https://doi.org/10.1126/science.1255641.

McClain CR, Balk MA, Benfield MC, Branch TA, Chen C, Cosgrove J, Dove ADM, Gaskins LC, Helm RR, Hochberg FG, Lee FB, Marshall A, McMurray SE, Schanche C, Stone SN and Thaler AD (2015) Sizing ocean giants: patterns of intraspecific size variation in marine megafauna. *PeerJ* **2**. https://doi.org/10.7717/peerj.715.

Mitchell E (1968) The Mio-Pliocene pinniped *Imagotaria*. *Journal of the Fisheries Board of Canada* **25**(9)**,** 1843-1900.

Moloshnikov S (2001) New data on *Pycnosteus palaeformis* Preobrazhensky (Heterostraci, Psammosteiformes) from the Aruküla Deposits. *Paleontological Journal* **35**(4)**,** 410-414.

Motani R (1996) Redescription of the dental features of an Early Triassic ichthyosaur, *Utatsusaurus hataii*. *Journal of Vertebrate Paleontology* **16**(3)**,** 396-402.

Nicholls EL and Manabe M (2004) Giant ichthyosaurs of the Triassic—a new species of *Shonisaurus* from the Pardonet Formation (Norian: Late Triassic) of British Columbia. *Journal of Vertebrate Paleontology* **24**(4)**,** 838-849.

Olden JD, Hogan ZS and Zanden MJV (2007) Small fish, big fish, red fish, blue fish: size-biased extinction risk of the world's freshwater and marine fishes. *Global Ecology and Biogeography* **16**(6)**,** 694-701.

Pacoureau N, Rigby CL, Kyne PM, Sherley RB, Winker H, Carlson JK, Fordham SV, Barreto R, Fernando D, Francis MP, Jabado RW, Herman KB, Liu K-M, Marshall AD, Pollom RA, Romanov EV, Simpfendorfer CA, Yin JS, Kindsvater HK and Dulvy NK (2021) Half a century of global decline in oceanic sharks and rays. *Nature* **589**(7843)**,** 567-571. https://doi.org/10.1038/s41586-020-03173-9.

Paillard A, Shimada K and Pimiento C (2021) The fossil record of extant elasmobranchs. *Journal of Fish Biology* **98**(2)**,** 445-455. https://doi.org/https://doi.org/10.1111/jfb.14588.

Payne JL, Boyer AG, Brown JH, Finnegan S, Kowalewski M, Krause RA, Lyons SK, McClain CR, McShea DW, Novack-Gottshall PM, Smith FA, Stempien JA and Wang SC (2009) Two-phase increase in the maximum size of life over 3.5 billion years reflects biological innovation and environmental opportunity. *Proceedings of the National Academy of Sciences* **106**(1)**,** 24-27. https://doi.org/doi:10.1073/nas.0806314106.

Payne JL, Bush AM, Heim NA, Knope ML and McCauley DJ (2016) Ecological selectivity of the emerging mass extinction in the oceans. *Science* **353**(6305)**,** 1284-1286. https://doi.org/10.1126/science.aaf2416.

Payne JL and Heim NA (2020) Body size, sampling completeness, and extinction risk in the marine fossil record. *Paleobiology* **46**(1)**,** 23-40.

Perez VJ, Leder RM and Badaut T (2021) Body length estimation of Neogene macrophagous lamniform sharks (*Carcharodon* and *Otodus*) derived from associated fossil dentitions. *Palaeontologica Electronica* **24**, a09.

Pimiento C (2018) Our shallow-water origins. *Science* **362**(6413)**,** 402-403. https://doi.org/doi:10.1126/science.aau8461.

Pimiento C and Benton MJ (2020) The impact of the Pull of the Recent on extant elasmobranchs. *Palaeontology* **63**(3)**,** 369-374. https://doi.org/https://doi.org/10.1111/pala.12478.

Pimiento C, Cantalapiedra JL, Shimada K, Field DJ and Smaers JB (2019) Evolutionary pathways toward gigantism in sharks and rays. *Evolution* **73**(3)**,** 588-599. https://doi.org/https://doi.org/10.1111/evo.13680.

Pimiento C and Clements CF (2014) When Did *Carcharocles megalodon* Become Extinct? A New Analysis of the Fossil Record. *PLoS ONE* **9**(10). https://doi.org/10.1371/journal.pone.0111086.

Pimiento C, Griffin JN, Clements CF, Silvestro D, Varela S, Uhen MD and Jaramillo C (2017) The Pliocene marine megafauna extinction and its impact on functional diversity. *Nature Ecology & Evolution* **1**(8)**,** 1100.

Pimiento C, Leprieur F, Silvestro D, Lefcheck J, Albouy C, Rasher D, Davis M, Svenning J-C and Griffin J (2020) Functional diversity of marine megafauna in the Anthropocene. *Science Advances* **6**(16)**,** eaay7650.

Pimiento C, MacFadden BJ, Clements CF, Varela S, Jaramillo C, Velez-Juarbe J and Silliman BR (2016) Geographical distribution patterns of *Carcharocles megalodon* over time reveal clues about extinction mechanisms. *Journal of Biogeography*.

Poust AW and Boessenecker RW (2017) Mandibles of the sea lion *Proterozetes ulysses* from the middle Pleistocene Port Orford Formation of Oregon. *Journal of Vertebrate Paleontology* **37**(3)**,** e1317637.

Pyenson ND (2017) The ecological rise of whales chronicled by the fossil record. *Current Biology* **27**(11)**,** R558-R564.

Pyenson ND and Sponberg SN (2011) Reconstructing Body Size in Extinct Crown Cetacea (Neoceti) Using Allometry, Phylogenetic Methods and Tests from the Fossil Record. *Journal of Mammalian Evolution* **18**(4)**,** 269-288. https://doi.org/10.1007/s10914-011-9170-1.

Reguero MA, Marenssi SA and Santillana SN (2012) Weddellian marine/coastal vertebrates diversity from a basal horizon (Ypresian, Eocene) of the Cucullaea I Allomember, La Meseta formation, Seymour (Marambio) Island, Antarctica.

Sallan L, Friedman M, Sansom RS, Bird CM and Sansom IJ (2018) The nearshore cradle of early vertebrate diversification. *Science* **362**(6413)**,** 460-464. https://doi.org/doi:10.1126/science.aar3689.

Sallan L and Galimberti AK (2015) Body-size reduction in vertebrates following the end-Devonian mass extinction. *Science* **350**(6262)**,** 812-815. https://doi.org/doi:10.1126/science.aac7373.

Sallan LC and Coates MI (2010) End-Devonian extinction and a bottleneck in the early evolution of modern jawed vertebrates. *Proceedings of the National Academy of Sciences* **107**(22)**,** 10131-10135.

Sander PM, Griebeler EM, Klein N, Juarbe JV, Wintrich T, Revell LJ and Schmitz L (2021) Early giant reveals faster evolution of large body size in ichthyosaurs than in cetaceans. *Science* **374**(6575)**,** eabf5787. https://doi.org/doi:10.1126/science.abf5787.

Sarko DK, Domning DP, Marino L and Reep RL (2010) Estimating body size of fossil sirenians. *Marine Mammal Science* **26**(4)**,** 937-959. https://doi.org/10.1111/j.1748-7692.2010.00384.x.

Scheyer TM, Romano C, Jenks J and Bucher H (2014) Early Triassic marine biotic recovery: the predators' perspective. *PLoS ONE* **9**(3)**,** e88987.

Seber GA (1965) A note on the multiple-recapture census. *Biometrika* **52**(1/2)**,** 249-259.

Silvestro D, Salamin N and Schnitzler J (2014a) PyRate: a new program to estimate speciation and extinction rates from incomplete fossil data. *Methods in Ecology and Evolution* **5**(10)**,** 1126-1131. https://doi.org/10.1111/2041-210x.12263.

Silvestro D, Schnitzler J, Liow LH, Antonelli A and Salamin N (2014b) Bayesian Estimation of Speciation and Extinction from Incomplete Fossil Occurrence Data. *Systematic Biology* **63**(3)**,** 349-367. https://doi.org/10.1093/sysbio/syu006.

Slack KE, Jones CM, Ando T, Harrison G, Fordyce RE, Arnason U and Penny D (2006) Early penguin fossils, plus mitochondrial genomes, calibrate avian evolution. *Molecular biology and evolution* **23**(6)**,** 1144-1155.

Stilwell JD and Zinsmeister WJ (1992) Molluscan systematics and biostratigraphy: lower tertiary, La Meseta Formation, Seymour Island, Antarctic Peninsula. *Antarctic Research Series*.

Südkamp WH and Burrow CJ (2007) The acanthodian Machaeracanthus from the Lower Devonian Hunsrück Slate of the Hunsrück region (Germany). *Paläontologische Zeitschrift* **81,** 97-104.

Swift CC and Barnes LG (1996) Stomach contents of *Basilosaurus cetoides*: implications for the evolution of cetacean feeding behavior, and evidence for vertebrate fauna of epicontinental Eocene seas. *The Paleontological Society Special Publications* **8,** 380-380.

Tambussi CP, Reguero MA, Marenssi SA and Santillana SN (2005) *Crossvallia unienwillia*, a new Spheniscidae (Sphenisciformes, Aves) from the late Paleocene of Antarctica. *Geobios* **38**(5)**,** 667-675.

Tavares DC, Moura JF, Acevedo-Trejos E and Merico A (2019) Traits shared by marine megafauna and their relationships with ecosystem functions and services. *Frontiers in Marine Science***,** 262.

Valenzuela-Toro A and Pyenson ND (2019) What do we know about the fossil record of pinnipeds? A historiographical investigation. *Royal Society open science* **6**(11)**,** 191394.

Vermeij GJ (1977) The Mesozoic Marine Revolution: Evidence from Snails, Predators and Grazers. *Paleobiology* **3**(3)**,** 245-258.

Voss M, Antar MSM, Zalmout IS and Gingerich PD (2019) Stomach contents of the archaeocete *Basilosaurus isis*: apex predator in oceans of the late Eocene. *PLoS ONE* **14**(1)**,** e0209021.

Weems RE and Sanders AE (2014) Oligocene pancheloniid sea turtles from the vicinity of Charleston, South Carolina, USA. *Journal of Vertebrate Paleontology* **34**(1)**,** 80-99.

Zmarzly D (1985) The shallow-water crinoid fauna of Kwajalein Atoll, Marshall Islands: ecological observations, interatoll comparisons, and zoogeographic affinities. *Pacific Science Volume* **39**(4), 340-358.

Appendix 7 | Candidate's extended scientific record

Jack Arthur Cooper

- Education
- Scientific publications
- Guest articles
- Invited seminars
- Conference presentations and published abstracts
- Media outreach
- Selected science communication
- Peer reviews
- Other experience

Education

Swansea University – PhD Biosciences   **2020-2024**

Project: Functional diversity of sharks through time: past, present and future

Supervisor(s): Dr Catalina Pimiento; Dr John Griffin

Funding: Fisheries Society of the British Isles (PhD studentship)

University of Bristol – MSc Palaeobiology (Distinction)   **2018-2019**

Thesis: External Anatomy of Megalodon

Supervisor(s): Dr Catalina Pimiento (External; Swansea University); Professor Mike Benton (Internal; University of Bristol)

University of St Andrews – BSc Evolutionary Biology (1st Class Honours)   **2014-2018**

Thesis: Intraspecific copulation in *Drosophila melanogaster*

Supervisor(s): Professor Mike Ritchie

Scientific Publications

2024:

- **Cooper JA** & Pimiento C, 2024. The rise and fall of shark functional diversity over the last 66 million years. *Global Ecology and Biogeography*, **33**, e13881.

- Pimiento C, Kocáková K, Mathes GH, Argyriou T, Cadena, E-A, **Cooper JA**, Cortes D, Field DJ, Klug C, Scheyer TM, Valenzuela-Toro AM, Buess T, Günter M, Gardiner AM, Hatt P, Holdener G, Jacober G, Kobelt S, Masseraz S, Mehli I, Reiff S,

Rigendinger E, Ruckstuhl M, Schneider S, Seige C, Senn N, Staccoli V, Bauman J, Flueler L, Guevara LJ, Ickin E, Kissling KC, Liechti J, Rogenmoser J, Spitznagel D, Villafaña JA & Zanatta C, 2024. The extinct marine megafauna of the Phanerozoic. *Cambridge Prisms: Extinctions*, **2**, e7, 1-17.

2023:

- **Cooper JA**, Griffin JN, Kindlimann R & Pimiento C, 2023. Are shark teeth proxies for functional traits? A framework to infer ecology from the fossil record. *Journal of Fish Biology*, **103**, 798-814.

2022:

- **Cooper JA**, Hutchinson JR, Bernvi DC, Cliff G, Wilson RP, Dicken ML, Menzel J, Wroe S, Pirlo J & Pimiento C, 2022. The extinct shark *Otodus megalodon* was a transoceanic super-predator: inferences from 3D modelling. *Science Advances*, **8**, eabm9424.

2020:

- **Cooper JA**, Pimiento C, Ferrón HG & Benton MJ, 2020. Body dimensions of the extinct giant shark *Otodus megalodon*: a 2D reconstruction. *Scientific Reports*, **10**, 14596.

Guest Articles

- Cooper JA, 2023. Meg 2: the truth about the extinct mega shark – and why even this ridiculous film could inspire future palaeontologists. *The Conversation*. https://theconversation.com/meg-2-the-truth-about-the-extinct-mega-shark-and-why-even-this-ridiculous-film-could-inspire-future-palaeontologists-210751.
- Cooper JA, 2020. Scaling a Giant. *Geoscientist*, **30**, 10-15.
- Cooper JA, 2020. A Shark Nerd's Guide to Megalodon. **Bristol Dinosaur Project Blog** (edited by Rhys Charles). https://dinoproject.blogs.bristol.ac.uk/category/shark-week/.

Invited Seminars

- Cooper JA, 2023. Three-minute thesis: Functional diversity of sharks: past, present and future (virtual). A breakdown of my PhD work for pupils to present as their entry to the three-minute thesis competition at their local school. **Cheadle Hulme High School, Manchester.**

- Cooper JA, 2023. Skype a Scientist: Palaeobiology and Megalodon (virtual). **Cheadle Hulme High School, Manchester.**

- Cooper JA, 2022. Mighty Megalodon family event. **Lapworth Museum of Geology, University of Birmingham**.

- Cooper JA, 2022. National Megalodon Day: Morphology and ecology based on 2D & 3D modelling. **Calvert Marine Museum**.

- Cooper JA, 2022. From giant sharks to a PhD in shark diversity: A brief history of my career so far. **University of Vienna**.

- Cooper JA, 2021 (virtual). SMUX Diving – In the Mind of a Shark: The Megalodon. **Singapore Management University**.

- Cooper JA, 2021 (virtual). More than teeth: megalodon's morphology and ecology. **Natural History Society of Maryland**.

Conference presentations and published abstracts

- **Cooper JA**, Mathes GH & Pimiento C (2024). Temporal and spatial declines of functional diversity in sharks and rays under simulated extinctions. *WEEN conference programme and abstract book*, p26. Oral presentation for WEEN (Welsh Ecology and Evolution Network) 2024.

- **Cooper JA** (2024). The future of elasmobranch functional diversity under a changing climate. Oral presentation for the 2024 Swansea University Biosciences PGR Conference.

- Cooke-Tapia I*, Pimiento C & **Cooper JA** (2024). Megalodon: A Tale in 3D. *Paleolusitana 2, p90*. Oral presentation for the second Proceedings of the Paleo Spring Meeting (*presented by Ian Cooke-Tapia).

- **Cooper JA** & Pimiento C (2023). How has the functional diversity of sharks changed over the last 66 million years? *WEEN conference programme and abstract book*, p17. Oral presentation for WEEN (Welsh Ecology and Evolution Network) 2023.

- **Cooper JA** & Pimiento C (2023). Shark functional diversity throughout the Cenozoic. 21st Swiss Geoscience Meeting Program booklet, p155. Oral presentation for the 21st Swiss Geosciences Meeting.

- **Cooper JA** & Pimiento C (2023). How has shark functional diversity changed through geological time? *PalAss 2023 abstract book*, p37. Oral presentation for the 2023 annual meeting of the Palaeontological Association.

- **Cooper JA** & Pimiento C (2023). How has shark functional diversity changed through geological time? *CPEG 2023 abstract book*, p26. Oral presentation for CPEG (Crossing the Palaeontological-Ecological Gap) 2023.

- **Cooper JA** & Pimiento C (2023). How has shark functional diversity changed through geological time? *Fisheries Society of the British Isles Annual International Symposium 2023 abstract book*, p126. Poster presentation for the 2023 Fisheries Society of the British Isles Annual International Symposium.

- **Cooper JA** (2023). Functional diversity of sharks through time: past, present and future. Oral presentation for the 2023 Swansea University Biosciences PGR Conference.

- **Cooper JA** & Pimiento C (2023). How has shark functional diversity changed through geological time? *4th Palaeontological Virtual Congress Book of Abstracts*, p106. Oral presentation for the 2023 Palaeontological Virtual Congress.

- **Cooper JA**, Hutchinson JR, Bernvi DC, Cliff G, Wilson RP, Dicken ML, Menzel J, Wroe S, Pirlo J & Pimiento C (2022). The extinct shark *Otodus megalodon* was a transoceanic super-predator: inferences from 3D modelling. *Fisheries Society of the British Isles Annual International Symposium 2022 abstract book*, p21. Oral presentation for the 2022 Fisheries Society of the British Isles Annual International Symposium.

- **Cooper JA,** Griffin JN & Pimiento C (2022). Are shark teeth proxies for functional traits? *Fisheries Society of the British Isles Annual International Symposium 2022 abstract book*, p70. Poster presentation for the 2022 Fisheries Society of the British Isles Annual International Symposium.

- **Cooper JA**, Hutchinson JR, Bernvi DC, Cliff G, Wilson RP, Dicken ML, Menzel J, Wroe S, Pirlo J & Pimiento C, 2021. 3D reconstruction reveals that the extinct giant shark *Otodus megalodon* was a transoceanic super-predator. *The Palaeontological Association Abstract Book 2021*, p60. Poster presentation for the 2021 annual meeting of the Palaeontological Association.

- **Cooper JA**, Hutchinson JR, Bernvi DC, Cliff G, Wilson RP, Dicken ML, Menzel J, Wroe S, Pirlo J & Pimiento C, 2021. 3D reconstruction reveals that the extinct giant shark *Otodus megalodon* was a transoceanic super-predator. *WEEN conference programme and abstract book*, p11. Oral presentation for WEEN (Welsh Ecology and Evolution Network) 2021.

- **Cooper JA**, Hutchinson JR, Wilson RP, Pirlo J, Dicken ML, Menzel J, Wroe S, Bernvi DC, Cliff G & Pimiento C, 2021. 3D model of the extinct giant shark *Otodus megalodon* suggests ability to undertake long migrations and a preference for large prey. *Progressive Palaeontology Abstract Booklet 2021*, p19-20. Oral presentation for Progressive Palaeontology 2021.

- **Cooper JA**, Pimiento C, Ferrón HG & Benton MJ, 2020. Body dimensions of the extinct giant shark *Otodus megalodon*: a 2D reconstruction. *WEEN conference programme and abstract book*, p18. Oral presentation for WEEN (Welsh Ecology and Evolution Network) 2020.

- **Cooper JA**, Hutchinson JR, Dicken ML, Menzel J & Pimiento C, 2020. A 3D reconstruction of the extinct giant shark *Otodus megalodon*. *Progressive Palaeontology Abstract Booklet 2020*, p43. Poster presentation for Progressive palaeontology 2020.

- **Cooper JA**, Benton MJ & Pimiento C, 2019. External anatomy of the extinct megalodon. *Progressive Palaeontology Abstract Booklet 2019*, p35. Poster presentation for Progressive palaeontology 2019.

Awards

2024: Best 10-minute talk (runner-up) – Swansea University Biosciences PGR Conference

2023: Best Oral Presentation (runner-up) – WEEN 2023

2023: Best 10-minute talk – Swansea University Biosciences PGR Conference

2022: Best Oral Presentation – Fisheries Society of the British Isles Symposium 2022

2022: International Travel Grant – University of Florida

2021: Best Oral Presentation – WEEN 2021

2020: Best Oral Presentation – WEEN 2020

2020: PhD Studentship – Fisheries Society of the British Isles

2018: Dean's List – University of St Andrews

Media Outreach

Documentaries

1. **Mentorn Media** (2024). "Monsters of the deep" – two-part documentary series on prehistoric and modern oceans for broadcast on Channel 5 on British television in Autumn 2024. Filmed with host Steve Backshall in July 2024.

2. **Good Thing Productions** (2024-present). Upcoming Australian documentary about Megalodon partially based on the popular science book "Big Meg" by Tim Flannery. Currently serving as a scientific consultant.

3. **Crackit Productions** (2024). "Sharks" – 3-part documentary series for broadcast on Channel 5 on British television. Filmed in April 2024, though ultimately cut.

4. **Off the Fence Productions** (2023). "Episode 4: Sharks". The documentary series "Giants" produced by Off the Fence Productions for CuriosityStream. Filmed 2 separate interviews in July and October 2022; and aired in May 2023.

5. **Storyhouse Productions** (2021). The documentary "Myths: Sea Monsters" by ZDF. Filmed in May 2021 and aired in October 2021.

Science animations

1. **TED-Ed** (2023). "Why did Megalodon go extinct? – Jack Cooper and Catalina Pimiento". Animated educational lesson with Ted-Ed with over a million views. https://www.youtube.com/watch?v=6LGCk08zMbg&t=143s.

2. **Cooked Illustrations** (2022). "The megalodon: A tale in 3D". Animated video accompanying scientific publication on megalodon. Produced in English, Spanish and German. https://www.youtube.com/watch?v=SBpIcsrof7M.

Selected science communication

Podcast, radio and news appearances

1. **World of Sharks** (2024). "Megalodon: Inside the life of a superpredator" – Podcast interview with Dr Isla Hodgson, sponsored by the Save our Seas foundation. https://saveourseas.com/worldofsharks/podcast/megalodon-inside-the-life-of-a-superpredator.

2. **The Pulse** (2024). "Why megalodons have captured our imagination and what researchers have learned from their extinction" – Podcast interview with Lauren Tran-Muchowski. https://whyy.org/segments/megalodons-and-what-researchers-have-learned-of-their-extinction/.

3. **Bearded Tit** (2024). "Megalodon: The Facts ft Jack Cooper #147" – Podcast interview with Jack Perks. https://beardedtit.podbean.com/e/megalodon-the-facts-ft-jack-cooper-147/.

4. **Let's Jaws for a Minute** (2023). "Episode 96: The Meg and Meg 2: The Trench" – Podcast interview with Sarah Buddery and MJ Smith. https://podcasters.spotify.com/pod/show/jawsforaminute/episodes/Episode-96-The-Meg-and-Meg-2-The-Trench-e292e3p.

5. **Let's Jaws for a Minute** (2022). "Patreon Exclusive 1: OnlyFins: an Interview with Jack Cooper" – Podcast interview with Sarah Buddery and MJ Smith. https://www.patreon.com/posts/patreon-1-with-71653987.

6. **Shark Stories** (2022). "The Meg" – Podcast interview with Madison Stewart. https://sharkstories.buzzsprout.com/1737603/9878878-the-meg.

7. **BBC Radio** (2021). "Shark enthusiast Jack Cooper on Megalodons and shark diving". Interview with Tim Wheeler. https://soundcloud.com/user-376006937/shark-enthusisast-jack-cooper-on-megalodons-and-shark-diving.

8. **Evolution Soup** (2021). "Megalodon – The shark that ate whales – with Jack Cooper". Interview with Mark Torrender. https://www.youtube.com/watch?v=EKqh3R8GliU.

9. **Let's Jaws for a Minute** (2021). "Episode 28 – Shark Autopsy" – Podcast interview with Sarah Buddery and MJ Smith. https://anchor.fm/jawsforaminute.

10. **Dinosaur George Podcast** (2020). "Megalodon body dimensions – Interview with Jack Cooper" by George Blasing. http://www.dinosaurgeorgepodcast.com/megalodon-body-dimensions-interview-with-jack-cooper/.

11. **BBC News** (2020). "Just how big were prehistoric mega-sharks?" Interview with Kasia Madera. https://www.youtube.com/watch?v=Ta6kzC9kCd4&t=2s.

News articles

12. **CBBC Newsround** (2024). "Megalodon: 10-year-old finds ancient tooth fossil on UK beach" – comments made for news story. Involved in confirming identity of the fossil tooth. https://www.bbc.co.uk/newsround/68887847.

13. **Discover Magazine** (2022). "Larger, 65-foot-long Megalodon might have fed on whales." By Sean Mowbray. https://www.discovermagazine.com/planet-earth/larger-65-foot-long-megalodon-might-have-fed-on-whales.

14. **Forbes Magazine** (2022). "Whale-Y Big Bites: Study shows the Meg could swallow modern predators whole" by Melissa Cristina Márquez.

https://www.forbes.com/sites/melissacristinamarquez/2022/08/22/whale-y-big-bites-study-shows-the-meg-could-swallow-modern-predators-whole/?sh=31f090121f2d.

15. **Popular Science** (2022). "3D models show that the megalodon was faster, fiercer than we ever thought" by Laura Baisas. https://www.popsci.com/science/3d-models-show-the-megalodon-was-faster-fiercer-than-we-ever-thought/.

16. **CNN** (2022). "The extinct superpredator megalodon was big enough to eat orcas, scientists say" by Zoe Sottile. https://edition.cnn.com/2022/08/20/world/megalodon-giant-shark-discovery-scn-trnd/index.html.

17. **The New York Times** (2022). "The Megalodon was bigger, faster and even hungrier" by Asher Elbein. https://www.nytimes.com/2022/08/17/science/how-big-was-megalodon.html.

18. **Associated Press News** (2022). "Giant sharks once roamed the sea, feasting on huge meals" by Maddie Burakoff. https://apnews.com/article/science-oddities-fossils-sharks-fish-cd87e463438196637b95b4d52832645d.

19. **The Guardian** (2022). "Ancient megalodon shark could eat a whale in a few bites, research suggests" https://www.theguardian.com/environment/2022/aug/17/ancient-megalodon-shark-could-eat-a-whale-in-a-few-bites-research-suggests.

20. **Science Alert** (2022). "The Megalodon was so huge it could have devoured an orca in just a few bites" by Michelle Starr. https://www.sciencealert.com/the-megalodon-was-so-huge-it-could-have-devoured-an-orca-in-just-a-few-bites.

21. **Ardrossan & Saltcoats Herald** (2020). "North Ayrshire man helps reveal enormity of the Megalodon shark" by Gianni Marini. https://www.ardrossanherald.com/news/18749842.north-ayrshire-man-helps-reveal-enormity-megalodon-shark/.

22. **Forbes Magazine** (2020). "Measuring Megalodon: Scientists Find Out How Large This Shark Once Was" by Melissa Cristina Márquez. https://www.forbes.com/sites/melissacristinamarquez/2020/09/10/measuring-megalodon-scientists-find-out-how-large-this-shark-once-was/.

23. **BBC Wales** (2020). "Shark researchers size up real 'Megalodon' for first time" by Matt Lloyd. https://www.bbc.co.uk/news/uk-wales-54011932.

24. **The Guardian** (2020). "Researchers reveal true scale of megalodon shark for first time" https://www.theguardian.com/environment/2020/sep/03/researchers-reveal-true-scale-of-megalodon-shark-for-first-time.

25. **CNN** (2020). "Vast size of prehistoric megalodon shark, which had a fin as long as a human, revealed for the first time" by Sara Spary. https://edition.cnn.com/2020/09/03/world/megalodon-shark-scli-intl-gbr-scn/index.html.

26. **Science Focus** (2020). "Prehistoric megalodon was a mega-shark that had 'fins as large as an entire adult human'" by Amy Barrett. https://www.sciencefocus.com/news/prehistoric-megalodon-was-a-mega-shark-that-had-fins-as-large-as-an-entire-adult-human/.

Additional projects

27. Two commissioned artworks of megalodon jaws and body outline with Jeff Maynard, PhD, director of Symbioseas. www.symbioseas.org.

Peer Reviews

During my PhD, I have been a peer reviewer of 18 different manuscripts across 11 journals:

Revista Brasileira de Paleontologia (1 paper)

Historical Biology (6 papers)

Paleoichthys – Journal of Fossil Fishes (3 papers)

PeerJ (1 paper)

Scientific Reports (1 paper)

Evolution (1 paper)

Royal Society Open Science (1 paper)

Communications Biology (1 paper)

Spanish Journal of Palaeontology (1 paper)

Canadian Journal of Earth Sciences (1 paper)

Evolution and Development (1 paper)

Other experience

Production consultation

May-Jul 2024   **Scientific Consultant/Interviewee**

                              Mentorn Media

Functional diversity of sharks through time: past, present and future

Consulted the production team on the science and modelling of *Otodus megalodon* for two-part documentary series "Monsters of the deep" on modern and Prehistoric Oceans to be broadcast on Channel 5.

Took part in subsequent filming in Dorset with host Steve Backshall as one of the interviewed megalodon scientists.

Feb-Oct 2022   **Scientific Consultant/Interviewee**

Off the Fence Productions

Consulted the production team on the science of *Otodus megalodon* for episode 4 of the programme "Giants" for Curiosity Stream.

Took part in two separate interviews with the presenter and crew.

Exhibit consultation

Feb 2022-Oct 2023   **Scientific consultant**

Royal Belgian Institute of Natural Sciences, Brussels, Belgium

Served as an advisor to the museum for their exhibit GIANTS, specifically for their *Otodus megalodon* specimen to go on display. My key roles were as a fact checker to the science being presented, and advising on the modelling process for the specimen.

Dec 2022-Jun 2023   **Scientific consultant**

Oriel Science, Swansea, Wales, UK

Primary advisor to a section of the "Imaging" exhibit in Swansea, specifically on a reconstruction of the head of the megalodon.

Committee roles

Dec 2020-Dec 2024   **Committee member**

Welsh Ecology & Evolution Network, Machynlleth, UK

Served as a committee member for Swansea University for the annual student-run WEEN conference. Roles included acquiring funding for the conference from the Fisheries Society of the British Isles and promoting the event to Swansea University postgraduates. Additionally, I arranged transport for Swansea University delegates to the venue and chaired presentation sessions based on Aquatic Ecology.

Appendix 8 | Ethics approval and risk assessment

Ethics approval

Project Ethics Assessment Confirmation|Cadarnhad o Asesiad Moeseg Prosiect

cosethics@swansea.ac.uk
To: COOPER J.
Cc: Catalina Pimiento

☀ ☺ ← Reply ← Reply all → Forward ⊞ ⋯
Mon 24/06/2024 15:46

This is an automated confirmation email for the following project. The Ethics Assessment status of this project is: APPROVED

Applicant Name: Jack Cooper
Project Title: Functional Diversity of Sharks Through Time: Past, Present and Future
Project Start Date: 1/10/20
Project Duration: 4 years
Approval No: SU-Ethics-Student-240624/3088

NOTE: This notice of ethical approval does not cover aspects relating to Health and Safety. Please complete any relevant risk assessments prior to commencing with your project.

Neges awtomataidd yw hon ar gyfer y prosiect canlynol. Statws Asesiad Moeseg y prosiect hwn yw: APPROVED

Enw'r Ymgeisydd: Jack Cooper
Teitl y Prosiect: Functional Diversity of Sharks Through Time: Past, Present and Future
Dyddiad Dechrau'r Prosiect: 1/10/20
Hyd y Prosiect: 4 years
Rhif y Gymeradwyaeth: SU-Ethics-Student-240624/3088

SYLWER: Nid yw'r hysbysiad hwn o gymeradwyaeth foesegol yn cynnwys agweddau sy'n ymwneud ag Iechyd a Diogelwch. Dylech gwblhau unrhyw asesiadau risg perthnasol cyn dechrau eich prosiect.

← Reply   ← Reply all   → Forward

Risk assessment

Swansea University Prifysgol Abertawe — HEALTH & SAFETY / IECHYD A DIOGELWCH

Risk Assessment

College/ PSU	College of Science	Assessment Date	01/10/20
Location	Desk-based	Assessor	Jack Cooper
Activity	Desk-based PhD project	Review Date (if applicable)	*
Associated documents	●	●	

Part 1: Risk Assessment

What are the hazards?	Who might be harmed?	How could they be harmed?	What are you already doing?	S	L	Risk (SxL)	Do you need to do anything else to manage this risk?
Display screen equipment	Student	Inappropriate working station set-up	Use of equipment in good working order; screen is at appropriate level, distance and brightness for student; mouse and keyboard used on flat desk surface; taking regular breaks from workstation; limiting use of portable devices such as laptops for short periods	2	1	2	No
Homeworking	Student	Unblanaced distribution of working and free time during the project's duration	Planning work in advance on a day-by-day basis; taking breaks throughout each work day; exercising regularly; remaining in touch with line manager and research team members at regular intervals	3	1	3	No

HEALTH & SAFETY
IECHYD A DIOGELWCH

Part 2: Actions arising from risk assessment

Actions	Lead	Target Date	Done Yes/No

HEALTH & SAFETY
IECHYD A DIOGELWCH

Appendix 1: Risk matrix

		Consequences				
		1 **Insignificant** No injuries/minimal financial loss	**2** **Minor** First aid treatment/medium financial loss	**3** **Moderate** Medical treatment/high financial loss	**4** **Major** Hospitalised/large financial loss	**5** **Catastrophic** Death/Massive Financial Loss
Likelihood	**5** **Almost certain** Often occurs/once a week	5 Moderate	10 High	15 High	20 Catastrophic	25 Catastrophic
	4 **Likely** Could easily happen/once a week	4 Moderate	8 Moderate	12 High	16 Catastrophic	20 Catastrophic
	3 **Possible** Could happen/happen once a year	3 Low	6 Moderate	9 Moderate	12 High	15 High
	2 **Unlikely** Hasn't yet happened but could happen	2 Low	4 Moderate	6 Moderate	8 High	10 High
	1 **Rare** Concievabe but 1/100 year event	1 Low	2 Low	3 Low	4 Moderate	5 Moderate